Version 8.0
January 2016

Cosmic Origins Spectrograph Instrument Handbook for Cycle 24

STScI | SPACE TELESCOPE SCIENCE INSTITUTE

3700 San Martin Drive
Baltimore, Maryland 21218
help@stsci.edu

Operated by the Association of Universities for Research in Astronomy, Inc., for the National Aeronautics and Space Administration

User Support

For prompt answers to any question, please contact the STScI Help Desk.

- Send e-mail to: help@stsci.edu.
- Phone: 410-338-1082.
- Within the USA, you may call toll free: 1-800-544-8125.

World Wide Web

Information and other resources are available on the STScI COS World Wide Web site:

http://www.stsci.edu/hst/cos

COS Handbook History

Version	Date	Editors
8.0	January 2016	Debes, J.
7.0	January 2015	Debes, J.
6.0	January 2014	Holland, S. T.
5.0	December 2012	Holland, S. T.
4.0	December 2011	Dixon, W. V.
3.0	December 2010	Dixon, W. V.
2.0	January 2010	Dixon, W. V., and Niemi, S.-M.
1.0	December 2007	Soderblom, D. R.

Citation

In publications, please refer to this document as
Debes, J., et al. 2016, Cosmic Origins Spectrograph Instrument Handbook, Version 8.0 (Baltimore: STScI)

Send comments or corrections to:
Space Telescope Science Institute
3700 San Martin Drive
Baltimore, Maryland 21218
E-mail:help@stsci.edu

Acknowledgments

The technical and operational information contained in this handbook is the summary of the experience gained by members of the STScI COS Team and by the COS IDT at the University of Colorado in Boulder.

Current and former members of the STScI COS Team include Alessandra Aloisi, Tom Ake, John Bacinski, Azalee Bostroem, John Debes, Rossy Diaz, Van Dixon, Tom Donaldson, Linda Dressel, Justin Ely, Scott Friedman, Parviz Ghavamian, Paul Goudfrooij, George Hartig, Svea Hernandez, Phil Hodge, Stephen Holland, Mary Beth Kaiser, Tony Keyes, Jerry Kriss, Claus Leitherer, Kevin Lindsay, Sean Lockwood, Chris Long, Matt McMaster, Melissa McGrath, Derck Massa, Sami Niemi, Cristina Oliveira (lead), Rachel Osten, Steven Penton, Charles Proffitt, Julia Roman-Duval, David Sahnow, Hugues Sana, Ken Sembach, Brittany Shaw, Ed Smith, David Soderblom, Paule Sonnentrucker, Joanna Taylor, Katya Verner, Nolan Walborn, Alan Welty, Tom Wheeler, Mike Wolfe, Brian York, and Wei Zheng. All of these individuals contributed to this volume, as did Russ Makidon.

The COS IDT includes James Green (Principal Investigator), Cynthia Froning (Project Scientist), Steven Penton, Steven Osterman (Instrument Scientist), Stéphane Béland, Eric Burgh, Charles Danforth, Kevin France, and Brian Keeney, all of whom provided information and assistance. COS co-investigators are Dennis Ebbets (Ball Aerospace), Sara R. Heap (GSFC), Claus Leitherer (STScI), Jeffrey Linsky (University of Colorado), Blair D. Savage (University of Wisconsin-Madison), Ken Sembach (STScI), J. Michael Shull (University of Colorado), Oswald Siegmund (University of California, Berkeley), Theodore P. Snow (University of Colorado), John Spencer and Alan Stern (Southwest Research Institute), and John T. Stocke (University of Colorado). K. Brownsberger, J. Morse, and E. Wilkinson have also been part of the COS IDT and have made significant contributions.

The prime contractor for COS is Ball Aerospace, Boulder, Colorado. The XDL detector was built at UC Berkeley by O. Siegmund, J. McPhate, J. Vallerga, and B. Welsh.

The Editor thanks Susan Rose (Senior Technical Editor) for her contributions to the production of this handbook.

References and Additional Information

This document relies heavily on information provided by the COS team in Boulder. The primary documents used are:

Morse, J. 2004, *Cosmic Origins Spectrograph Science Operations Requirements* Document (referred to as OP-01);

Wilkinson, E. 2002, *COS Calibration Requirements and Procedures, rev. B*. (referred to as AV-03); and

Wilkinson, E. 2008, *COS Prelaunch Calibration Data* (referred to as AV-04).

We also used the *STIS Instrument Handbook* (J. Ely et al. 2011, v11.0).

CHAPTER 1:

An Introduction to COS

In this chapter…

1.1 Overview

The Cosmic Origins Spectrograph (COS) was installed on the *Hubble Space Telescope (HST)* in May 2009. Working at far-ultraviolet wavelengths, COS was designed to study the origins of large-scale structure in the Universe, the formation and evolution of galaxies, the origin of stellar and planetary systems, and the cold interstellar medium. COS significantly enhances the spectroscopic capabilities of *HST* at ultraviolet wavelengths, and provides observers with unparalleled opportunities for observing faint sources of ultraviolet light.

COS offers two independent observing channels, a far-ultraviolet (FUV) detector, which is sensitive to wavelengths between 900 and 2150 Å, and a near-ultraviolet (NUV) detector for wavelengths from 1650 to 3200 Å. Both channels are equipped with medium-resolution ($R \sim 20{,}000$) and low-resolution ($R \sim 3000$) gratings. The NUV channel can also be used in imaging mode for both target acquisitions and scientific observations. The COS field of view is approximately 2.5 arcsec in diameter.

In this chapter, we provide a brief overview of COS operations, tables of instrument and detector parameters, a list of frequently-asked questions, and a guide to using this handbook.

1.2 Observing with COS

1.2.1 Target Acquisitions

The COS entrance apertures are 2.5 arcsec in diameter. To ensure that the target is centered in the aperture a target-acquisition procedure must be performed at the beginning of each visit.

The COS flight software provides two methods for acquiring and centering a target in the aperture. The first method obtains a direct image of the aperture with the NUV channel and moves the telescope to the center of light. The second method centers the target using its dispersed spectrum and can be performed with either the NUV or FUV channel. For both methods the target's center of light can be computed from either a single exposure or from a series of exposures that map out a grid on the sky. Target acquisitions are described in Chapter 8.

1.2.2 Observing Modes: Spectroscopic and Imaging

While COS was designed as a spectrograph, the NUV channel can be used for imaging observations. The COS/NUV plate scale of 23.5 mas per pixel provides the highest spatial sampling of any instrument aboard *HST*. The image is corrected for the telescope's spherical aberration, but is degraded by zonal (polishing) errors on its primary and secondary mirrors (see Chapter 3). The NUV imaging count-rate limit of 50 counts per second per pixel (Table 10.1) corresponds to a *GALEX* NUV magnitude of 17.6.

1.2.3 Observing Modes: TIME-TAG and ACCUM

COS provides two observing modes, `TIME-TAG` and `ACCUM`. In `TIME-TAG` mode the position, arrival time, and (for the FUV channel) pulse height of each detected photon are recorded in the memory buffer. In `ACCUM` mode only the locations of arriving photons are recorded.

`TIME-TAG` mode is preferred because it allows for more sophisticated data reduction. For example, an observer may compare data from the night and day sides of the orbit or compute the count rate of an object whose intensity varies on short time scales. `TIME-TAG` observations through the primary science aperture (PSA) allow the taking of occasional wavelength-calibration spectra during an exposure. These spectra are used by the COS data-reduction pipeline, **calcos,** to correct drifts in the spectrum due to small motions of the Optics Select Mechanism (OSM). `ACCUM` mode is designed for observations of targets that are too bright for `TIME-TAG` mode. Because the lower information content of `ACCUM` data reduces their utility for archival researchers, its use must be justified for each target.

Both `TIME-TAG` and `ACCUM` modes may be used with either the FUV or NUV channel. For more information comparing `TIME-TAG` and `ACCUM` see Section 5.2.

1.2.4 Typical Observing Sequences

In the majority of cases the following sequence of events will produce high-quality data.

- Acquire the object using `ACQ/IMAGE`. This should take about three minutes. See examples in Chapter 9
- Obtain spectra in `TIME-TAG` mode using the `FP-POS=ALL` setting and `FLASH=YES` so the spectra can be corrected for flat-field anomalies and OSM drifts. The COS Exposure Time Calculator webpage (ETC) provides a means of calculating essential parameters, such as the `BUFFER-TIME`.
- Obtain additional spectra during subsequent orbits to achieve the desired signal-to-noise ratio or wavelength coverage.

1.3 COS Quick Reference Guide

Table 1.1: COS Instrument Characteristics

Property	FUV channel	NUV channel
Entrance apertures	2.5 arcsec diameter circle: clear (PSA) or attenuated (BOA)	
Detector plate scale	0.11 arcsec per pixel 1.1 arcsec per resel (G130M cross-dispersion)	23.5 mas per pixel 70.5 mas per resel (imaging mode)
	0.0285 arcsec per pixel 0.171 arcsec per resel (G130M along-dispersion[1])	23.8 mas per pixel 71.4 mas per resel (G185M along- and cross-dispersion directions)

1. Raw plate scale.

Table 1.2: COS Detector Characteristics

	FUV XDL (A / B)	NUV MAMA
Photocathode	CsI (opaque)	Cs_2Te (semi-transparent)
Window	None	MgF_2 (re-entrant)
Wavelength range	< 900 – 2150 Å	1650 – 3200 Å
Active area	85 × 10 mm (two)	25.6 × 25.6 mm
Pixel format (full detector)	16,384 × 1024 (two)	1024 × 1024
Image size recorded per spectrum	16,384 × 128 (two, `ACCUM`) 16,384 × 1024 (two, `TIME-TAG`)	1024 × 1024
Pixel size	6 × 24 μm	25 × 25 μm
Spectral resolution element size (= resel)	6 × 10 pix	3 × 3 pix
Quantum efficiency	~26% at 1335 Å ~12% at 1560 Å	~10% at 2200 Å ~8% at 2800 Å
Typical dark-count rate (away from SAA)[1]	2.77 cnt s^{-1} cm^{-2} 4×10^{-6} cnt s^{-1} pix^{-1} 2.56×10^{-4} cnt s^{-1} $resel^{-1}$	143 cnt s^{-1} cm^{-2} 8.9 cnt s^{-1} pix^{-1} 8.0×10^{-3} cnt s^{-1} $resel^{-1}$
Detector Global Count rate limit[2]	60,000 cnt s^{-1}	117,000 cnt s^{-1}
Local count-rate limit[2, 3]	~1.67 cnt s^{-1} pix^{-1} ~100 cnt s^{-1} $resel^{-1}$	~200 cnt s^{-1} pix^{-1} ~1800 cnt s^{-1} $resel^{-1}$
Screening limits for bright objects	see Table 10.1	
Dead-time constant	7.4 μs	280 ns

1. The dark-count rate values are projections to the middle of Cycle 23 (April 2016).
2. Count rates higher than these limits will trigger a detector shut-down. Bright-object screening limits are lower. See Chapter 10.
3. The FUV values are not applicable to the COS FUV G130M blue cenwaves, 1055 and 1096. The local count rate limit for these two modes is 0.2 cnt s^{-1} pix^{-1}.

Table 1.3: COS Calibration Accuracies

Property	FUV channel	NUV channel
Wavelength zero point: M gratings	15 km s^{-1}	15 km s^{-1}
Wavelength zero point: L gratings	150 km s^{-1}	175 km s^{-1}
Wavelength scale	15 km s^{-1}	15 km s^{-1}
Absolute photometry	5%	5%
Relative photometry (same object at a different times)	2%	2%
Flat field quality (spectral S/N) per resel, using standard techniques	35:1	100:1
Flat field quality (spectral S/N) per resel, using special techniques	100:1[1]	100:1

1. See Section 5.8.1.

Table 1.4: Useful Figures and Tables

Topic	Source	Content
Usage planning	Table 5.1	Grating parameters
	Table 5.3	FUV grating wavelength ranges
	Table 5.4	NUV grating wavelength ranges
	Table 10.1	Count-rate screening limits
Aperture parameters and PSFs	Figure 3.2	BOA transmission
	Figure 3.6	Model LSFs for the COS FUV channel
	Figure 4.10	Model LSFs for the COS NUV channel
	Figure 3.7	Resolving Power of FUV gratings
	Figure 6.4	Cross section of the COS imaging PSF
	Figure 8.5	Relative transmission of the COS PSA in the NUV
	Figure 13.29	*HST* focal plane and COS aperture
Effective Area	Figure 5.1	FUV spectroscopy
	Figure 5.2	NUV spectroscopy
	Figure 6.3	NUV imaging
Acquisitions	Figure 8.1	Examples of spiral search patterns
	Figure 8.2	Point-source images with all apertures and mirrors
	Figure 8.3	ACQ/IMAGE exposure times
	Figure 8.4	Dispersed-light exposure times
Detector characteristics	Figure 4.1	FUV XDL detector schematic layout
	Figure 4.9	NUV MAMA detector layout
	Table 7.1	Detector background count rates
Overheads and observing parameters	Table 5.2	TAGFLASH exposure durations
	Table 9.1	Overhead estimates for Phase I proposals
	Table 9.2	Generic observatory overhead times
	Table 9.3	Overhead times for OSM1 movements
	Table 9.4	Overhead times for OSM2 movements
	Table 9.5	Science exposure overhead times
Celestial backgrounds	Figure 7.1	Sky background versus wavelength
	Figure 7.2	Moon, Earth and zodiacal-light background levels
	Figure 7.2	Galactic extinction model
	Table 7.3	Earthshine and zodiacal light fluxes
	Table 7.4	Strengths of airglow lines
Data quality	Figure 5.13	FUV flat-field example
	Figure 5.17	NUV flat-field example

1.4 COS FAQ

Table 1.5: COS Frequently–Asked Questions

Question	Answer
Should I use COS or STIS? Does COS have an imaging mode?	Section 2.7 Chapter 6
What detectors are available? What apertures? What gratings? What are their properties?	Chapter 4 Section 3.1.2 Tables 5.1, 5.3, 5.4
What do COS images look like? What do COS spectra look like? Do the spectra have gaps?	Figure 6.1 Figures 4.2, 4.9 Section 5.5
What is the difference between `ACCUM` and `TIME-TAG` mode? How do I estimate the `BUFFER-TIME` for `TIME-TAG` exposures? How do I obtain wavelength-calibration exposures?	Section 5.2 Section 5.4 Section 5.7
What are the science impacts of the COS line-spread function? What is the COS sensitivity and resolution below 1150 Å? Which COS gratings suffer from second-order contamination?	Section 3.3 Figures 5.3, 5.1.4, 5.5 Section 5.1.3
How accurate is COS absolute/relative photometry? How accurate are the COS wavelength scale and zero point?	Section 5.1.10 Section 5.1.11
How do I plan a successful target acquisition?	Chapter 8
What are the bright-object limits? How do I confirm that my target/field is safe to observe?	Table 10.1 Section 10.5
How much time should I request for my observations?	Chapter 9

1.5 Purpose of this Handbook

The *COS Instrument Handbook* describes the design, performance, operation, and calibration of the Cosmic Origins Spectrograph. It is meant to be the principal reference manual for users of COS. This handbook is written and maintained at STScI. While it presents the best available information about COS at the time of the most recent update, tabulated parameters, such as dark rates or sensitivities, can evolve with time during a cycle.

The handbook is designed for readers who are

- preparing a Phase I proposal to observe with *HST*,
- writing a Phase II program once a proposal has been accepted, or
- analyzing data from observations that have already been made.

This handbook is not meant to be the primary reference for COS data reduction or analysis. That information is provided in the *COS Data Handbook*. For quick reference, information on COS data products is provided in Chapter 11.

1.5.1 Document Conventions

This document follows the usual STScI conventions:

- Terms, words, or phrases that are to be entered by the user in a literal way in an *HST* proposal are shown in a typewriter or Courier font, such as "`COS/FUV`" or "`TIME-TAG`".
- Names of software packages or commands (such as **calcos**) are shown in boldface.

Wavelengths in this handbook, and in COS data products, are always measured in vacuum and are quoted in Angstroms (Å).

CHAPTER 2:

Special Considerations for Cycle 24

In this chapter…

2.1 COS FUV Detector Lifetime Positions

Prolonged exposure to light causes the COS FUV detectors to become less efficient at photon-to-electron conversion, a phenomenon called “gain sag”. The more a particular region of the detector has been used, the smaller the “pulse height” of the charge cloud generated by an individual photon becomes. As long as all pulse heights are above the minimum threshold needed to distinguish real photons from background events there is no loss in sensitivity. However, as the average pulse height at a location on the detector approaches, and then drops below this threshold, real photon pulses are increasingly misidentified as background and the effective throughput decreases. Since the amount of gain sag increases with the total amount of previous illumination, these effects appear first on regions of the detector that are illuminated by the bright Lyman-α airglow line, but eventually the entire spectrum becomes affected. STScI is undertaking a number of actions to mitigate the effects of gain sag and extend the lifetime of the COS FUV XDL detector. These are discussed in detail in Chapter 4.

On July 23, 2012 the COS FUV spectral location was moved to its second lifetime position (LP2). This changed the COS aperture position location from its original lifetime 1 (LP1) position by 3.5" in the *HST* field of view, and shifted the spectral location by about 1 mm to a part of the detector where significant gain sag had not yet

occurred. This change temporarily eliminated the "Lyman-α" gain sag holes and other gain sag artifacts for data obtained during Cycle 20, 21, and the early parts of Cycle 22. By February 9, 2015, new gain-sagged regions at LP2 degraded enough to require a move of most FUV modes to the third lifetime position (LP3).

For LP3 a smaller shift of ~2.5" from LP1 has been performed in the opposite direction from that done for LP2. This closer placement to LP1 is needed to keep the spectral resolution as high as possible, though it places the FUV spectra significantly closer to the severely gain-sagged detector regions of LP1. Observations with the G130M 1055 and 1096 central wavelength settings, which have wide cross-dispersion profiles that would be severely impacted by this overlap, continue to be executed at LP2. The G130M 1222 central wavelength will execute at LP3, but has been operated at a higher voltage setting to minimize the impact of gain-sagged regions.

For point source observations at LP3, the close proximity to the sagged detector regions require the implementation of a new extraction algorithm that uses the shape of a point source profile to define the region over which counts are included in the extracted spectrum and to decide when bad pixels in the profile wings compromise the accuracy of the spectral extraction. Sources that have substantial spatial extent may have significant overlap with the gain-sagged regions and may require specialized extractions that are currently not performed with **calcos**. For these reasons, observations of extended sources will not be optimally calibrated. Users should set the optional APT parameter EXTENDED=YES to flag such sources (see Section 5.9), even if the **calcos** pipeline calibration will not treat extended sources differently from point sources.

Throughput, and most other calibrations at LP3, are very similar to those at the original position, but the spectral resolution may be up to 15-20% lower than it was at the original lifetime position and about 10% lower than at LP2. See the COS website and the COS Instrument Science Reports (ISRs) for additional information about the calibration of the second and third lifetime positions.

Gain sag is an inevitable result of using the detector. Gain sag holes will eventually appear at LP3 as well, with the timing of their appearance depending on the locally accumulated signal. The use of all four `FP-POS` positions, which is now required for most COS FUV observations (see Section 4.1.7), will distribute the high geocoronal Lyman-α flux more uniformly over the detector, and thus will significantly delay the re-appearance of these holes.

2.2 COS Observations Below 1150 Å: Resolution and Wavelength Calibration Issues

Starting in Cycle 21 the spectral resolutions of the FUV G130M 1055 and 1096 central wavelengths settings were substantially increased above the values offered during earlier cycles and, when combined with the 1222 setting first offered in Cycle 20, this now allows resolutions of 7300 to 11,000 to be obtained (estimated for LP3) at any wavelength between 900 and 1150 Å (see Figure 5.5). Users should note, however, that for each of these modes the focus values have been set to optimize the resolution over a limited part of their wavelength range, and it will be necessary to use

multiple settings to get the maximum resolution over this full range. At longer wavelengths the resolutions offered by any of these settings will be inferior to those available with the original complement of G130M central wavelength settings (1291, 1300, 1309, 1318, and 1327).

Users should also note that targets that are too bright to observe at longer wavelengths with the COS G130M grating may be observable on Segment B with the 1055 and 1096 settings by turning off Segment A, which covers longer wavelengths. However, in this case there is no usable TAGFLASH wavelength calibration lamp spectrum recorded because there are no visible wavelength calibration lines that fall on Segment B. As a result, the spectrum observed on Segment B cannot be corrected for mechanism drift or zero-point offsets. *In such cases, for each* `CENWAVE` *and* `FP-POS` *position, a separate GO-wavecal exposure should be taken with Segment A "on" immediately adjacent to the Segment B science observations. This Segment A wavecal will allow the zero-point offset of the wavelength scale of Segment B to be corrected to within 10 pixels.* Several minutes are required to reconfigure the COS FUV detector each time the segments are powered on or off. However, with careful planning much of this overhead can often be hidden in the occultations or other overheads. Additional details and examples of observing scenarios can be found in Chapter 5 and in Section 9.7 "Examples of Orbit Estimates".

The 1280 setting of G140L also covers from below 900–1185 Å on Segment B of the FUV detector with resolution of 900–1800 (estimates for LP3) over this range. In principle, the spectral format of this setting may allow observations at even shorter wavelengths; however, the throughput and resolution between 500 and 900 Å are poorly characterized.

Limited amounts of data were taken using the G130M 1055 and 1096 central wavelength settings at the first lifetime position (before July 23, 2012). Calibrated data from these observations can be obtained by contacting the STScI Help Desk.

2.3 Time-Dependent Sensitivity Changes

During Cycle 17 the throughputs of some COS modes—the bare-aluminum NUV G225M and G285M gratings and the FUV channels—were found to be declining with time significantly more rapidly than had been expected. Since that time the decline of the G225M and G285M grating throughputs has continued at approximately the same rate. However, the rate of decline of the throughput of the FUV channels has fluctuated, first becoming more modest and later showing variations that appear to be correlated with Solar activity (Section 5.1.5). It is believed that these latter changes are due to degradation of the photocathode caused by reactions with residual atmospheric atomic oxygen. As Solar activity increases, the Earth's atmosphere becomes slightly inflated, exposing the open-faced COS FUV XDL detector to increased levels of atomic oxygen

Despite these challenges, the COS FUV sensitivity is still outstanding, and COS remains the instrument of choice for most spectroscopic observations of faint FUV targets.

The figures and tables in this handbook were constructed using projected instrumental sensitivities for the middle of Cycle 23 (April 2016). Observers are reminded to use the COS Exposure Time Calculator (ETC; see Chapter 7) to design their proposals. It will be updated as the instrument sensitivity and background rates evolve.

2.4 Spectroscopic Use of the Bright Object Aperture

Spectroscopic observations with the BOA have had very little demand over the past cycles. For that reason, it has been decided that spectroscopic observations with the BOA will not be supported at the level that is used for the PSA. Spectroscopic observations with the BOA should be performed only if the technical requirement and scientific justification are particularly compelling. Proposers should be aware of the following caveats regarding use of the BOA:

- Further calibrations for the BOA will not be provided by STScI. Either users must determine that they can create calibration files from data in the HST Archive or they must obtain calibrations as part of their observations. Spectroscopic observations using the BOA will be calibrated by **calcos**, but will be based on reference files primarily derived for use with the PSA and will use a the new TWOZONE extraction algorithm described in Section 3.2.1 of the *COS Data Handbook*.
- User support from STScI for observation planning, as well as data reduction and analysis, with the BOA will be limited. Users taking spectroscopic data with the BOA should be prepared to shoulder the increased burden of the planning, calibration, reduction, and analysis.

Cycle 24 Phase I proposals that include spectroscopic use of the BOA must include a justification of why the science cannot be done with the PSA.

2.5 Non-Optimal Observing Scenarios

To optimize the scientific return of COS, we recommend that all observations be performed in `TIME-TAG` mode, employ the default wavelength-calibration procedures (i.e., `TAGFLASH=YES`), and with all four `FP-POS` positions (See Section 5.8) of each `CENWAVE` setting for the FUV gratings. Observers who wish to employ non-optimal observing techniques must strongly justify their observing strategy in the "Description of Observations" section of their Phase I proposal. A modest reduction in observational overheads will not normally be a sufficient justification for adopting

non-optimal observing techniques. Whenever possible, observers should use the recommended techniques, even if this requires requesting additional resources in their Phase I proposal.

2.6 SNAP, TOO, and Unpredictable Source Programs with COS

The COS photon-counting detectors can be harmed by exposure to bright light. Because all COS observations must be checked at STScI by a Contact Scientist to confirm that both the intended target and all nearby objects lie within safe-brightness limits, the total number of targets accepted for all COS and STIS MAMA SNAP programs will be limited to 150 per cycle.

For similar reasons, when planning Target of Opportunity (TOO) observations COS observers must ensure that sufficient time is available to allow for STScI screening of targets for compliance with safety limits. Ultra-rapid TOOs, (< 2 days), are not allowed with COS. *No COS observations will be performed until the bright object screening has been completed.* This process can be greatly accelerated by preliminary discussions with the assigned Contact Scientist to clarify the information that the observer will need to provide to STScI and the criteria that will be used to determine if the target is safe to observe.

In the case of irregular variables that are either known to undergo unpredictable outbursts, or belong to classes of objects that are subject to outbursts, the proposer must determine whether the target will violate the bright object limits during outburst. If a violation is possible, the proposer must outline a strategy that will ensure that the target is safe to observe with COS. The observing strategy might include additional observations, obtained over a timescale appropriate to the particular type of variable object, with either HST or ground-based telescopes. If HST data are to be used for this purpose, the required orbits must be requested in Phase I (see Section 4.1.3 of the *Call for Proposals*). STScI reserves the right to limit the number of visits requiring quiescence verification observations within 20 days or less of an HST observation to no more than 12 such visits per Cycle. Further details about these procedures are presented in ACS ISR 06-04. The general policies described there apply to the STIS/MAMA and COS detectors as well, with suitable scaling for the differences in the exact Bright Object Protection (BOP) limits for each detector and mode. These limits are described in the individual instrument handbooks.

For more information on these and other policies pertaining to *HST* observing, please see the *Call for Proposals*.

2.7 Should I Use COS or STIS?

With the installation of COS and the repair of the Space Telescope Imaging Spectrograph (STIS) *HST* has two spectrographs with significant overlap in spectral range and resolving power. Each has unique capabilities, and the decision of which to use will be driven by the science goals of the program and the nature of the target to be observed.

In the far-UV (from about 1100 to 1800 Å), the throughput of the COS FUV channel exceeds that of the STIS FUV MAMA by factors of 10 to 30, and the combination of the spectroscopic resolving power (~17,000) and wavelength coverage (300 to 370 Å per setting) of the medium-resolution COS FUV modes, as well as the extremely low detector dark rate of the XDL detector, results in a discovery space (throughput times wavelength coverage) for observations of faint FUV point sources that is at least 10 times greater for most targets than that of STIS modes with comparable resolution, and as much as 70 times greater for faint, background-limited point sources.

Because of its MgF_2 windows, the STIS FUV MAMA is insensitive to wavelengths below about 1150 Å. The COS FUV XDL detector is windowless and provides useful throughput to at least 900 Å. See Section 5.1.2 for details.

In the near-UV (~ 1700 to 3200 Å), COS and STIS have complementary capabilities. To accommodate the NUV detector format the COS NUV spectrum is split into three non-contiguous stripes, each of which covers a relatively small range in wavelength. Obtaining a full NUV spectrum of an object requires several set-ups and exposures (six or more for the medium-resolution gratings and three for G230L grating). When broad NUV wavelength coverage is needed obtaining a single STIS spectrum will often be more efficient than taking separate COS spectra. Users should note that for the shorter NUV wavelengths COS modes often have a substantial throughput advantage over the comparable STIS modes, while at the longer NUV wavelengths it can be STIS that has the advantage. They should also consider that the STIS NUV modes have produced a large set of existing observations, while the COS NUV modes have so far seen limited use. As a result, the calibration of the STIS NUV modes is likely to be superior to that of comparable COS modes for the foreseeable future.

After installation into HST in 2009, the dark rate of the COS NUV detector had initially been substantially lower than that of STIS NUV detector. However, the dark rates for the two detectors have converged over the years. Observers are advised to perform detailed calculations using both the COS and STIS ETCs and to consider carefully the relative instrument overheads to determine which combination of instruments and modes is best for their science.

For observations of extended sources, the spatial resolution offered by STIS must be weighed against the superior sensitivity of COS. One of the primary design goals of STIS was to provide spatially-resolved spectra in the UV, optical, and near-IR. The STIS long slits, when used with the first-order gratings, allow spatially-resolved observations that exploit the intrinsically high resolution of *HST* over the full width of the detectors (approximately 0.05 arcsec per 2-pixel spatial resolution element over a

length of 25 arcsec with the NUV and FUV MAMAs, and approximately 0.1 arcsec per 2-pixel spatial-resolution element over a length of 52 arcsec with the CCD).

COS was optimized for point-source observations. While COS has relatively large entrance apertures (2.5 arcsec diameter), flux from regions more than 0.4 arcsec from the aperture center is significantly vignetted. These large apertures also mean that objects extended in the dispersion direction will yield spectra with lower spectral resolution. In addition, the optical design of the FUV channel limits the achievable spatial resolution; measured values of the FWHM in the spatial dimension vary between about 0.25 and 1.5 arcsec, depending on grating and wavelength (Section 5.1.9). The COS NUV channel uses a different optical design and has a spatial resolution comparable to that of the STIS first-order NUV modes (~ 0.05 arcsec), with somewhat better sampling. However, for sources extending more than 1 arcsec in the spatial direction, the various NUV spectral segments will begin to overlap.

The line-spread functions (LSFs) of both instruments exhibit non-Gaussian wings due to mid-frequency zonal (polishing) errors in the Optical Telescope Assembly (OTA). Using STIS, one can minimize their effects through the use of narrow apertures. Narrow apertures are not available on COS. The broad wings of the LSF, especially in the short wavelengths of the FUV band, can limit the ability of COS to resolve faint, narrow features, and blend closely-spaced lines. Studies that require accurate knowledge of the line profile will require full consideration of the COS LSF (Section 3.3). The non-Gaussian wings of the COS LSF should have only modest impact on science programs targeting broad lines and continuum sources.

Both COS detectors and the STIS MAMA detectors are prohibited from observing objects that exceed specific brightness levels (see Chapter 10 in this handbook and Sections 13.8 and 14.8 of the *STIS Instrument Handbook*). Some brightness limits have been established for the health and safety of the instrument, while others are practical limits that are set to ensure good data quality. Because STIS is less sensitive than COS, the brightness limits for STIS tend to be significantly less stringent. In the NUV range, the STIS G230LB and G230MB gratings can also be used with the STIS CCD, which has no bright-object limitations. STIS also has a number of small and neutral-density apertures that can be used with the MAMA detectors to attenuate the light of a too-bright object. COS has only a single neutral-density filter that attenuates by a factor of about 200, but also degrades the spectral resolution by a factor of 3 to 5. In most cases some combination of STIS gratings and apertures will be a better choice for observing a UV-bright object than COS with its neutral-density filter. Users are advised to compare results from the COS and STIS ETCs when deciding on an appropriate strategy for their target.

The STIS high-dispersion echelle modes E140H and E230H have resolving powers of ~114,000 (or even $R \sim 200{,}000$ with the 0.1×0.03 aperture and specialized data reduction; see Section 12.6, "Improving the Sampling of the Line Spread Function," of the *STIS Instrument Handbook*), significantly higher than the best COS resolution. Also, STIS can obtain spectra in the optical and near-IR at wavelengths up to 10,200 Å, while the maximum wavelength observable by COS is about 3200 Å.

Both STIS and COS can perform observations in `TIME-TAG` mode, whereby the time of each photon's arrival is recorded. STIS is capable of a much finer time

resolution (125 μs vs. 32 ms for COS), although few programs require such a high sampling rate. Due to its lower sensitivity STIS may be able to observe a target in TIME-TAG mode that is too bright for TIME-TAG observations with COS. On the other hand, TIME-TAG data acquired with the COS FUV detector includes information on the pulse-height distribution, while TIME-TAG data acquired with the STIS and COS MAMAs do not. Pulse-height information can be valuable in identifying and rejecting background counts in the spectra of faint sources.

CHAPTER 3:

Description and Performance of the COS Optics

In this chapter…

3.1 The Optical Design of COS

In most spectrographs the light from the telescope is focused onto a slit, which is then re-imaged onto the detector. In such a design the slit width and the way that the slit is illuminated determine the resolving power and LSF. COS is different. It is essentially a slitless spectrograph with an extremely small field of view. In this section we follow the light from the *HST* Optical Telescope Assembly (OTA) as it progresses through COS to each optical element and mechanism. The optical path and mechanism locations are shown in Figure 3.1.

3.1.1 External Shutter

The external shutter is located at the front of the COS enclosure. When closed the shutter blocks all external light from entering the COS instrument and prevents light from the COS internal lamps from exiting the instrument. The opening and closing of the external shutter does not define the duration of an exposure, as the shutter may be opened before an exposure begins to allow for target acquisition and bright-object checking.

Figure 3.1: The COS Optical Path and the Locations of the Mechanisms
The optical path is drawn to scale, with all elements in proportion and in their correct relative locations.

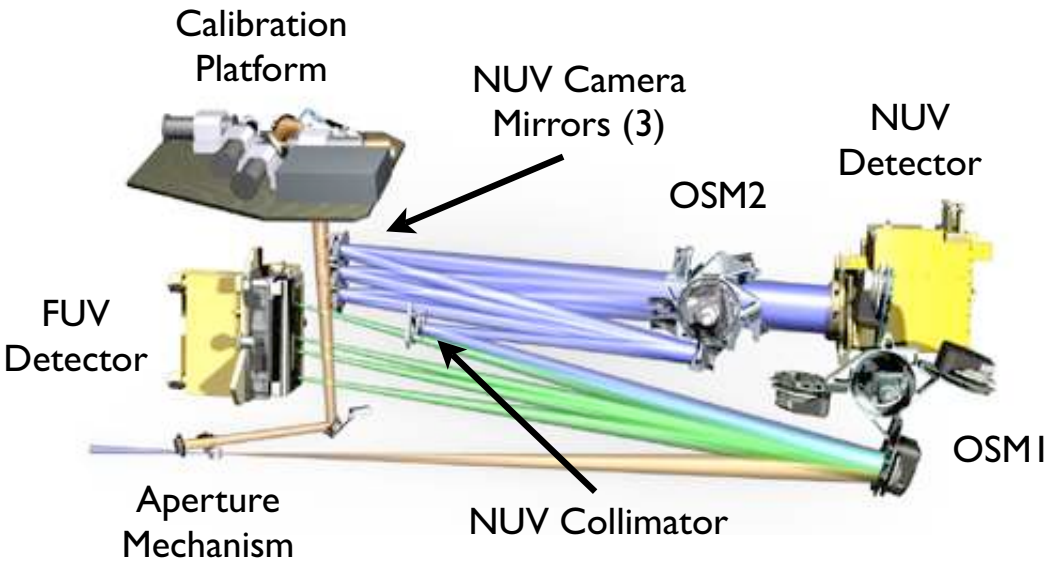

3.1.2 The Apertures and Aperture Mechanism

After passing through the external shutter, the light from the OTA first encounters one of the COS entrance apertures (Table 3.1), which are mounted on the Aperture Mechanism (ApM). Selecting an aperture can involve movement of the Aperture Mechanism.

Primary Science Aperture

The Primary Science Aperture (PSA) is a circular field stop 2.5 arcsec (700 μm) in diameter. It is located, not at the *HST* focal surface, but near the point of the circle of least confusion. The aperture transmits ≥ 95% of the light from a well-centered, aberrated point-source image delivered by the *HST* optics. The PSA is used for almost all COS science observations. It is in place, ready to use, at the start of a new visit. Note that, when the PSA is in place, the Wavelength Calibration Aperture (WCA; see below) is also in place and available to acquire simultaneous wavelength-calibration spectra. External light entering the PSA and internal light entering the WCA are dispersed by the same grating. Thus, for a given grating and central-wavelength setting, no additional motion of the Aperture Mechanism is required to obtain a wavelength-calibration exposure.

Table 3.1: COS Entrance Apertures

Aperture	Full Name	Purpose	Size (mm)
PSA	Primary Science Aperture	science aperture	0.700 diameter
BOA	Bright Object Aperture	science aperture with ND2 filter	0.700 diameter
WCA	Wavelength Calibration Aperture	wavecals with Pt-Ne lamp	0.020 × 0.100
FCA	Flat-Field Calibration Aperture	Flat field with deuterium lamp	0.750 × 1.750

Wavelength Calibration Aperture

The Wavelength Calibration Aperture (WCA) is offset from the PSA by 2.5 mm (about 9 arcsec) in the cross-dispersion direction. The WCA is illuminated by one of two Pt-Ne wavelength-calibration (wavecal) lamps. It does not receive light from external sources. The wavecal spectrum is used by the COS pipeline to assign wavelengths to the science spectra obtained through either the PSA or BOA. During target acquisitions light from the Pt-Ne lamps provides a reference from which the location of the target aperture is determined.

Bright Object Aperture

Like the PSA, the Bright Object Aperture (BOA) is 2.5 arcsec (700 μm) in diameter, but it incorporates a neutral-density (ND2) filter. The transmission of the ND2 filter varies with wavelength (Figure 3.2), but is roughly 0.6%. The BOA is offset from the PSA by 3.7 mm (about 13 arcsec) in the cross-dispersion direction opposite the WCA. For scientific observations the aperture block is shifted, via movement of the Aperture Mechanism, to place the BOA in the position normally occupied by the PSA. Thus, spectra obtained through either the PSA or BOA use the same optical path and detector region (for a given channel), and so may employ the same fixed pattern calibrations. *Moving the BOA into place for scientific use shifts the WCA as well, precluding simultaneous use of the WCA for a wavecal exposure*. Before or after an observation through the BOA the Aperture Mechanism must be moved to properly position the WCA, so that a wavecal exposure may be obtained. Currently, the BOA has not been calibrated to the same accuracy as other modes and is an available-but-unsupported option in Cycle 23.

Flat-Field Calibration Aperture

The Flat-Field Calibration Aperture (FCA) is used to obtain flat-field exposures using one of the two deuterium hollow-cathode flat-field calibration lamps. The FCA is used only for calibration and is not available to general observers.

3.1.3 Gratings and Mirrors: The Optics Select Mechanisms

After passing through one of the COS apertures light next encounters the Optics Select Mechanism 1 (OSM1), a rotating mechanism that can bring one of four optical elements into the beam. One of these, NUV Collimating Mirror 1 (NCM1), is a flat mirror that directs the beam to the NUV channel. The other three elements are the

G130M, G160M, and G140L gratings for the FUV channel. As a consequence of this design the FUV and NUV channels cannot be used simultaneously.

Figure 3.2: Transmission of the COS BOA as a Function of Wavelength

Dashed lines represent the ratio of BOA to PSA spectra of the standard star LDS749b obtained using all three FUV gratings. The thick red curve is a spline fit to the dashed curves.

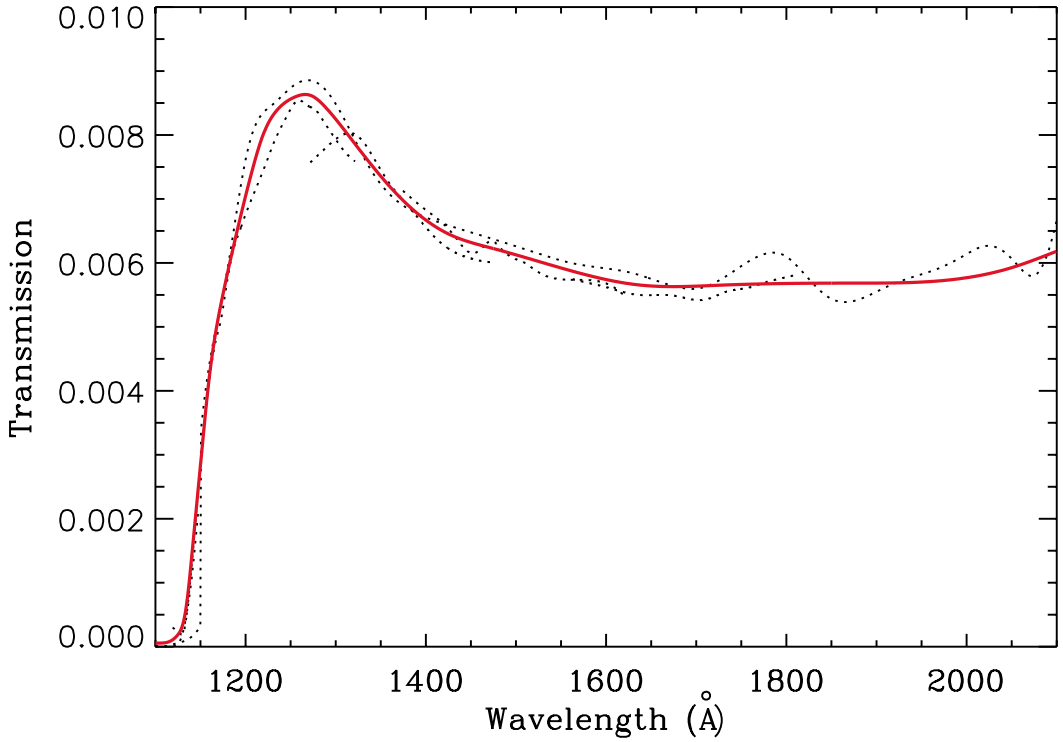

Figure 3.3: The COS FUV Optical Path

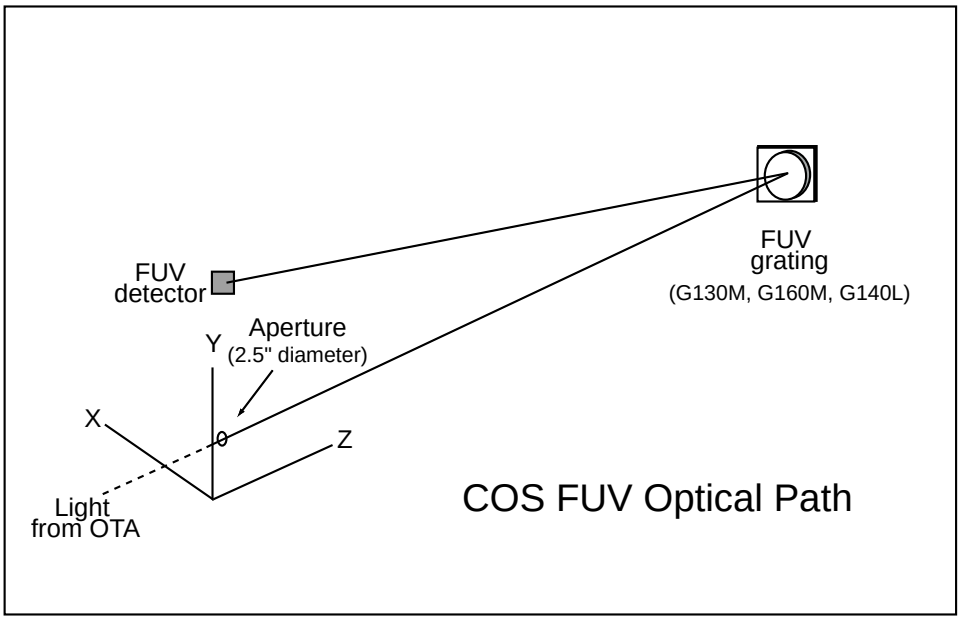

FUV Channel Optical Design

The COS FUV optical path is illustrated schematically in Figure 3.3. To maximize throughput a single FUV grating is used to disperse the light, remove the spherical aberration introduced by the *HST* primary mirror, and focus the beam onto the detector. Because the FUV gratings introduce astigmatism in the direction perpendicular to dispersion, the height of the spectrum varies with wavelength (Section 5.1.9). Given the location of OSM1 in the *HST* optical path it is possible for the FUV gratings to disperse, focus, and correct the beam optimally only for a point source that is centered in the aperture. Performance is degraded when the source is moved away from the aperture center. Fortunately, this degradation is low for displacements up to about 0.4 arcsec (Section 8.8).

The COS FUV channel provides spectra from 900 to 2150 Å at low and moderate spectral resolution (Section 5.1). The FUV detector is described fully in Chapter 4, but it is important to note that it consists of two independent detector segments with a small physical gap between them. Light falling into the gap is not recorded. Though the gap prevents a continuous spectrum from being obtained at a single central-wavelength setting, the missing wavelengths can be recovered by obtaining additional exposures at other central-wavelength settings (corresponding to small rotations of the OSM1 mechanism; see Section 5.5).

Figure 3.4: The COS NUV Optical Path for Spectroscopic Observations

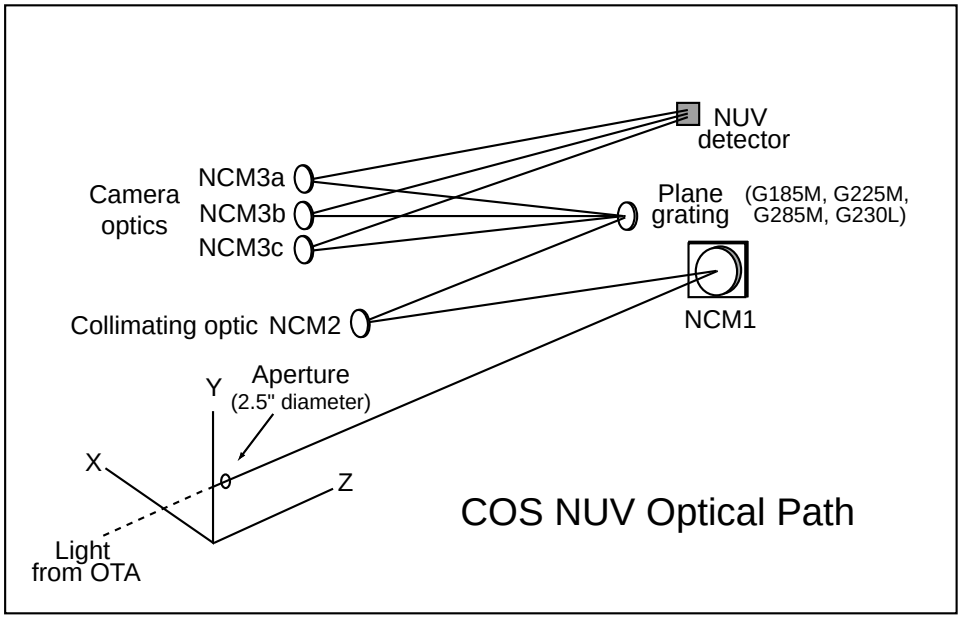

OSM2 and the NUV Channel

The COS NUV channel, illustrated schematically in Figure 3.4, provides coverage from about 1650 to 3200 Å at low and moderate spectral resolution. If the NUV channel is to be used OSM1 is turned to place mirror NCM1 in the beam. NCM1 corrects the beam for the spherical aberration of *HST*, magnifies it by a factor of four, and directs it to the NUV Collimating Mirror 2 (NCM2). The NCM2 collimates the light and directs it to Optics Select Mechanism 2 (OSM2). OSM2 holds five optical

elements: the four NUV diffraction gratings (G185M, G225M, G285M, and G230L), and a mirror for target acquisitions or imaging.

To accommodate the NUV detector format, dispersed light from the NUV gratings is imaged onto the detector by three parallel mirrors (NCM3a, 3b, 3c). For the medium-dispersion gratings the spectra appear as three non-contiguous 35–40 Å stripes on the MAMA detector, providing 105–120 Å wavelength coverage per exposure. The low-dispersion grating provides ~400 Å per stripe. The layout of the stripes is shown in Figure 4.9. The gratings can be shifted via slight rotations of OSM2 to cover the entire NUV wavelength band. The NCM3 mirrors are spaced such that several correctly-chosen exposures will produce a complete spectrum, from the low end of the short-wavelength stripe to the high end of the long-wavelength stripe.

Imaging with the NUV Mirror

For imaging observations OSM2 is turned to place a mirror (TA1) in the light path instead of a grating (Figure 3.5). When used in direct specular reflection this mirror is designated as `MIRRORA`. For bright targets, the flux can be attenuated by adjusting OSM2 so that the order-sorting filter in front of the mirror reflects the light onto the detector. This configuration is referred to as `MIRRORB`. COS imaging is described in Chapter 6.

Figure 3.5: COS NUV Optical Path for Imaging Observations

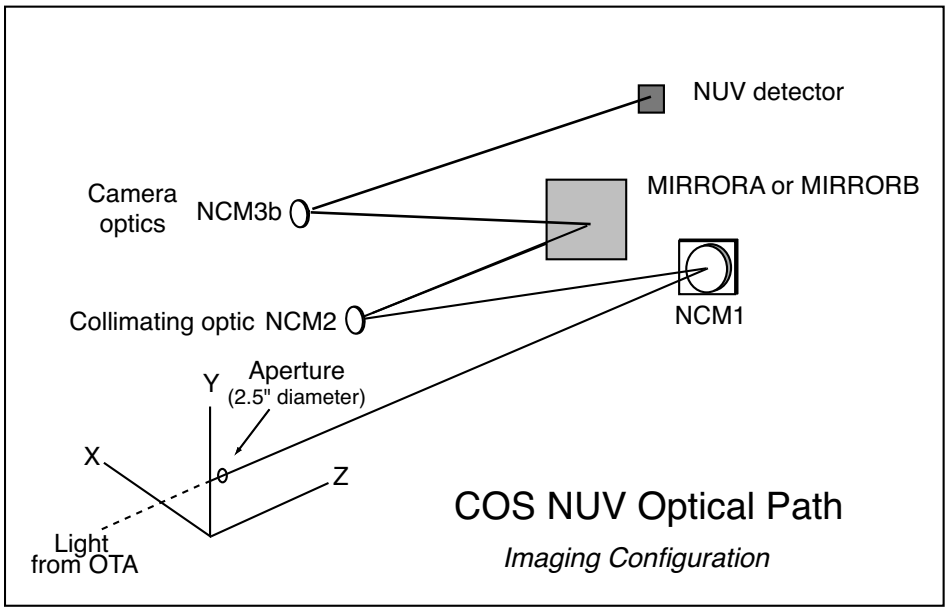

3.2 Size of a Resolution Element

Throughout this document, we assume that a resolution element (resel) spans 6 × 10 pixels on the FUV detector (in the dispersion and cross-dispersion directions, respectively) and 3 × 3 pixels on the NUV detector (Table 1.2). These values were determined before launch. Even then, it was known that the true size of a resel would vary with wavelength. In-flight data suggests that the FUV resel is somewhat larger than previously assumed (see the discussion of the line-spread function in Section 3.3), while the NUV resel is smaller. For the G130M 1055 Å and 1096 Å settings the resel is between 8 and 32 pixels. For the 1222 Å setting it is 7–13 pixels. We will continue to refine our analysis of the instrument parameters. In the mean time, keep in mind that, for the FUV, the *COS Exposure Time Calculator* (ETC) uses a 6-pixel resel size (dispersion) in all of its calculations in the FUV. It uses resel sizes of 8, 9, and 6 for the G130M/1055, G130M/1096, and G130M/1222 blue modes respectively. Users who adopt a larger or smaller resel should adjust the ETC results accordingly.

3.3 The COS Line-Spread Function

The COS optics correct for the spherical aberration of the *HST* primary mirror, but not for the mid-frequency wavefront errors (MFWFEs) due to zonal (polishing) irregularities in the *HST* primary and secondary mirrors. As a result, the COS spectroscopic line-spread function (LSF) has extended wings and a core that is slightly broader and shallower than a Gaussian. The extended wings of its LSF limit the ability of COS to detect faint, narrow spectral features. The effect is greater at short wavelengths, and it may have consequences for some COS FUV science. The most severely impacted programs are likely to be those that

- rely on models of the shapes of narrow lines,
- search for very weak lines,
- aim to measure line strengths in complex spectra with overlapping, or nearly overlapping, lines, or
- require precise estimates of residual intensity in very strong or saturated lines.

3.3.1 Non-Gaussianity of the COS LSF

Initial results from an analysis of the on-orbit COS LSF at the original lifetime position are reported by Ghavamian et al. (2009) in COS ISR 2009-01. They find that model LSFs incorporating *HST* MFWFEs are required to reproduce the absorption features observed in stellar spectra obtained with COS. Figure 3.6 shows model LSFs computed for grating G130M at 1309 Å. The solid line represents a model incorporating the spherical aberration of the *HST* OTA. It is well-fit by a Gaussian with FWHM = 6.5 pixels. The dot-dash line represents a model that includes the MFWFEs at the original lifetime position while the dashed line represents a model that also includes the MFWFEs at the second lifetime position. The model at the

original lifetime position has a FWHM of 7.9 pixels, slightly larger than that of the solid curve, and broad non-Gaussian wings. The model at the second lifetime position has a very similar FWHM. The non-Gaussian wings can hinder the detection of closely-spaced narrow spectral features. Model LSFs for all of the COS gratings at the original and second lifetime positions are available on the COS website.

Figure 3.6: Model Line-Spread Functions for the COS FUV Channel.
Model LSFs for G130M at 1309 Å normalized to a sum of unity. The solid line represents a model LSF that incorporates the spherical aberration of the OTA. It is well fit by a Gaussian with FWHM = 6.5 pixels. The dashed line represents a model that also includes the **HST** mid-frequency wave-front errors at the second lifetime position. The dot-dash line represents a model that also includes the **HST** mid-frequency wave-front errors at the original lifetime position. These latter two LSFs show a larger FWHM and broad non-Gaussian wings.

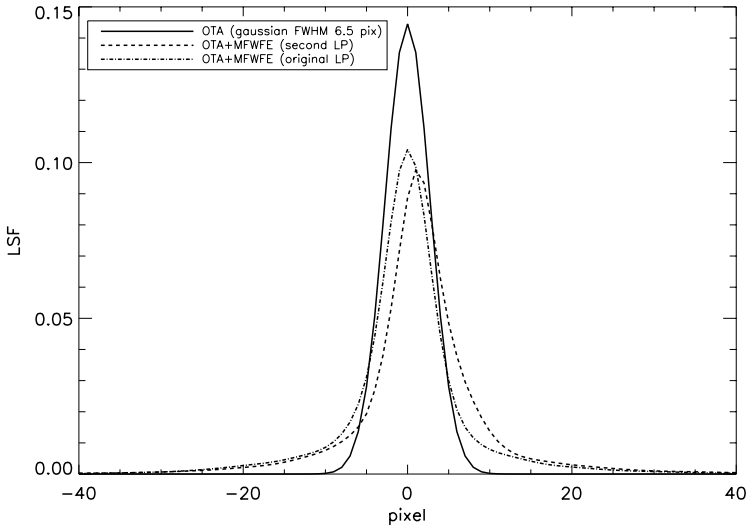

3.3.2 Quantifying the Resolution

When a substantial fraction of the power in an LSF is transferred to its extended wings traditional measures of resolution, such as the FWHM of the line core, can be misleading. For example, an observer assuming that the resolving power R = 16,000 at 1200 Å quoted for the G130M grating represents the FWHM of a Gaussian would mistakenly conclude that COS can resolve two closely-spaced narrow absorption features, when in fact it may not be able to. Nevertheless, the FWHM is a convenient tool, and we use it to describe the COS gratings in tables throughout this handbook. When using these tables keep in mind that the quoted resolving power R is computed from the empirically-determined FWHM of the line core, and careful modeling may be needed to determine the feasibility of a particular observation or to analyze its result.

Figure 3.7 shows the resolving power of the FUV gratings for three cases: the first assumes a Gaussian LSF of FWHM = 6.5 pixels with no MFWFEs from the *HST* OTA (solid lines), the second is an LSF model with the MFWFEs included for the original lifetime position (dot-dash lines), and the third is an LSF model with the MFWFEs included for the second lifetime position (dashed lines). In the second case the FWHM of the LSF is calculated directly from the line profile by taking the width at half the peak (from Table 1 of COS ISR 2009-01). The MFWFEs reduce the resolving power

of the G130M and G160M gratings by ~20%. The G140L profile is least affected by the MFWFEs, due to its lower dispersion. Measurements of the resolving power of the G130M grating at λ < 1150 Å are presented in Section 5.1.4.

Figure 3.7: Resolving Power of FUV Gratings

The resolving power (**R** = λ / FWHM) for the three gratings of the COS FUV channel for observations through the PSA aperture. The solid lines represent a Gaussian with FWHM = 6.5 pixels. The dashed lines are the values predicted by the LSF model with the on-orbit MFWFEs included at the second lifetime position. The dot-dash lines are the values predicted by the LSF model with the on-orbit MFWFEs included at the original lifetime position. (The dashed, dot-dash, and solid lines for G140L nearly overlap.)

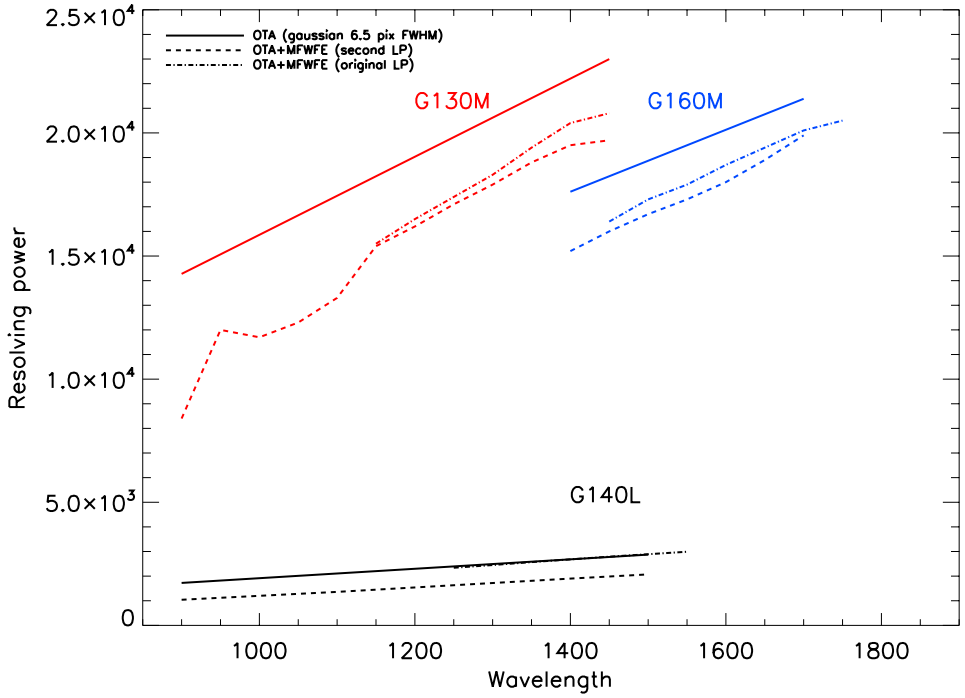

3.3.3 Impact on Equivalent Width Measurements

The broad core and extended wings of the COS LSF increase the limiting equivalent width for absorption features in COS spectra. Figure 3.8 shows the limiting equivalent widths as a function of wavelength for a 3σ FUV detection of absorption features at S/N = 10 per pixel at lifetime position 2. A series of Gaussian spectral features with nominal Doppler parameters of b = 0, 10, 25, 50, and 100 km/s have been convolved with both a Gaussian instrumental LSF and the modeled on-orbit COS LSF for the G130M and G160M gratings. The results are similar for the NUV gratings, although the effect of the MFWFEs is more moderate for the long-wavelength G285M grating.

Figure 3.8: Limiting Equivalent Width of FUV Medium-Resolution Gratings

Limiting equivalent width as a function of wavelength for 3σ detections of absorption features at a S/N of 10 per pixel at lifetime position 2. Dashed lines represent the full on-orbit LSFs including MFWFEs. Solid lines represent Gaussian LSFs without MFWFEs. The colors correspond to features with intrinsic Doppler parameters **b** = 0 km s^{-1} (black), 10 km s^{-1} (red), 25 km s^{-1} (green), 50 km s^{-1} (blue) and 100 km s^{-1} (magenta).

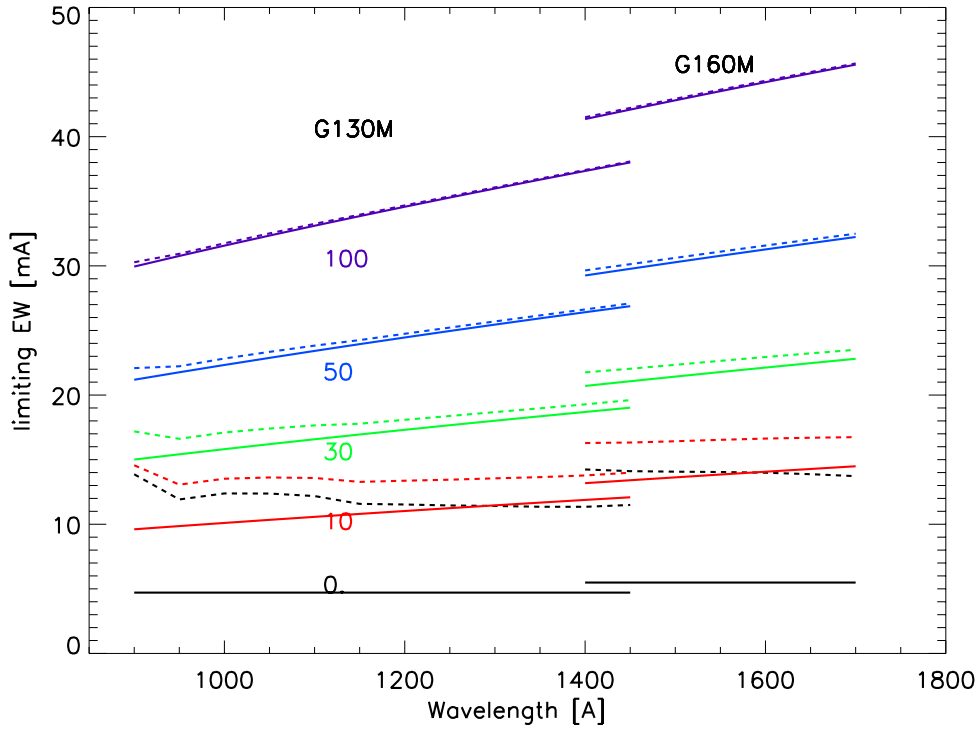

3.3.4 Extended Wings of the COS LSF

The LSF models of Ghavamian et al. (2009) successfully characterize the basic profile and integrated properties of narrow spectral features in COS spectra. However, scientific investigations that depend on characterizing the depth of saturated or nearly-saturated absorption features may require a more careful treatment of the light scattered into the wings of the LSF. To address this concern Kriss (2011) has developed empirical LSF models for the G130M and G160M gratings. These models differ in two ways from the preliminary models discussed above. First, while the preliminary models extend only ±50 pixels from the line center, the new models extend ±100 pixels, which is the full width of the geocoronal Lyman-α line. Second, the new models include scattering due to the micro-roughness of the surface of the primary mirror, an effect that transfers an additional 3% of the light from the center of the line into its extended wings (Figure 3.9). For details, see COS ISR 2011-01. The LSF models computed by Ghavamian et al. (2009), the empirical models of Kriss (2011), and predicted LSFs for the lifetime positions are available on the COS website.

Figure 3.9: Comparison of LSF Models for Medium–Resolution FUV Gratings

Comparison between a simple Gaussian LSF model (red line, FWHM = 6.5 pixels), the LSF profile from Ghavamian et al. (2009) that includes MFWFEs from the **HST** OTA (blue line, calculated at 1200 Å), and the new LSF that includes power-law scattering wings of index –2.25 extending ± 100 pixels from line center (Kriss et al., 2011;black line). In the latter two cases solid lines represent the original lifetime position and the dot-dash lines represent the second lifetime position. Figure based on figure 2 from Kriss (2011).

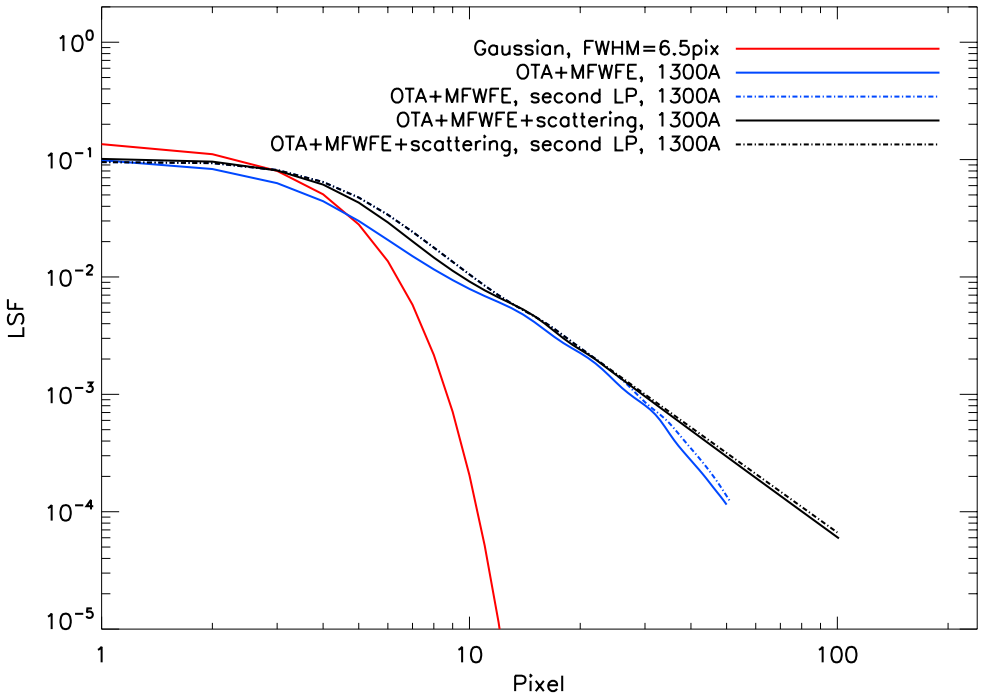

3.3.5 Enclosed Energy of COS LSF

Figure 3.10 shows the fraction of enclosed energy within the LSF, measured from the center of the profile, for both the FUV and NUV channels. The differences between the modeled on-orbit LSFs (MFWFEs included) and the Gaussian LSFs without MFWFEs are apparent in both spectroscopic channels. Though inclusion of the MFWFEs at longer NUV wavelengths widens the FWHM of the on-orbit LSF models only slightly, the wider wings decrease noticeably the spectral purity and the contrast level of the observed spectra.

Figure 3.10: Enclosed Energy Fraction of the COS Line-Spread Function

The enclosed energy fraction of the COS LSF for an unresolved spectral feature as measured from the center of the profile (collapsed along the cross-dispersion direction). The top panel shows a Gaussian with FWHM = 6.5 Å and FUV model profiles with and without scattering due to micro roughness on the surface of the **HST** primary mirror (Kriss 2011). The 1150 Å data (blue) use the G130M grating while the 1450 Å (green) and 1750 Å (red) data use the G160M grating. The solid lines indicate results for the original lifetime position while the dot-dash lines indicate data for the second lifetime position. In the bottom panel, NUV model profiles with and without the effects of the OTA MFWFEs are shown (Ghavamian et al. 2009). The 1700 Å data (blue) use the G185M grating, the 2500 Å data (green) use the G225M grating, and 3200 Å data (red) use the G285M grating.

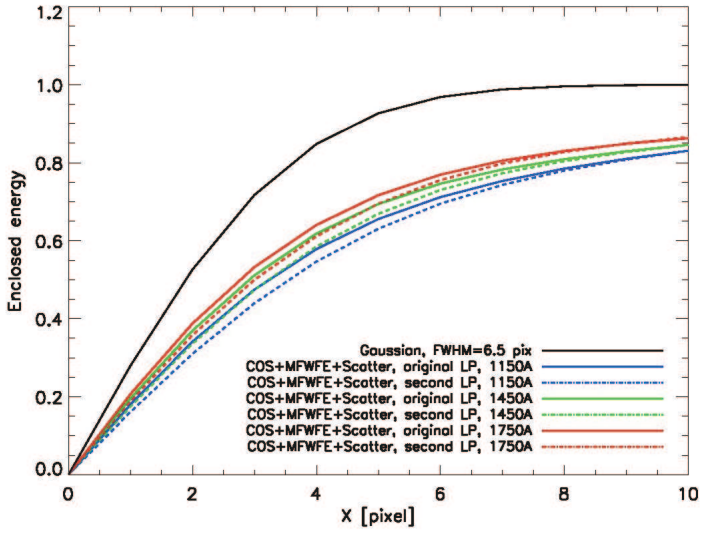

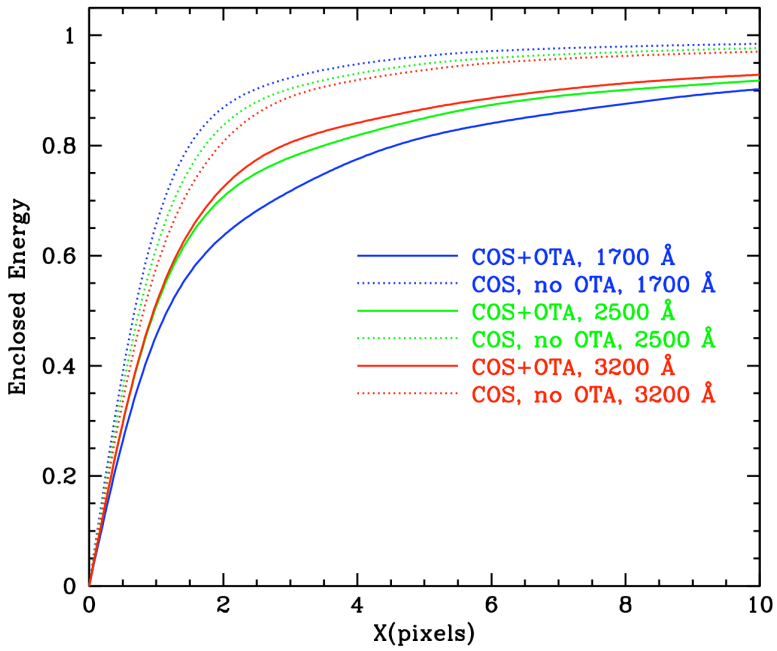

Table 3.2: Distance from Line Center (in Pixels) Versus Enclosed Energy Fraction and Wavelength for the G130M Grating.[1]

Enclosed Energy Fraction	Wavelength (Å)						
	1150	1200	1250	1300	1350	1400	1450
0.90	14.9/15.2	15.0/15.1	15.0/14.9	14.9/15.2	14.8/14.5	14.7/14.2	14.4/14.7
0.95	24.3/24.7	24.4/24.6	24.4/24.3	24.5/24.8	24.4/23.9	24.3/23.3	23.8/24.3
0.99	58.1/58.6	58.3/58.4	58.3/58.0	58.4/58.7	58.3/57.5	58.2/57.1	57.5/58.1

Table 3.3: Distance from Line Center (in Pixels) Versus Enclosed Energy Fraction and Wavelength for the G160M Grating.[2]

Enclosed Energy Fraction	Wavelength (Å)						
	1450	1500	1550	1600	1650	1700	1750
0.90	14.7/14.4	14.6/14.9	14.4/14.2	14.2/14.0	14.0/13.8	13.6/13.7	13.2/13.2
0.95	24.5/24.0	24.3/24.7	24.0/23.8	23.8/23.7	23.5/23.4	23.1/23.1	22.6/22.8
0.99	58.3/57.6	58.1/58.7	57.8/57.4	57.4/57.1	57.0/56.8	56.3/56.4	55.6/55.9

Table 3.4: Distance from Line Center (in Pixels) Versus Enclosed Energy Fraction and Wavelength for the G140L Grating[3].

Enclosed Energy Fraction	Wavelength (Å)											
	1250	1300	1350	1400	1450	1500	1550	1600	1650	1700	1750	1800
0.90	12.1	12.1	12.1	12.1	12.1	12.1	12.0	11.9	11.8	11.7	11.6	11.4
0.95	17.9	18.1	18.2	18.4	18.5	18.6	18.7	18.7	18.7	18.7	18.7	18.7
0.99	30.5	30.7	31.0	31.3	31.6	31.9	32.1	32.4	32.6	32.9	33.2	33.3

Table 3.2, Table 3.3, and Table 3.4 present the enclosed-energy fractions for gratings G130M, G160M, and G140L respectively. The G130M and G160M data include the effects of scattering and are for both the original and the second lifetime position. Information on values for the third lifetime position will be made available in the future, but are not expected to change appreciably. The G140L data are taken from Ghavamian et al. (2009) and are for the original lifetime position. The G140L data do not include the effects of micro-roughness.

1. The values in each cell are from the original lifetime position / second lifetime position.
2. The values in each cell are from the original lifetime position / second lifetime position.
3. The values in each cell are from the original lifetime position.

CHAPTER 4:

Description and Performance of the COS Detectors

In this chapter…

4.1 The FUV XDL Detector

4.1.1 XDL Properties

The COS FUV detector is a windowless cross delay line (XDL) device that is similar to the detectors used on the *Far Ultraviolet Spectroscopic Explorer (FUSE)*. The XDL is a photon-counting micro-channel plate (MCP) detector with two independently-operable segments (FUVA and FUVB). Each segment has an active area of 85 × 10 mm; they are placed end to end and separated by a 9-mm gap. When the locations of detected photons are digitized they are placed into a pair of arrays (one per detector), each 16,384 × 1024 pixels, though the active area of the detector is considerably smaller. Individual pixels span 6 × 24 μm. The long dimension of the array is in the direction of dispersion; increasing pixel number (the detector's *x* axis in user coordinates) corresponds to increasing wavelength. The XDL format is shown schematically in Figure 4.1. Detector parameters are listed in Table 1.2.

The FUV XDL is optimized for the 1150 to 1775 Å bandpass, with a cesium iodide photocathode on the front MCP. The front surfaces of the MCPs are curved with a radius of 826 mm to match the curvature of the focal plane. When photons strike the photocathode they produce photoelectrons that are multiplied by a stack of MCPs. The charge cloud that comes out of the MCP stack, several millimeters in diameter, lands on the delay-line anode. There is one anode for each detector segment, and each anode

has separate traces for the dispersion (x) and cross-dispersion (y) axes. The location of an event on each axis is determined by measuring the relative arrival times of the collected charge pulse at each end of the delay-line anode for that axis. The results of this analog measurement are digitized to 14 bits in x and 10 bits in y. In `TIME-TAG` mode the total charge collected from the event, called the pulse height, is saved as a 5-bit number.

Figure 4.1: The FUV XDL Detector.

This diagram is drawn to scale, and the slight curvature at the corners is also present on the masks of the flight detectors. Wavelength increases in the direction of the increasing X coordinate. The red and blue dots show the approximate locations of the stim pulses on each segment. The numbers in parentheses show the pixel coordinates at the corner of the segment's digitized area; the two digitized areas overlap in the region of the inter-segment gap.

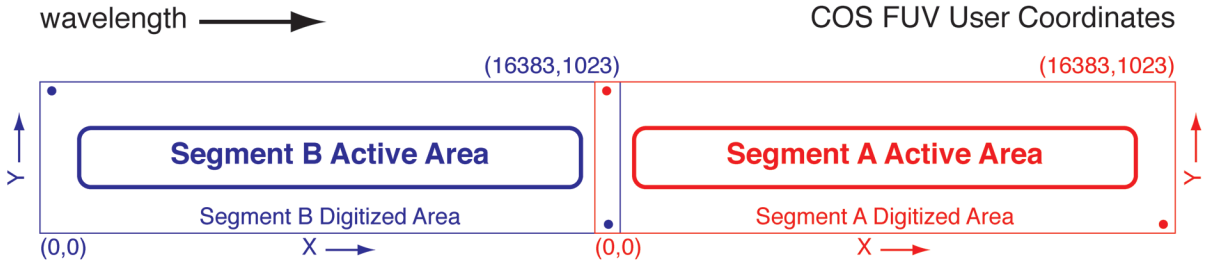

The detector electronics generate pulses that emulate counts located near the corners of the anode, outside the active area of the MCPs. These "stim pulses" (see Section 4.1.6) provide a means of tracking and correcting thermal distortions.

The XDL's quantum efficiency is improved by the presence of a series of wires, called the quantum-efficiency (QE) grid, placed above the detector (i.e., in the light path). These wires create shadows in the spectrum that are flagged and corrected by **calcos** during data reduction. The XDL also includes an ion-repeller grid that reduces the background rate by preventing low-energy thermal ions from entering the open-faced detector. It acts as a 95% transmission neutral-density filter.

4.1.2 XDL Spectrum Response

COS is considerably more sensitive than STIS and earlier-generation *HST* instruments at comparable spectral resolutions in the FUV. Effective areas for the COS FUV gratings are shown in Figure 5.1. The maximum count rates for the FUV detector are listed in Table 10.1. The time-dependent changes in the sensitivity of the COS FUV channel are discussed in Section 5.1.5.

4.1.3 XDL Dark Rate

The XDL detector segments have extremely low intrinsic dark rates, on the order of 10^{-6} count/s/pixel; see Section 7.4.1. Background counts can also be caused be external events, such as proximity to the South Atlantic Anomaly (SAA). **Calcos** estimates the dark rate by measuring the counts in an unilluminated region on the detector and subtracting this from the spectrum during processing. Each segment has a distinct dark current that varies with time and may be correlated with the Solar Cycle (see Figure 4.2). The dark rates vary with time, so observers, particularly those with faint, background-limited targets, should consider how the changing dark rates may affect their orbital estimates. In particular, some exposures experience sharp increases in the dark rate over short periods of time. The COS spectroscopic ETC estimates the dark rate for a typical exposure and segment based on the value that encompasses 95% of all observations. For the 24.1 ETC version, the dark rate for both segments is around 4.0×10^{-6} counts/s/pixel for science exposures.

Figure 4.2: COS FUV Dark Rates and the Solar Cycle

Upper panel: Global dark rate of the FUVA detector as a function of time. The orange curve shows the corresponding Solar Radio Emission, which is a proxy for stellar activity, a smoothed version of which is shown in red. The gap in data corresponds to the shutdown of COS due to a detector anamoly on April 30, 2012. Lower panel: This is the same as the upper panel, but for the COS FUVB detector.

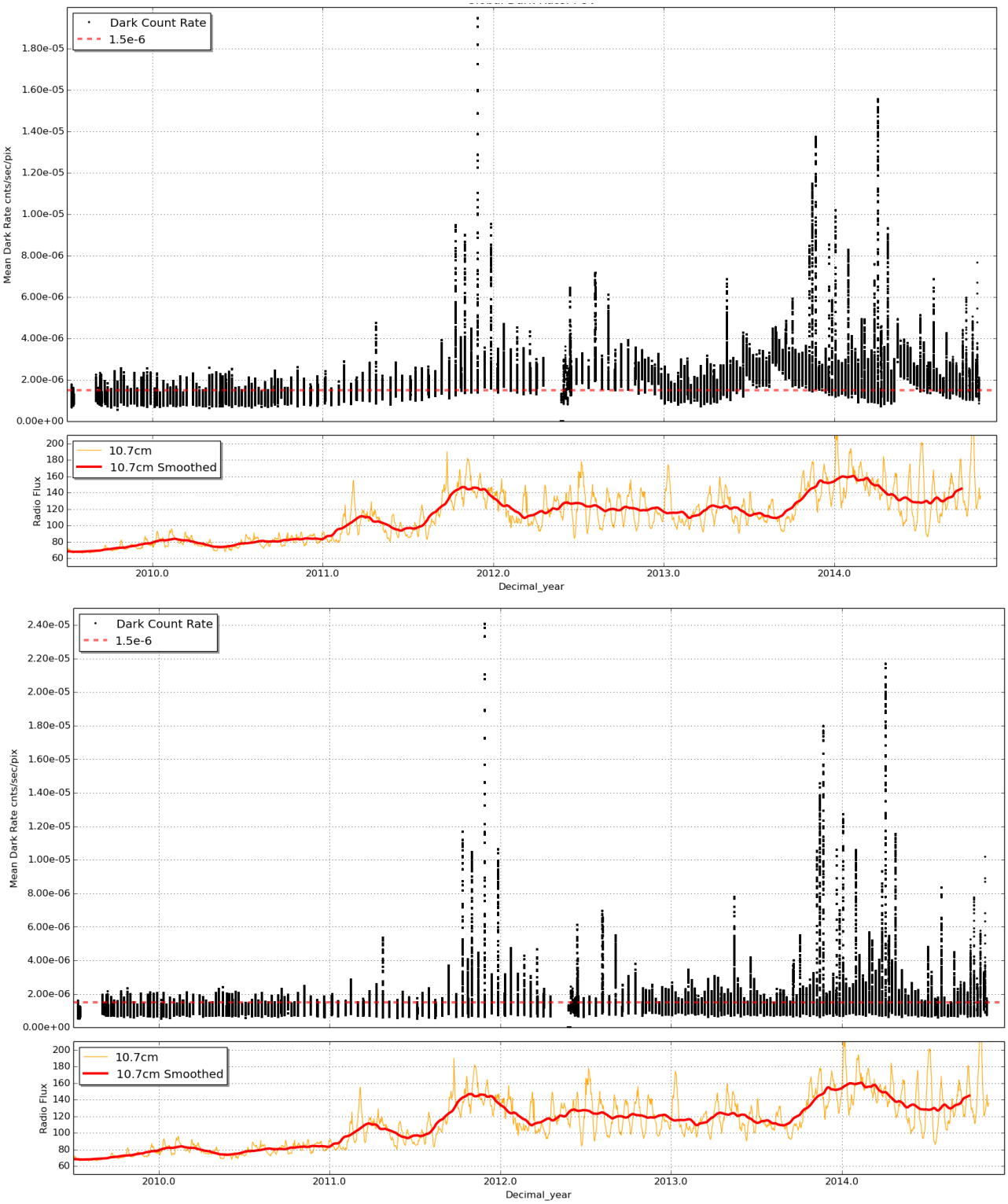

4.1.4 XDL Read-out Format

The FUV channel creates one spectral stripe on each detector segment for the science spectrum and another for the wavelength-calibration spectrum. The aperture not being used for science may also create a spectrum. If so, it will appear below the science spectrum if the PSA is being used, and above it if the target is in the BOA. Since the non-target aperture is usually observing blank sky, it will normally be visible only if airglow lines fall in the spectral range. Figure 4.3 shows an example of an FUV spectrum obtained on orbit with Segment B. The upper panel shows the two-dimensional image; the lower panel shows the extracted PSA spectrum. Note the difference in the *x* and *y* axis scales in the upper figure.

Although the gap between the two FUV detector segments prevents the recording of an uninterrupted spectrum, it can be made useful. For example, when the G140L grating is used with a central wavelength of 1280 Å, the bright Lyman-α airglow feature falls in the gap. For suggestions on spanning the gap, see Section 5.5.

Should a high count rate on one of the segments be a safety concern, the detector can be operated in single-segment mode, whereby the high voltage on one segment is lowered to a value that prevents it from detecting light. This adjustment is required for central wavelength 1105 Å on G140L, since the zero-order light falling on Segment B in that mode is too bright.

Figure 4.3: Example of a COS FUV Spectrum

Upper panel: A stellar spectrum obtained with Segment B of the COS FUV detector using the G130M grating at a central wavelength of 1309 Å. The wavelength calibration (WCA) spectrum is on top, and the stellar spectrum (PSA) is below. Both the PSA and BOA are open to the sky when the COS shutter is open, so Lyman-α airglow through the BOA is also visible below the PSA. The **HST** +V2 and +V3 axes are over plotted. Note that the size of the active area of the MCP is smaller than the overall digitized area (16,384 × 1024). Lower panel: the extracted stellar spectrum from the PSA.

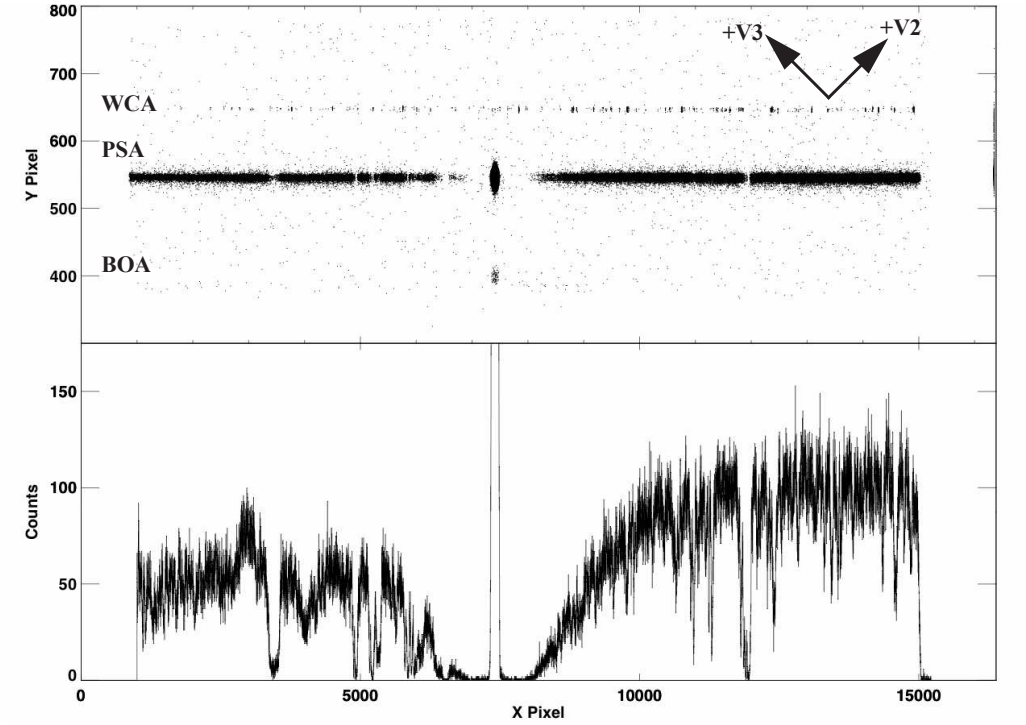

4.1.5 Non-linear Photon Counting Effects (Dead Time)

The electronics that control the COS detectors have a finite response time t, called the dead time, that limits the rate at which photon events can be processed. If two photons arrive within time t the second photon will not be processed. For the FUV channel three factors limit the detected count rate. The first is the Fast Event Counter (FEC) for each segment, which has a dead time of 300 ns. The FEC dead time matters only at count rates well above what is usable, introducing a 1% error at a count rate of 33,500 per segment per second.

The second factor is the time required to digitize a detected event. For a given true count rate C, the detected count rate D is

$$D = \frac{C}{1 + C \cdot t}$$

where t is the dead-time constant. For the COS FUV detector t = 7.4 μs, so the apparent count rate deviates from the true count rate by 1% when C = 1350 counts/s and by 10% when C = 15,000 counts/s. Note that, when the effect is near the 10% level, then the FUV detector is near its global count-rate limit (see Table 10.1), so non-linear effects are relatively small.

Finally, the Detector Interface Board (DIB) combines the count streams from the two FUV segments and writes them to a single data buffer. The DIB is limited to processing about 250,000 count/s in `ACCUM` mode and only 30,000 count/s in `TIME-TAG` mode (the highest rate allowed for `TIME-TAG` mode). The DIB interrogates the A and B segments alternately; because of this a count rate that is high in one segment, but not the other, could cause a loss of data from both segments. Tests have shown that the DIB is lossless up to a combined count rate for both segments of 20,000 count/s; the loss is 100 count/s at a rate of 40,000 count/s. Thus, this effect is less than 0.3% at the highest allowable rates. Furthermore, information in the engineering data characterizes this effect.

Corrections for dead-time effects are made in the **calcos** pipeline, but they are not included in the ETC, which will over-predict count rates for bright targets.

4.1.6 Stim Pulses

The signals from the XDL anodes are processed by Time-to-Digital Converters (TDCs). Each TDC contains a circuit that produces two alternating, periodic, negative-polarity pulses that are capacitively coupled to both ends of the delay-line anode. These stim pulses emulate counts located near the corners of the anode, beyond

the active area of the detector. Stim pulses provide a means for **calcos** to correct the temperature-dependent shift and stretch of the image during an exposure, and they provide a first-order check on the dead-time correction. They are recorded in both TIME-TAG and ACCUM modes, and appear in the data files.

Four stim-pulse rates are used: 0 (i.e., off), 2, 30, and 2000 Hz per segment. These rates, which are only approximate, are *not* user selectable. Exposures longer than 100 s will use the 2 Hz rate, those between 10 and 100 s use 30 Hz, and those shorter than 10 s use 2000 Hz.

4.1.7 Pulse-height Distributions

An ultraviolet photon incident on the front MCP of the XDL detector creates a shower of electrons, from which the detector electronics calculate the x and y coordinates and the total charge, or pulse height. The number of electrons created by each input photon, or "gain" of the MCPs, depends on the high voltage across the MCPs, the local properties of the MCPs at that location, and the high voltage across the plates. *It is not a measure of the energy of the incident photon*. A histogram of pulse heights for multiple events is called a pulse-height distribution (PHD).

The PHD from photon events on a particular region of the detector typically shows a peaked distribution, which can be characterized by the modal gain (the location of the peak) and its width. Background events, both internal to the detector and induced by cosmic-rays, tend to have a falling exponential PHD, with most events having the lowest and highest pulse heights. On-board charge-threshold discriminators filter out very large and small pulses to reduce the background and improve the signal-to-noise ratio. In TIME-TAG mode the pulse height is recorded for each detected photon event. By rejecting outlier pulse-height events **calcos** further reduces the background rate. In ACCUM mode only the integrated pulse-height distribution is recorded (Section 5.2.2), so pulse-height filtering is not possible.

Figure 4.4: Spectra Showing the Effects of Gain Sag on FUV Detector Segment B

Spectra (G160M/1623/FP-POS=4) of a target observed five times over 19 months: from top to bottom, September 2009, June 2010, September 2010, January 2011, and May 2011. The blue curve includes only photon events with pulse heights in the range 4–30; the red curve includes pulse heights 2–30. The spectral features near pixels 7200 and 9011 are not astrophysical, but represent the effect of gain sag on regions of the detector illuminated by Lyman-α in other observing modes. These features become more pronounced with time until March 2011, when the Segment B high voltage was raised.

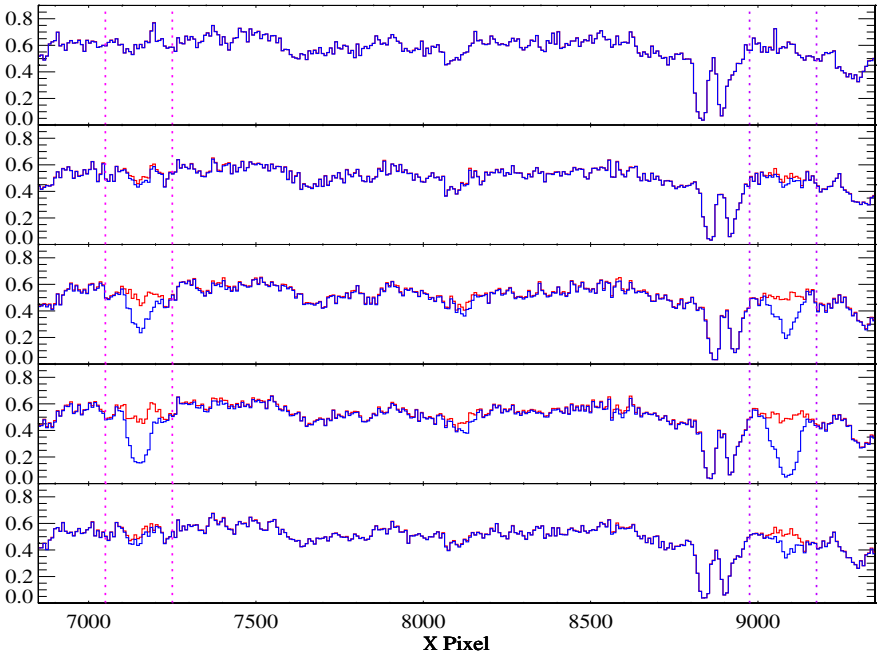

Gain Sag

Prolonged exposure to light causes the number of electrons per incident photon to decrease, a phenomenon known as "gain sag." As a result, the peak of the PHD in each region of the detector shifts to lower values as the total (time-integrated) illumination of that region increases. As long as all pulse heights are above the minimum threshold imposed by the onboard electronics and **calcos**, there is no loss in sensitivity. However, if the gain drops low enough that the pulse heights of the photon events from the target fall below the threshold, these events are discarded and the apparent throughput decreases. The amount of gain sag increases with the total amount of previous illumination at that position on the detector, so gain sag appears first in regions of the detector that are illuminated by bright airglow lines, but eventually affects the entire spectrum. Figure 4.4 shows the effect of gain sag on Segment B of the COS FUV detector. These data were obtained using the grating setting G160M/1623/FP-POS=4. A portion of the extracted spectrum from the same object taken at five different times is shown. The blue curve was constructed using only photon events with pulse heights in the range 4–30, while the red curve includes pulse heights of 2–30. The current pulse height limits used by the COS pipeline are 2-23. Two regions that suffer the most serious gain sag are marked: the region near pixel 7200 is illuminated by Lyman-α when grating setting G130M/1309/FP-POS=3 is used, and the region near pixel 9100 is illuminated by Lyman-α when the setting is G130M/1291/FP-POS=3. Initially, the pulse heights were well above either threshold, so the blue and red curves are indistinguishable. As time progressed all of

the pulse heights decreased. However, the two Lyman-α regions decreased faster, causing the blue spectra to exhibit spurious absorption features. This trend continued until the Segment B high voltage was raised in March 2011. The bottom plot shows that increasing the voltage has recovered most of the lost gain.

More details on the gain sag can be found in the *COS Data Handbook* and COS ISR 2011-05.

Detector Walk

As the pulse height of a photon event decreases the detector electronics begin to systematically miscalculate its position. On the COS FUV detector this effect, called detector walk, occurs in both *x* and *y*, but is much larger in the *y* (cross-dispersion) direction. The shift is approximately 0.5 pixel per pulse-height bin, which means that the entire spectrum may be shifted by several pixels, and the regions with the lowest gain may be noticeably shifted relative to the rest of the spectrum (Figure 4.5). **Calcos** applies a *y*-walk correction to `TIME-TAG` data, but the current algorithm does not completely correct the data; future versions of **calcos** will improve the correction. In addition, the walk is uncorrected in `ACCUM` mode, where no pulse-height information is available. The spectral extraction should remain unaffected, because the extraction regions are large enough to include the misplaced counts.

Figure 4.5: Y-Walk on the FUV Detector

Two-dimensional spectra, uncorrected for walk, taken in September 2009 (left) and December 2010 (right). The entire spectrum has shifted down by several pixels due to gain sag and detector walk. A larger shift is seen in the region near X = 9100, where the gain sag is greater due to the geocoronal Lyman-α feature that falls there when the G130M/1291 with the FP-POS=3 setting is used.

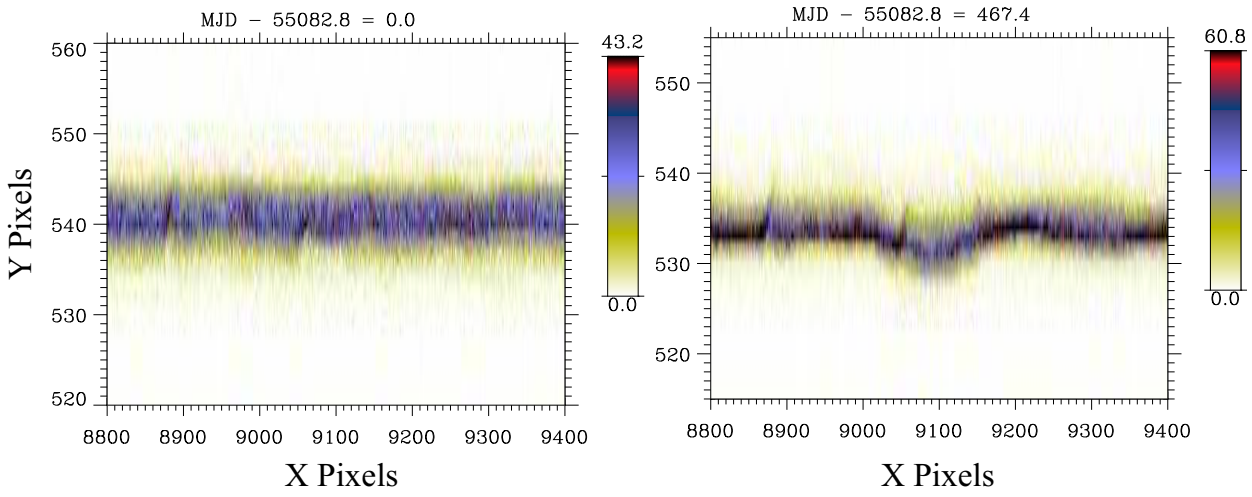

Mitigation Strategies

A range of strategies have been used to minimize the effects of gain sag and detector walk on the science data. Several of these are modifications to **calcos**, which means that previously collected data can be improved by reprocessing. Others involve changes to the on-orbit settings, and thus only affect exposures taken after the changes are made.

Calcos Changes

*Pulse Height Threshold*ing: At present, the lower pulse height threshold used by **calcos** when processing `TIME-TAG` data has been decreased to near its minimum value (2). This ensures that as few events as possible are lost due to low gain, but it will have the effect of slightly increasing the detector background. We hope to eventually implement time- and position-dependent pulse height thresholds in **calcos**.

Walk Correction: **Calcos** applies a walk correction to `TIME-TAG` events. The pulse height and measured position of an event are used to apply a correction factor to its position. Although the walk correction is not time-dependent, it may be modified as we learn more about the walk properties of the detector.

Gain Sag Table: Low-gain pixels are flagged by **calcos** and excluded when combining spectra taken at multiple `FP-POS` positions.

Onboard Changes

Voltage Adjustments: In an effort to keep the MCP gain in the spectral regions within the range that gives acceptable position determination, while simultaneously minimizing gain sag, the high voltage on each segment has been adjusted numerous times since launch. The voltages used for a particular exposure can be found in the file headers, but the effects should be transparent to the user, since any effects on the data will be handled by **calcos**. More details on the high voltage changes are given in the *COS Data Handbook*.

Change in Lifetime Position: After years of collecting exposures—and tens of thousands of counts per pixel in the most exposed areas—the gain at certain areas on the MCPs drops so much that none of the techniques described above can return the detector to an acceptable level of performance. Once that occurs the only way to obtain satisfactory data is to move the spectra to a new location on the detector, which can be accomplished by adjusting the position of the aperture and the pointing of *HST*. This moves the spectra to a pristine region on the detector which defines a new lifetime position. COS has been operated at a total of three lifetime positions; Cycle 24 will use the third lifetime position. Because the optical path is slightly different for each lifetime position the properties of the spectrograph are also slightly different. Thus, the resolving power, throughput, flat field, etc. may differ at different lifetime positions. A keyword in the header of the data files tells **calcos** which lifetime position was used, and reference files appropriate to that position are applied when processing the data.

The first change in lifetime position, to lifetime position 2, was made on July 23, 2012. The second change to lifetime position was to lifetime position 3, which occurred on February 9, 2015. At this time, multiple LPs are in use simultaneously, with both the LP and high voltage chosen to optimize performance on the grating and central wavelength of each exposure. The position and voltage values are determined by STScI based on the performance of the detector, so they cannot be specified by general observers. The appropriate lifetime position is determined by STScI based on the performance of the detector, so it cannot be specified by the observer.

Further adjustments to the lifetime position will be made as necessary. Details on these new calibrations are reported in ISRs that are available on the COS website. The *COS Data Handbook* and periodic STANs will also document these changes.

4.1.8 Spatial Variation of the Dark Rate

The dark rate varies spatially over the FUV detector. Figure 4.6 shows the sum of approximately 80,000 s of dark exposures taken over a five-month period in 2011. With the standard lower pulse-height threshold of 2, Segment A is relatively featureless away from the edges of the active area, except for a few small spots with a higher rate. Segment B shows several large regions with a slightly elevated rate; they are enhanced by less than a factor of two over the quieter regions.

For most `TIME-TAG` observations these features will have a negligible effect on the extracted spectra, because the variation is small and the overall rate is low (see Table 7.1). In `ACCUM` mode, where no lower pulse-height threshold is used, additional features appear. `ACCUM` mode is used only for bright targets, so these features should constitute a negligible fraction of the total counts.

Figure 4.6: FUV Detector Dark Features

Summed dark exposures showing spatial variations on the detector. The approximate position of the G130M extraction window for the original lifetime position is marked in blue, and a sum of the dark counts in this extraction window as a function of x pixel is shown in red below the image. A sum as a function of y pixel is shown on the right side of the figure. Segment A is nearly featureless aside from a few small hot spots, while Segment B shows larger variations. Both segments show a slightly lower dark rate in the region where the most counts have fallen. This is due to gain sag. The data are binned by 8 pixels in each dimension for display purposes.

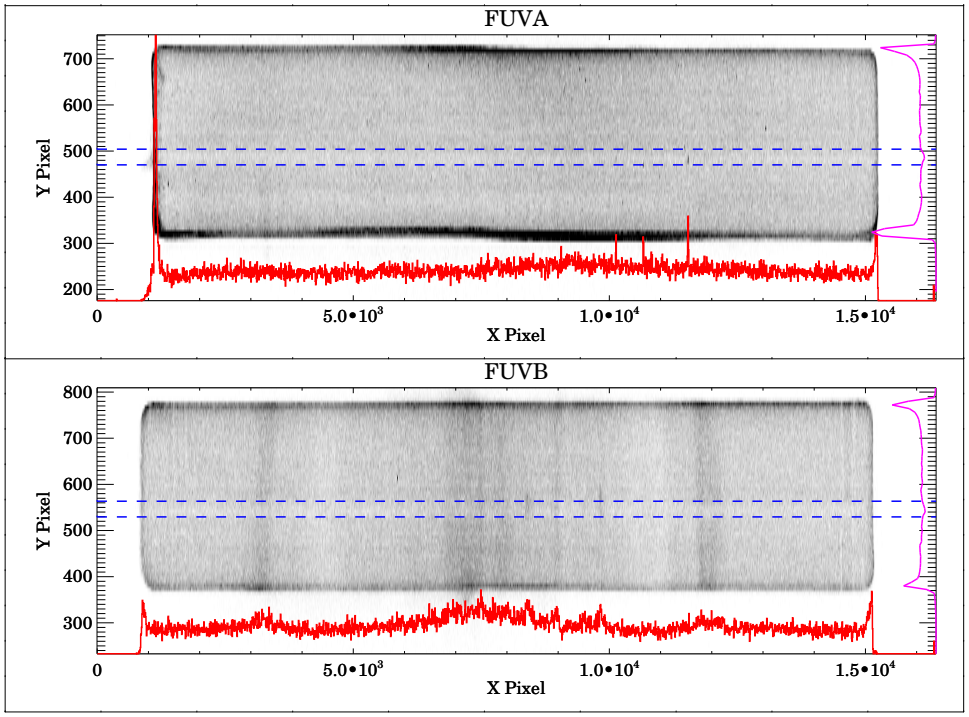

4.2 The NUV MAMA Detector

4.2.1 MAMA Properties

The COS NUV detector is a Multi-Anode Micro-channel Array (MAMA) identical to that used for the NUV in STIS. (In fact, it is the STIS NUV flight spare.) The COS MAMA has a semi-transparent cesium telluride photocathode on a magnesium fluoride window and is sensitive to photons with wavelengths from 1150 to 3200 Å. The NUV optics focus light through the MgF_2 window onto the Cs_2Te photocathode. A photoelectron generated by the photocathode then falls onto a curved-channel micro-channel plate (MCP), which generates a cloud of electrons. The active area of the anode array is 25.6 mm square and is divided into 1024 × 1024 pixels on 25 μm centers. The spatial resolution at 2500 Å is 35 μm FWHM. Detector parameters are listed in Table 1.2.

4.2.2 MAMA Spectrum Response

The inherent spectral response of the COS NUV MAMA is essentially identical to that of the STIS NUV MAMA. However, the overall optical train of COS differs from that of STIS, so the throughputs are different (Figure 5.2). The maximum count rates for the NUV detector are listed in Table 10.1.

4.2.3 MAMA Dark Rate

A sum of dark exposures taken away from the SAA shows a relatively featureless background, with slight enhancements at two of the corners (Figure 4.7). Although the early dark rate was lower than had been measured on the ground, the rate has steadily increased since launch, as shown in Figure 4.8. For version 24.1 of the COS ETC a value of 8.9 x 10^{-4} counts/s/pixel was adopted, encompassing 95% of observations through September 2015.

Figure 4.7: Spatial Variation in the NUV Dark Rate

Summed dark exposures show the uniformity of the NUV dark rate across the detector. There is very little variation across the detector, with only a small depression in the dark rate in the lower left corner. The cumulative histograms show the collapsed rows (above) and columns (right).

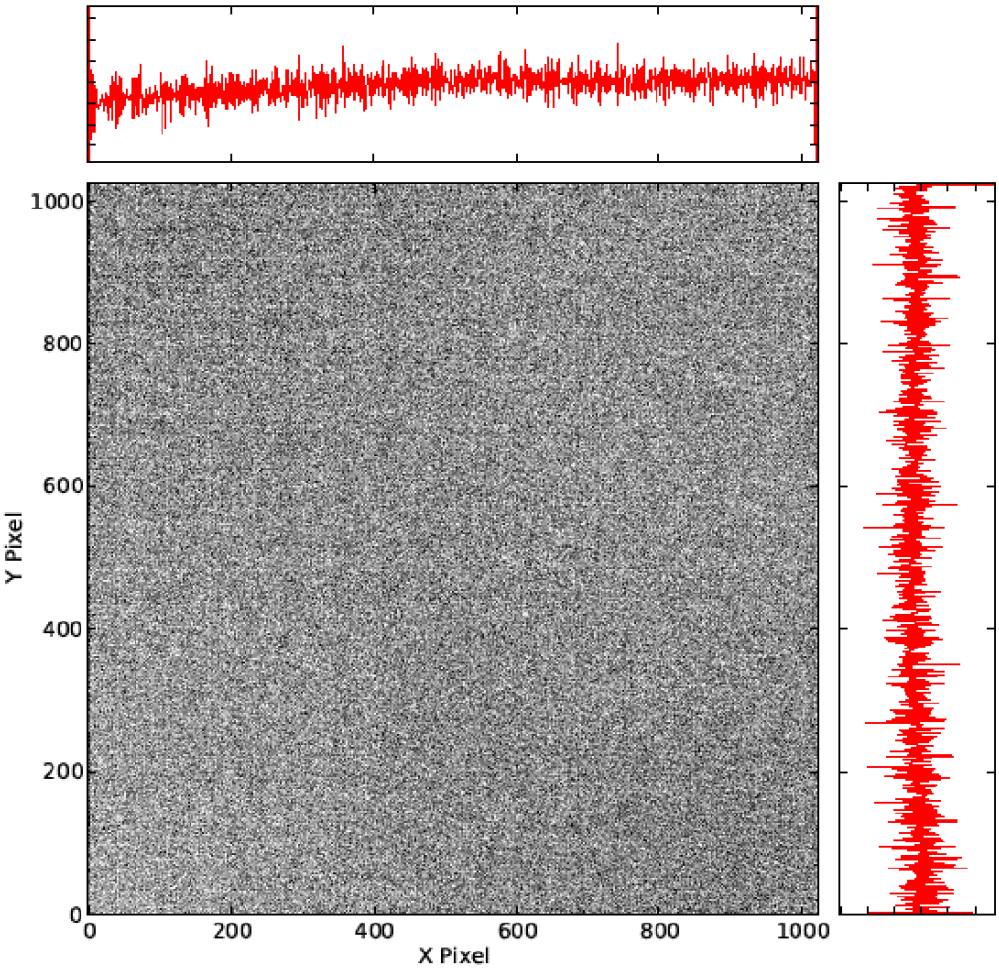

Figure 4.8: NUV Detector Dark Rate versus Time

Measured dark rate as a function of time through August 2014. When the periods affected by the SAA are excluded, the dark rate increased by roughly 200 count/s per year until 2013, when the trend flattened. Neither the increase in the dark rate, nor the increase in the scatter that is seen in the later observations, are understood. The middle panel shows the radio flux of the sun for comparison. The lower panel shows the detector temperature (LNTUBET). This demonstrates the temperature dependence of the dark rate. The two observations of exceptionally low dark rate at 2012.35 are due to a much lower than normal temperature caused by the shut-off of the FUV detector.

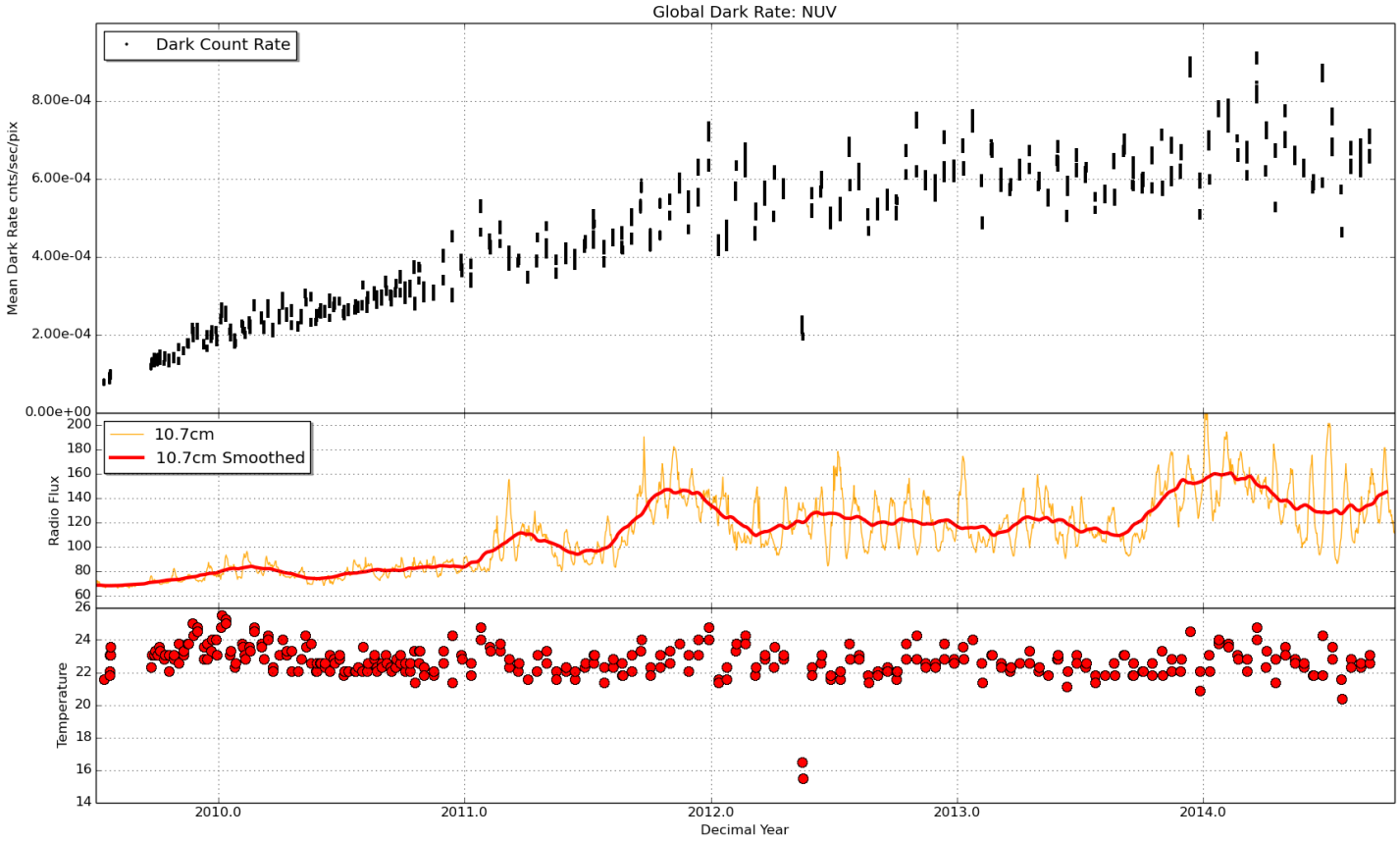

Figure 4.9: Example of a COS NUV Spectrum.
A COS NUV spectrum obtained in TIME-TAG mode with FLASH=YES. The stellar spectrum (labeled PSA) is on the bottom, and the wavelength-calibration spectrum (labeled WCA) on the top; each has three stripes. From bottom to top, these stripes are designated A, B, and C, as illustrated. Wavelength increases to the right and toward the top of the detector. The **HST** +V2 and +V3 axes are also shown. The SHORT, MEDIUM, and LONG designations are used in Phase II with the ACQ/PEAKXD command and the STRIPE optional parameter.

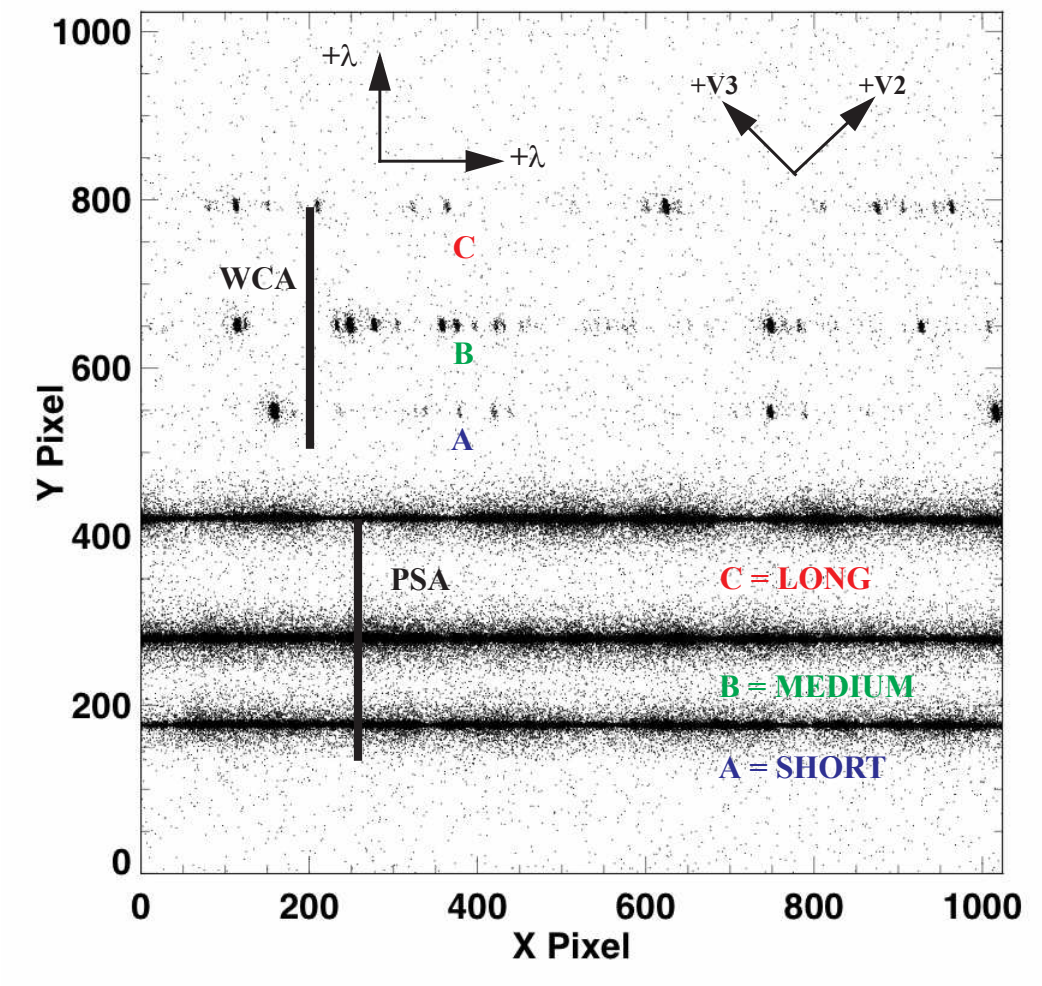

4.2.4 MAMA Read-Out Format

The NUV channel creates six spectral stripes on the MAMA detector, three for the science data and three for the wavelength-calibration data. Stripes are separated by 94 to 143 pixels (2.1 to 3.3 arcsec), center to center, in the cross-dispersion direction. The NUV detector is read out as a 1024 × 1024 array, but in all other respects the data are handled in the same way as for the FUV detector. No pulse-height information is provided for MAMA data. An NUV spectrum obtained in `TAGFLASH` mode is shown in Figure 4.9.

Figure 4.10: Model LSFs for the COS NUV Channel
LSFs including the MFWFEs are plotted as solid lines, those without as dotted lines.

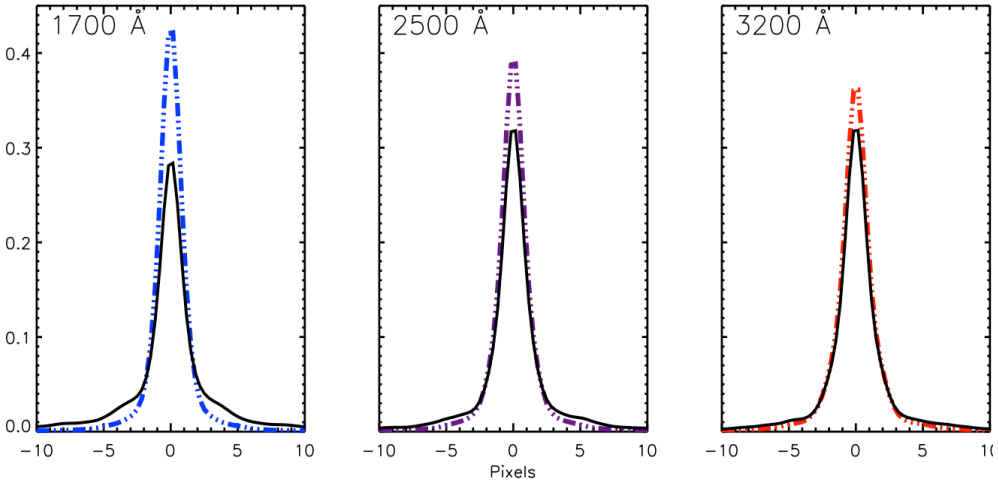

4.2.5 MAMA Dead Time

The dead time for the COS NUV MAMA is 280 ns, the same as for the STIS NUV MAMA. The 1% level of non-linearity is reached for $C = 36{,}000$ count/s. Corrections for dead-time effects are made in the **calcos** pipeline, but they are not included in the ETC, which will over-predict count rates for bright targets.

4.2.6 Non-Gaussian Wings in the MAMA PSF

While most NUV observations should be minimally affected by the mid-frequency wavefront errors (MFWFEs) discussed in Section 3.3, they will reflect the point-spread function of the COS MAMA detector, which exhibits faint, extended wings that are unrelated to the telescope optics. While the telescope-induced wings weaken as wavelength increases, the detector wings become stronger with increasing wavelength. Figure 4.10 shows model NUV detector LSFs with and without the MFWFEs at various wavelengths. Beyond 2500 Å, the detector wings dominate.

CHAPTER 5:

Spectroscopy with COS

In this chapter…

5.1 The Capabilities of COS

COS has two detectors and seven diffraction gratings (three for FUV, four for NUV), which enable high-sensitivity spectroscopy at low and moderate resolution across the FUV and NUV bands. The bandpass and resolution of each grating are presented in Table 5.1. In addition to the standard G130M central wavelengths, the first two rows of Table 5.1, give the bandpass and resolution for the 1055/1096 and 1222 central wavelengths respectively.

For each exposure the observer selects a detector (FUV or NUV), a grating, a central wavelength, an `FP-POS` setting, one of the two apertures (PSA or BOA), and a data-taking mode (`TIME-TAG` or `ACCUM`). Chapter 13 provides detailed specifications for each grating and aperture. Note that the two channels cannot be used simultaneously as the NUV channel is fed by the NCM1 mirror on the FUV optics select mechanism (OSM1). As of this cycle, FUV science observations with the BOA aperture are considered "available-but-unsupported" (See Section 2.4).

Table 5.1: COS Grating Parameters

Grating	Approximate Wavelength Range (Å)	Bandpass per Exposure and FUV Gap[1] (Å)	Inferred PSA Resolving Power $R = \lambda$ / FWHM[2]	Approximate BOA Resolving Power	Dispersion (mÅ pixel^{-1})
FUV Channel					
G130M	900 – 1236	295 / 16	up to ~11,500[3]	—	9.97
	1065 – 1365	296 / 15.7	10,000 – 15,000[3]	—	9.97
	1150 – 1450	292 / 14.3	16,000 – 20,000	7600[4] / 9200[5]	9.97
G160M	1405 – 1775	360 / 18.1	16,000 – 21,000	4400[4]	12.23
G140L	< 900 – 2150	> 1150 / 112	1500 – 4000	1100[4]	80.3
NUV Channel					
G185M	1700 – 2100	3 × 35	16,000 – 20,000	3500	37
G225M	2100 – 2500	3 × 35	20,000 – 24,000	4600	33
G285M	2500 – 3200	3 × 41	20,000 – 24,000	5000	40
G230L	1650 – 3200[6]	(1 or 2) × 398	2100 – 3900	500	390

1. Width of gap between FUV detector segments; see Section 5.5.
2. Empirically-determined FWHM of the LSF, which is not Gaussian. *R* increases approximately linearly with wavelength.
3. *R* falls with increasing wavelength. *R* ~ 8500 – 11,500 between 940 and 1080 Å
4. Lifetime position 1.
5. Lifetime position 2.
6. Some shorter wavelengths are recorded in second-order light. They are listed in Table 5.4.

5.1.1 First-Order Sensitivity

COS is considerably more sensitive than STIS and earlier-generation *HST* instruments at comparable spectral resolutions, particularly in the far ultraviolet. Effective areas for targets observed through the PSA are shown in Figure 5.1, Figure 5.2, and Figure 5.3. Note that the COS sensitivity changes with time (Section 5.1.5), so the plots and tables in this handbook are based on predictions for the middle of Cycle 23 (April 2016). Please consult the COS website for updated information.

While the figures and tables in this handbook can be used to estimate count rates and exposure times, we recommend the use of the COS ETC in all cases, because it properly computes instrument throughput, accounts for detector and astronomical backgrounds, and checks for violations of local and global count-rate limits.

Figure 5.1: Effective Areas for the FUV Channel through the PSA

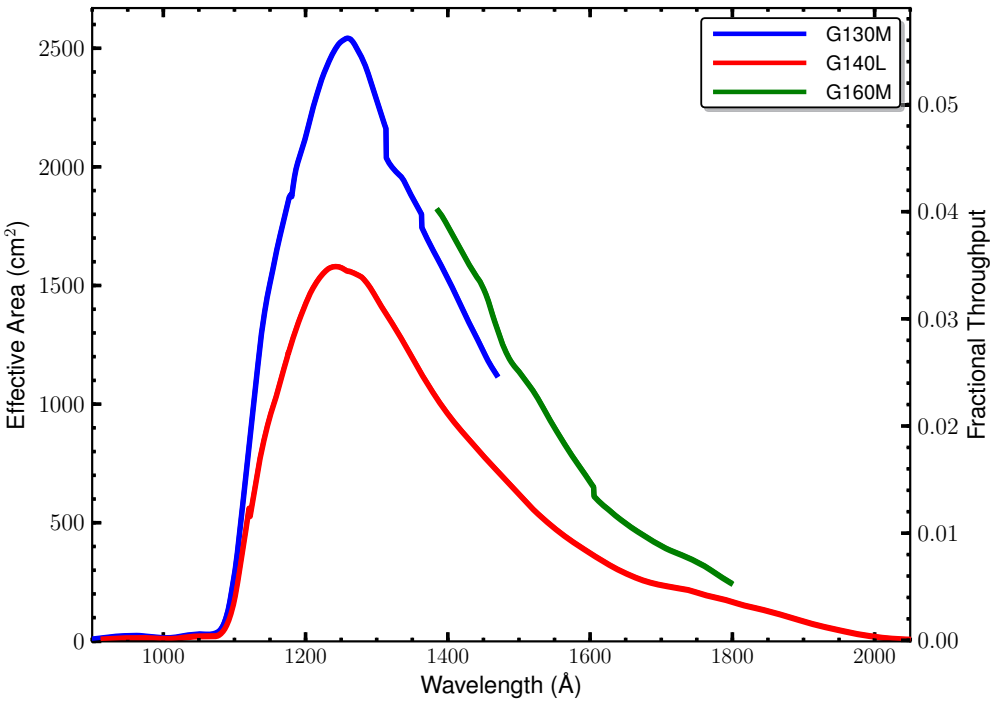

Figure 5.2: Effective Areas for the NUV Channel through the PSA

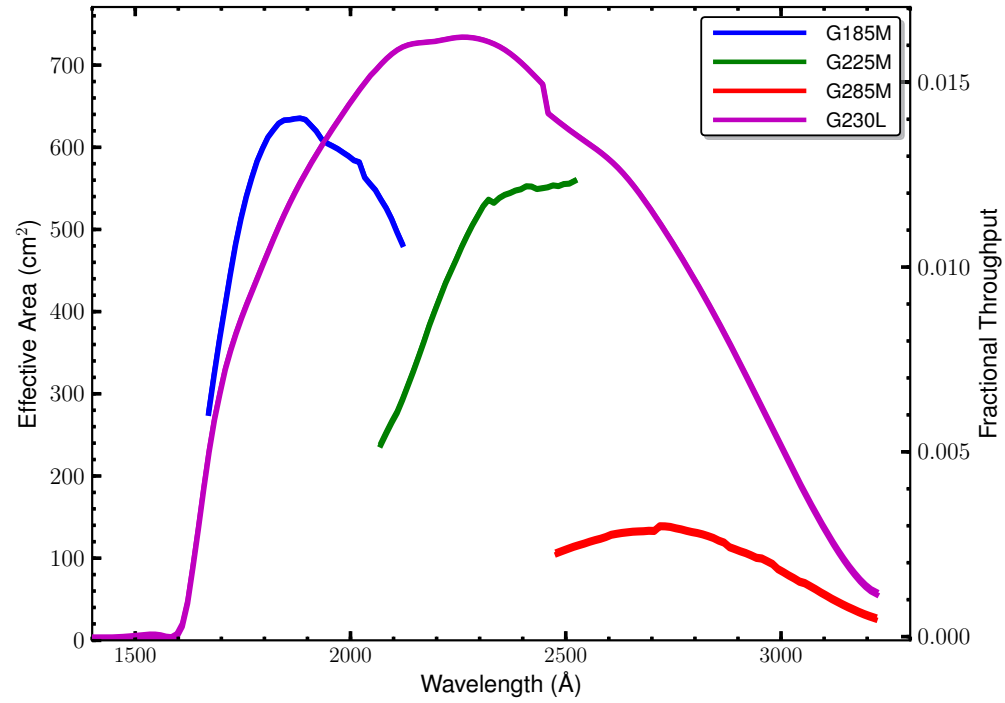

Figure 5.3: Effective Area at Wavelengths below 1400 Å

The effective areas of the various G130M central-wavelength settings are compared with those of G140L and STIS. Effective areas are not well characterized below 920 Å.

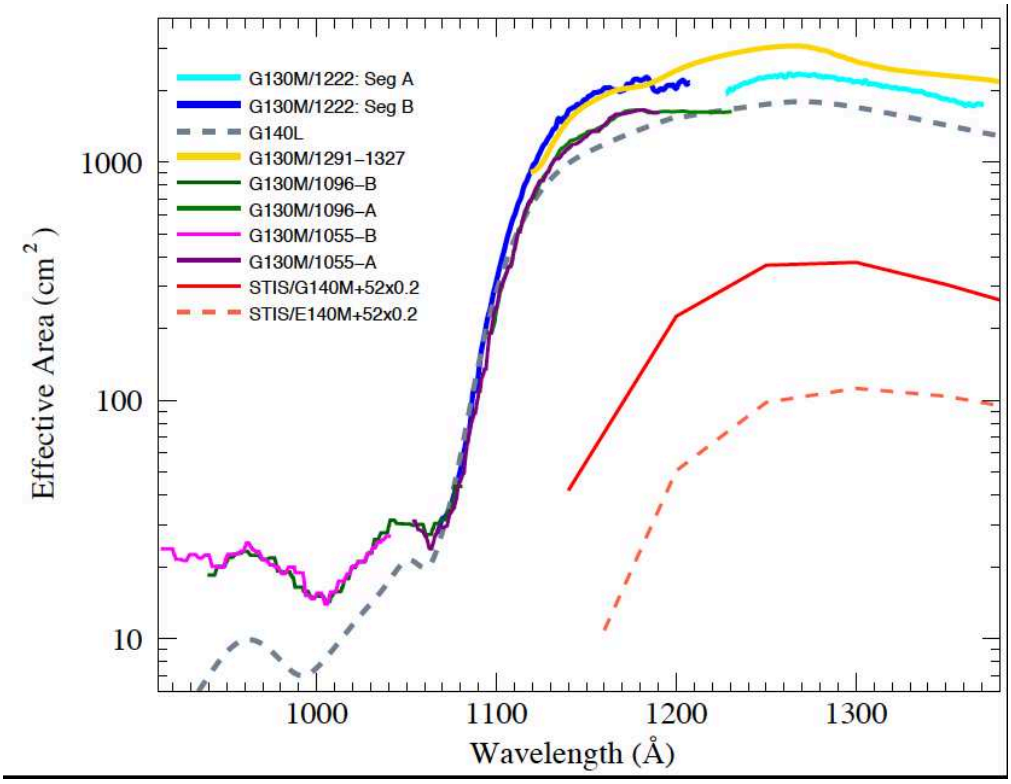

5.1.2 Sensitivity below 1150 Å

Figure 5.3 compares the effective areas of the G130M and G140L gratings at the short-wavelength end of the COS bandpass. From this figure we can draw two fundamental conclusions. First, COS can obtain useful spectra at wavelengths between 900 and 1150 Å. Second, the contrast between the throughputs at 1070 and 1150 Å is roughly a factor of 100.

When G140L is used with `CENWAVE=1280` wavelengths as long as 1200 Å can fall on Segment B. For many targets the count rate at 1150 Å will exceed the local bright limit, while the count rate at shorter wavelengths is perfectly safe. Consequently, turning Segment A off and using `FP-POS=4` is the recommended approach for observing bright objects below 1150 Å with the G140L grating.

When grating G130M is used with `CENWAVE=1055` Segment B records wavelengths shortward of ~1050 Å, depending on the `FP-POS` setting employed (Section 13.3). Using this grating mode with Segment A turned off further reduces the danger of high count rates at longer wavelengths. Special configurations to allow proper wavelength calibration must be used (see Section 5.7.4). Note that both the sensitivity and resolving power (Section 5.1.4) of G130M are greater than those of G140L in this wavelength range.

The Segment B sensitivity for the G140L/1280 setting changes by a factor of 100 between the wavelengths of 1070 Å and 1150 Å, so the flux vs. wavelength calibration is extremely sensitive to small misalignments in the wavelength scale. This is complicated by the absence of usable calibration lamp lines on Segment B for this

setting (see Section 5.7.4). Therefore, even small wavelength misalignments will lead to sizable artifacts in the extracted flux for the calibrated spectra. The flux and wavelength calibrations should be used with caution when interpreting the default pipeline products.

5.1.3 Second-Order Sensitivity

Because the MAMA detector is sensitive to wavelengths as short as 1150 Å, NUV spectra longward of 2300 Å are vulnerable to contamination from second-order light. To mitigate this problem the COS NUV optics were designed to provide peak reflectivities between 1600 and 2000 Å. Gratings G225M and G285M are coated with bare aluminum, which, when oxidized, has poor reflectivity below 1800 Å. After six reflections (two MgF_2 mirrors in the *HST* OTA and four bare-Al optics in COS) light from below 1250 Å is attenuated by 99%. Mounted directly on gratings G230L and G285M are order-sorting filters that block most light from below 1700 Å.

For the G230L grating stripes B and C are still affected by second-order flux. When `CENWAVE=3360` stripe B is contaminated by second-order light beyond 3200 Å. In a spectrum of the planetary nebula NGC 6833 obtained with `CENWAVE=3360` second-order light accounts for roughly 40% of the flux at 3320 Å, and more that 50% at 3500 Å (Figure 5.4). Above 1700 Å stripe C is more sensitive to second-order light than first-order by design (Table 5.4), but on-orbit observations reveal that first-order light is detectable at a level of 5% from wavelengths greater than 3700 Å at all central-wavelength settings (COS ISR 2010-01).

In the FUV channel second-order light is present at long wavelengths ($\lambda > 2150$ Å) in spectra taken with G140L `CENWAVE=1280` FUVA. These photons are rejected by the COS pipeline during processing, but available in the "net counts" column of the `*x1d*.fits` files.

Figure 5.4: Second–Order Light in G230L Spectrum

The black curve is stripe B of the G230L CENWAVE=3360 spectrum of NGC 6833. The blue curve is an FOS spectrum over the same wavelength range (units are Å). The red curve is an FOS spectrum of the 1600–1800 Å region, plotted as f(2λ). The FOS spectra have been rescaled by arbitrary amounts for display purposes. The dashed black curve, a combination of the two FOS spectra, reasonably reproduces the COS spectrum.

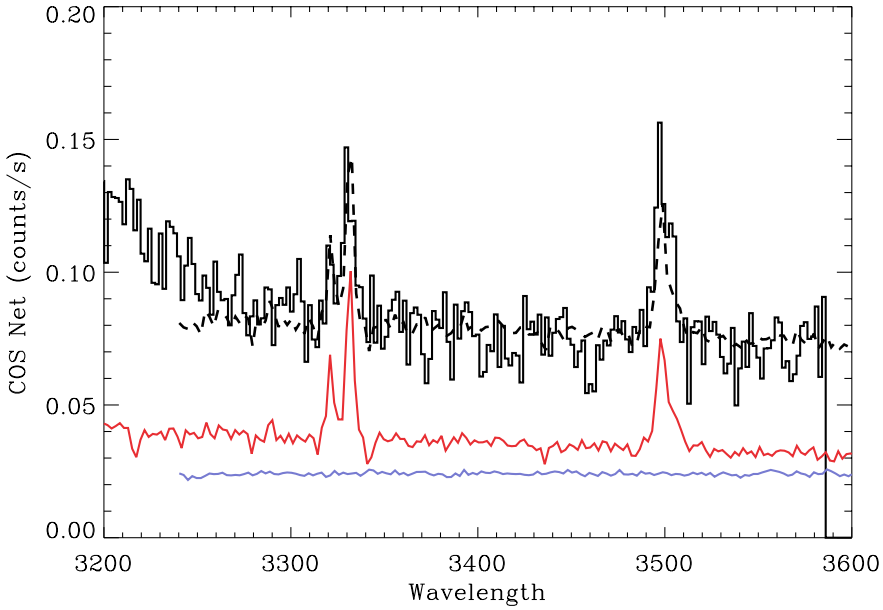

5.1.4 Spectroscopic Resolving Power

The spectroscopic resolving power ($R = \lambda$ / FWHM) of each COS grating is listed in Table 5.1, and plotted as a function of wavelength for the FUV gratings in Figure 3.7 and Figure 5.5. These values correspond to the FWHM of the model line-spread functions (LSFs) that are described in Section 3.3, which have been validated with on-orbit measurements (COS ISR 2013-07, Roman-Duval et al., 2013). Preliminary measurements and model predictions of the resolving power for the new 1055, 1096, and 1222 Å central wavelength settings of the G130M grating are shown in Figure 5.5. Recent adjustments made during Cycle 20 to the focus for the 1055 and 1096 central wavelength settings of the G130M grating have increased their short wavelength resolution by a factor of several over that available before Cycle 20. The quantitative values quoted here for this improved resolution are based on ray-trace models and actual resolution may be slightly different. However, preliminary comparison with on-orbit test data appears consistent with the predictions of these models. A comparison of data obtained with these revised 1055 and 1096 settings with archival *FUSE* data for the same target is shown in Figure 5.6. Users should note, however, that for each of these modes the focus values have been set to optimize the resolution over a limited part of their wavelength range, and it will be necessary to use multiple settings to get the maximum resolution over the full FUV wavelength range (Figure 5.5).

The COS LSF is not a Gaussian, so simple rules relating *R* to the observability of narrow spectral features may not apply. Careful modeling of the LSF may be required to determine the feasibility of an observation. See Section 3.3, COS ISR 2009-01, and COS ISR 2013-07 for further information about the COS LSF.

Figure 5.5: Resolving Power of G130M/1055, G130M/1096, G130M/1222, G130M/1291, and G140L/1280.

The predicted spectral resolving power (R = λ/ FWHM) as a function of wavelength for each segment of the COS FUV detector is shown for the G130M grating at the 1055, 1096, 1222, and 1291 central wavelength settings. The G140L and G160M gratings are shown for comparison. These predictions are based on ray-trace models that include the MFWFEs of the HST primary and secondary mirrors.

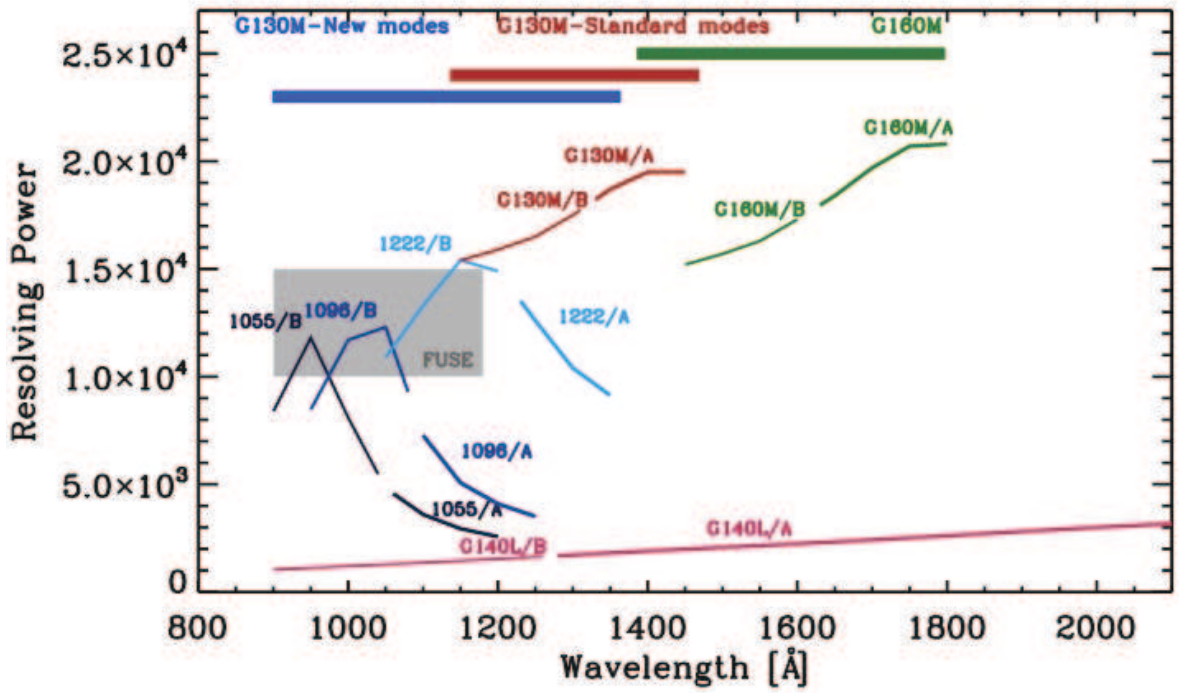

Figure 5.6: Comparison of COS and FUSE Spectra.
The profiles of selected interstellar H_2 lines in the spectrum of the O3.5V binary HD 93205 as seen in COS exposures (black lines) at the 1055 (left, association lc3n02010q, 1320 s) and 1096 (right, association lc3n03010q, 1000 s) central wavelength settings done using the newly optimized focus values are compared with the 4265 s FUSE observation E1590103 (red lines) of the same target.

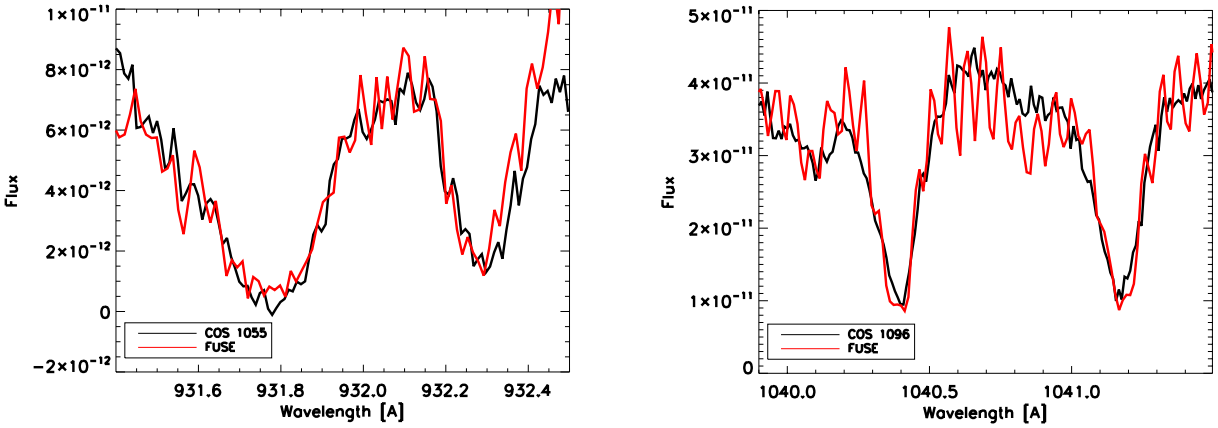

5.1.5 Time-Dependent Sensitivity Changes

Observations of *HST* primary spectrophotometric standard stars show that there is a significant time dependence of the COS sensitivity for some spectrographic modes. The reflectivity of the G225M and G285M NUV gratings, which are coated with bare aluminum (rather than MgF_2 over aluminum like the other gratings), showed a time-dependent degradation before launch that has continued on orbit, decreasing at a rate of ~3% and ~10% per year respectively, independent of wavelength.

Throughout 2009 the FUV modes showed a wavelength-dependent sensitivity decline, falling ~3% per year below 1400 Å, and as much as 11% per year at 1800 Å. The decline slowed to ~5% per year in 2010 and to 3% in 2011, independent of wavelength. In the last quarter of 2011 the sensitivity decline increased again to as much as ~25% per year at 1300 Å, recovering to ~10% per year in the first quarter of 2012, and to ~5% per year up to mid-2013. Since late 2013, the sensitivity decline has decreased more quickly, especially on Segment A. As shown in Figure 5.7 these variations appear to be correlated with Solar activity, and they are consistent with a degradation of the quantum efficiency of the CsI photocathode of the FUV detector caused by reactions with residual atmospheric atomic oxygen. As Solar activity increases the Earth's atmosphere becomes slightly inflated exposing the open-faced COS FUV XDL detector to increased levels of atomic oxygen. For details, see COS ISR 2011-02 and the COS website.

The COS data-reduction pipeline **calcos** includes a time-dependent sensitivity calibration, and regular monitoring of standard stars is used to update the sensitivity reference files. The ETC reflects the best estimate of the sensitivity for the middle of Cycle 24.

Figure 5.7: Relative throughput of the COS FUV over time

Relative throughput of the COS FUV settings as a function of time. The Solar activity, as measured by the 10.7 cm radio flux, is overplotted in blue (and a smoothed curve is shown in green). Dashed vertical lines (red) mark the breakpoints in the time-dependent sensitivity curve. These are the times when the slope of the sensitivity decline changed. The breakpoints appear to be correlated with changes in the intensity of the 10.7 cm radio flux.

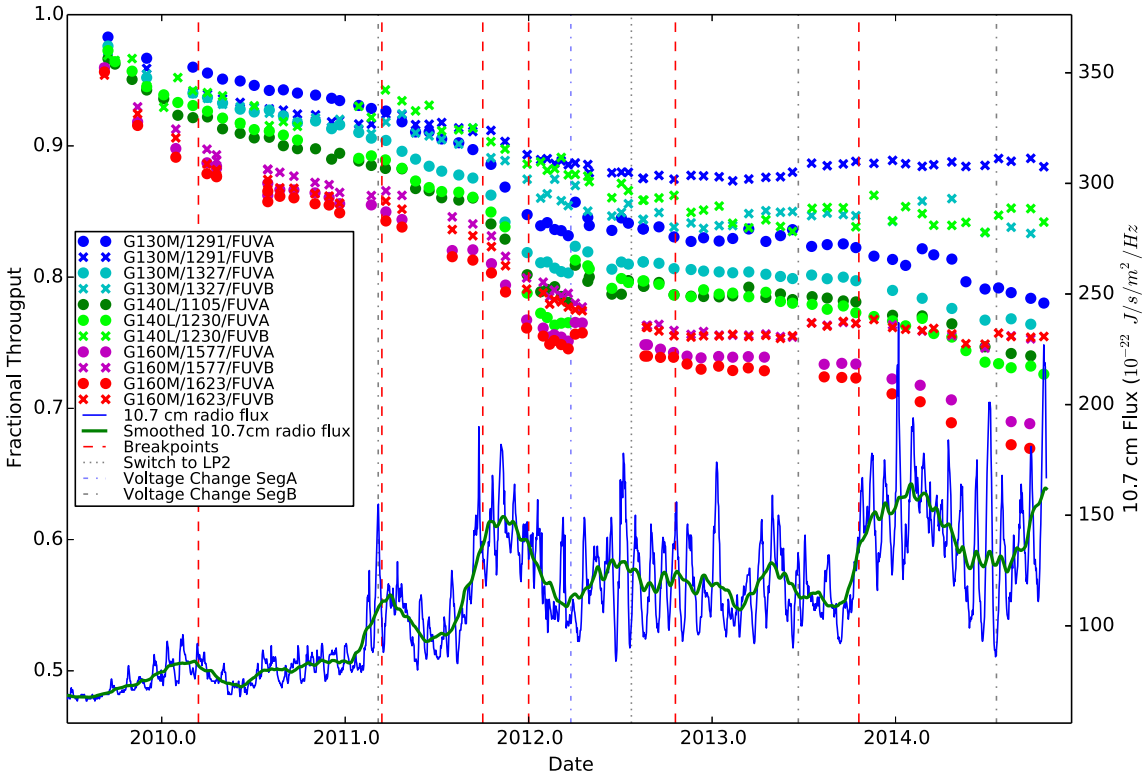

5.1.6 Dip in Sensitivity around 1180 Å

High S/N observations of standard stars have allowed us to uncover what is likely an optical effect that leads to a dip in the sensitivity at about 1180 Å. Figure 5.8 shows the spectrum of WD0320-539 observed in Program 12086 with the G130M/1291 and G130M/1327 settings. The sensitivity dip, of ~10% of the continuum value, is seen near 1180 Å in the G130M/1291 data and near 1190 Å in the G130M/1327 data. This effect is not currently corrected by **calcos**. The data shown in Figure 5.8 were taken at the original lifetime position, but this feature is also present in data taken at the second lifetime position. Preliminary analysis indicates that this feature is not fixed in pixel or wavelength space, but that it moves to longer wavelengths with increasing `CENWAVE` settings. More details about this feature will be posted on the COS website as they become available.

Figure 5.8: The 1180 Å Dip

The spectrum of WD0320-539 (from Program 12086) observed with the G130M/1291 (black) and G130M/1327 (red) settings. A dip of approximately 10% in sensitivity is seen between 1180Å and 1190 Å.

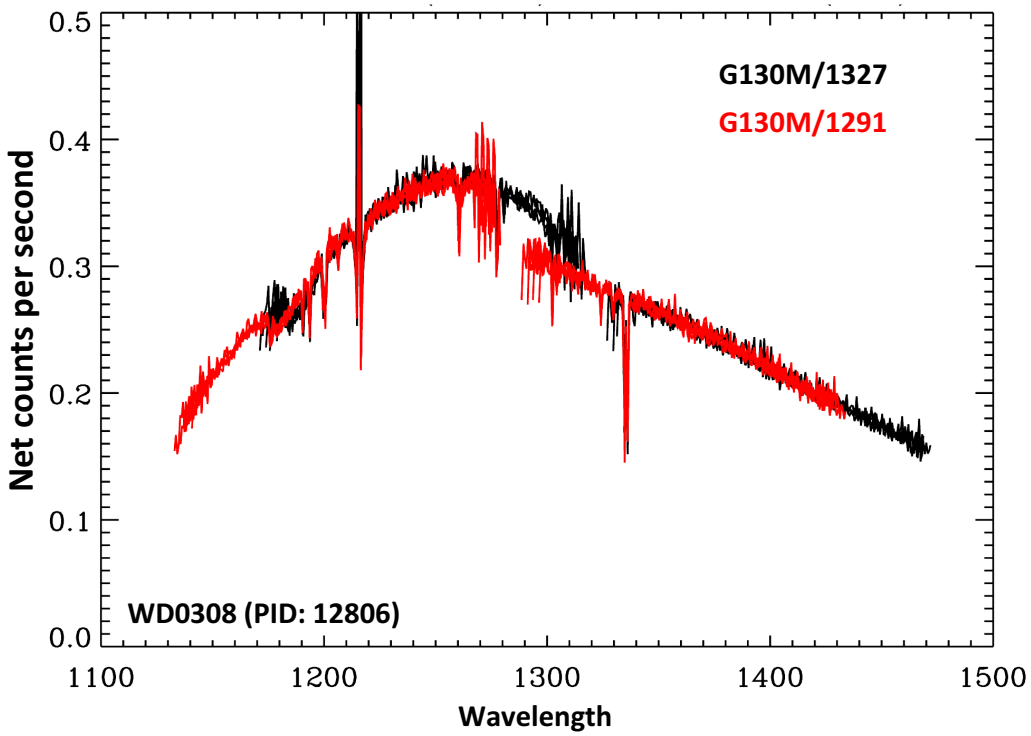

5.1.7 Zero-Order Image

The 1105 Å central-wavelength setting of grating G140L places the zero-order image from the grating on Segment B of the FUV detector, violating detector count-rate limits, while a useful first-order spectrum falls onto Segment A. For this central wavelength observations can be made only in single-segment mode, with the high voltage for Segment B reduced (Section 5.6). After final alignment of COS on-orbit the zero-order image was also found to fall on Segment B for the 1230 Å setting with `FP-POS=4`. In Cycle 18, `CENWAVE=1230` was replaced with `CENWAVE=1280` to keep the zero-order image off the detector. Two-segment observations are allowed for all `FP-POS` settings with `CENWAVE=1280`.

5.1.8 Internal Scattered Light

The internal scattered-light level within COS is quite low. In ground-test measurements light scattered along the dispersion axis represents less than 1% of the nearby continuum. On orbit the COS LSF dominates the scattered light (Chapter 3). Scattering within the instrument is negligible (Kriss 2011).

5.1.9 Spatial Resolution and Field of View

The spatial resolution of COS is affected by the mid-frequency wavefront errors (MFWFEs) via the non-Gaussian wings they introduce (Section 3.3). The NUV channel corrects for the telescope's spherical aberration, but not for the MFWFEs. For PSA observations the spatial resolution is ~ 0.07 arcsec for G185M and G230L, and 0.06 arcsec for G225M and G285M. For BOA observations, the spatial resolution is 0.29 arcsec for G185M, 0.22 arcsec for G225M, 0.24 arcsec for G285M, and 0.30 arcsec for G230L.

In the FUV the situation is more complex, because of the uncorrected astigmatism in the cross-dispersion direction. Figure 5.9 and Figure 5.10 show the strong dependence on wavelength of the FWHM of the cross-dispersion profiles for each of the FUV gratings at the first and second lifetime positions, respectively. The spatial resolutions at LP1 and LP2 differ by not more than 3 pixels (0.3 arcsec). At wavelengths for which the profile width is large the spectra of two objects separated by less than the profile width in the cross-dispersion (XD) direction would be combined.

The COS field of view is determined by the entrance apertures, which are 1.25 arcsec in radius, but the aberrated beam entering the aperture allows objects up to 2 arcsec from the center of the aperture to contribute to the recorded spectrum.

For additional information, please see "FUV Spectroscopic Performance" (COS ISR 2010-09, Ghavamian et al. 2010), "NUV Spectroscopic Performance" (COS ISR 2010-08, Béland et al. 2010), and "COS/FUV Spatial and Spectral Resolution at the New Lifetime Position" (COS ISR 2013-07, Roman-Duval et al. 2013).

Figure 5.9: Cross-Dispersion Profile Widths for FUV Gratings at Lifetime Position One

Variation in the width of the FUV spatial profile at the original lifetime position. The widths are obtained via Gaussian fits to the cross-dispersion profiles of a point source observed through the PSA. (Empirically-determined FWHM values may be slightly smaller.) Widths are plotted as a function of wavelength for each of the central-wavelength settings. Dips in the G130M and G140L spectra mark airglow features.

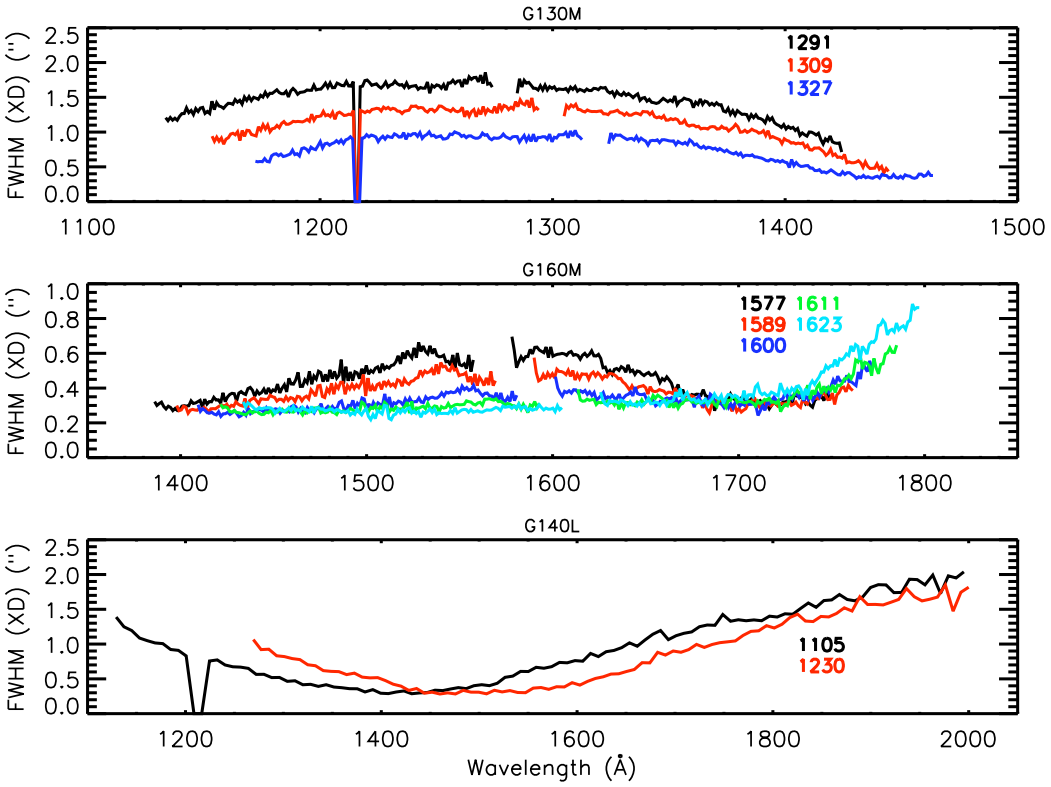

Figure 5.10: Cross-Dispersion Profile Widths for FUV Gratings at Lifetime Position Two.

Variation in the width of the FUV spatial profile at the second lifetime position. The widths are obtained via Gaussian fits to the cross-dispersion profiles of a point source observed through the PSA. (Empirically-determined FWHM values may be slightly smaller.) Widths are plotted as a function of wavelength for each of the central-wavelength settings. Top is G130M, middle is G160M, and bottom is G140L.

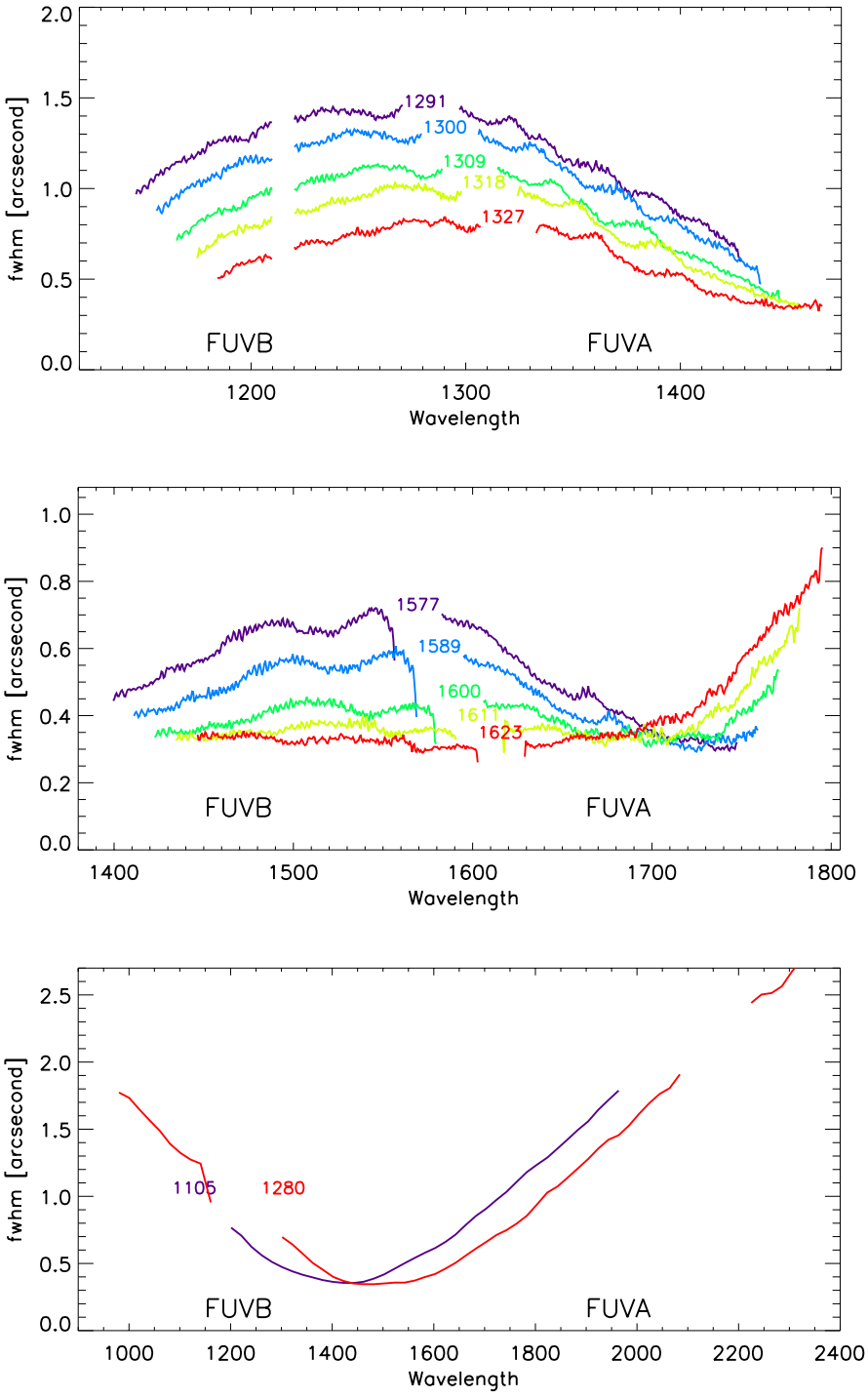

5.1.10 Photometric (Flux) Precision

Based on measurements made during and since SMOV, we estimate that the absolute flux calibration of COS is accurate to about 5% in the FUV, though uncertainties may be larger at wavelengths less than 1150 Å. The relative flux calibration is good to about 2%. In the NUV the calibration is accurate up to 3% for the medium-resolution gratings, and is slightly less accurate in some parts of the G230L bandpass. Time-dependent sensitivity corrections should be accurate to about 2% (Section 5.1.5).

5.1.11 Wavelength Accuracy

The COS medium-resolution gratings are required to achieve a wavelength accuracy of 15 km/s (resel 0.06 Å). For G140L the requirement is 150 km/s. It is 175 km/s for G230L. Analysis of COS data obtained on orbit suggest that these requirements are routinely met. To do so, targets must be properly centered in the desired aperture. Target acquisitions are discussed in Chapter 8.

For modes where the wavelength shift determined from FUV Segment A is applied to Segment B (for example, if there are no lines present on FUVB) there is an additional uncertainty of up to 10 pixels that must be applied. For the G140L grating this corresponds to a wavelength accuracy of 250 km/s. Neither the wavelength solution for the BOA nor the throughput at blue wavelengths is not well characterized, so we recommend that the BOA *not* be used for wavelengths bluer than 1200 Å. See Section 2.4 for further discussion of BOA usage for FUV science observations.

5.1.12 Vignetting of the NUV Channel

After on-orbit alignment of COS in *HST*, fluxes of external targets in the PSA were found to be depressed at the short wavelength ends of the NUV stripes. For the medium-resolution gratings the reduction is about 20% at the first pixel and rises linearly to expected levels over approximately the next 160 pixels (Figure 5.11). For G230L the reduction is about 15% at the first pixel and extends about 110 pixels. (The slope is the same as in Figure 5.11; it is as though the ramp were shifted by 50 pixels.) The depression is thought to be due to vignetting of the beam at the NUV camera mirrors that image the spectrum on the detector. Corrections for this vignetting are not included in either the ETC or the **calcos** data-reduction pipeline. Users are advised to consult the COS webpages, where additional information will be posted as it becomes available.

Figure 5.11: Vignetting Profile for NUV M Gratings

Vignetting profile of the medium-resolution gratings as a function of pixel location showing the linear decrease in throughput near the low-pixel edge of the NUV detector. The red line shows the best fit to the profile obtained from observations of the white dwarf G191-B2B.

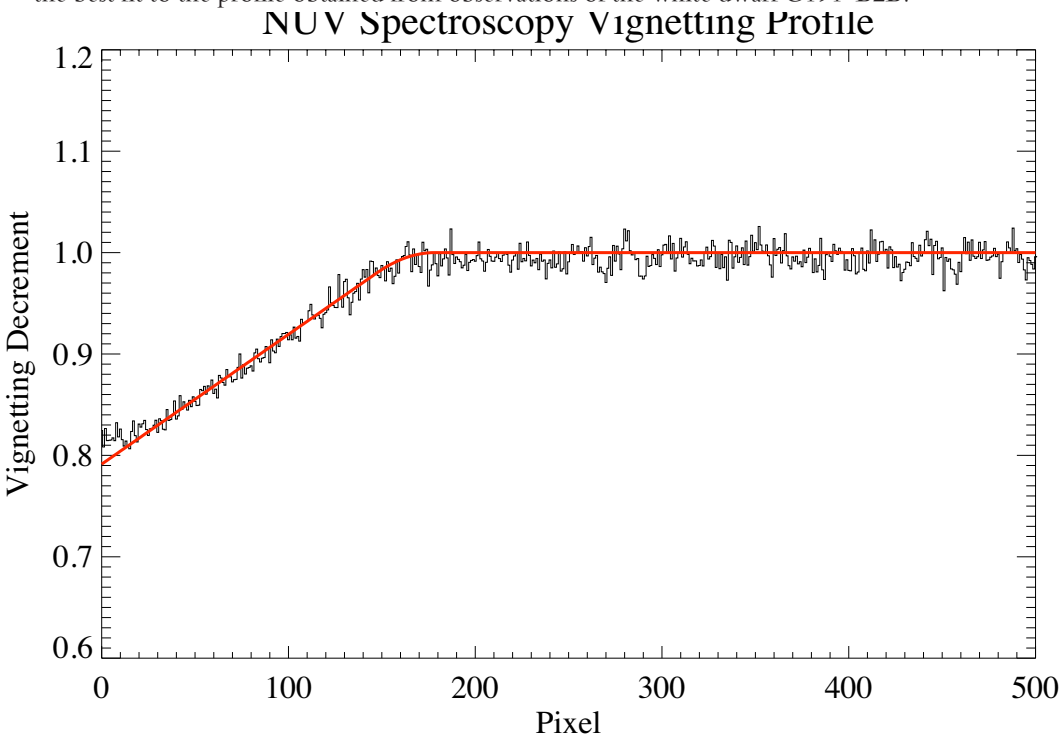

5.2 TIME-TAG vs. ACCUM Mode

COS exposures may be obtained in either a time-tagged photon-address mode (TIME-TAG), in which the position, arrival time, and pulse height (for FUV observations) of each detected photon are saved in an event stream, or in accumulation (ACCUM) mode, in which only the positions of the photon events are recorded.

5.2.1 TIME-TAG Mode

In TIME-TAG mode each photon is kept as a separate event in a list in COS memory. Each entry in that list contains the (*x, y*) coordinates of the photon together with the pulse height of the charge cloud generated by it (for FUV observations). Time markers are inserted in the list every 32 ms by the instrument electronics. When data are processed by the ground system arrival times are assigned to the events according to the time marker preceding the event.

COS observations should be obtained in TIME-TAG mode whenever possible because it provides significant opportunities for temporal sampling, exclusion of poor quality data, and, for the FUV, improved thermal correction (by tracking the stim-pulse positions as a function of time) and background removal (by using the pulse-height information). TIME-TAG mode should always be used for exposures that will generate count rates of 21,000 count/s or less from the entire detector (including both detector segments for the FUV). At count rates between 21,000 and 30,000

count/s, TIME-TAG may be used to obtain properly flux-calibrated data, but the loss of some continuous time periods within extended exposures will occur (see the discussion of the buffer time in Section 5.4). At present, TIME-TAG should not be used for count rates greater than 30,000 count/s. ACCUM mode should be used for such high count-rate targets.

We recommend that TIME-TAG mode always be used with FLASH=YES (the so-called TAGFLASH mode) unless circumstances prevent it (see Section 5.7.1).

Doppler Correction for TIME-TAG Mode

No on-board corrections are made for shifts in the spectrum due to the orbital motion of *HST* while in TIME-TAG mode. This is done later in pipeline processing.

Pulse-Height Data for TIME-TAG

In FUV TIME-TAG mode the pulse height of each photon event is recorded, along with its position and arrival time. Pulse heights are stored as 5-bit words, so their values range from 0 to 31. Post-observation pulse-height screening is useful for rejecting unwanted background events, and can often improve the S/N ratio in the extracted science spectrum. Pulse-height information is not provided by the NUV detector.

5.2.2 ACCUM Mode

In ACCUM mode an image of the detector is stored in a 16-bit memory buffer. As each photon arrives from the detector the location in the buffer at coordinates *(x, y)* is incremented by one. Each location can hold at most 65,535 counts; the next event will cause the value to roll over to zero. To conserve memory only a 16,384 × 128 region of each segment is stored, as well as the regions around each stim pulse. Timing and pulse-height information are not saved, preventing the application of the data-correction techniques available in TIME-TAG mode.

ACCUM mode is designed for bright targets whose high count rates would fill the on-board buffer memory too rapidly if the data were taken in TIME-TAG mode. In some instances one may observe a relatively bright object in TIME-TAG mode by using the BOA instead of the PSA, but the BOA degrades the spectroscopic resolution. Starting in Cycle 23, use of the BOA will be available-but-unsupported (See Section 2.4 for further discussion of BOA usage for FUV science observations). Observers wishing to use ACCUM mode will be asked to justify doing so when submitting their Phase II program.

Observing Efficiencies with ACCUM

FUV ACCUM images do not include the entire detector. To conserve memory photons are collected only from the stim regions and that portion of the detector actually illuminated by the target (1/8 of the full detector area, or 128 pixels in *y*). Each FUV ACCUM image fills one-half of the total COS memory, so it is possible to acquire two FUV images before dumping the on-board buffer.

NUV ACCUM images cover the entire detector. Because they are smaller, up to nine of them can be stored in the memory buffer. Unlike TIME-TAG mode, no data may be acquired during an ACCUM readout. NUV ACCUM mode is thus most efficient when repeated identical observations are stored in memory, then read out all at once. (Within APT, the Astronomer's Proposal Tool, one may easily schedule multiple iterations of an exposure using the Number_of_Iterations parameter.)

Doppler Correction for ACCUM Mode

In ACCUM mode, the COS flight software adjusts the pixel coordinates of detected events to correct for the orbital motion of *HST*. The correction (always by an integer number of pixels) is updated whenever *HST*'s velocity with respect to the target changes enough to shift the spectrum by an additional pixel. This is done via a small table, computed on the ground, that lists the time of each pixel shift based on the orbital motion and the dispersion of the grating in use.

Note that ACCUM mode exposures longer than 900 s that use the G130M or G160M gratings may blur the FUV spectra by 1 to 2 pixels (about 1/6 to 1/3 of a resolution element) since shifts are performed in pixel, not wavelength, space.

Pulse-Height Distribution Data for ACCUM Mode Observations

Some pulse-height information is available for FUV ACCUM observations. A pulse-height histogram, consisting of 256 bins (128 bins for each detector segment) of 32 bits each, is dumped for every ACCUM mode image obtained with the FUV detector. (Why 128 bins? In ACCUM mode individual pulse heights are stored as 7-bit words, so their values range from 0 to 127.) Pulse-height data are not provided for NUV exposures.

5.3 Valid Exposure Times

The minimum COS exposure duration is 0.1 s (but FLASH=YES TIME-TAG exposures impose a longer minimum; see Section 5.7.1). The maximum is 6500 s. Between these extremes COS exposure times must be integer multiples of 0.1 s. If the observer specifies an exposure time that is not a multiple of 0.1 s, its value is rounded *down* to the next lower integer multiple of 0.1 s, (or set to 0.1 s if a smaller value is specified). Exposure times larger than about 3000 s are normally appropriate only for visits with the Continuous Viewing Zone (which is a special requirement that must be requested and justified in the Phase I proposal) because the visibility period of a typical orbit is ~50 minutes. See the *HST Primer* for information about *HST*'s orbit and visibility periods.

For TARGET=WAVE exposures, DEF (default) must be entered as the exposure time. The value appropriate for the optical configuration will be chosen from a table established at STScI for best performance. At present TARGET=WAVE flash durations are identical to those given in Table 5.2.

Table 5.2: TAGFLASH Exposure Durations

Grating	Central Wavelength (Å)	Flash duration (s)	Grating	Central Wavelength (Å)	Flash duration (s)
G130M	1055	142	G225M (cont.)	2339	12
	1096	52		2357	12
	1222	52		2373	22
	all others	12		2390	7
G160M	all	12		2410	7
G140L	all	7	G285M	2617	12
G185M	1786	12		2637	12
	1817	12		2657	7
	1835	12		2676	22
	1850	22		2695	22
	1864	32		2709	12
	1882	17		2719	7
	1890	12		2739	7
	1900	22		2850	22
	1913	17		2952	7
	1921	12		2979	17
	1941	12		2996	17
	1953	17		3018	22
	1971	17		3035	27
	1986	12		3057	32
	2010	12		3074	32
G225M	2186	7		3094	32
	2217	12	G230L	2635	7
	2233	7		2950	7
	2250	22		3000	7
	2268	12		3360	12
	2283	12	MIRRORA	...	7
	2306	12	MIRRORB	...	27
	2325	12			

5.4 Estimating the BUFFER-TIME in TIME-TAG Mode

COS maintains two on-board data buffers, each with a capacity of 9 MBytes (2.35×10^6 counts). The BUFFER-TIME is the time that it takes to fill one of these buffers. COS uses the BUFFER-TIME to establish the pattern and timing of memory dumps during a TIME-TAG exposure. For the first BUFFER-TIME of an exposure counts are recorded in the first COS data buffer. At the end of this time data recording switches to the second data buffer and the first buffer is read out while the second is being filled.

For all external TIME-TAG observations a value of the BUFFER-TIME must be specified in the Phase II proposal. The BUFFER-TIME is 2.35×10^6 counts divided by the anticipated count rate in photons per second. The BUFFER-TIME calculation should include counts from the detector dark current and stim pulses (for FUV) as well as the detected photon events, and factor in the instrument quantum efficiency and dead time. It is strongly recommended that the COS ETC be used to compute an accurate value of the BUFFER-TIME. *In addition, to prevent the loss of data should your target be brighter than specified in the ETC calculation, give yourself a margin of error of about 50%; i.e., multiply the ETC BUFFER-TIME by 2/3.*

If the BUFFER-TIME is overestimated the buffer may fill before input switches to the other buffer. Subsequently-arriving photons will be lost, leaving a gap in the data. The pipeline will correct the exposure times for any such gaps, so flux calibrations will be correct, but the overall S/N will be lower than expected. If BUFFER-TIME is underestimated input will switch to the second buffer before the first buffer is full. No data will be lost, but the resulting drain on spacecraft resources could preclude other activities, including parallel observations. There are, however, some instances when it is advantageous to use a slightly smaller BUFFER-TIME to minimize the overhead when the buffer is being read (see the discussion below).

Figure 5.12 shows a flow chart that illustrates the process of selecting a BUFFER-TIME value for all possible combinations of exposure time and BUFFER-TIME. Each of the options is discussed in detail in Sections 5.4.1 through 5.4.5.

Figure 5.12: BUFFER–TIME Selection Flow Chart

Flow chart for guiding the selection of BUFFER–TIME based on different combinations of exposure time and buffer size. BT_{ETC} is the value of BUFFER–TIME returned by the ETC, $BT_{2/3}$ is 2/3×BT_{ETC}, and T_{EXP} is the exposure time.

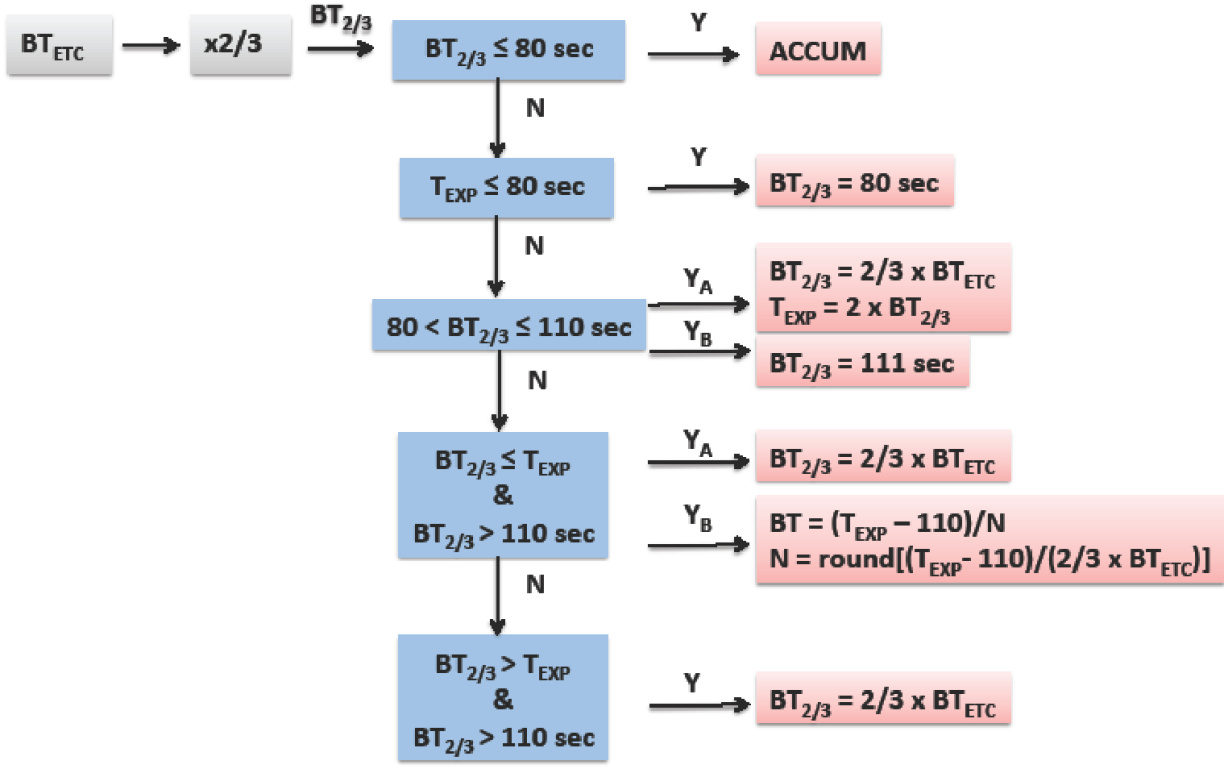

5.4.1 BUFFER-TIME > 110 s and BUFFER-TIME > Exposure Time

For exposures where 2/3 of the BUFFER-TIME returned by the ETC is larger than the exposure time and larger than 110 s the BUFFER-TIME should be set to 2/3 of the value returned by the ETC. In this case the time allocated to read the last buffer dump is proportional to the number of events in the buffer, and some overhead can be saved if only a portion of the buffer needs to be read out. By specifying 2/3 of the BUFFER-TIME returned by the ETC a margin of error of 50% in the observed count rate is used. However, if the observed count rate is actually higher than the 50% margin of error then those events will not be read out of the buffer and will be lost. *If there is a concern that this may happen the BUFFER-TIME should be set to the exposure time. This will ensure that the entire buffer is read out at the end of the exposure.* The FUV dark current fluctuates and occasionally the combined global dark rate for both segments has exceeded 90 count/s (Sections 4.1.3 and 7.4.1). To ensure that all detected events are dumped from the COS buffer, even for a very faint target, the use of BUFFER-TIME > 20,000 s should normally be avoided.

5.4.2 BUFFER-TIME > 110 s and BUFFER-TIME ≤ Exposure Time

In this case 2/3 of the BUFFER-TIME returned by the ETC should be used. As a special case, to minimize the overhead associated with reading the buffer, the BUFFER-TIME can be specified such that there are only between 100 and 110 s left of exposure for the last buffer dump. This new BUFFER-TIME can be calculated using BUFFER-TIME_{new} = (Exposure Time – 110) / *n*, where *n* is the value of (Exposure Time – 110) / (2/3 × ETC Buffer Time) rounded to the next higher integer. For example, suppose that the exposure time is 2300 s and that 2/3 of the BUFFER-TIME returned by the ETC is 2/3 × 1050 = 700 s. Then (2300 – 110) / 700 = 3.13, which is rounded up to *n* = 4 and BUFFER-TIME_{new} = (2300 – 110) / 4 = 547.5 s, which we round up to 548 s. This means that the buffer will be read out every 548 s, and after four buffer reads there will be 2300 – 4×548 = 108 s left in the exposure. This last buffer read has a lower overhead and allows the next exposure to start sooner.

5.4.3 80 s < BUFFER-TIME ≤ 110 s)

It takes 110 s to empty a COS data buffer. A BUFFER-TIME of 110 s corresponds to a count rate of 21,000 count/s. If the count rate exceeds this value, then the second data buffer will be filled before the first buffer has been completely read out. In this situation, you have two options. You can either shorten your exposure, or you can accept gaps in the recorded data stream. In either case **calcos** will compute the actual exposure time and will calculate fluxes correctly, but the total number of collected counts, and hence the S/N, will be limited by the 21,000 count/s per rate.

- Option A: You wish to receive all the data and are willing to shorten the exposure time. In this case use 2/3 of the BUFFER-TIME returned by the ETC. If the BUFFER-TIME is less than 111 s, the APT will issue a warning and truncate the exposure time at 2 × BUFFER-TIME to ensure that all data are recorded.
- Option B: You can tolerate data drop-outs, but want control of the total exposure time. In this case choose a BUFFER-TIME of 111 s. You will lose some fraction of the data during each BUFFER-TIME interval (see example below), but the APT will not truncate your exposure.

As an example, suppose that 2/3 × (BUFFER-TIME returned by the ETC) is 100 s, and you want an exposure time of 360 s.

- With Option A, you would specify BUFFER-TIME=100. Because it takes longer than that to read out the buffer, the APT limits you to an exposure time of 2 × 100 = 200 s. In this case COS records all the events that arrived during the exposure.
- With Option B, you would specify BUFFER-TIME=111 s. Since the COS buffer may be full after the first 100 s the last 11 s of data may not be recorded, and are lost each time the buffer fills. With this option you will get a series of data blocks as follows: **100**, *11*, **100**, *11*, **100**, *11*, **27**, where the bold

numbers represent periods when the data are recorded, and the italic numbers represents periods when the data are lost. The COS shutter remains open for the full 360 s, and the data are properly flux calibrated by the pipeline.

5.4.4 BUFFER-TIME ≤ 80 s

The minimum allowed value of the BUFFER-TIME is 80 s. This value corresponds to a count rate of 30,000 count/s over the entire detector, the maximum rate at which the flight electronics are capable of processing counts. If 2/3 of the ETC BUFFER-TIME is less than 80 s, then the source is very bright and should be observed in ACCUM mode. If your exposure is less than 80 s in length set BUFFER-TIME=80 s. The buffer will be read out immediately after the exposure ends, and there will be no idle time.

The software and parameters that control dumps of the data buffer have been designed to avoid any loss of data from an observation. The duration and timing of data dumps depend on several factors, and observers are urged to experiment with APT to optimize the efficiency of their observations.

5.4.5 BUFFER-TIME and AUTO-ADJUST

If you use the AUTO-ADJUST feature in the APT to set your exposure times do it first, then adjust the BUFFER-TIME of each exposure according to the rules above.

5.5 Spanning the Gap with Multiple CENWAVE Settings

COS spectra exhibit wavelength gaps due to the physical layout of the detectors and the optics. The FUV detector consists of two segments whose active areas are separated by a gap approximately 9 mm wide. The optical image of the spectrum is continuous across the segments, but the wavelengths that fall in the gap (which depend on the CENWAVE selected) are not recorded. These wavelengths can be brought onto the active area of the detector by choosing one of the alternate central-wavelength settings listed in Table 5.3. For the FUV M gratings, the gap (14–18 Å) is about twice the size of the difference in central wavelength shifts (9 Å). To span it we recommend obtaining exposures at two or more FP-POS positions at each of two non-consecutive CENWAVE settings. For the G140L grating, both CENWAVEs are needed to obtain a complete spectrum.

Table 5.3: Wavelength Ranges for FUV Gratings for FP–POS=3

Grating	Central wavelength setting (Å)[1]	Recorded wavelengths[2]	
		Segment B	Segment A
G130M	1055	899 – 1040	1055 – 1196
	1096	940 – 1080	1096 – 1236
	1222	1067 – 1207	1223 – 1363
	1291	1134 – 1274	1291 – 1431
	1300	1144 – 1283	1300 – 1441
	1309	1154 – 1294	1309 – 1450
	1318	1163 – 1303	1319 – 1460
	1327	1172 – 1313	1328 – 1469
G160M	1577	1386 – 1559	1577 – 1751
	1589	1397 – 1571	1589 – 1762
	1600	1409 – 1581	1601 – 1774
	1611	1420 – 1594	1612 – 1786
	1623	1432 – 1606	1625 – 1798
G140L	1105	HV OFF	1118 – 2251[3]
	1280	<900 – 1165	1280 – 2391[3]

1. The central wavelength is (approximately) the shortest wavelength recorded on Segment A.
2. All wavelength ranges quoted here are approximate, due to uncertainties in the position of the OSM1 mechanism.
3. G140L spectra are flux calibrated up to 2150 Å. At longer wavelengths, second-order light may be present (see Section 5.1.3).

For the NUV channel dispersed light from the gratings is imaged onto the detector by three camera mirrors resulting in three non-contiguous spectral stripes being recorded at once. The gaps between the stripes are approximately 64 Å for the G185M and G225M gratings, 74 Å for G285M, and 700 Å for G230L (Table 5.4). To acquire a complete medium-resolution spectrum requires six settings with G185M, six with G225M, and eight with G285M (Table 5.5). A full spectrum with G230L requires three `CENWAVE` settings (Table 5.4). Such a complete spectrum can probably be acquired more efficiently with STIS, but COS may be a better choice when a limited number of specific wavelengths is desired.

Table 5.4: Wavelength Ranges for NUV Gratings for FP–POS=3

Grating	Central wavelength setting (Å)[1]	Recorded wavelengths		
		Stripe A	Stripe B	Stripe C
G185M	1786	1670 – 1705	1769 – 1804	1868 – 1903
	1817	1701 – 1736	1800 – 1835	1899 – 1934
	1835	1719 – 1754	1818 – 1853	1916 – 1951
	1850	1734 – 1769	1833 – 1868	1931 – 1966
	1864	1748 – 1783	1847 – 1882	1945 – 1980
	1882	1766 – 1801	1865 – 1900	1964 – 1999
	1890	1774 – 1809	1872 – 1907	1971 – 2006
	1900	1783 – 1818	1882 – 1917	1981 – 2016
	1913	1796 – 1831	1895 – 1930	1993 – 2028
	1921	1804 – 1839	1903 – 1938	2002 – 2037
	1941	1825 – 1860	1924 – 1959	2023 – 2058
	1953	1837 – 1872	1936 – 1971	2034 – 2069
	1971	1854 – 1889	1953 – 1988	2052 – 2087
	1986	1870 – 1905	1969 – 2004	2068 – 2103
	2010	1894 – 1929	1993 – 2028	2092 – 2127
G225M	2186	2070 – 2105	2169 – 2204	2268 – 2303
	2217	2101 – 2136	2200 – 2235	2299 – 2334
	2233	2117 – 2152	2215 – 2250	2314 – 2349
	2250	2134 – 2169	2233 – 2268	2332 – 2367
	2268	2152 – 2187	2251 – 2286	2350 – 2385
	2283	2167 – 2202	2266 – 2301	2364 – 2399
	2306	2190 – 2225	2288 – 2323	2387 – 2422
	2325	2208 – 2243	2307 – 2342	2406 – 2441
	2339	2223 – 2258	2322 – 2357	2421 – 2456
	2357	2241 – 2276	2340 – 2375	2439 – 2474
	2373	2256 – 2291	2355 – 2390	2454 – 2489
	2390	2274 – 2309	2373 – 2408	2472 – 2507
	2410	2294 – 2329	2393 – 2428	2492 – 2527

Grating	Central wavelength setting (Å)[1]	Recorded wavelengths		
		Stripe A	Stripe B	Stripe C
G285M	2617	2480 – 2521	2596 – 2637	2711 – 2752
	2637	2500 – 2541	2616 – 2657	2731 – 2772
	2657	2520 – 2561	2636 – 2677	2751 – 2792
	2676	2539 – 2580	2655 – 2696	2770 – 2811
	2695	2558 – 2599	2674 – 2715	2789 – 2830
	2709	2572 – 2613	2688 – 2729	2803 – 2844
	2719	2582 – 2623	2698 – 2739	2813 – 2854
	2739	2602 – 2643	2718 – 2763	2837 – 2878
	2850	2714 – 2755	2829 – 2870	2945 – 2986
	2952	2815 – 2856	2931 – 2972	3046 – 3087
	2979	2842 – 2883	2958 – 2999	3073 – 3114
	2996	2859 – 2900	2975 – 3016	3090 – 3131
	3018	2881 – 2922	2997 – 3038	3112 – 3153
	3035	2898 – 2939	3014 – 3055	3129 – 3170
	3057	2920 – 2961	3036 – 3077	3151 – 3192
	3074	2937 – 2978	3053 – 3094	3168 – 3209
	3094	2957 – 2998	3073 – 3114	3188 – 3229
G230L	2635	1334 – 1733[2]	2435 – 2834	**1768 – 1967[3,5]**
	2950	1650 – 2050	2750 – 3150	**1900 – 2100[5]**
	3000	1700 – 2100	2800 – 3200	**1950 – 2150[5]**
	3360	2059 – 2458[4]	3161 – 3560[5]	**2164 – 2361[5]**

1. The central wavelength setting corresponds to the approximate midpoint of stripe B.
2. For central wavelength 2635 Å, the stripe A wavelengths are listed for completeness only (and in case a bright emission line falls onto the detector). The NUV detector's sensitivity at these wavelengths is extremely low. To obtain a low-resolution spectrum at wavelengths below ~ 1700 Å, we recommend the FUV grating G140L.
3. The values in shaded cells are wavelength ranges observed in second order light. Their dispersion is twice that of the first-order spectrum. First-order flux, from wavelengths twice those of the listed range, will be present at the ~ 5% level.
4. Lyman-α may be present in second order light.
5. Longward of 3200 Å, second-order light may be present. At these wavlengths, the flux calibration applied by **calcos** is unreliable (Section 5.1.3).

Table 5.5: COS modes required to obtain a complete medium–resolution NUV spectrum

Grating	Central Wavelength (Å)	Stripe Wavelength Ranges (Å)			Cumulative Wavebands (Å)		
G185M	1786	1670 – 1705	1769 – 1804	1868 – 1903	1670 – 1705	1769 – 1804	1868 – 1903
	1817	1701 – 1736	1800 – 1835	1899 – 1934	1670 – 1736	1769 – 1835	1868 – 1934
	1850	1734 – 1769	1833 – 1868	1931 – 1966	1670 – 1966		
	1953	1837 – 1872	1936 – 1971	2034 – 2069	1670 – 1971	2034 – 2069	
	1986	1870 – 1905	1969 – 2004	2068 – 2103	1670 – 2004	2034 – 2103	
	1921	1804 – 1839	1903 – 1938	2002 – 2037	1670 – 2103		
G225M	2217	2101 – 2136	2200 – 2235	2299 – 2334	1670 – 2136	2200 – 2235	2299 – 2334
	2250	2134 – 2169	2233 – 2268	2332 – 2367	1670 – 2169	2200 – 2268	2299 – 2367
	2283	2167 – 2202	2266 – 2301	2364 – 2399	1670 – 2399		
	2410	2294 – 2329	2394 – 2428	2492 – 2527	1670 – 2428	2492 – 2527	
	2339	2223 – 2258	2322 – 2357	2421 – 2456	1670 – 2456	2492 – 2527	
	2373	2256 – 2291	2355 – 2390	2454 – 2489	1670 – 2489	2492 – 2527	
G285M	2617	2480 – 2521	2596 – 2637	2711 – 2752	1670 – 2527	2596 – 2637	2711 – 2752
	2657	2520 – 2561	2636 – 2677	2751 – 279>	1670 – 2561	2596 – 2677	2711 – 2792
	2695	2558 – 2599	2674 – 2715	2789 – 2830	1670 – 2830		
	2952	2815 – 2856	2931 – 2972	3046 – 3087	1670 – 2856	2931 – 2972	3046 – 3087
	2979	2842 – 2883	2958 – 2999	3073 – 3114	1670 – 2883	2931– 2999	3046 – 3114
	3018	2881 – 2922	2997 – 3038	3112 – 3153	1670 – 2922	2931 – 3038	3046 – 3153
	3057	2920 – 2961	3036 – 3077	3151 – 3192	1670 – 3192		
	3094	2957 – 2998	3073 – 3114	3188 – 3229	1670 – 3229		

This table gives the NUV medium–resolution grating and central wavelength combinations that are needed to create a continuous COS NUV spectrum from 1670 Å to 3229 Å. The Stripe Wavelength Ranges columns give the wavelength ranges covered by each of the three NUV stripes, using the nominal FP–POS=3 setting, corresponding to each of the grating and central wavelength values on the left. The Cumulative Wavebands columns give the cumulative wavebands covered by the current setting, and all the grating and central wavelength settings above it.

5.6 FUV Single-Segment Observations

The FUV detector segments are operated and read out independently. For all FUV gratings Segment A detects the longer-wavelength light and Segment B the shorter wavelengths. Normally both segments are used for a science exposure, but there are circumstances in which operating with one detector segment at the nominal high voltage and the other effectively turned off may be beneficial. The `SEGMENT` optional parameter allows this choice. STScI strongly recommends use of both segments (the default for all but the G140L 1105 Å setting) unless special circumstances exist. Such circumstances include

- Sources with unusual spectral energy distributions at FUV wavelengths (bright emission lines or rapidly increasing/decreasing continuum slopes), for which the count rate on one detector segment exceeds the bright-object protection limit, while the other segment is safe for observing. In some cases, this problem may be mitigated by adjusting the central wavelength or `FP-POS` setting.
- Sources for which the count rate on one detector segment is high but safe, while the other segment has a relatively low count rate. If the science to be done were on the low count-rate segment, operating just that segment would reduce data losses due to dead-time effects and increase the S/N of the resulting spectrum.

The optional parameter `SEGMENT` specifies which segment of the FUV detector to use for an observation. A value of `BOTH` will activate both segments. This is the default setting. If `SEGMENT=A` is selected, only Segment A of the detector will be activated for photon detection, and the spectrum will contain data from only the long-wavelength half of the detector. If `SEGMENT=B` is selected, only the short-wavelength Segment B of the detector will be activated and used to generate data. Wavelength and flat-field calibration procedures remain the same for a particular segment whether or not the other segment is operating. Observers should take care to set `SEGMENT` appropriately when using the new blue mode settings for the G130M (the 1055, 1096, and 1222 `CENWAVE` settings).

If grating G140L is specified with the 1105 Å wavelength setting, then the value defaults to `SEGMENT=A`. Switching from two-segment to single-segment operation (or back again) incurs a substantial overhead time; see Table 9.5.

5.7 Internal Wavelength Calibration Exposures

Three types of internal wavelength calibration exposures may be inserted in the observation sequence by the scheduling system or by the observer:

1. FLASH=YES (so-called TAGFLASH) lamp flashes (TIME-TAG observing with the PSA only),
2. AUTO wavecals, and
3. user-specified GO wavecals.

Note that *all* wavelength-calibration exposures are taken in TIME-TAG mode. Wavelength calibration exposure overheads are higher when the BOA is used for science observation because the aperture mechanism must be moved to place the WCA in the wavelength-calibration beam.

While it is possible to suppress the taking of any wavelength-calibration spectra, doing so significantly lessens the archival quality of COS data and must be justified on a case-by-case basis.

5.7.1 Concurrent Wavelength Calibration with TAGFLASH

The optional parameter FLASH indicates whether or not to "flash" the wavelength calibration lamp during TIME-TAG exposures utilizing the PSA. These flashes provide data used by the **calcos** pipeline to compensate for drifts of the Optics Select Mechanisms. In this mode, when the external shutter is open to observe an external target, the wavecal lamp is turned on briefly at the beginning of, and at intervals throughout, the exposure. Light from the science target and the internal wavelength calibration source is recorded simultaneously on different portions of the detector. Other than the flash at the start, the timing of flashes is determined by the elapsed time since the last OSM motion. As a result flashes may occur at different times in different exposures. The grating-dependent flash durations (Table 5.2) and the flash intervals are defined and updated as necessary by STScI. Observers may not specify either flash duration or interval. (Details of TAGFLASH execution are presented in COS ISR 2011-04.) When flashing is enabled the exposure time must be at least as long as a single flash. Science exposures shorter than the flash durations listed in Table 5.2 may be obtained by setting FLASH=NO, in which case a wavecal exposure will automatically be inserted after the science exposure.

TIME-TAG sequences with FLASH=YES provide the highest on-target exposure time, as no on-target time is lost to wavelength-calibration exposures. Therefore, we strongly recommend use of the optional parameter FLASH=YES with all TIME-TAG observations through the PSA. (Since FLASH=YES is the default for TIME-TAG spectroscopic exposures, the observer need not specify it.) FLASH=YES may not be specified for ACCUM mode or when the BOA is selected. Users should be aware that the BOA is not well calibrated at wavelengths below 1200 Å.

5.7.2 AUTO Wavecals (when TAGFLASH is not used)

For ACCUM, BOA, or FLASH=NO, TIME-TAG exposures a separate wavelength calibration exposure will be automatically scheduled by the APT for each set of external spectrographic science exposures using the same spectral element, central wavelength, and FP-POS value. These AUTO wavecals are always obtained in TIME-TAG mode with the external shutter closed. This automatic wavelength calibration exposure will be added before the first associated science exposure, and after each subsequent science exposure if more than 40 minutes of visibility time has elapsed since the previous wavelength calibration exposure and if the same spectrograph set-up has been in use over that time. The calibration exposure will often use some science target orbital visibility. The calibration lamp configuration and exposure time will be based on the grating and central wavelength of the science exposure. Utilization of a GO wavecal (see below) resets the 40 minute interval timer. Insertion of a FLASH=YES exposure in the timeline does not affect the 40-minute clock.

AUTO wavecals may not be turned off by the observer. If there is a science requirement to turn off AUTO wavecals, specific permission must be sought from the STScI Contact Scientist.

FLASH=NO observations will be less efficient than FLASH=YES observations in terms of on-target utilization of orbital visibility, and in the quality of their wavelength calibration, due to possible OSM residual motions.

5.7.3 GO Wavecals (User-Specified)

Observers may request additional wavelength-calibration exposures, called GO wavecals, by selecting TARGET=WAVE, EXPTIME=DEF, and FLASH=NO. The exposure must be made in TIME-TAG mode. GO wavecals use the same calibration lamp configuration and exposure times as the automatic wavelength calibrations discussed above. The default modes of operation automatically secure needed wavelength-calibration information to go with your science data, so GO wavecals are rarely required.

5.7.4 No-Cal Wavecals

The COS Pt-Ne wavelength-calibration lamps produce no lines on FUV Segment B in the following observing modes:

- G130M, central wavelength 1055 Å, all FP-POS settings;
- G130M, central wavelength 1096 Å, all FP-POS settings;
- G140L, central wavelength 1280 Å, all FP-POS settings.

To reduce these data **calcos** assigns the wavelength shifts derived from the Segment A spectrum. If no Segment A data are present (*i.e.,* if SEGMENT=B), then no shift is assigned.

5.7.5 Inserting Wavecals in Observations with G130M/1055 and G130M/1096, SEGMENT=B

Due to the 100x difference in sensitivity between the COS FUVA and FUVB segments when observing with the G130M/1055 and 1096 CENWAVEs, it is expected that many observers will need to turn off FUVA when observing bright targets. Only those observers using these two configurations are affected by this issue.

Under these conditions the zero point of the wavelength solution cannot be determined because the MgF_2 window on the PtNe lamps (WAVECAL) blocks light below ~ 1180Å (all WAVECAL light falls on FUVA). This results in a degradation of the resolution when FP-POS are combined by **calcos** and decreases the archival value of the COS data. *In these cases, normal TAGFLASHs are not available and WAVECAL exposures with FUVA turned ON must be inserted into the observing sequence adjacent to each CENWAVE/FP-POS setting used.* As a result, in these cases FP-POS=ALL should not be used. Individual FP-POS science exposures should be used instead.

For non-CVZ science exposures at the start of an orbit not containing a target acquisition (TA) sequence, the WAVECAL can be inserted into the prior occultation with no impact on the timeline. For non-CVZ science exposures at the end of an orbit, the WAVECAL can be inserted into the following occultation with no impact on the timeline. For science exposures that immediately follow TA, or do not start or end an orbit, a WAVECAL must be inserted. This can take anywhere from 500 to 900 s (8–15 minutes) depending on configuration and observing sequence. See COS Newsletter at:

http://www.stsci.edu/hst/cos/documents/newsletters/cos_stis_newsletters/full_stories/2013_06/bm_detail.

5.8 Fixed-Pattern Noise

The S/N of COS observations in **calcos** is improved through two techniques, flat fielding and coadding spectra taken at different central wavelengths or FP-POS settings. Flat fielding removes low-frequency variations on the detector by dividing the data by a high S/N flat-field response image. FP-POS exposures smooth out pixel-to-pixel detector variations by combining in wavelength space data taken at different positions on the detector.

5.8.1 COS Flat Fielding

The internal flat-field calibration system consists of two deuterium lamps and the flat-field calibration aperture (FCA). The system was designed such that light from the lamps follows nearly the same optical path as that from an external target. The FCA is placed near the usual location of the PSA, and the lamp beam illuminates the gratings and mirrors from this slightly offset position.

The deuterium lamps are not bright enough to map out the flat field at FUV wavelengths, so the FUV flats are constructed from on-orbit observations of bright white dwarfs. An image of the FUV detector using the deuterium lamp is shown in Figure 5.13. The light, vertical stripe is a shadow cast by a grid wire in front of the detector (Section 4.1.1). A detector dead spot and the hexagonal pattern of the fiber bundles in the micro-channel plate are also visible. Although significant structure is present in the FUV flats, it is reproducible and can be removed during data reduction.

Figure 5.13: Section of a Flat-Field Image for the FUV XDL

A section of the FUV flat field showing representative detector features and a grid wire (the light vertical stripe at a pixel position of 4720).

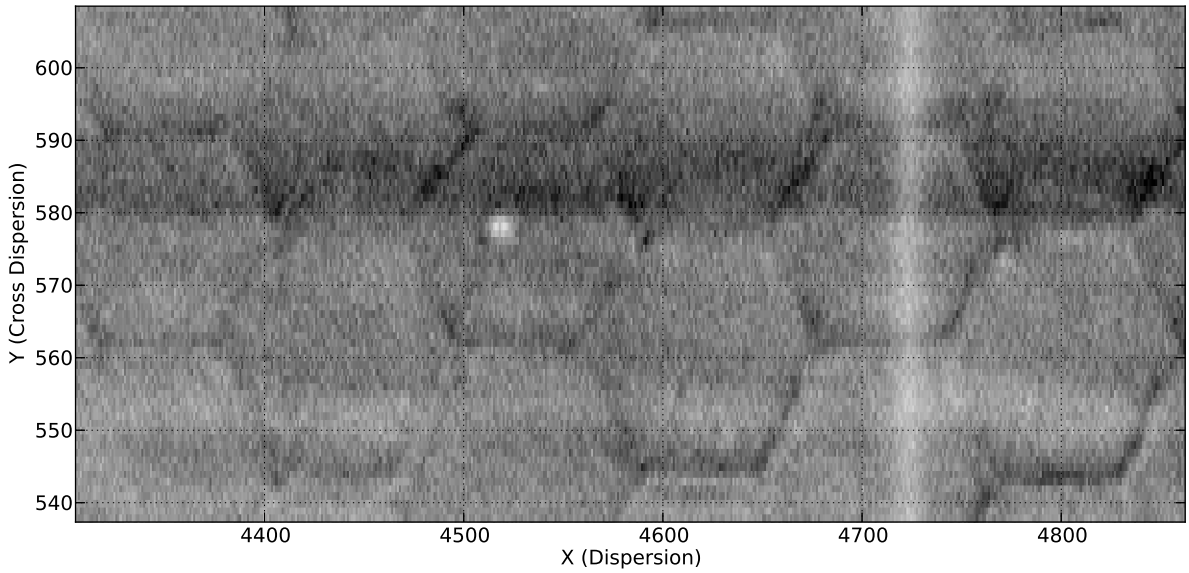

Grid-wire shadows are the greatest source of fixed-pattern noise. In the past **calcos** flagged these regions and eliminated their contributions to the final, summed spectra. During Cycle 18 a grid-wire flat-field calibration file was developed for the G130M and G160M gratings, and it was updated in Cycle 21 for all FUV gratings. Pixels affected by grid wires are still flagged by **calcos**, but their corrected values are included in the summed spectra. Figure 5.14 shows the effect of correcting the grid-wire shadows on a single G130M FUVB exposure of the white dwarf WD0320-539 obtained at the original lifetime position. This star has a relatively smooth continuum, making the corrections obvious. The upper (blue) spectrum contains grid-wire shadows (indicated by the vertical lines), which are corrected in the lower (green) spectrum. The affected regions are clearly improved, but residual structure, much of it fixed-pattern noise in the FUV detector, remains. This structure can be reduced through the use of multiple `FP-POS` settings (Section 5.8.2).

Figure 5.14: Correcting Grid–Wire Shadows with Flat–Field Reference File

G130M FUVB exposure of the white dwarf WD0320–539 obtained at the original lifetime position. The upper (blue) spectrum contains grid–wire shadows (indicated by the vertical lines), which are corrected in the lower (green) spectrum.

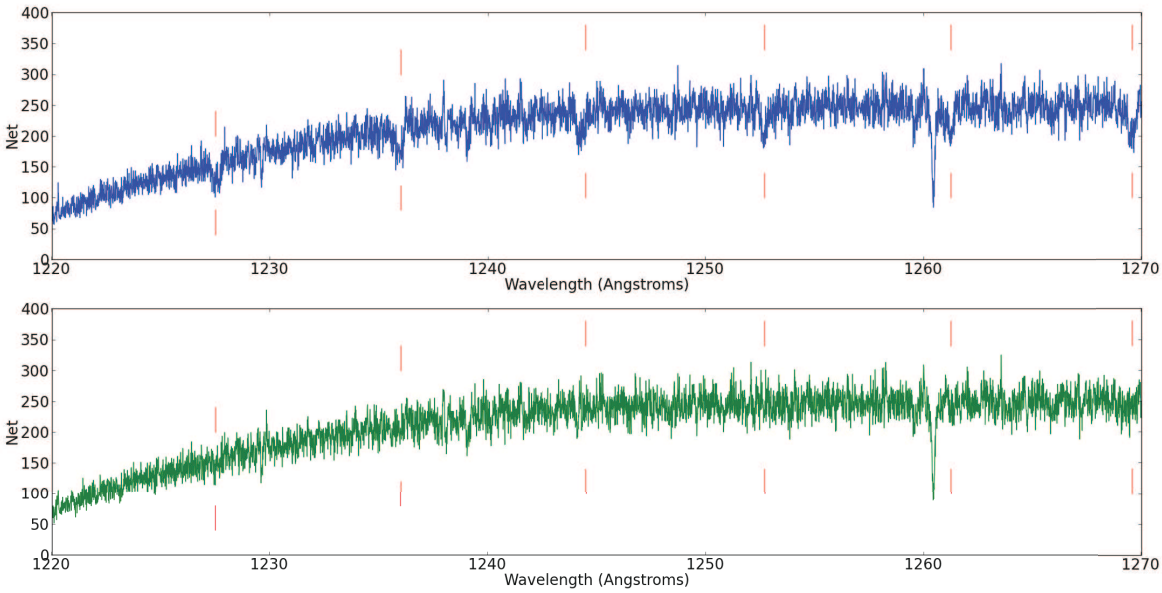

Table 5.6 gives the limiting S/N for the G130M and G160M gratings when the grid-wire flat field is used, both with and without multiple FP-POS settings. To attain higher S/N ratios special analysis procedures, such as those described in the January 2011 COS STAN, are required.

Table 5.6: Limiting S/N for FUV Spectroscopy

Grating	FUVA	FUVB
Single FP-POS Exposure		
G130M	17.9	23.8
G160M	14.9	20.4
Combining 4 FP-POS Exposures		
G130M	35.7	47.6
G160M	29.9	40.8

Because the grid wires are oriented perpendicular to the spectrum, their effect on the data is relatively insensitive to the location of the spectrum in the cross-dispersion direction. Much of the remaining fixed-pattern noise depends strongly on the spectrum location, and will require considerably more effort to characterize and correct. The grid-wire flats have been shown to be independent of the *y* position on the detector, so they can be applied at both lifetime positions.

In addition to grid-wire shadows "grid-wire impostors" were recently discovered in COS FUV Data. The morphology of the impostor in the extracted spectra is similar overall to that of the grid-wire shadows. However, unlike the grid-wire shadows the impostor features depend strongly on the *y* position on the detector. From the appearance of these features in the dark exposures it had been determined that the impostors are artifacts introduced by the geometric distortion correction. However, due to the way that the geometric distortion corrections are integrated into nearly every other aspect of calibration changing this reference file cannot be done quickly. Therefore, a 2D correction for the "impostors" has been incorporated into the FLATFIELD reference file until a fix to the geometric distortion correction can be fully investigated and tested. As a result **calcos** now corrects these features through the flat-field correction.

Comparison of extracted spectra at difference `FP-POS` and `CENWAVE` settings has revealed *y*-independent illumination variations on each detector segment. These variations are now being corrected in **calcos** by applying a low-order flat-field correction (L-flat) that has been incorporated into the FLATFIELD reference file. The L-flat applicable to the original and second lifetime positions is shown in Figure 5.15 and an example of the improvement obtained using the L-flat is shown in Figure 5.16.

Figure 5.15: L–Flat Amplitudes for the COS FUV
The amplitudes of the L–flats for the COS FUV A and B Segments.

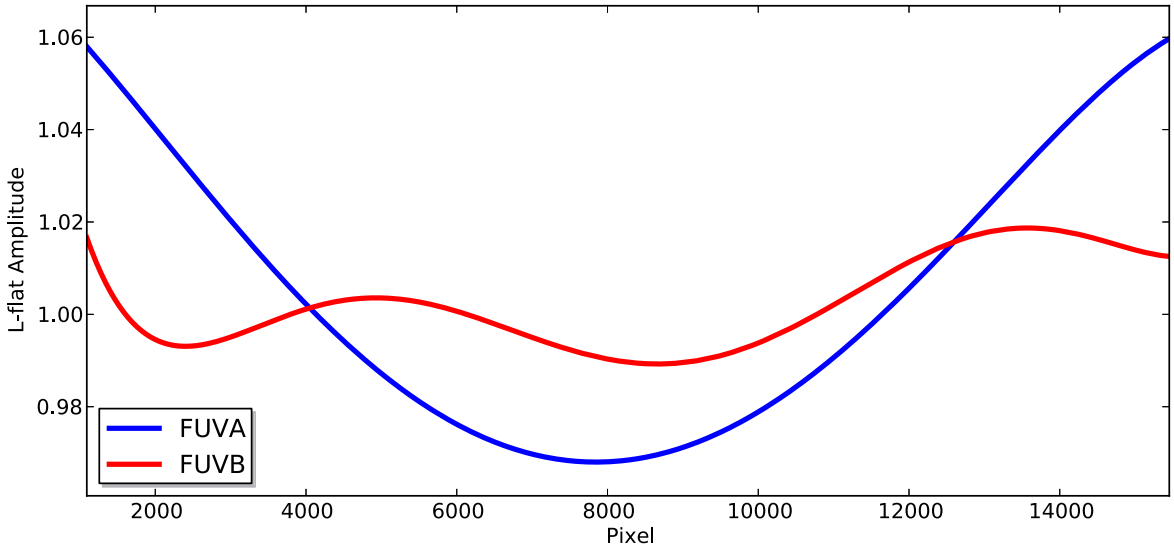

Figure 5.16: A Comparison of COS Spectra with and without the L–Flat Correction.

The top panel shows two COS spectra without the L–flat correction. The bottom panel shows the same two spectra with the L–flat correction.

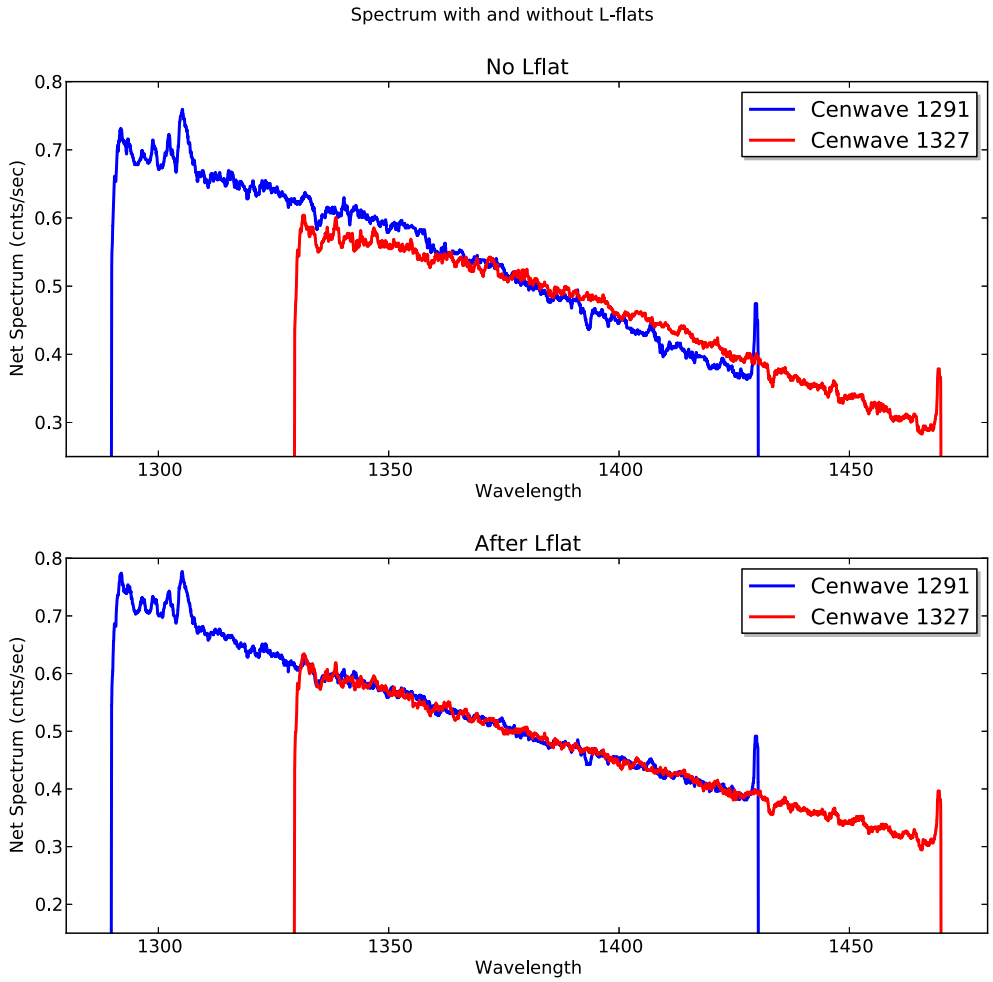

The NUV flat field used by **calcos** was built from a combination of external PSA deuterium lamp exposures taken on the ground and internal FCA observations taken on the ground and on orbit. Figure 5.17 presents a comparison between two NUV flat-field frames, one obtained on orbit and one on the ground. Each image was divided by a low-order polynomial to isolate the high-order fringe pattern characteristic of the NUV detector. Their ratio is consistent with the noise in the on-orbit image, confirming that the two flat fields may be safely combined. Pre-flight ground tests with COS show that the NUV MAMA can deliver S/N up to about 50 without using a flat field. Using a flat field it should be possible to routinely achieve S/N of 100 or more per resolution element.

Figure 5.17: Flat–Field Exposures for the NUV MAMA

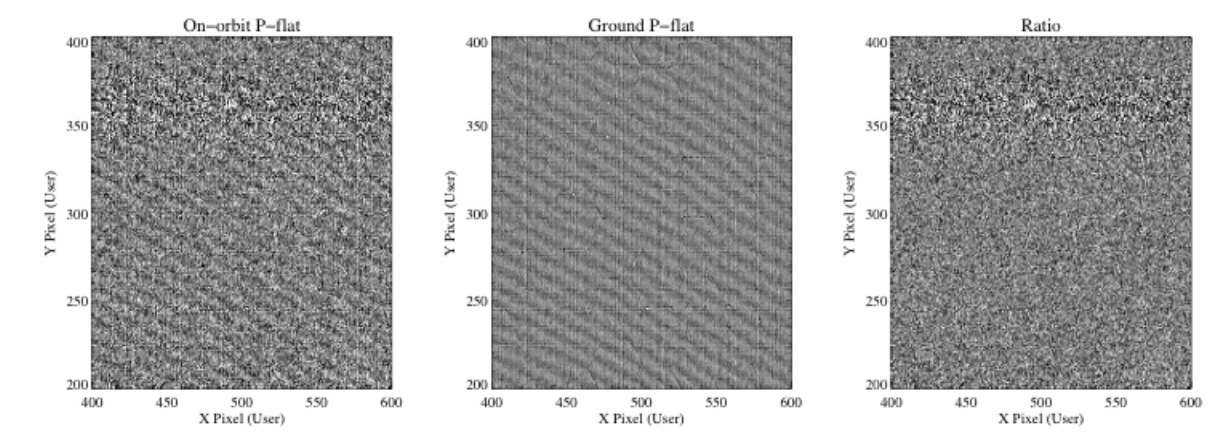

5.8.2 Use of Multiple FP-POS Settings

Fixed-pattern noise in the COS detectors limits the S/N that can be achieved in a single exposure to 15–25 per resolution element for the FUV and 50 for the NUV. To achieve higher S/N ratios one can obtain a series of exposures, each slightly offset in the dispersion direction, causing spectral features to fall on a different part of the detector. For STIS and GHRS these motions are known as FP-SPLITs. For COS these motions are specified by the `FP-POS` optional parameter.

Four `FP-POS` offset positions are available: a nominal position (0), two positions toward longer wavelengths (–2 and –1), and one position toward shorter wavelengths (+1). Positions –2, –1, 0, and +1 are designated respectively as `FP-POS=1`, `2`, `3`, and `4`. The nominal position, `FP-POS=3`, is the setting used to define the wavelength range associated with the grating central wavelengths (Table 5.3 and Table 5.4). In pipeline processing **calcos** creates individual calibrated spectra for each `FP-POS` position, then aligns and combines them into a merged spectral product, using only good-quality data at each wavelength.

The optical mechanism on which the grating is mounted is rotated by one step for each adjacent `FP-POS` position. The amount that a particular spectral feature moves in the dispersion direction on the detector is approximately 250 pixels per step for the FUV channel and 52 pixels for the NUV. The corresponding wavelength shifts for each grating are given in Chapter 13. There is a preferred direction for moving the grating mechanism. Overheads are reduced if `FP-POS` exposures are obtained in increasing order (see Section 9.5). When moving to a new grating or central-wavelength setting you may select any `FP-POS` position without paying an additional overhead penalty. Thus, the most efficient order is `FP-POS=1, 2, 3, 4`, as it requires no backward motion of the grating mechanism.

A wavelength calibration exposure will be obtained each time the `FP-POS` changes. For `FLASH=YES` exposures the time-since-last-grating-motion clock is not reset by an `FP-POS` movement. However, there will always be at least one lamp flash during each individual `FP-POS` exposure. For `FLASH=NO` exposures a separate wavelength calibration exposure will be taken for each `FP-POS` position change.

Using all four FP-POS for each CENWAVE can be achieved by using the FP-POS=ALL parameter in APT for each CENWAVE or by spreading out the four FP-POS positions over multiple orbits within a visit for each CENWAVE or over multiple visits to the same target.

Requirements for Use of Multiple FP-POS Settings

The use of multiple `FP-POS` positions for each `CENWAVE` setting of the COS FUV detector is required unless a strong scientific justification to do otherwise is provided in Phase I. Using multiple `FP-POS` positions improves the limiting S/N and minimizes the effects of flat-field artifacts. The use of multiple `FP-POS` positions is especially important for the FUV detector as the fixed pattern noise is larger and more poorly characterized than that of the NUV detector. In addition the consistent use of multiple FP-POS positions in the G130M and G140L/1105 settings will spread the bright geocoronal Lyman-α illumination and significantly delay the appearance of gain sag effects.

Since this simple shift-and-add technique significantly improves the signal-to-noise ratio of the resulting spectrum, and will extend the lifetime of the COS FUV detector, the use of multiple FP-POS for each CENWAVE setting is required for science observations. *Proposers using the FUV channel of COS, but who do not intend to use* ***all four*** *`FP-POS` settings for each `CENWAVE` setting, must justify their observing strategy in their Phase I proposals. A modest reduction in observational overheads will not normally be considered sufficient justification for not using all four `FP-POS` settings.* Using all four FP-POS for each CENWAVE can be achieved by using the FP-POS=ALL parameter in APT for each CENWAVE or by spreading out the four FP-POS positions over multiple orbits within a visit for each CENWAVE or over multiple visits to the same target.

5.9 COS Spectroscopy of Extended Sources

COS spectra of extended objects can have significantly lower resolution than those of point sources, depending on the spatial distribution of the source. For example, measurements of Lyman-α airglow lines, which uniformly fill the COS aperture, show R = 1450 for G130M and R = 165 for G140L. Filled-aperture observations of SNR N132D confirm R ~ 1500 for both FUV M gratings (France et al. 2009, ApJL, 707, L27). In the NUV the situation is much worse, because a source that fills the aperture will lead to cross-contamination among the three spectral stripes on the MAMA detector.

A similar situation arises when multiple point sources fall within the aperture. COS was designed to resolve two point sources separated by 1 arcsec in the cross-dispersion direction, but on-orbit measurements of the XD profile reveal that such observations are possible only for selected grating and central-wavelength settings (Section 5.1.9). Note that light from a point source falling more than 0.4 arcsec from the center of the PSA will be attenuated (Section 8.8.2).

While the performance of COS when observing extended targets was never optimal, the extended target flux calibration was still reasonably accurate up to the COS/FUV move to Lifetime Position 3 (LP3) in February 2015. This is however not the case at LP3 due to its location, close to the gain-sagged Lifetime Position 1 (LP1) regions, and the new two-zone extraction algorithm required by the small LP1-LP3 separation (see February 2015 COS STAN).

For extended targets larger than ~0.6" (FWHM), the spatial distribution of incoming light on the COS/FUV detector is significantly wider than that of a point source. As a result, the light distribution of extended targets may overlap low-gain regions at LP1, located 2.5" above LP3, and may incur significant flux loss.

In addition, the two-zone extraction algorithm implemented to support LP3 science observations extracts counts in 2D profiles that tightly follow the optical footprint of the light from a point source on the detector, thus reducing the number of dark counts and avoiding large chunks of spectra from being discarded when bad or LP1 sagged pixels overlap with the wings of those profiles. This algorithm therefore provides accurate calibration for point sources, but the flux calibration of extended targets (i.e., with FWHM larger than ~0.6") may be significantly off because the spatial distribution of their flux on the detector is wider than that of a point source.

Combined with the aperture vignetting, these effects may result in an unreliable flux calibration for COS/FUV/LP3 observations of extended targets (larger than 0.6" FWHM).

Starting with Cycle 23 and continuing in Cycle 24, COS observers are required to define their targets as EXTENDED = "YES" or "NO" at the target description level. This new field is required for COS observations only. This change is intended to provide an indication as to whether the source extent might be large enough to affect the reliability of the default pipeline extraction which is currently optimized for point source targets. In the future this keyword may also be used to allow the pipeline to use an alternate extraction procedure better suited to extended sources. Both COS FUV and NUV observations of targets with FWHM larger than about 0.6 arcsec or radius larger than 0.35 arcsec should be considered as extended. "YES" should be selected for such targets and "NO" for targets of smaller angular extent. The field should be left blank if the target is not being observed by COS. If this new target-level description keyword is not provided, APT will trigger a warning message asking the PI to define it, and any proposals submitted without a value specified for all COS targets will be sent back to the PI to be corrected. See the COS STAN articles from February and March 2015 for further details. Note that the old exposure-level EXTENDED keyword, set via the "optional parameters" prior to Cycle 23, is still present in APT but has been deprecated. As a result, the exposure-level EXTENDED keyword should no longer be selected for any exposure in Cycle 23 or later.

5.10 Wavelength Settings and Ranges

Table 5.3 and Table 5.4 show the wavelength ranges recorded on the detectors for each valid combination of grating and central-wavelength setting at the nominal `FP-POS=3` position (Section 5.8.2). The wavelength ranges spanned at other `FP-POS` settings may be estimated using the `FP-POS` step values provided in Chapter 13. Note, however, that uncertainties in the positioning of the Optics Select Mechanisms (Section 3.1.3) correspond to about half of an `FP-POS` step. These wavelength ranges are subject to change as the instrumental calibration evolves. The most recent measurements are available from the COS website

CHAPTER 6:

Imaging with COS

In this chapter…

6.1 Introduction to COS Imaging

The COS NUV channel has a plate scale of 23.5 mas per pixel, which provides the highest spatial sampling of any instrument aboard *HST*. Figure 6.1 shows an image of Pluto and its moon Charon obtained with COS. COS images are fully corrected for the telescope's spherical aberration, though not for the zonal (polishing) errors on its primary and secondary mirrors (Section 3.3). Because the optics image the sky onto the detector, rather than the aperture, COS images extend to a radius of 2 arcsec, but suffer considerable vignetting at radii greater than 0.4 arcsec, as shown in Figure 6.2.

To request an imaging observation specify `CONFIG = COS/NUV` and `MODE = TIME-TAG` or `ACCUM`. In `TIME-TAG` mode the minimum `BUFFER-TIME` is `80` seconds, which may be longer than the expected exposure time. ACCUM mode is recommended for such short exposures. The minimum COS exposure duration is 0.1 s, as discussed in Section 5.3. MIRRORB and/or the BOA can be used to obtain images of bright objects, but at some cost in spatial resolution; see Section 8.4 for details.

For long exposures, drifting of the Optics Select Mechanisms (OSMs) can be significant, ~ 3.5 pixels in the *x* dimension with an *e*-folding time of ~ 50 minutes (COS ISR 2010-10). Observers taking images with exposure times longer than ~ 200 s are urged to use `MODE=TIME-TAG` and `FLASH=YES`. The resulting lamp flash will illuminate the WCA, allowing one to track the drift accurately. By default, `FLASH=NO` for all imaging modes.

COS imaging in `TIME-TAG` mode allows for high-speed NUV photometry with a temporal resolution of 32 ms. STIS is capable of much finer time resolution (125 μs), but at lower sensitivity.

Figure 6.1: Pluto and Charon Observed with COS

NUV exposure of Pluto and Charon, separated by 0.8 arcsec. The exposure time is 25 s. Note that the pixel numbers refer only to this sub-section of the full image. Image courtesy of J. Green.

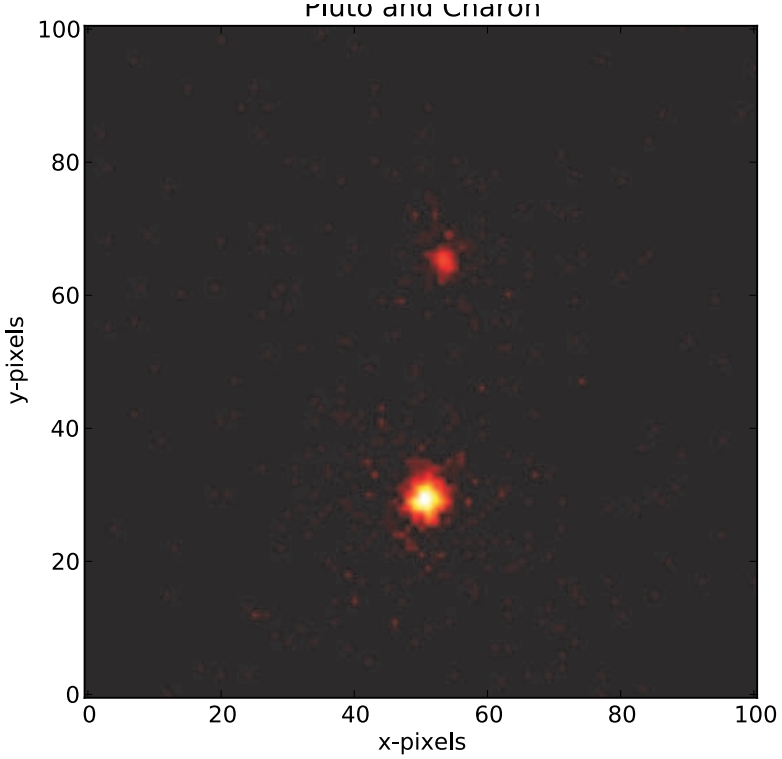

Figure 6.2: Relative Throughput of the COS PSA in NUV Imaging Mode

Throughput variation as a function of the offset position. See "COS NUV Image Performance" (COS ISR 2010-10, Goudfrooij 2010).

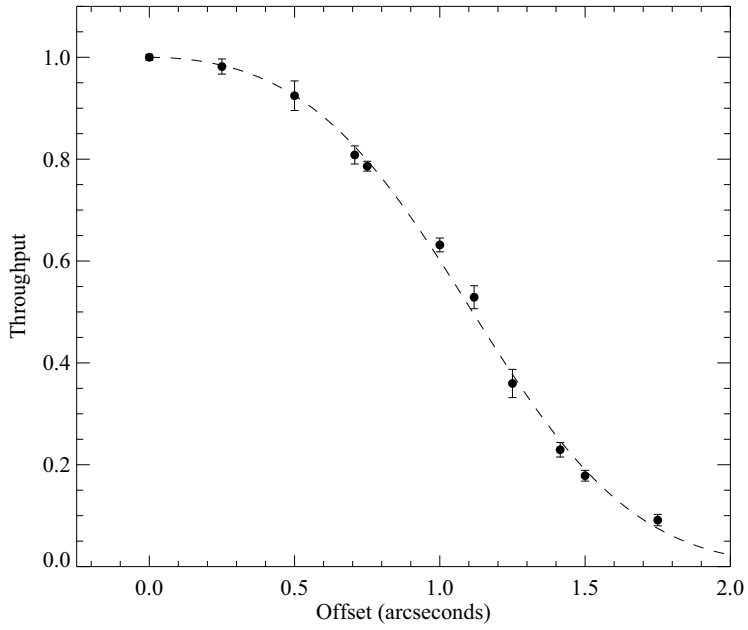

6.2 Sensitivity

When used in imaging mode, COS concentrates the target's NUV flux into a diffraction-limited image rather than dispersing the light. The local count rate limit for COS/NUV, 50 count/s/pixel (Table 10.1), is easily reached, even for fairly faint objects. Observers should use the COS Exposure Time Calculator (ETC) to get an accurate estimate of expected count rates, but the following values will provide a guide. These have been calculated for a flat-spectrum source (flux independent of wavelength). The approximate flux levels where the limiting count rate is reached are listed in Table 6.1.

Table 6.1: Approximate Flux Limits for a Flat Spectrum

Aperture and Mirror	Flux Limit (erg cm^{-2} s^{-1} $Å^{-1}$)
PSA + MIRRORA	2×10^{-15}
BOA + MIRRORA	4×10^{-13}
PSA + MIRRORB	4×10^{-14}
BOA + MIRRORB	7×10^{-12}

When `MIRRORA` is used for imaging observations, sensitivity extends from about 1600 to 3300 Å, peaking at ~ 2300 Å (Figure 6.3). Both `MIRRORA` and `MIRRORB` have sensitivity tails that extend to about 8000 Å (see COS ISR 2010-10, Goudfrooij 2010), so care must be taken when observing cool stars ($T_{eff} < 5000$ K) and other red objects, as high count rates at long wavelengths could damage the detector. When MIRRORB is employed, its use of a first-surface reflection allows short-wavelength light to reach the detector. Sensitivity extends to the NUV detector cut-off, about 1150 Å, for the primary image.

Figure 6.3: Effective Area for COS NUV Imaging with the PSA

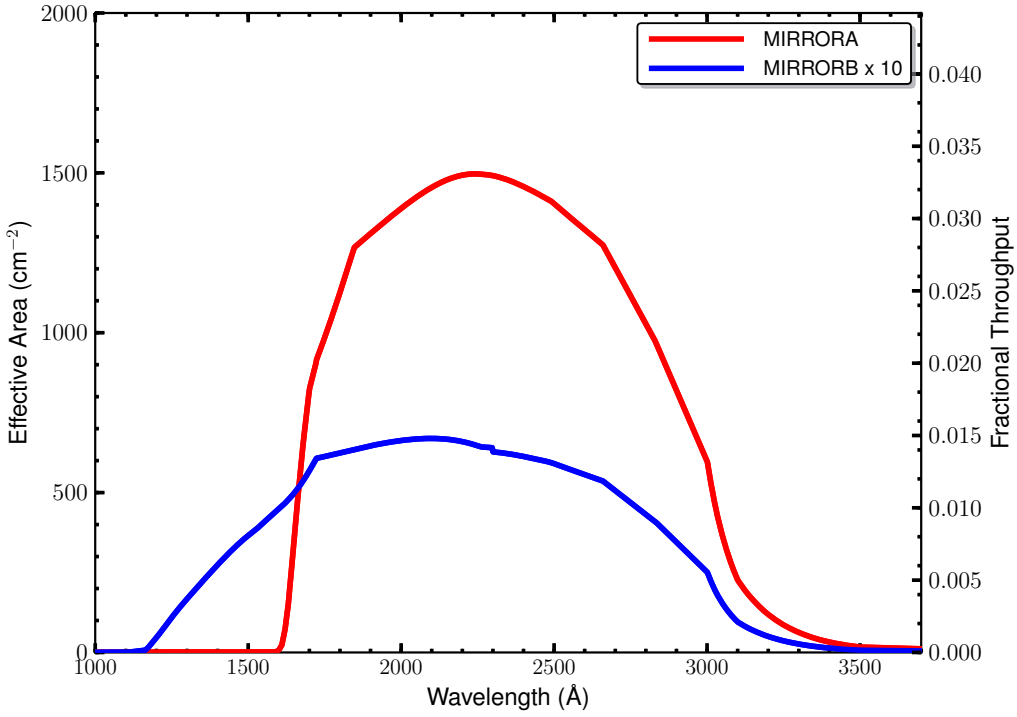

6.3 Image Characteristics

A two-dimensional Gaussian fit to a typical imaging point-spread function (PSF) has a FWHM of 1.97 pixels (47.1 mas), with 13.4% of the light in the brightest pixel. Because the *HST* focus varies with orbital phase, FWHM values can range from 1.8 to 2.4 pixels.

As discussed in Section 3.3, mid-frequency wavefront errors (MFWFEs) contribute significantly to the PSF wings at wavelengths < 2500 Å, so the spatial resolution of a point source will depend somewhat on its spectral energy distribution. For an M star, which has little photospheric flux at the shortest wavelengths, the image would be close to diffraction limited. For a hot white dwarf, the MFWFEs would have the maximum impact on the spatial resolution.

Deep images reveal the detailed shape of the COS imaging PSF. Figure 6.4 shows the PSF, averaged over 180 degrees of azimuth and plotted on a log scale to reveal its extended wings. Figure 6.5 shows a 2-dimensional gray-scale image of a deep imaging observation that reveals two low-level "ghosts" located approximately 20 pixels to the right and the upper left of the center of the PSF. The peak intensity of the brightest of the two ghosts is roughly 0.1% of that of the main PSF. These features may complicate the analysis of faint objects located in the wings of a brighter object.

Figure 6.4: Extended Wings in the COS Imaging PSF

Azimuth-averaged COS imaging PSF plotted with a logarithmic intensity scale.

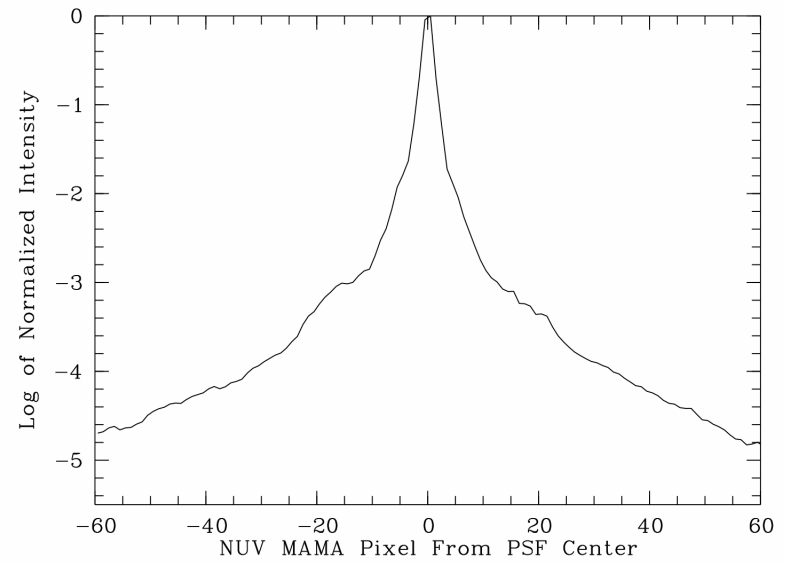

Figure 6.5: Ghosts in COS NUV Images

Negative gray-scale rendering of a deep COS NUV image of a point source. This figure is plotted with a logarithmic intensity scale and covers about 6.5 arcsec along each axis. Note the two ghost images to the right and upper left of the center of the PSF.

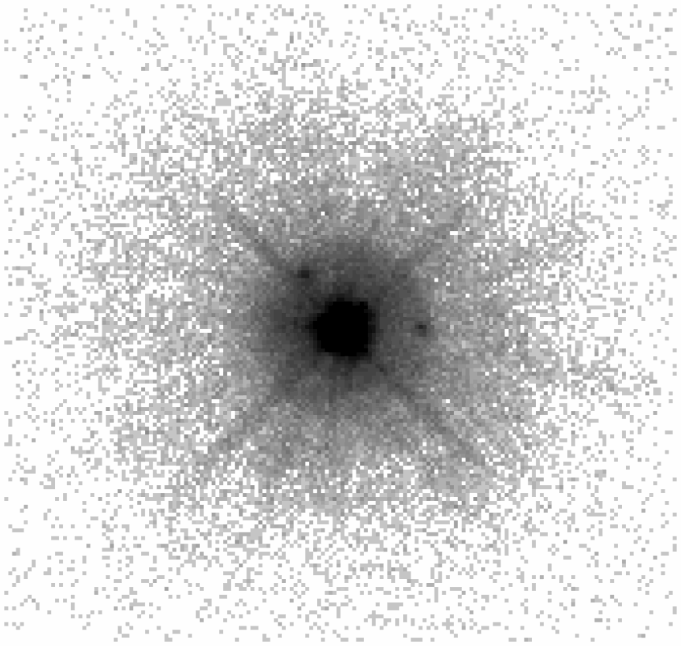

CHAPTER 7:

Exposure-Time Calculator (ETC)

In this chapter…

7.1 The COS Exposure Time Calculators

To help with proposal preparation, four COS Exposure Time Calculators (ETCs) are available on the STScI ETC webpage:

`http://etc.stsci.edu`

These calculators model spectroscopic and imaging exposures for both target acquisitions and scientific observations. They estimate count rates for given source and background parameters, and calculate either the signal-to-noise ratio for a given exposure time or the exposure time needed to achieve a desired signal-to-noise ratio. If you have a calibrated spectrum of your source you can upload it to the Exposure Time Calculators. The ETCs warn you if your observations exceed local or global brightness limits (see Table 10.1). The ETCs offer extensive on-line help that provides instructions and explains their calculations.

A unique exposure ID is assigned to each calculation performed by the ETCs, allowing results from previous calculations to be retrieved easily. *This number must be included in the appropriate box in your Phase II proposal to document your work and to facilitate Phase II review.* Proposers are urged to check the COS ETC webpage for any updates or issues related to the COS ETCs before performing ETC simulations.

The spectroscopic ETC can display the input spectrum, a simulated one-dimensional output spectrum, the S/N as a function of wavelength, and the number of counts per resolution element for the selected instrument configuration and source. These outputs can be downloaded in ASCII format. The ETC also computes the `BUFFER-TIME`, which is required for `TIME-TAG` observations. Scale this value by 2/3 and, following the discussion in Section 5.4, enter it in the Astronomer's Proposal Tool.

The imaging ETC allows for the selection of either the PSA or BOA and either MIRRORA or MIRRORB. It reports the count rate in the brightest pixel, total counts in the detector, and S/N per resolution element.

The target-acquisition ETCs return the acquisition exposure time to be entered in APT for both imaging and spectroscopic acquisitions. Target acquisition is described in Chapter 8.

7.2 Imaging Observations of Red Objects

As shown in Figure 6.3, the COS NUV channel is sensitive to wavelengths above 3200 Å, an important consideration when imaging red objects. For stars with effective temperatures above 6000 K, the effect is negligible, but it grows to about 20% at 5000 K, and below 5000 K it quickly becomes large.

If you upload a spectrum into the ETC to calculate exposure time of an imaging exposure, whether for a target acquisition or a scientific observation, be sure that the spectrum spans the full range of wavelengths to which the NUV channel is sensitive, from about 1600 Å to 12,000 Å. Failure to do so can produce a misleading result.

The COS ETC expects input spectra to extend out to 12,000 Å and will return a warning message ("Partial overlap between instrument throughput band and input spectrum") if they do not. This message indicates that the ETC may return incorrect results due to the incomplete source spectrum. Users should take care to be sure that the input source spectrum covers the entire wavelength range of the detector, accounting for any impact to the spectral coverage due to the redshift of the source.

7.3 Sensitivity, Count Rate, and S/N

A complete theoretical discussion of the exposure time as a function of instrument sensitivity and signal-to-noise ratio is given in Chapter 6 of the *STIS Instrument Handbook* and will not be repeated here. However, COS has several characteristics that simplify signal-to-noise calculations.

Both COS detectors are photon counters, which means that they have no read noise and their gain is unity. COS is optimized for point sources, and in this case the signal-to-noise ratio is given by,

$$\frac{S}{N} = \frac{C \cdot t}{\sqrt{C \cdot t + N_{pix}(B_{sky} + B_{det}) \cdot t}}$$

where

C = the signal from the astronomical source, in count s^{-1}

t = the integration time, in seconds

N_{pix} = the total number of detector pixels integrated to achieve C

B_{sky} = the sky background, in count s^{-1} $pixel^{-1}$

B_{det} = the detector dark count rate, in count s^{-1} $pixel^{-1}$

With no detector read noise, the signal-to-noise ratio is proportional to the square root of the exposure time whether the target is bright or faint compared to the backgrounds and dark count.

Note that the detector dead-time effects discussed in Section 4.1.5 and Section 4.2.5 are not included in the ETC, which will over-predict the count rates and resulting S/N ratios for bright targets.

7.4 Detector and Sky Backgrounds

The primary background sources that affect COS observations are detector dark count, earthshine, zodiacal light, and airglow emission; neither of the COS detectors suffers from read noise. The ETC allows the user to select among several levels of intensity for each of the sky backgrounds, corresponding to a variety of observing environments.

7.4.1 Detector Dark Count

Table 7.1 lists the detector dark-count rates assumed by the ETC. The dark rate values are projections for mid-Cycle 24 (April 2017). We assume that a resolution element, or "resel," spans 6 × 10 pixels on the FUV detector and 3 × 3 pixels on the NUV MAMA. The dark rate on the FUV detectors can sometimes vary by a factor of a few on very short timescales, impacting less than 5% of observations. See Sections 4.1.3 and 4.2.3 for more information.

Beginning with Cycle 21, the ETC uses separate dark rates for science observations and target acquisitions obtained with the FUV detector. **Calcos** filters the data by pulse height, while the COS flight software does not, so the effective dark rate for science data is lower than that for target acquisitions. In either mode the dark rate on the FUV detector is truly small, due in part to its windowless design. The NUV detector has a window and thus a higher dark rate.

Table 7.1: Assumed Detector Dark Count Rates

	FUV (A / B) in ACQ Mode	FUV (A / B) in Science Mode	NUV
Dark rate (counts s^{-1})	4.3 / 4.5 per cm^2 6.4×10^{-6} / 6.7×10^{-6} per pixel 3.8×10^{-4} / 4.0×10^{-4} per resel[1]	2.6 / 2.6 per cm^2 4.0×10^{-6} / 4.0^{-6} per pixel $2.4e^{-6}$ / $2.4e^{-6}$ per resel[1]	142 per cm^2 $8.9e^{-4}$ per pixel $8.0e^{-3}$ per resel[1]

1. Resel size can vary for the 1055 and 1096 central wavelengths. See Appendix B of the ETC User's Guide for more information

Figure 7.1: Sky Background Intensity as a Function of Wavelength

Earthshine (red curve) for a target 24° above the limb of the sunlit Earth, corresponding to the "high" level in the ETC. Use Figure 7.2 to estimate background contributions at other angles. The zodiacal light level (m_V = 22.7 mag per $arcsec^2$, the "average" level in the ETC, blue curve) corresponds to a helio-ecliptic latitude and longitude of 30° and 180°, respectively. The airglow line intensities are integrated fluxes, corresponding to the "Day" level in Table 7.4. The upper limit to the [OII] λ2471 intensity is shown.

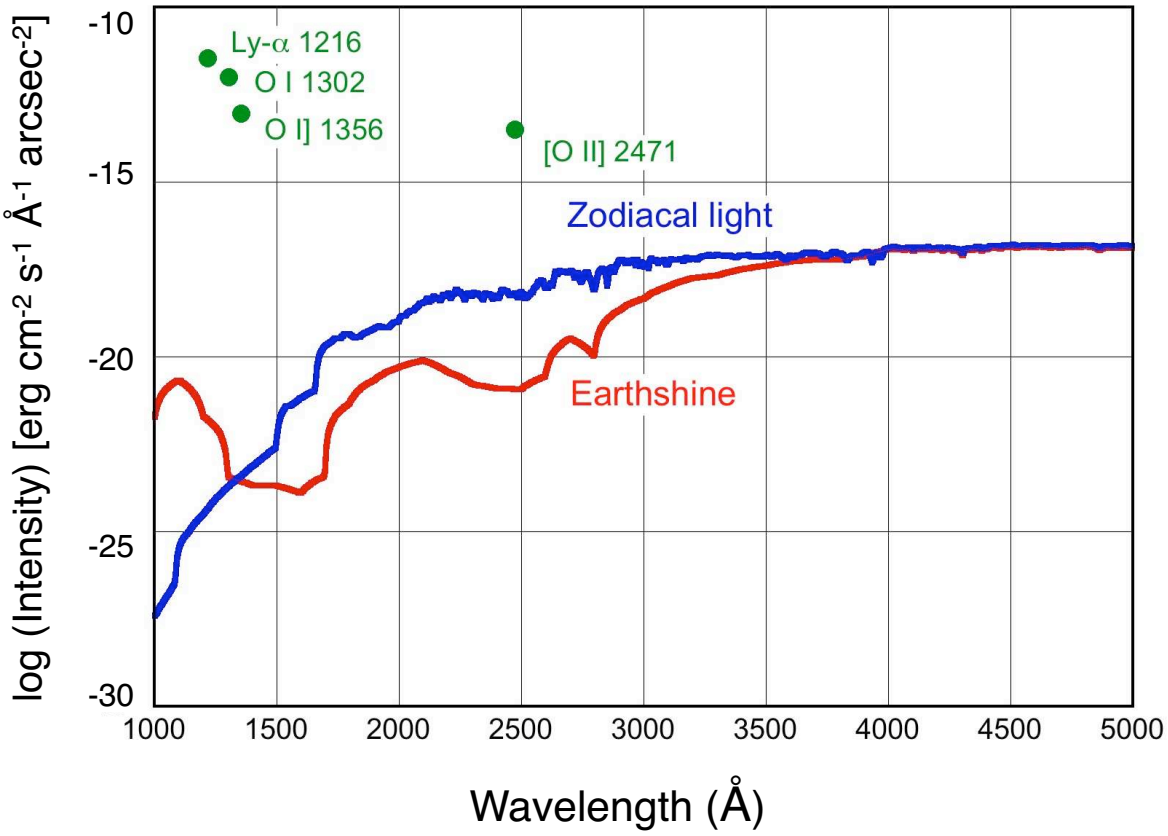

7.4.2 Earthshine

Four earthshine intensity levels, with scaling factors of (`none`, `average`, `high`, `extremely high`) = (0.0, 0.5, 1.0, 2.0), are available in the ETC. Earthshine intensity is a strong function of the angle between the target and the bright Earth limb. The earthshine surface brightness for a target 24° degrees above the limb, corresponding to the "`high`" level, is shown in Figure 7.1. The limb angle is approximately 24° when *HST* is aligned toward its orbit pole (*i.e.,* the center of the CVZ). The variation of earthshine with limb angle is shown in Figure 7.2.

Figure 7.2: Background Contributions from the Moon, Earth, and Zodiacal Light

The values are V magnitude per square arcsec due to the moon and the sunlit Earth as a function of angle between the target and the limb of the bright Earth or moon. Zodiacal light levels range between m_V = 22.1 and 23.3 mag arcsec^{-2}.

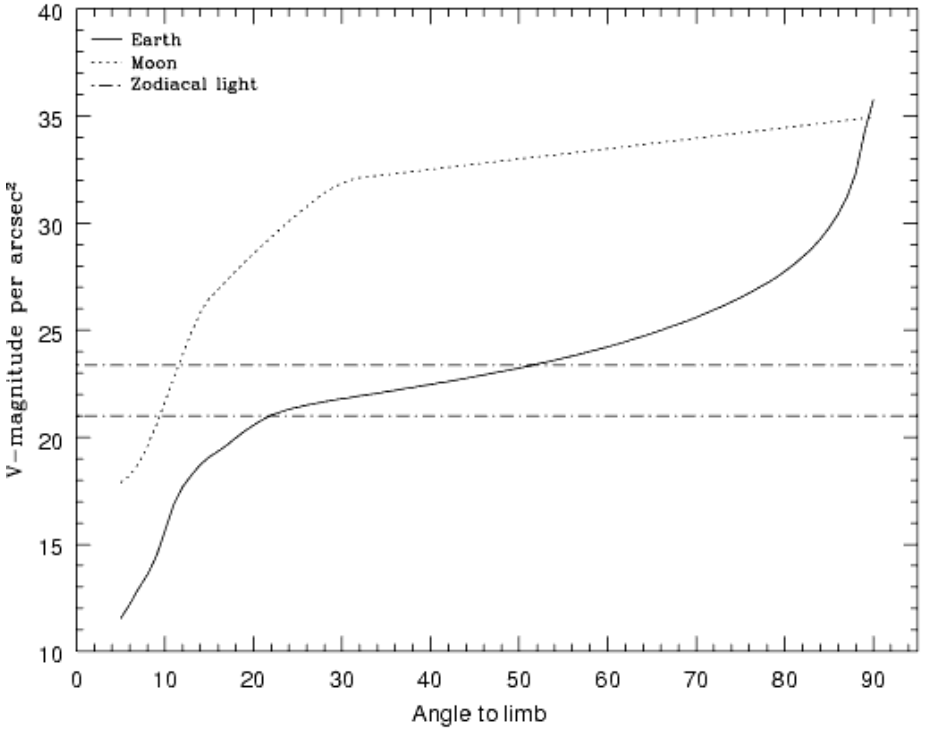

7.4.3 Zodiacal Light

Away from the airglow lines, at wavelengths between about 1300 and 3000 Å the sky background is dominated by zodiacal light, which is generally fainter than the intrinsic detector background, especially for the NUV detector. Figure 7.1 shows the zodiacal light for the "average" level in the ETC. Table 7.2 gives the variation of the zodiacal background as a function of helio-ecliptic longitude and latitude. For a target near (50°,0°) or (–50°,0°), the zodiacal light is relatively bright at m_V = 20.9 mag arcsec^{-2}, about 9 times the polar value of m_V = 23.3 mag arcsec^{-2}. These limits are plotted in Figure 7.2. The intensity levels and the factors by which they are scaled in the ETC are (`none`, `low`, `average`, `high`) = (0.0, 0.576, 1.0, 1.738), corresponding to m_V = (none, 23.3, 22.7, 22.1) mag arcsec^{-2}.

Observations of the faintest objects may need the special requirement `LOW-SKY` in the Phase II observing program. `LOW-SKY` observations are scheduled during the part of the year when the zodiacal background is no more than 30% greater than the minimum possible value for the given sky position. `LOW-SKY` also invokes the restriction that exposures will be obtained at angles greater than 40° from the bright Earth limb to minimize earthshine and the UV airglow lines. The `LOW-SKY` requirement limits the times at which targets within 60° of the ecliptic plane will be scheduled and limits visibility to about 48 minutes per orbit.

Table 7.2: Approximate Zodiacal Sky Background (V mag arcsec^{-2}) as a Function of Helioecliptic Coordinates

Helioecliptic Longitude (deg)	Helioecliptic Latitude (deg)						
	0°	15°	30°	45°	60°	75°	90°
180°	22.1	22.4	22.7	23.0	23.2	23.4	23.3
165°	22.3	22.5	22.8	23.0	23.2	23.4	23.3
150°	22.4	22.6	22.9	23.1	23.3	23.4	23.3
135°	22.4	22.6	22.9	23.2	23.3	23.4	23.3
120°	22.4	22.6	22.9	23.2	23.3	23.3	23.3
105°	22.2	22.5	22.9	23.1	23.3	23.3	23.3
90°	22.0	22.3	22.7	23.0	23.2	23.3	23.3
75°	21.7	22.2	22.6	22.9	23.1	23.2	23.3
60°	21.3	21.9	22.4	22.7	23.0	23.2	23.3
45°	SA	SA	22.1	22.5	22.9	23.1	23.3
30°	SA	SA	SA	22.3	22.7	23.1	23.3
15°	SA	SA	SA	SA	22.6	23.0	23.3
0°	SA	SA	SA	SA	22.6	23.0	23.3

Note: A value of "SA" denotes positions in the solar avoidance zone

The ETC provides the user with the flexibility to adjust both the zodiacal (`none, low, average, high`) and earthshine (`none, average, high, extremely high`) sky background components to determine if the use of `LOW-SKY` is advisable for a given program. However, the absolute sky levels that can be specified in the ETC may not be achievable for a given target. As shown in Table 7.2, the minimum zodiacal background level for an ecliptic target is m_V = 22.4 mag, which is brighter than both the low and average options with the ETC. By contrast, a target near the ecliptic pole would always have a zodiacal = `low` background in the ETC. The user is cautioned to consider sky levels carefully, as the backgrounds obtained in *HST* observations can span a significant range.

7.4.4 Airglow Emission

In the ultraviolet, the sky background contains important contributions from airglow emission lines, which vary from day to night and as a function of *HST* orbital position. These features originate mainly from hydrogen and oxygen atoms in the exosphere of the Earth. Airglow lines may be an important consideration for spectroscopic observations at wavelengths near the lines.

The brightest airglow line by far is Lyman-α at 1216 Å. The strength of the Lyman-α line varies between about 2 and 20 kilo-Rayleighs (i.e., between 6.3×10^{-14} and 6.3×10^{-13} erg/cm^2/s/arcsec^2, where 1 Rayleigh = 10^6 photons/cm^2/s per 4π steradians, which equals 3.15×10^{-17} erg/cm^2/s/arcsec^2 at Lyman-α) depending on the time of the observation and the position of the target relative to the Sun. The next-strongest feature is the O I line at 1302 Å, which rarely exceeds 10% of Lyman-α. The typical strength of the O I λ1302 line is about 2 kilo-Rayleighs (about 7×10^{-14} erg/cm^2/s/arcsec^2) on the daylight side and about 150 times fainter on the night side of the *HST* orbit. The O I] λ1356 and [O I] λ2471 lines may appear in observations on the daylight side of the orbit, but these lines are at least 10 times weaker than the O I λ1302 line. The widths of the lines also vary, but a representative value for a temperature of 2000 K is about 3 km/s. Airglow emission from N I λ1200 is also seen, particularly on the day side of the orbit, with fluxes up to 1.6×10^{-16} erg/cm^2/s/arcsec^2. The N I line is not included in the ETC. Airglow emission lines are essentially unresolved at the resolution of COS, but the emission fills the aperture in the spectral and spatial directions. For the FUV modes, the aperture width is approximately 114 pixels, or 1.12, 1.36, and 9.46 Å for G130M, G160M, and G140L, respectively. For the NUV modes, the aperture width is approximately 105 pixels, or 3.87, 3.46, 4.18, and 41.21 Å for G185M, G225M, G285M, and G230L, respectively.

The COS ETC provides four airglow intensity levels (`none`, `low`, `average`, `high`), whose scaling factors depend on the airglow line considered: (0.0, 0.1, 0.5, 1.0) for Lyman-α, (0.0, 0.0667, 0.5, 1.0) for O I λ1302, (0.0, 0.006, 0.5, 1.0) for O I] λ1356, and (0.0, 0.005, 0.5, 1.0) for [O II λ2471.

It is possible to request that exposures be taken when *HST* is in the earth's shadow to minimize airglow emission (e.g., if you are observing weak lines at 1216 Å or 1302 Å) using the special requirement `SHADOW`. Exposures using this special requirement are limited to roughly 25 minutes per orbit, exclusive of the guide-star acquisition (or reacquisition) and can be scheduled only during a small percentage of the year. `SHADOW` reduces the contribution from the airglow emission lines by roughly a factor of ten, while the continuum earthshine is essentially nil. If you require `SHADOW`, you should request and justify it in your Phase I proposal (see the *Call for Proposals*).

An alternate strategy for reducing the effects of airglow emissions is to use time-resolved observations, so that any data badly affected by airglow emission can simply be excluded from the final co-addition. This can be done either by using `TIME-TAG` mode, the default for all COS observations if the target is not too bright, or by taking a series of short (~ 5 min) `ACCUM` mode exposures over the course of each orbit.

As noted, geocoronal Lyman-α is by far the strongest airglow feature. On the day side of the *HST* orbit, when Lyman-α is at its strongest, it will produce a net count rate

of 20 counts/s/resel, too faint to be a safety concern, but bright enough to make a significant contribution to gain sag on the FUV detector (Section 4.1.7).

7.4.5 Tabular Sky Backgrounds

Table 7.3 lists the `high` sky background numbers as plotted in Figure 7.1. The *high* sky values are defined as the earthshine at 24° from the limb and by the average zodiacal light of m_V = 22.7 mag. The quoted values represent the zodiacal and earthshine backgrounds (excluding the contributions from airglow emission lines) averaged over each wavelength interval. The line intensities of some important airglow lines in the COS bandpass are listed in Table 7.4.

Table 7.3: Earthshine and Zodiacal Light in the COS PSA

Wavelength (Å)	Earthshine	Zodiacal Light	Total
1000	6.48 E–7	1.26 E –12	6.48 E –7
1100	1.66 E –6	6.72 E –11	1.66 E–6
1200	4.05 E–7	6.23 E–10	4.06 E –7
1300	2.66 E–8	3.38 E –9	2.99 E–8
1400	2.28 E –9	1.32 E–8	1.54 E–8
1500	1.95 E–9	2.26 E–7	2.28 E–7
1600	1.68 E–9	1.14 E–6	1.14 E–6
1700	6.09 E–8	3.19 E–5	3.19 E–5
1800	6.19 E–7	6.63 E–5	6.69 E–5
1900	2.30 E–6	1.05 E–4	1.07 E–4
2000	5.01 E–6	2.07 E–4	2.12 E–4
2100	6.97 E–6	5.95 E–4	6.02 E–4
2200	3.94 E–6	9.82 E–4	9.86 E–4
2300	1.83 E–6	9.67 E–4	9.69 E–4
2400	1.27 E–6	1.05 E–3	1.05 E–3
2500	1.37 E–6	1.01 E–3	1.01 E–3
2600	6.33 E–6	2.32 E–3	2.32 E–3
2700	2.66 E–5	4.05 E–3	4.08 E–3
2800	3.79 E–5	3.67 E–3	3.71 E–3
2900	2.17 E–4	7.46 E–3	7.68 E–3
3000	4.96 E–4	8.44 E–3	8.94 E–3
3100	1.04 E–3	9.42 E–3	1.05 E–2
3200	1.72 E–3	1.10 E–2	1.27 E–2
3300	2.18 E–3	1.34 E–2	1.56 E–2

Table 7.3: Earthshine and Zodiacal Light in the COS PSA (Continued)

Wavelength (Å)	Earthshine	Zodiacal Light	Total
3400	3.12 E–3	1.30 E–2	1.62 E–2
3500	4.06 E–3	1.31 E–2	1.72 E–2
3600	5.15 E–3	1.24 E–2	1.77 E–2
3700	5.89 E–3	1.49 E–2	2.18 E–2
3800	6.19 E–3	1.41 E–2	2.03 E–2
3900	7.80 E–3	1.39 E–2	2.17 E–2
4000	1.14 E–2	2.07 E–2	3.21 E–2
4250	1.13 E–2	2.17 E–2	3.40 E–2
4500	1.33 E–2	2.53 E–1	3.86 E–2
4750	1.35 E–2	2.57 E–2	3.92 E–2
5000	1.30 E–2	2.50 E–2	3.80 E–2

These rates correspond to the high level in the ETC and are listed in units of 10^{-15} erg cm^{-2} s^{-1} Å^{-1} for the total COS PSA, which is 4.91 arcsec^2 in area.

Table 7.4: Typical Strengths of Important Ultraviolet Airglow Lines

Airglow features	Intensity					
	Day			Night		
	Rayleighs	10^{-15} erg cm^{-2} s^{-1} arcsec^{-2}	10^{-15} erg cm^{-2} s^{-1} per PSA	Rayleighs	10^{-15} erg cm^{-2} s^{-1} arcsec^{-2}	10^{-15} erg cm^{-2} s^{-1} per PSA
O I λ911	17	0.7	3.5	8.3	0.35	1.7
O I λ989	161	6.2	30	0.6	–	–
H I λ1026	571	21	105	2.7	–	–
O I λ1027	64	2.4	12	0	–	–
O I λ1152	28	0.93	4.6	0	–	–
N I λ1200[1]	5.2	0.16	0.8	0.26	0.008	0.04
H I λ1216	20,000	630	3100	2,000	63	310
O I λ1302	2,000	59	290	13	0.38	1.9
O I] λ1356	204	5.8	28	1.3	0.035	0.17
[O II λ2471	45	0.70	3.4	1	–	–

1. This feature is not included in the ETC.

7.5 Extinction Correction

Extinction can dramatically reduce the observed intensity of your source, particularly in the ultraviolet. Figure 7.3 shows A_λ/A_V values applicable to our Galaxy, taken from Cardelli, Clayton, & Mathis (1989, ApJ, 345, 245) assuming R_V = 3.1. This corresponds to the *Milky Way Diffuse (Rv=3.1)* selection of the ETC.

Extinction curves have a strong metallicity dependence, particularly at ultraviolet wavelengths. Sample extinction curves are presented in Gordon et al. [2003, ApJ, 594, 279 (LMC Average, LMC 30 Dor Shell, and SMC Bar)], Calzetti et al. [2000, ApJ, 533, 682 (starburst galaxies)], and references therein. At lower metallicities, the 2200 Å bump that is so prominent in the Galactic extinction curve disappears, and $A_\lambda/E(B–V)$ increases at shorter UV wavelengths.

The ETC allows the user to select among a variety of extinction curves and to apply the extinction correction either before or after the input spectrum is normalized. Be aware that not all extinction laws in the ETC extend below 1200 Å, which may cause incorrect calculations for the 1222, 1055, and 1096 Å central wavelengths.

Figure 7.3: Extinction in Magnitude as a Function of Wavelength
The Galactic extinction model of Cardelli et al. (1989), computed for R_V = 3.1.

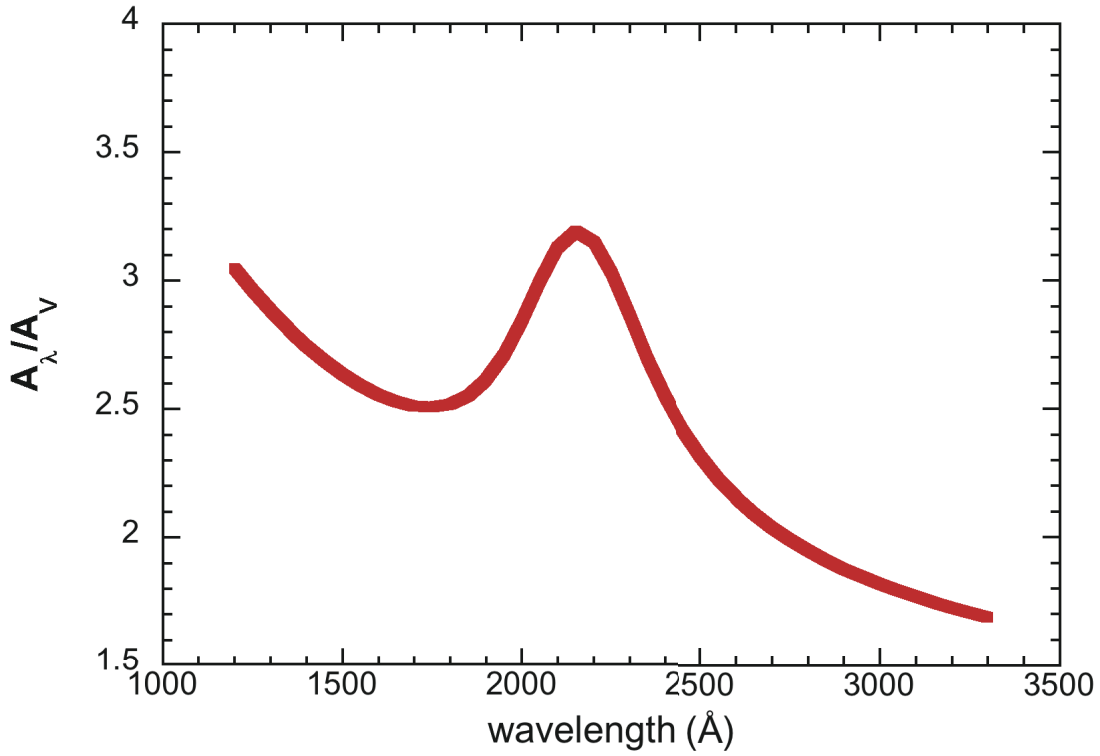

7.6 Examples

We present a few examples of how the COS ETCs may be used. They illustrate the information that is returned by the ETCs and how they can be used to plan your observations. Please note that the calculations presented have not been updated for Cycle 24.1 and as such some discrepancies between the results below and current ETC predictions might exist.

7.6.1 A Flat-Spectrum Source

One often does not know the exact spectrum shape of the object to be observed, so the answer to a simple question is desired: how long will it take to achieve a given signal-to-noise ratio at a given wavelength if the flux at that wavelength is specified? The easiest way to determine this is to use a flat spectrum as input. How long will it take to achieve S/N = 10 per resolution element at 1320 Å for a point source with a flux of 10^{-15} erg cm^{-2} s^{-1} Å^{-1} using a medium resolution grating?

Only the G130M grating covers the desired wavelength at medium resolution, but several choices of central wavelength are available. We select the 1309 Å setting. We enter these values into the spectroscopic ETC, select the Primary Science Aperture (PSA), select "Exposure time needed to obtain a S/N ratio of 10.0", enter the specified wavelength of 1320 Å, and select "Point Source" as the source type. For the spectrum distribution, choose a flat continuum in F_λ. Make sure the reddening, *E(B–V)*, is set to 0. Normalize the target to 10^{-15} erg cm^{-2} s^{-1} Å^{-1} at 1320 Å. The zodiacal light, earthshine, and airglow were not specified, so we choose average values.

When this case is computed with the ETC, we find the required time is 17,660 s; the total count rates are 66 and 271 counts s^{-1} in detector Segments A and B, respectively, well below the safety limit; the count rate in the brightest pixel has 0.096 counts s^{-1}, also well within the safe range (but see below); and the buffer time indicated by the ETC is 7004 seconds (COS.sp.539442).

What if somewhat higher *S/N* were desired and one were willing to devote 10 *HST* orbits to the observation? Assuming that each orbit allows 50 minutes of observing time (ignoring the acquisition time here), we find that in 30,000 seconds we will get S/N = 13.0 per resel. Note that $(30{,}000/17{,}660)^{1/2} = (13.0/10.0)$. That is, the *S/N* ratio scales as $t^{1/2}$, as stated in Section 7.3.

If a low-resolution observation is acceptable, then one could switch to the G140L grating. With a grating setting of 1105 Å and S/N = 10 per resel, we find the required exposure time is 2833 s, considerably less than the medium-resolution case required.

Note that the sensitivity of G130M is higher than that of G140L once resolving power is taken into account. In other words, a G130M spectrum that is rebinned to the same resolution as a G140L spectrum can be obtained in less time for a given S/N, although, of course, with diminished wavelength coverage. If only a limited portion of the source's spectrum is of interest, using G130M is more efficient than using G140L.

These cases also illustrate that the earthshine and zodiacal light are completely negligible in the FUV, unless the target flux is much lower than that considered here.

This is also true of the airglow if the wavelength of interest is far from the airglow lines. Of course, the airglow cannot be ignored in terms of the total count rate on the detector, or the local count rate if the source contributes at the same wavelengths as the airglow lines.

This is a toy example. For most targets, a more realistic model spectrum would be used to estimate exposure times and test for bright-object violations.

If only a limited portion of the source's spectrum is of interest, using G130M and binning over wavelength is more efficient than using G140L.

7.6.2 An Early-Type Star

We wish to observe an O5V star at medium spectral resolution at a wavelength of 1650 Å. We know that the star has a magnitude of $V = 16$. How long will it take to obtain S/N = 15?

We select the G160M grating with a central wavelength of 1623 Å. We select a Kurucz O5V stellar model and set the normalization to be Johnson $V = 16$ mag. We find that the required exposure time is 910 s.

Suppose this star is reddened, with $E(B–V) = 0.2$. We select the *Milky Way Diffuse* (R_V=*3.1)* extinction law, which is shown in Figure 7.3. We must now decide if this extinction is to be applied before or after the normalization. Since the star has a measured magnitude, we want to apply the reddening before normalization. Otherwise, the extinction would change the V magnitude of the stellar model. Making this selection, we find that S/N = 15 can be obtained in 2165 s (COS.sp.539447). The ETC returns a `BUFFER-TIME` of 2753 s. To be conservative, we scale it by 2/3 to get 1835 s.

7.6.3 A Solar-Type Star with an Emission Line

We want to observe a solar-type star with a narrow emission line. Consider the Si II λ1810 feature with the following parameters: FWHM = 30 km s^{-1} or 0.18 Å at 1810 Å, and integrated emission line flux of 1×10^{-14} erg cm^{-2} s^{-1}. The measured magnitude of the star is $V = 12$ mag. The desired exposure time is 1000 s.

In the ETC we select a G2V star and an NUV grating, G185M, set to a central wavelength of 1817 Å. We request an exposure time of 1000 s and specify that the S/N be evaluated at 1810 Å. We add an emission line with the line center at 1810 Å, FWHM=0.18 Å, and an integrated flux of 10^{-14} erg cm^{-2} s^{-1}. We specify the normalization as Johnson $V = 12$ mag. We set the zodiacal and earthshine to be `average`.

The ETC returns S/N = 16.4 per resel (COS.sp.539448). The local and global count rates are within safe limits. The recommended buffer time is 2326 s. This `BUFFER-TIME` exceeds the exposure time of 1000 s, so, following the procedure

outlined in Section 5.4 we set the BUFFER-TIME to 2/3 of the BUFFER-TIME value returned by the ETC, which is 1551 s.

7.6.4 A Faint QSO

An important science goal for the design of COS was to obtain moderate S/N spectra of faint QSOs in the FUV. In the ETC, use the FOS-based QSO spectrum (in the Non-Stellar Objects menu) and choose G130M at 1309 Å, S/N = 20, and a continuum flux of 10^{-15} erg cm^{-2} s^{-1} $Å^{-1}$ at 1320 Å. The indicated exposure time is 69,843 s, or about 23.3 orbits (COS.sp.539450). The source count rate is 0.001 count/s, with a background rate of 1.410×10^{-4} count/s, seven times less than that of the source. The background is completely dominated by the dark current of the detector. The count rate over the entire detector is 352 count/s, well below any safety limits, and the maximum BUFFER-TIME is 6705 s. Scaling by 2/3 yields 4470 s for the BUFFER-TIME.

CHAPTER 8:

Target Acquisitions

In this chapter…

8.1 Introduction

The COS science apertures are 2.5 arcsec in diameter. An observation will yield high-quality data only if the target is properly centered in the science aperture. This chapter discusses the available target-acquisition (TA) methods, demonstrates the dependence of data quality on centering accuracy, and recommends acquisition scenarios for various combinations of target coordinate accuracy and brightness. Recommended parameters for all COS TA modes are presented in Section 8.9.

Based on improvements in the COS-to-FGS alignment, together with an analysis of the distribution of positional errors in the GSC2, we estimate that an *HST* guide-star acquisition will place a target with good coordinates in the COS aperture 98.5% of the time. As a result, we do not require that all COS observations begin with an ACQ/SEARCH sequence if the uncertainty of the target coordinates is ≤ 0.4 arcsec. We do, however, recommend in almost all cases that some sort of target acquisition be performed to center the target in the aperture. The APT (the Astronomer's Proposal Tool) will issue a warning if an acquisition is omitted. Target acquisition is required only once for a series of observations in contiguous orbits (i.e., once per visit). Moving targets require an acquisition at the beginning of each orbit.

Bright-Object Protection

The COS detectors are vulnerable to damage or performance degradation if exposed to too much light. Imaging acquisitions present a special risk because they concentrate the light of an object on a small area of the detector. Users of COS must demonstrate that their targets are safe. Information on bright-object protection and screening is provided in Chapter 10.

8.2 Target Acquisition Overview

COS has four TA modes:

- **ACQ/SEARCH** performs a spiral search by executing individual exposures at each point in a square grid pattern on the sky (details are in Section 8.3). This mode can use either dispersed-light or imaging exposures.
- **ACQ/IMAGE** obtains an NUV image of the target field, moves the telescope to center the object, and obtains a second NUV image as confirmation (details are in Section 8.4). This is generally the fastest and most accurate method of target acquisition, but covers a limited area on the sky.
- **ACQ/PEAKXD** determines the centroid of the dispersed-light spectrum in the cross-dispersion (XD) direction and moves the telescope to center the object in the XD direction (details are in Section 8.5).
- **ACQ/PEAKD** centers the target in the along-dispersion (AD) direction by executing individual exposures at each point in a linear pattern along the dispersion axis (details are in Section 8.6). `ACQ/PEAKXD` should always precede `ACQ/PEAKD`, and the two should always be performed together.

Coordinate accuracy and target brightness will inform your choice of target-acquisition strategy and optional parameters. Imaging acquisitions are more precise and often faster, but restrictions on the local count rate (Chapter 10) can prevent their use. While the TA modes can be used in any order or even repeated, the recommended strategies are given in Table 8.1. We suggest evaluating these strategies in the following order:

1. NUV imaging with the fastest allowable combination of aperture and mirror to achieve the desired S/N, even if the science to follow is performed with the FUV channel.
2. Dispersed-light acquisition using the same configuration as the first science exposure, if it will use less time overall, or if the target violates local count limits.
3. Dispersed-light acquisition with a different configuration, if it will use less time overall, or if the target violates local count limits.

The scenarios outlined here are for isolated point sources. See Section 8.10 for additional information regarding crowded or complex fields and offset-target TAs.

Table 8.1: Basic COS Target Acquisition Strategies

Type	Step 1	Step 2	Step 3
Imaging (if coordinates are good to 0.4")	ACQ/IMAGE	none	none
Imaging (if coordinates are less accurate)	ACQ/SEARCH	ACQ/IMAGE	none
Dispersed-Light (coordinates good to 0.4")	ACQ/PEAKXD	ACQ/PEAKD	none
Dispersed-Light (coordinates less accurate)	ACQ/SEARCH	ACQ/PEAKXD	ACQ/PEAKD
Either Imaging or Dispersed-Light (e.g. small, extended sources)	ACQ/SEARCH	2 × 2 × 1.767" ACQ/SEARCH	none

Please Note...

- It is the responsibility of the observer to provide coordinates and proper motions with the required accuracy. Be especially mindful of nearby white dwarfs, which generally have high proper motions, and binary stars, whose motions on the sky are highly non-linear. Observations that fail because of an inaccurate target position will not be repeated. STScI cannot be responsible for target-coordinate or proper-motion errors in published or on-line catalogs, or in the literature. If there is any doubt that the available coordinates meet the required accuracy, then an ACQ/SEARCH should be performed.
- If a target falls near the edge of the aperture at the initial pointing, the ACQ/IMAGE and ACQ/PEAKXD algorithms may miscalculate its position. Users who require the best possible photometric or absolute wavelength accuracy may wish either to begin with an ACQ/SEARCH to ensure that the target is reasonably well centered before the final stages of the acquisition are performed, or to perform an extra ACQ/IMAGE or ACQ/PEAKXD in case the observation at the initial pointing was partially vignetted.
- At the present time, the new central-wavelength settings for G130M (1055, 1096, and 1222 Å) cannot be used for target acquisitions.
- For ACQ/IMAGE exposures, both the preliminary and confirmation images are downlinked and delivered to the observer. For the other three TA modes, no images or spectra are recorded.

8.3 ACQ/SEARCH Acquisition Mode

In ACQ/SEARCH mode, the telescope is moved in a spiral pattern on the sky to cover a square grid up to 5 × 5 steps in size. At each scan point, the telescope stops and data are collected. A two-dimensional array containing the total counts measured at

each dwell point is constructed. After completion of the full $n \times n$ pattern, the target position is calculated as described below, and the telescope is moved to center the target. Figure 8.1 illustrates the spiral search patterns that are used for ACQ/SEARCH.

Figure 8.1: The Spiral Search Patterns Used for ACQ/SEARCH

This Figure shows the 2 × 2, 3 × 3, 4 × 4, and 5 × 5 spiral search patterns executed with the default STEP-SIZE of 1.767 arcsec. The black circles represent the positions of the 2.5 arcsec-diameter science aperture, and the numbers show the sequence of steps on the sky. The outer circle in red has a radius of 3 arcsec. The green pattern represents the approximate COS science aperture PSF.

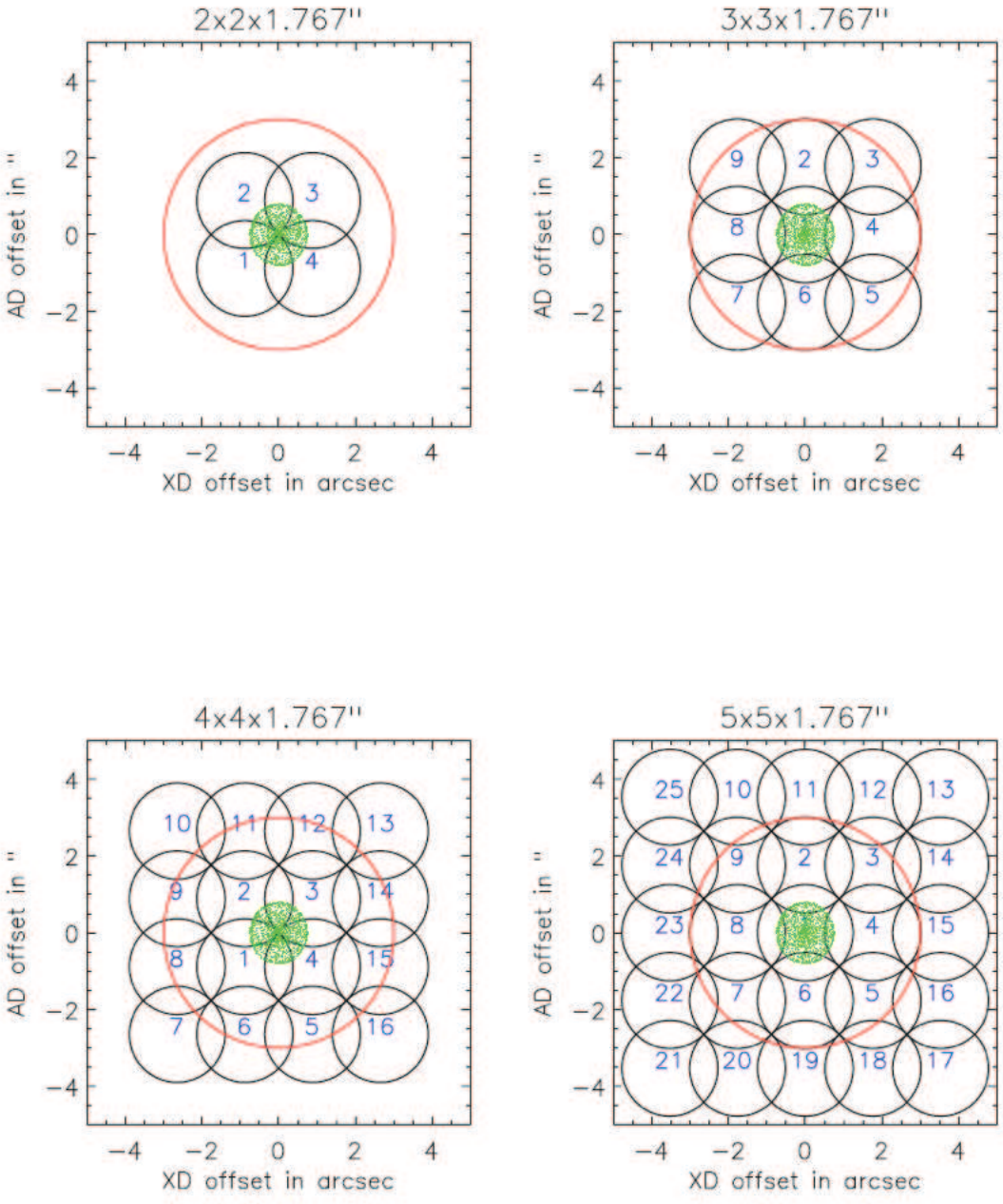

For an ACQ/SEARCH, the user must specify:

- The aperture to use, either PSA or BOA.

- The spectral element (grating or mirror) and the central-wavelength setting (if applicable). For a spectroscopic ACQ/SEARCH these will generally be the grating and central wavelength of the initial science observation. However, an observer may specify ACQ/SEARCH with a different grating and central-wavelength setting if there are advantages to doing so.
- The SCAN-SIZE, which is 2, 3, 4, or 5, corresponding to spiral patterns of 2 × 2, 3 × 3, etc.
- The STEP-SIZE, or spacing between grid points. It may be any value from 0.2 to 2.0 arcsec, but we strongly recommend using the default value of 1.767 arcsec in most cases. This value has been chosen so that no part of the sky is missed, given the aperture diameter of 2.5 arcsec ($2.5 / \sqrt{2} = 1.767$).
- The exposure time per dwell point.
- For FUV searches, users may choose to use just one of the segments, A or B, but the use of both (the default for all but G140L) is recommended. In the case of G140L ACQ/SEARCH, only Segment A data is used. However, there is a substantial overhead associated with switching from two-segment to single-segment operation (and back again); see Table 9.5.

Once the scan is complete, the flight software computes the centroid of the array and thus the position of the target. There are three centroiding options:

1. The first option is CENTER=FLUX-WT, which uses a flux-weighted centroiding algorithm to determine the center of light. It is the default for SCAN-SIZE=2.
2. A variation on CENTER=FLUX-WT is CENTER=FLUX-WT-FLR. In this case, a floor is subtracted from the counts at each dwell point before the centroid is computed. The floor is taken as the minimum number of counts seen at any one dwell point. FLUX-WT-FLR has the advantage of removing background counts, but leaves one or more points in the array with zero counts. As it can cause computational problems, FLUX-WT-FLR should not be used with SCAN-SIZE=2. CENTER-FLUX-WT-FLR should be used for SCAN-SIZE > 2 × ACQ/SEARCHs.
3. The last option for centering is CENTER=BRIGHTEST, which simply centers the dwell point with the most counts. This is straightforward, but not as accurate as the other centroiding methods. CENTER=BRIGHTEST is appropriate if coordinates are uncertain and the ACQ/SEARCH is followed by either a second ACQ/SEARCH using flux-weighted centering or an ACQ/IMAGE, or if the source is extended and it is only desired that the brightest point be in the aperture.

Table 8.2 presents the recommended ACQ/SEARCH parameters as a function of coordinate uncertainty. For all values of SCAN-SIZE > 2 we recommend CENTER=FLUX-WT-FLR as it is more accurate due to better sky and detector background suppression. The CENTER values in Table 8.2 are the current default

values for each SCAN-SIZE. Note that even SCAN-SIZE values (2 or 4) trigger additional overhead because of the telescope motion required to displace the aperture by half of a STEP-SIZE in both the dispersion and cross-dispersion directions, so that the overall pattern remains centered on the initial pointing.

Analysis of COS acquisitions indicate that a single ACQ/SEARCH acquisition, whether spectroscopic or imaging, provides a centering accuracy of 0.3 arcsec only 75% of the time. Additional TA stages are thus necessary to achieve the centering accuracy necessary to meet wavelength and photometric requirements.

Table 8.2: Recommended ACQ/SEARCH Parameters versus Coordinate Uncertainty

Coordinate uncertainty (arcsec)	SCAN-SIZE	STEP-SIZE	CENTER
$\sigma \leq 0.4$	ACQ/SEARCH not required.		
$0.4 < \sigma < 0.7$	2	1.767[1]	FLUX-WT
$0.7 < \sigma < 1.0$	3	1.767[2]	FLUX-WT-FLR
$1.0 < \sigma < 1.3$	4	1.767[2]	FLUX-WT-FLR
$1.3 < \sigma \leq 1.6$	5	1.767[2]	FLUX-WT-FLR

1. This is the default STEP-SIZE value and the largest to cover the search area without holes or gaps.
2. If target coordinate uncertainty is on the lower edge of the given range, the STEP-SIZE may be reduced slightly (*e.g.*, 1.5 arcsec) to improve centering accuracy at the expense of total area covered by the search.

8.4 ACQ/IMAGE Acquisition Mode

In ACQ/IMAGE mode COS obtains an NUV image of the target field, moves the telescope to center the object, and obtains a second NUV image as confirmation. ACQ/IMAGE may use either the primary science aperture (PSA) or the bright object aperture (BOA) and either MIRRORA or MIRRORB. All four combinations are illustrated in Figure 8.2. Note the additional structures present in images obtained with MIRRORB or the BOA: The secondary image produced by MIRRORB is half the intensity of the primary image and is displaced by 20 pixels (about 0.5 arcsec) in the direction. The BOA produces a chevron-like image whose peak is displaced in both the along-dispersion (AD) and cross-dispersion (XD) directions. When the BOA is used with MIRRORB, two distorted peaks result. In this configuration, there is some overlap between the wings of the primary and secondary peaks, but they are well enough separated to allow for reliable acquisitions. The lamp and target images of MIRRORA and MIRRORB images are offset, and vary from exposure to exposure.

Users should expect MIRRORB images to be offset from MIRRORA images by ~214 pixels in AD, and ~160 pixels in XD.

An `ACQ/IMAGE` exposure consists of the following steps:

1. An exposure of the internal Pt-Ne lamp is obtained through the WCA aperture. The onboard COS Flight Software (FSW) sets the exposure time for the lamp exposure automatically. The centroid of the WCA image is calculated by the FSW. Using the known offset between the center of the WCA and the science aperture (PSA or BOA), the location of the center of the science aperture on the detector is computed.
2. The shutter is opened and a TA image of the field is obtained. The telescope is not moved, meaning that an acquisition using `ACQ/IMAGE` will be successful only if the target lies within (or just outside of) the aperture. An area of 170 × 170 pixels, which corresponds to approximately 4 × 4 arcsec^2, centered on the aperture, is read out. This image is recorded and downlinked and becomes part of the archived data package. (It is stored in the first extension of the `_rawacq`.file).
3. A 9 × 9 pixel checkbox array is then passed over the 170 × 170 pixel image. First, the checkbox with the most counts is identified. In the unlikely instance that two checkboxes have equal counts, the first one encountered is used. The brightest 9 × 9 array is then analyzed using a flux-weighted centroiding algorithm to calculate the target position.
4. Finally, *HST* is moved to place the calculated centroid at the center of the selected aperture. A second exposure, identical to the first, is taken and recorded for later downlink as a verification of the centering. (It is stored in the fourth extension of he `_rawacq`.file). It is important to consider the throughput of the NUV MIRRORA or MIRRORB combinations when selecting a TA strategy (Section 6.2 and Figure 6.3).

Figure 8.2: Point Sources Observed with all Four Aperture/Mirror Combinations

NUV images of point sources observed through the PSA (top) and BOA (bottom) using MIRRORA (left) and MIRRORB (right). The limits of each plot represent the 170 × 170 pixel image used by ACQ/IMAGE. Also shown are the COS aperture (blue circle of radius 1.25") and the 9 × 9 checkbox used by ACQ/IMAGE. Histograms show the AD and XD profiles. The pointing is typical of that expected after an ACQ/SEARCH, but before additional peak-ups.

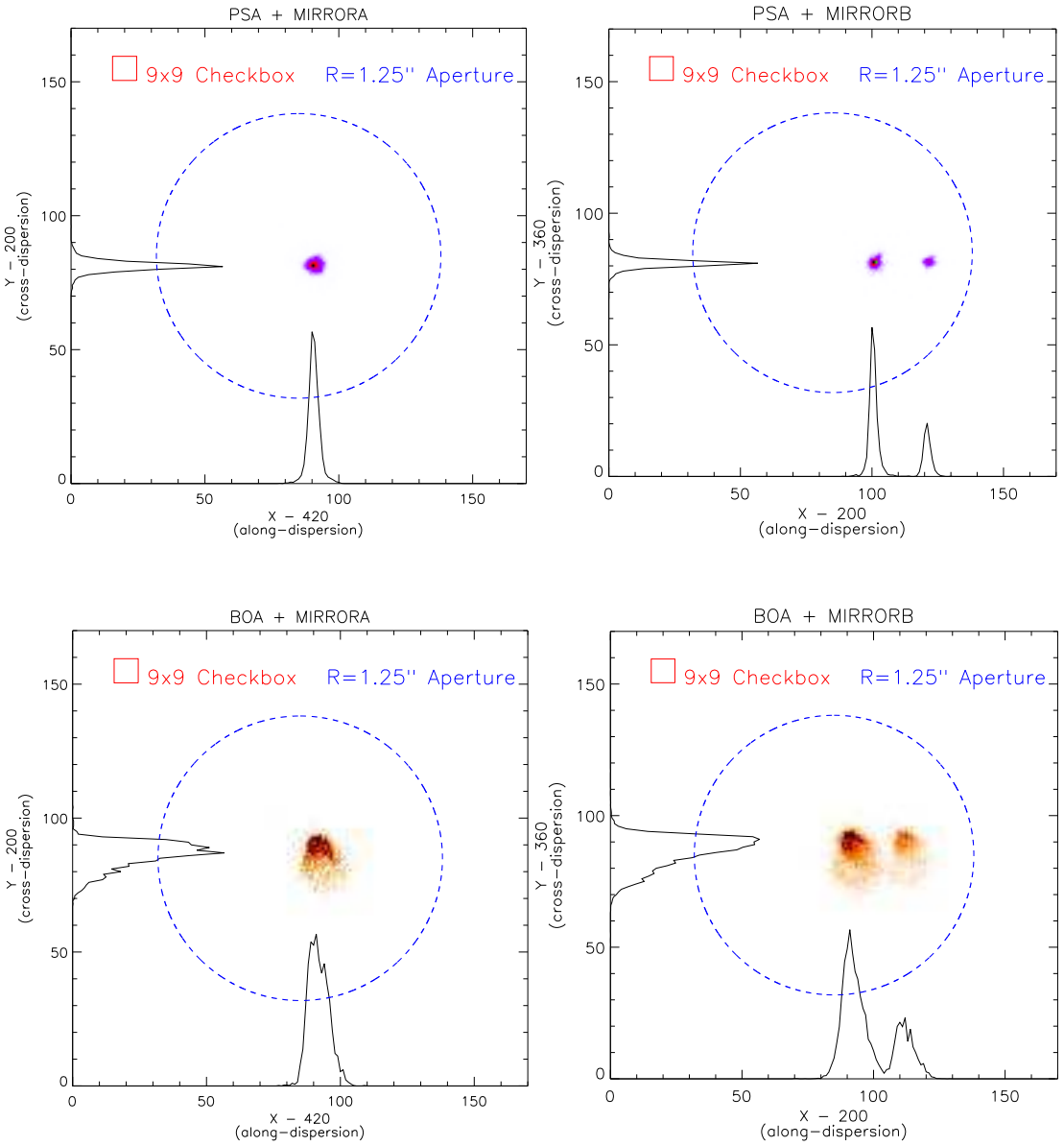

8.5 ACQ/PEAKXD Acquisition Mode

8.5.1 Description

An ACQ/PEAKXD sequence is used to improve centering in the cross-dispersion (XD) direction. The steps executed in an ACQ/PEAKXD sequence are

1. A short exposure of the Pt-Ne wavelength calibration lamp through the WCA aperture is obtained. The spectrum is collapsed along the dispersion direction, its centroid is calculated, and the center of the target aperture is computed.
2. A target spectrum is recorded for the user-specified time using a sub-array tailored to each grating and central wavelength (excluding edge effects and airglow lines). The spectrum is collapsed along the dispersion direction.
3. The target XD location is assumed to be the median position (NUV) or mean position (FUV) of the collapsed spectrum.
4. The slew required to move the target spectrum in the XD direction to the center of the aperture is computed.
5. The telescope is slewed by the calculated offset to center the target in the XD direction.

The user must specify the aperture (PSA or BOA, typically the same as for the science exposure), the grating and central wavelength, and the exposure time. The use of MIRRORA or MIRRORB is not allowed. For NUV ACQ/PEAKXD acquisitions, the stripe (SHORT, MEDIUM, or LONG, corresponding to stripes A, B, or C) to be used in the computation may be specified; however, the default stripe B (MEDIUM) is recommended, as it achieves the best centering. For FUV ACQ/PEAKXD acquisitions, only data from Segment A are used to compute the centroid; data from Segment B are ignored.

We recommend a minimum S/N of 40 for all dispersed-light target acquisition exposures, except for FUV ACQ/PEAKXD exposures, which require only S/N = 25 in detector Segment A.

Note: Because light from the three spectral stripes will overlap, PEAKXD acquisitions will fail—and should thus be avoided—for extended sources observed with the NUV detector.

8.5.2 Effects of FUV Detector Y Walk

As described in Section 4.1.7, the COS FUV detector exhibits gain sag. Gain sag effects at the original lifetime position led to the need to move the location of the FUV spectrum to the second lifetime position on July 23, 2012. Continued operations at lifetime position 2 have resulted in the gradual sag of the gain at this new position. It is expected that COS FUV operations will move to a third lifetime position by the spring of 2015.

One consequence of the gain sag effect is the mis-registration of photon events in the cross-dispersion (XD) or Y direction, commonly referred to as Y walk. While Y walk does not adversely affect science data, it can reduce the accuracy of target

acquisitions obtained in dispersed light. If the target is centered in the aperture, but the Y walk shifts its spectrum in the XD direction, then the ACQ/PEAKXD algorithm will miscalculate its centroid and move the target away from the aperture center.

The FUV Segment B is more affected by Y walk and gain sag than Segment A, mainly due to the intense geocoronal Lyman-α emission that hits the detector during G130M observations. To combat the effects of Y walk we have modified the FUV ACQ/PEAKXD algorithm to only use Segment A data as this has been shown to give better cross-dispersion centering.

8.6 ACQ/PEAKD Acquisition Mode

ACQ/PEAKD exposures are used to improve centering in the along-dispersion (AD) direction after an ACQ/PEAKXD. ACQ/PEAKD works much like ACQ/SEARCH except that, instead of a spiral, the spacecraft is moved linearly along the AD axis between exposures. An array containing the total counts at each dwell point is constructed. Its centroid is computed, and the telescope is moved to center the target in the aperture in the AD direction.

The user must specify the aperture, grating, central wavelength, and the exposure time at each dwell point. The use of MIRRORA or MIRRORB is not allowed. The number of steps, here called NUM-POS, may be 3, 5, 7, or 9. The STEP-SIZE is given in arcseconds. There are three options for the centering algorithm, CENTER=FLUX-WT, FLUX-WT-FLR, and BRIGHTEST, and they work just as described in Section 8.3.

For most applications, we recommend the use of NUM-POS=5, STEP-SIZE=0.9, and CENTER=FLUX-WT-FLR, as this combination is the least sensitive to high or variable background rates and covers a large area on the sky. Observers who wish to use NUM-POS=3 are advised to use STEP-SIZE=1.3 and CENTER=FLUX-WT. The special parameter CENTER=DEFAULT sets CENTER=FLUX-WT if NUM-POS=3 and CENTER=FLUX-WT-FLR if NUM-POS=5, 7, or 9. For FUV ACQ/PEAKD acquisitions, either segment A or B may be used, but use of the SEGMENT=DEFAULT (both, except for G140L) is recommended. All G140L ACQ/PEAKD acquisitions use only segment A data.

8.7 Exposure Times

While the figures in this section will help you to estimate exposure times for various acquisition scenarios, the COS Exposure Time Calculator (ETC) should be used for all proposal preparation.

8.7.1 Imaging Acquisitions

Acquisition images obtained through the PSA should strive for a minimum S/N of 40. Due to the complex shape of images obtained through the BOA, a S/N > 60 is recommended. For MIRRORB acquisitions, the recommended S/N refers only to the primary image; the ETC performs this calculation appropriately. Figure 8.3 shows approximate exposure times needed to reach these S/N levels for various target fluxes. A flat source spectrum (F_λ = constant) is assumed.

Figure 8.3: Exposure Time Needed for an ACQ/IMAGE Acquisition

Approximate exposure time needed to achieve S/N = 40 (PSA) or 60 (BOA) as a function of target flux. This calculation assumes a flat source spectrum.

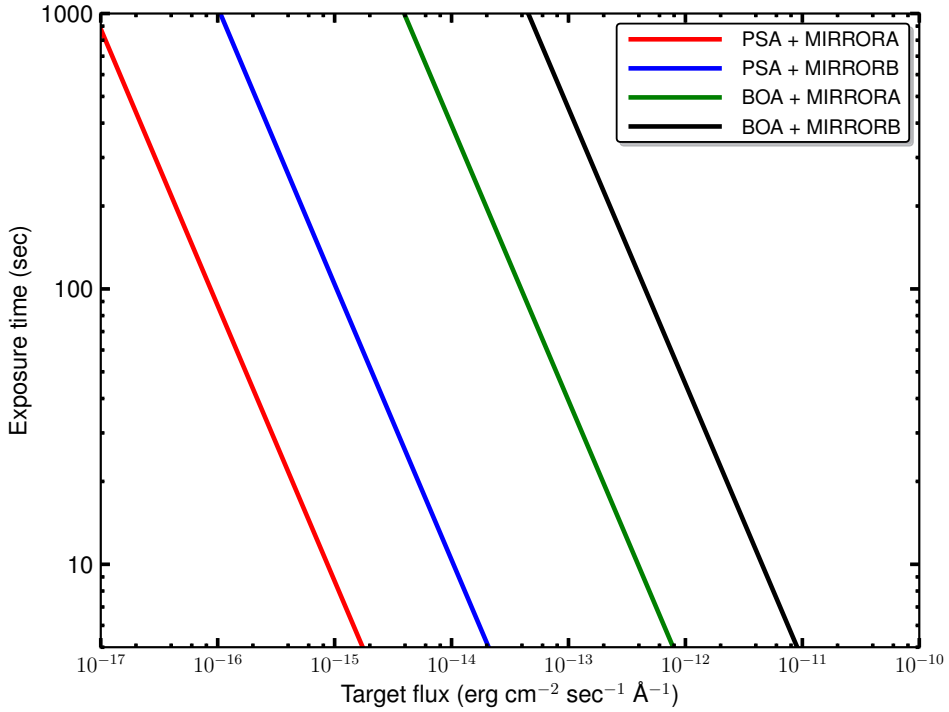

Figure 8.4: Exposure Time Needed for a Dispersed–Light Acquisition with the PSA

Approximate exposure time needed to achieve a S/N of 40, assuming a flat source spectrum.

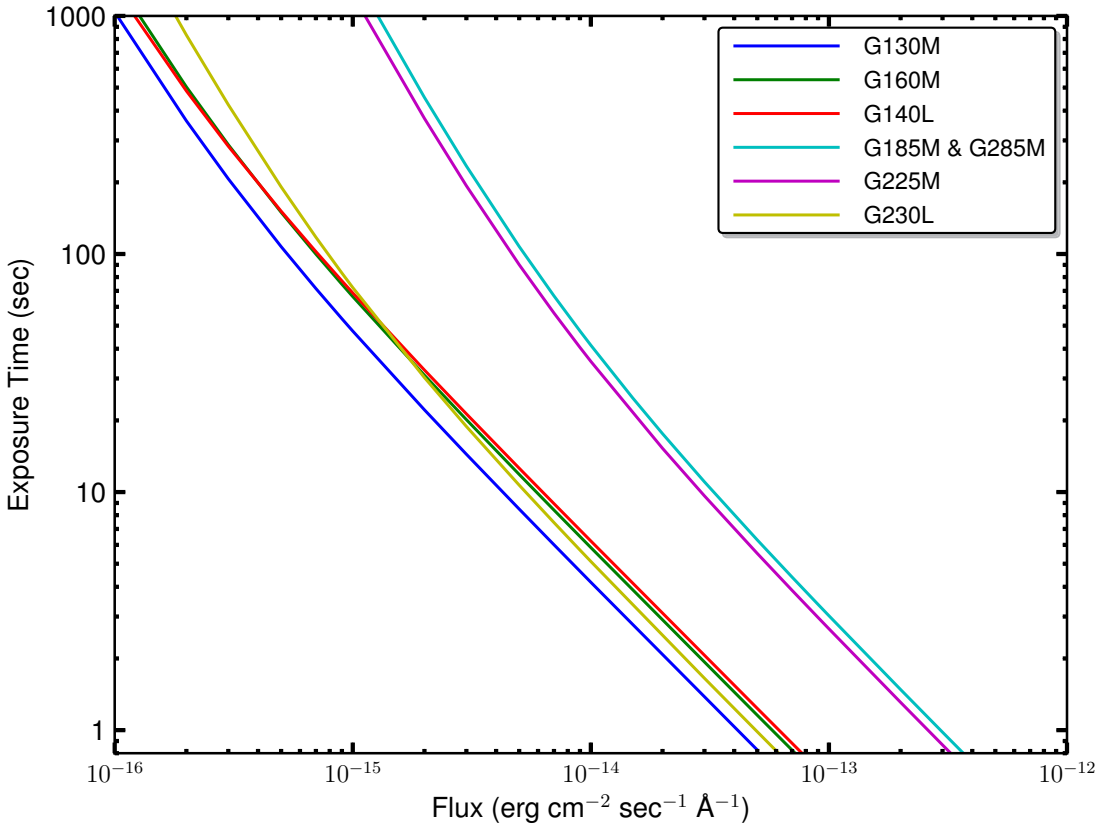

8.7.2 Dispersed-Light Acquisitions

We recommend a minimum S/N of 40 for all dispersed-light acquisition exposures, except for FUV `ACQ/PEAKXD` exposures, which require only S/N = 25 in detector segment A (Section 8.5.2). STScI calibration programs routinely use up to S/N = 100 to minimize the influence of Poisson noise and background when very precise pointing is required. Figure 8.4 is a guide to the exposure time needed for a dispersed-light acquisition with the PSA, assuming a flat source spectrum (F_λ = constant). Note that these exposure times apply to each separate dwell point of a pattern, which is the quantity entered into APT in Phase II.

8.8 Centering Accuracy and Data Quality

A centering accuracy of 0.3 arcsec in the cross-dispersion (XD) direction is required to achieve optimum photometric accuracy and spectral resolution. In the along-dispersion (AD) direction, the minimum accuracy is set by velocity requirements: ±15 km/s for the medium-resolution modes, ±150 km/s for G140L, and ±175 km/s for G230L. Since the AD requirements are in units of km/s, they are grating and wavelength dependent. Assuming that the wavelength error budget is split evenly between the COS TA and wavelength scale accuracy, the strictest pointing requirements are ±0.041 arcsec for the NUV channel and ±0.106 arcsec for the FUV channel.

8.8.1 Centering Accuracy and Wavelength Accuracy

To achieve a wavelength accuracy of ±15 km/s, the target should be centered to within about 0.04–0.07 arcsec for NUV observations and 0.1–0.2 arcsec for FUV observations. The throughput of COS is not affected by centering errors of less than 0.4 arcsec, so high centering precision is not strictly necessary if science goals do not require that the wavelength zero point be well constrained. For example, the spectra of some objects may include foreground interstellar or inter-galactic absorption lines that can be used to establish the zero point of the wavelength scale.

8.8.2 Centering Accuracy and Photometric Precision

Figure 8.5 shows the relative transmission of the PSA as a function of the displacement of a point source from the aperture center, as measured using each of the four NUV gratings. These and the corresponding FUV curves are nearly identical and show that the transmission of the COS apertures is essentially flat within the central ±0.4 arcsec, then tails off in a non-linear but approximately symmetrical profile (COS ISR 2010-09).

Figure 8.5: Relative Transmission of the COS PSA at NUV Wavelengths

Transmitted flux as a function of displacement from aperture center for all four NUV gratings. The dotted lines mark the edge of the aperture (1.25"). The two curves labeled D and XD refer to offsets along the dispersion and cross-dispersion axes, respectively. The other curves trace offsets in the cross-dispersion direction. For all gratings, the absolute transmission through the PSA for a centered point source is at least 95%.

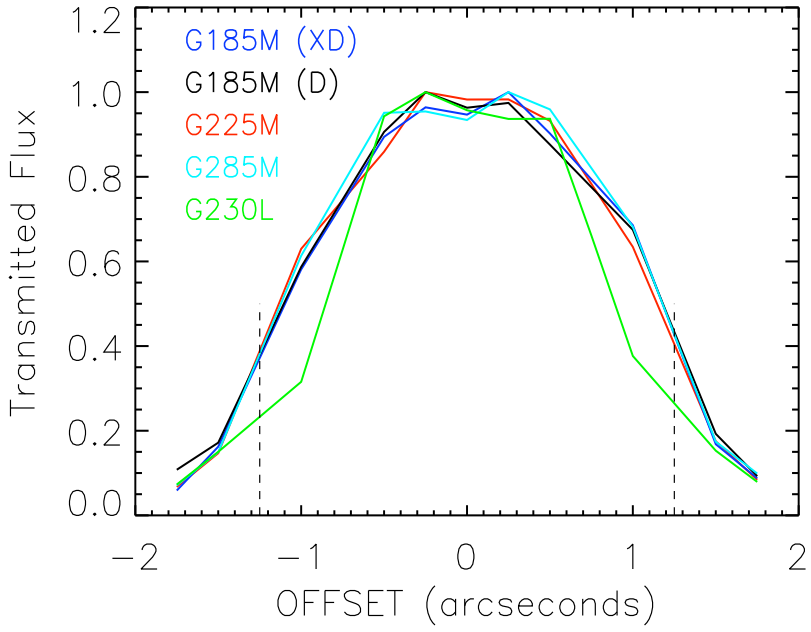

8.8.3 Centering Accuracy and Spectroscopic Resolution

Targets placed within 0.3 arcsec of the aperture center will achieve maximum spectral resolution. Centering errors larger than 0.3 arcsec will lead to progressively poorer resolution. Targets at the edge of the aperture have approximately half the spectral resolution of well-centered targets.

8.9 Recommended Parameters for all COS TA Modes

As the result of our analysis of the target acquisition (TA) performance of COS during SMOV and during Cycles 17 through 21, we have adjusted many COS TA parameters and have refined our recommendations and guidelines for routine COS TAs. We present these recommendations and guidelines in the previous sections and summarize the most significant instructions below. Table 8.3 provides our recommended values for optional parameters for each COS TA type.

- All TA modes provide good centering. For optimal wavelength accuracy, use NUV imaging mode; otherwise, use the mode that is fastest, based on ETC simulations.
- Signal-to-noise (S/N) is important. Use S/N > 40 for PSA and BOA TAs, except for BOA `ACQ/IMAGE`, which should have S/N > 60. A S/N of 25 on detector segment A is sufficient for FUV `ACQ/PEAKXD` exposures.

- A single ACQ/SEARCH is not sufficient to center a COS point-source target in the aperture. Always follow the first ACQ/SEARCH with an ACQ/IMAGE, ACQ/PEAKXD+ACQ/PEAKD, or a second 2 × 2 ACQ/SEARCH which uses FLUX-WT weighting.
- ACQ/SEARCH exposures are not required for targets with coordinate accuracies of ±0.4 arcsec or better in the ICRS/GSC2 frame. Spending extra time to validate target coordinates is the best way to save TA time. On-line catalogs often have coordinate errors that exceed 0.4 arcsec. *It is the user's responsibility to verify that target coordinates are correct.*
- If at all possible, use STRIPE=MEDIUM (stripe B) for NUV spectroscopic ACQ/PEAKXDs. (This is the default.) Primarily, this is because the WCA-to-PSA offsets in the flight software are optimized for stripe B in most modes. Choosing a different stripe will result in systematic offsets of the initial spectrum of order of a few pixels, which generally are still within typical target coordinate uncertainties.
- Use NUM-POS=5, STEP-SIZE=0.9, and CENTER=FLUX-WT-FLR for most ACQ/PEAKD centerings. For the most accurate AD centering possible, use NUM-POS=9, STEP-SIZE=0.6, and CENTER=FLUX-WT-FLR. When a fast TA is required and lower centering accuracy can be tolerated, use NUM-POS=3, STEP-SIZE=1.3, and CENTER=FLUX-WT.

Table 8.3: COS Acquisition Modes, Options, and Recommended Values

Acquisition Type	Description	SCAN-SIZE or NUM-POS	STEP-SIZE (arcsec)	Optional Parameters	Recommended Values	Recommended S/N
ACQ/SEARCH	Spiral pattern; multiple exposures	2	1.767	CENTER=FLUX-WT, FLUX-WT-FLR, BRIGHTEST For FUV: SEGMENT=A, B, BOTH	FLUX-WT	40 (PSA and BOA)
		3[1]			FLUX-WT-FLR	
		4			FLUX-WT-FLR	
		5			FLUX-WT-FLR	
ACQ/IMAGE	Initial and confirmation images (NUV only)					40 (PSA) 60 (BOA)
ACQ/PEAKXD	One exposure			For NUV: STRIPE=SHORT, MEDIUM, LONG For FUV: SEGMENT=A, BOTH[2]	For NUV: STRIPE=MEDIUM For FUV: SEGMENT=BOTH (These are the default values.)	For NUV: 40 For FUV: 25 on segment A
ACQ/PEAKD	Linear pattern; multiple exposures	3	1.3	CENTER=FLUX-WT, FLUX-WT-FLR, BRIGHTEST, DEFAULT[3] For FUV: SEGMENT=A, B, BOTH	FLUX-WT	40
		5[1]	0.9		FLUX-WT-FLR	
		7	0.6		FLUX-WT-FLR	
		9	0.6		FLUX-WT-FLR	

1. Recommended number of acquisition steps.
2. For FUV exposures, data from detector Segment B are ignored by the ACQ/PEAKXD centroiding algorithm, regardless of the value of the SEGMENT parameter.
3. For ACQ/PEAKD, use of the special parameter CENTER=DEFAULT is recommended. This parameter sets CENTER=FLUX-WT if NUM-POS=3 and CENTER=FLUX-WT-FLR if NUMPOS=5, 7, or 9.

8.10 Special Cases

8.10.1 Early Acquisitions and Preliminary Images

In some situations an observer may need to obtain an independent ultraviolet image of a region in order to ensure that no objects violate safety limits and that the target to be observed can be acquired by COS successfully. Such an early acquisition should be included in the Phase I proposal, and the observation should not use a photon-counting detector. The UVIS channel on WFC3 is recommended, but observers are encouraged to consult with an STScI instrument scientist.

8.10.2 Extended or Multiple Targets

Because most COS target-acquisition schemes were developed with the implicit assumption that the target is a point source, acquisitions of extended or multiple sources may require more careful planning.

If the target is sufficiently uniform and its coordinates are well known, then a target acquisition may not be required. To ensure that the brightest region of an extended source falls into the aperture, an `ACQ/SEARCH` with `CENTER=BRIGHTEST` may be sufficient (Section 8.3). `ACQ/PEAKXD` acquisitions with the NUV detector should be avoided for extended sources, because light from the three spectral stripes will overlap on the detector (Section 8.5).

Complex targets—such as two stars with very small angular separation, multiple bright knots, etc.—may confuse the acquisition algorithms. In such cases, consider an offset target acquisition, discussed in Section 8.10.3. Take care when doing target acquisition for a target in a binary system since it is possible for the pointing to end up between the two stars. The coordinates of the target must be corrected for the orbital phase of the target in the binary system.

8.10.3 Offset Target Acquisitions

When targets are faint or lie in crowded fields, direct acquisition of the primary science target may be difficult or uncertain. In such cases, an offset acquisition, in which acquisition of a nearby field target is followed by a short slew to the science target, may be appropriate.

The size of the offset is limited by the requirement that the guide stars remain within the fields of view of their respective FGSs. Offset acquisition slews routinely involve displacements up to 1 arcmin and can be larger. Offset slews have a typical accuracy of ±0.003 arcsec. The centering of the initial offset target should be refined (via either `ACQ/IMAGE` or `ACQ/PEAKXD+ACQ/PEAKD`) before the offset maneuver. For offset acquisitions, bright-object considerations apply over the entire offset region. Refer to Chapter 9 for a discussion of the modest overheads associated with the offset-acquisition spacecraft movement.

In unusual cases, including highly uncertain target coordinates or knotty, extended sources for which high wavelength accuracy is required, an offset target acquisition, followed by an additional ACQ/IMAGE or ACQ/PEAKXD+ACQ/PEAKD on the primary target, may be employed.

8.10.4 Acquisition Failure Actions and Diagnostics

Should any stage of the TA fail or a Local Rate Check (LRC) violation occur during a TA exposure, then the subsequent acquisition procedures in that visit (such as ACQ/PEAKXD or ACQ/PEAKD) will not be executed, but the science exposures will still occur. Note that *HST* will be left pointing at the last commanded position, which may differ substantially from the initial pointing.

Many quantities useful for evaluating the success of COS TAs are recorded in the COS TA data products (the _rawacq and _spt files). Table 5 of COS ISR 2010-14 lists these keywords and their meanings.

CHAPTER 9:

Scheduling Observations

In this chapter…

9.1 Introduction

Once you have established the series of target-acquisition, scientific, and (if necessary) calibration exposures required for your program you are ready to determine the total number of orbits to request. Generally, this is a straightforward exercise: compile the overheads on the individual exposures, assign the exposures to orbits, and tally the results to determine your orbit request. In some cases, it may be an iterative process, as you refine your observing plan to use each orbit most efficiently. This chapter provides simple tools to help you perform these calculations.

Once your proposal has been accepted you will return to this chapter to construct your Phase II proposal, which is the detailed observing plan that will eventually be transmitted to the telescope. Our goal is to help you schedule your observations as efficiently as possible.

Table 9.1: Phase I Estimates of Observatory and Instrument Overheads

Acquisition or Exposure	Overhead Time (minutes)	Notes
Guide-star acquisition	6	First orbit of each visit
Guide-star re-acquisition	4	Each subsequent orbit
ACQ/IMAGE	3	Typical imaging acquisition
ACQ/SEARCH	7	Imaging or dispersed light, NUV or FUV
ACQ/PEAKXD + ACQ/PEAKD	7	Typical dispersed light acquisition, NUV or FUV
Science (Imaging or Dispersed Light)	5	First exposure in series
	2	Each subsequent exposure in series
	1	Add 1 minute for each instrument change (except to increment FP-POS)

9.1.1 Phase I Proposal

The *HST Primer* provides simple guidelines for estimating the overheads associated with a COS observation. These guidelines are summarized in Table 9.1. These numbers are estimates only, and will usually overestimate the amount of time needed for overheads. However, additional observing time will not be granted in Phase II if the Phase I overheads were underestimated, so it is important that overhead times not be underestimated.

Each orbit must begin with a guide-star acquisition, which takes 6 minutes on the first orbit of a visit and 4 minutes on subsequent orbits. Next, the target must be acquired via an ACQ/SEARCH (7 min) and/or centered in the aperture via an ACQ/IMAGE (3 min) or a pair of ACQ/PEAKXD and ACQ/PEAKD exposures (7 min for both). The first science exposure requires 5 minutes of overhead. Subsequent identical exposures incur 2 minutes of overhead each. Add 1 minute for each instrument change (e.g., new grating or central wavelength; incrementing the FP-POS takes only 3 s, if ordering is efficient-see Table 9.5). If the same target is observed on contiguous orbits, a target acquisition is not required on the second and subsequent orbits.

These simple rules are remarkably successful at reproducing the total time required for a COS observation. To demonstrate, we list in Section 9.7 both the Phase I times and the final times predicted by APT for a series of observing scenarios. These rules assume that acquisition exposure times are on the order of 20 s. If your targets are extremely faint, you must increase the length of the acquisition exposures accordingly (Section 9.4). Finally, note that some instrument changes, such as turning a detector segment on or off, take considerably longer than 1 minute (Section 9.5).

Allowing sufficient time for overheads in your Phase I proposal is important; additional time to cover unplanned or overlooked overheads will not be granted later. *Do not underestimate the amount of time that will be needed for overheads.*

9.1.2 Phase II Proposal

Once your proposal is approved, you will be responsible for building the observing sequences that will be executed by the telescope. The APT (Astronomer's Proposal Tool) scheduling software is used to prepare the Phase II; it automatically incorporates the appropriate overheads into your observing plan. While all COS overheads are automatically scheduled by APT, it is useful to understand where they come from. To that end, this chapter discusses the various observatory and instrument overheads in some detail, and Section 9.7 provides observing scenarios as examples. Note that, when this chapter and the APT disagree, the APT overheads are the definitive values.

Accounting properly for all the overheads involved in an observation can be complicated. The information provided here is meant only to be illustrative. Proposers are urged to use APT to derive a complete and accurate determination of overhead times.

9.2 Generic Observatory Overheads

The first time that you acquire an object, you must include a 6-minute overhead for the *HST* guide-star acquisition. In all subsequent orbits of the same visit, you must include the 4-minute overhead for the guide-star reacquisition. If you are observing an object in the Continuous Viewing Zone (CVZ), then no guide-star re-aquisitions are required.

You must allocate additional time for each deliberate movement of the telescope; e.g., if you are performing a target-acquisition exposure on a nearby object and then offsetting to your target, or if you are taking a series of exposures in which you move the target on the detector (`POS-TARG`), then you must allow time for telescope motion. The time varies depending on size of the slew; see Table 9.2.

Table 9.2: Generic Observatory Overhead Times

Action	Overhead type	Time needed
Guide-star acquisition	Initial acquisition	6 min
	Re-acquisition	4 min per orbit
Spacecraft movements	10 arcsec < Offset < 1.5 arcmin[1]	60 s
	1.25 arcsec ≤ Offset ≤ 10 arcsec	30 s
	Offset < 1.25 arcsec	20 s

1. Spacecraft motions larger than ~ 1.5 arcmin are likely to result in the loss of guide stars.

9.3 Spectral Element Movement Overheads

For any COS exposure, including target-acquisition exposures, any change of spectral elements incurs an overhead. A transition from FUV to NUV requires movement of OSM1 to the NCM1 position, followed by a possible OSM2 movement. On the other hand, a transition from NUV to FUV requires only the movement of OSM1 from NCM1 to the desired FUV grating. Table 9.3 gives the times required for movement between OSM1 spectral elements and Table 9.4 gives the times for movement between OSM2 spectral elements.

All COS visits start with OSM1 at the G130M position (with central wavelength 1309 Å) and OSM2 at the G185M position (with central wavelength 1850 Å). These gratings are highlighted in Table 9.3 and Table 9.4. OSM1 and OSM2 move sequentially, so the total overhead is the sum of the two separate overheads. The time required to move from one optical element to another is independent of the initial and final central-wavelength and FP-POS settings.

Table 9.3: Overhead Times for Motions Between OSM1 Spectral Elements

Movement times (s) from	to G140L	to G130M	to G160M	to NCM1
G140L	—	158	200	115
G130M	164	—	112	116
G160M	206	116	—	159
NCM1	121	109	154	—

Table 9.4: Overhead Times for Motions Between OSM2 Spectral Elements

Movement times (s) from	to G230L	to G185M	to G225M	to G285M	to MIRRORA	to MIRRORB
G230L	—	209	140	176	105	99
G185M	204	—	136	102	169	175
G225M	135	141	—	108	100	106
G285M	170	107	103	—	136	142
MIRRORA	100	174	105	141	—	71
MIRRORB	94	181	112	147	77	—

9.4 Acquisition Overheads

The various target-acquisition procedures are described in detail in Chapter 8. The exposure overheads associated with each are given below:

ACQ/SEARCH: Add 20 s to the exposure time and multiply by the number of dwell points. Add the grating-change overheads from Table 9.3 and Table 9.4. Even `SCAN-SIZE` values (2 or 4) trigger an additional overhead because of the telescope motion required to displace the aperture by half of a `STEP-SIZE` in both the dispersion and cross-dispersion directions, so that the overall pattern remains centered on the initial pointing.

ACQ/IMAGE: The associated overhead is 120 s plus twice the specified exposure time; this includes both the OSM1 and OSM2 movements and the overhead adjustment discussed in Section 9.6. The exposure time is doubled because, after *HST* is slewed to center the target, a confirmation image is obtained. Dumping the two images to memory requires an additional 58 s.

ACQ/PEAKXD: The overhead is 70 s (NUV) or 80 s (FUV) plus exposure time. Add the grating-change overhead from Table 9.3 and Table 9.4.

ACQ/PEAKD: Add 20 s to the exposure time and multiply by the number of dwell points. Add the grating-change overhead from Table 9.3 and Table 9.4. Add 39 s for memory readout.

9.5 Science Exposure Overheads

Science-exposure overheads are dominated by the time required to move OSM1 and OSM2 and to read out the on-board memory buffer at the end of each exposure. While the Phase II overheads computed by APT may be less than the values presented below, it is important to plan Phase I proposals using the conservative overheads given below to ensure adequate time for each exposure.

The full overhead calculation for science exposures depends upon a number of factors including generic exposure set-ups (which depend on the detector and observing mode), whether an aperture change is required, whether a grating change is required, whether the central wavelength setting for the grating is changed, and the directional sense of any required motion to implement an FP-POS change. Table 9.5 lists these additional overheads.

When moving to a new grating, you may specify any combination of central wavelength and FP-POS setting with no additional overhead penalty. As a result, the FP-POS sequence 1,2,3,4 is more efficient than 3,4,1,2, because no backward motion is required.

Table 9.5: Science Exposure Overhead Times

Overhead times (s)	FUV		NUV	
	TIME-TAG	ACCUM	TIME-TAG	ACCUM
Exposure set-up	71	79	36	38
Grating change	see Table 9.3		see Table 9.4	
Central wavelength change	72		75	
FP-POS forward[1]	3		3	
FP-POS backward[1]	70		70	
PSA – BOA Change	8		8	
WCA – BOA Change	10		10	
SEGMENT reconfiguration	330		N/A	
Memory readout[2]	116	108[2]	116	48[2]

1. "Forward" refers to the preferred direction of motion of OSM1 or OSM2 and "backward" to the opposite direction. The preferred direction is toward larger FP-POS values.
2. ACCUM mode readout overheads can be hidden within subsequent exposures under certain circumstances, but the rules are complex. Use these values as safe upper limits for proposals.

To estimate the overhead for an exposure, round the desired exposure time up to the next whole second and add the generic exposure setup overhead from Table 9.5. If a grating change has occurred from the previous exposure, add the appropriate values from Table 9.3 and/or Table 9.4. If a central wavelength change is made, add the appropriate value from Table 9.5. If an FP-POS movement is made, add the appropriate value for motion in the preferred direction (toward larger FP-POS) or non-preferred direction. Note that all dispersed-light target-acquisition exposures are obtained with FP-POS=3. For all FUV observations except the G140L 1105 Å setting, both detector segments are powered on by default. To turn one of them off, set SEGMENT to A or B and add the associated overhead. Lastly, add the appropriate detector memory readout overhead.

Due to the 100x difference in sensitivity between the COS FUVA and FUVB segments when observing with the G130M/1055 and 1096 CENWAVEs, it is expected that many observers will need to turn off FUVA when observing bright targets. (We refer to these SEGMENT=B observations here as either C1055B or C1096B). Only those observers using these two configurations are affected by this issue.

Under these conditions the zero point of the wavelength solution cannot be determined because the MgF_2 window on the PtNe lamps (WAVECAL) blocks light below ~ 1180Å (all WAVECAL light falls on FUVA). This results in a degradation of the resolution when FP-POS are combined by **calcos** and decreases the archival value of the COS data. In these cases, normal TAGFLASHs are not available and WAVECAL

exposures with FUVA turned ON must be inserted into the observing sequence adjacent to each CENWAVE/FP-POS setting used. As a result, in these cases FP-POS=ALL should not be used. Individual FP-POS science exposures, and their associated WAVECALs, should be used instead. A detailed description of how to insert these WAVECALs can be found at the following website:

http://www.stsci.edu/hst/cos/documents/newsletters/cos_stis_newsletters/full_stories/2013_06/bm_detail

9.6 First Exposure Overhead Adjustment

To increase observing efficiency, a special feature of the COS instrument commanding allows a portion of the instrumental overheads for the first exposure of a visit to be performed during the initial guide-star acquisition. These will usually be target-acquisition exposures. As a result, up to 340 s of instrumental overheads (Table 9.3, Table 9.4, and Table 9.5), but ***not*** observatory or acquisition overheads (Table 9.2 and Section 9.4), may be hidden in this fashion. See Section 9.7 for examples.

9.7 Examples of Orbit Estimates

In this section we present five example COS observations using both detectors and all of the target-acquisition modes. Besides the topics discussed in the previous sections we include examples of

- **Multiple FP-POS settings** (Section 5.8.2)**:** To minimize the damage to the FUV detector caused by strong Lyman-α airglow lines and to improve the limiting S/N of an observation. Proposers using the FUV channel of COS, but who do not intend to use all four FP-POS settings for each central wavelength setting, must justify this choice in the observing strategy section of their Phase I proposal. A modest reduction in observational overheads will not normally be considered sufficient justification for not using all four FP-POS settings.
- **Adjusting the BUFFER-TIME (**Section 5.4**):** If BUFFER-TIME is greater than the exposure time, one would normally set BUFFER-TIME = EXP-TIME. In orbits with a series of long FUV exposures, one can minimize overheads by setting BUFFER-TIME = EXPTIME-100. The full buffer takes 116 s to empty, so most of the data will be read out before the exposure is completed. The post-exposure data dump then requires only 40 s. For the final exposure of an orbit, the buffer dump can occur during the occultation, so adjusting the BUFFER-TIME will not save time. See the example in Section 9.7.5.

While the overhead rules presented in this chapter may appear complex, the actual rules used by the *HST* scheduling software are even more so. It is thus imperative that

you use APT to construct your Phase II proposal. In the examples that follow, we present three sets of overhead estimates: one using the Phase I rules (Section 9.1), one using the rules in this chapter (Sections 9.2 to 9.6), and one computed using APT version 20.2.3. The APT estimates should be considered definitive. COS is a relatively new instrument, and the overhead rules will continue to evolve as we learn how to use it more efficiently. The version of APT available for constructing Cycle 22 Phase II proposals may return values that differ slightly from those given below. An up-to-date version of the APT *must* be used for the Phase II planning of each visit.

9.7.1 Target Acquisition Using ACQ/IMAGE

In this example, we begin with an NUV `ACQ/IMAGE` target acquisition, then add two NUV `TIME-TAG` exposures using the same grating but different central wavelengths. For NUV observations, the use of multiple `FP-POS` settings is not required (though it useful to reduce flat-field noise).

Table 9.6: Overhead Values for ACQ/IMAGE Acquisition

Action	Phase I (s)	Chapter 9 (s)	APT Time (s)	Comment
Initial guide star acquisition	360	360	333	Required at start of a new visit
NUV `ACQ/IMAGE` with 2 s exposure	180	116 + 169 + 120 + 4 + 58 = 467	419 + 56 (dump)	COS starts at G130M on OSM1, so move to NCM1 requires 116 s. OSM2 home position is G185M, so move to `MIRRORA` takes 169 s. Add 2 min `ACQ/IMAGE` setup, twice the exposure time, and memory readout.
First exposure overhead adjustment	N/A	–(116 + 169) = –285	–333	OSM1 and OSM2 movements may be hidden in guide-star acquisition.
NUV G185M at 1850 Å, `TIME-TAG`, `FP-POS=3`, 1175 s exposure	300 + 1175	36 + 174+ 1175 + 116 = 1501	204 + 1175 + 116	Generic NUV `TIME-TAG` setup; change from `MIRRORA` to `G185M` (174 s); exp time; `TIME-TAG` memory readout
NUV G185M at 1817 Å, `TIME-TAG`, `FP-POS=3`, 1175 s exposure	120 + 60 + 1175	36 + 75 + 1175 + 116 = 1402	102 + 1175 + 116	Generic NUV `TIME-TAG` exposure setup; central-wavelength change (75 s); exp time; `TIME-TAG` memory readout
Total science time	2350	2350	2350	
Total time used in orbit	3370	3445	3363	

9.7.2 ACQ/SEARCH plus ACQ/IMAGE Acquisition

In this example, we begin with an NUV ACQ/SEARCH followed by an ACQ/IMAGE target acquisition. We obtain an NUV TIME-TAG exposure, then switch to the FUV channel for a pair of FUV TIME-TAG exposures. To minimize damage to the detector, we employ two FP-POS settings.

Table 9.7: Overhead Values for ACQ/SEARCH plus ACQ/IMAGE

Action	Phase I (s)	Chapter 9 (s)	APT Time (s)	Comment
Initial guide star acquisition	360	360	333	Required at start of a new visit
NUV ACQ/SEARCH, MIRRORA, 3 × 3 pattern, 10 s exposure	420	116 + 169 + 9×(20+10) = 555	696	COS starts at G130M on OSM1, so move to NCM1 requires 116 s. OSM2 home position is G185M, so move to MIRRORA takes 169 s. 9 ACQ/SEARCH sub-exposures, so overhead includes 9 slews (20 s each) plus 9 exposures (10 s each)
First exposure overhead adjustment	N/A	–(116 + 169) = –285	–291	OSM1 and OSM2 movements may be hidden in guide-star acquisition.
NUV ACQ/IMAGE with 10 s exposure	180	120 + 2×10 + 58 = 198	131 + 56 (dump)	No OSM2 movement; ACQ/IMAGE setup, twice exp time, and memory readout
NUV G225M at 2250 Å, TIME-TAG, FP-POS=3, 1200 s exposure	300 + 1200	36 + 105 + 1200 + 116 = 1457	135 + 1200 + 114	Generic NUV TIME-TAG setup; change from MIRRORA to G225M (105 s); exp time; TIME-TAG memory readout
FUV G130M at 1309 Å, TIME-TAG, FP-POS=2, 300 s exposure	120 + 60 + 300	71 + 109 + 300 + 116 = 596	197 + 300 + 114	Generic FUV TIME-TAG setup; OSM1 move from NCM1 to G130M (109 s); exp time; TIME-TAG memory readout
FUV G130M at 1309 Å, TIME-TAG, FP-POS=4, 300 s exposure	120 + 300	71 + 6 + 300 + 116 = 493	64 + 300 + 114	Generic FUV TIME-TAG setup; increment FP-POS by 2 settings (6 s); exp time; TIME-TAG memory readout
Total science time	1800	1800	1800	
Total time used in orbit	3360	3374	3463	

9.7.3 FUV Acquisition plus TIME-TAG

In this example, we begin with an FUV ACQ/SEARCH, followed by ACQ/PEAKXD and ACQ/PEAKD, all with G130M, then change to G140L and SEGMENT=A for a set of FUV TIME-TAG exposures using FP-POS=ALL.

Table 9.8: Overhead Values for FUV Acquisition and FP–POS=ALL

Action	Phase I (s)	Chapter 9 (s)	APT Time (s)	Comment
Initial guide-star acquisition	360	360	333	Required at start of a new visit
FUV ACQ/SEARCH, G130M at 1309 Å, 3 × 3 pattern, 15 s exposure	420	9 × (20 + 15) = 315	441	COS starts from G130M 1309 Å on OSM1, so no initial move. 9 ACQ/SEARCH sub-exposures, so overhead includes 9 slews (20 s each) plus 9 exposures (15 s each)
First exposure overhead adjustment	N/A	0	–12	No instrument movements prior to first exposure in this example.
FUV ACQ/PEAKXD, G130M at 1309 Å, 25 s exposure	420	80 + 25 = 105	103 + 25	PEAKXD overhead; exp time
FUV ACQ/PEAKD, G130M at 1309 Å, 5 steps, 25 s exposure		5 × (20 + 25) + 39 = 264	293+ 37	5 slews plus 5 exposures; memory readout
FUV G140L at 1280 Å, TIME-TAG, FP-POS=ALL, SEGMENT=A, 268 s exposure	330[1] + 300 + 268	330[1]+ 71 + 164 + 268+ 116 = 949	300 (reconfig) + 243 + 268 + 114	SEGMENT reconfiguration change; generic FUV TIME-TAG setup; OSM1 grating change (164 s); exposure time; TIME-TAG memory readout (note: FP-POS=1)
	120 + 268	71 + 3 + 268 + 116 = 458	67 + 268 + 114	Generic FUV TIME-TAG setup; change to FP-POS=2 (3 s); exp time; TIME-TAG memory readout
	120 + 268	71 + 3 + 268 + 116 = 458	67 + 268 + 114	Same as above, but with FP-POS=3
	120 + 268	71 + 3 + 268 + 116 = 458	67 + 268 + 114	Same as above, but with FP-POS=4
Total science time	1072	1072	1072	
Total time used in orbit	3262	3367	3492	

1. We include the 330 s required to shut off detector Segment B (Table 9.5).

9.7.4 FUV TIME-TAG with BOA and Multiple FP-POS

In this example, we start with an NUV ACQ/IMAGE, followed by a switch to the FUV channel and a TIME-TAG science exposure using G160M, FP-POS=ALL, the BOA, and, as required with the BOA, FLASH=NO. The science exposure will be followed automatically by a 12 s wavecal (see Table 5.2). As required, we obtain two exposures with FP-POS=1 and 2. In the second orbit (not shown), we obtain exposures with FP-POS=3 and 4.

Table 9.9: Overhead Values for FUV TIME–TAG Using the BOA

Action	Phase I (s)	Chapter 9 (s)	APT Time (s)	Comment
Initial guide-star acquisition	360	360	333	Required at start of a new visit
NUV ACQ/IMAGE with 2 s exposure	180	116 + 169 + 120 + 4 + 58 = 467	421 + 56 (dump)	OSM1 starts at G130M, so move to NCM1 requires 116 s. OSM2 starts at G185M, so move to MIRRORA takes 169 s. Add 2 min ACQ/IMAGE setup, twice the exposure time, and memory readout.
First exposure overhead adjustment	N/A	–(116 + 169) = –285	–333	OSM1 and OSM2 movements may be hidden in guide star acquisition.
FUV G160M at 1600 Å, TIME-TAG, BOA, FLASH=NO, FP-POS=1, 1100 s exposure	300 + 1100	71 + 154 + 8 + 116 + 1100 = 1449	233 + 1100 + 114	Generic FUV TIME-TAG setup; change from NCM1 to G160M (154 s); aperture change from PSA to BOA (8 s); exp time; TIME-TAG memory readout
FUV G160M at 1600 Å, TIME-TAG, AUTO WAVECAL, WCA, FP-POS=1, 12 s exposure	120 + 12	71 + 10 + 12 + 116 = 209	75 + 12 + 38	AUTO WAVECAL inserted, since FLASH=YES is not allowed with BOA; generic FUV TIME-TAG setup; aperture change from BOA to WCA (10 s); exp time; TIME-TAG memory readout
FUV G160M at 1600 Å, TIME-TAG, BOA, FLASH=NO, FP-POS=2, 1100 s exposure	120 + 1100	71 + 3+ 10 + 1100 + 116 = 1300	73 + 1100 + 114	Generic FUV TIME-TAG setup; increment FP-POS (3 s); aperture change from WCA to BOA (10 s); exp time; TIME-TAG memory readout
FUV G160M at 1600 Å, TIME-TAG, AUTO WAVECAL, WCA, FP-POS=2, 12 s exposure	120 + 12	71 + 10 + 12 + 116 = 209	75 + 12 + 38	Another AUTO WAVECAL required as FP-POS has changed; again generic FUV TIME-TAG exposure setup; aperture change from BOA to WCA (10 s); exp time; TIME-TAG memory readout
Total science time in orbit 1	2200	2200	2200	
Total time used in orbit 1	3424	3709	3461	
Note: Two additional exposures, using FP-POS=3 and 4 in a second orbit, are not shown.				

9.7.5 FUV TIME-TAG with Modified BUFFER-TIME

In this example, we begin with an NUV ACQ/IMAGE exposure, then switch to the FUV channel for four long G130M exposures, one at each FP-POS position. We use a couple of tricks to maximize the exposure time. First, we shorten the BUFFER-TIME for the first exposure of each orbit as described in Section 5.4.2, which reduces the length of the memory read-out following the exposure from 116 to 40 seconds. Second, we extend the exposure times, pushing the final memory read-out of each orbit into the occultation period. Note that we do not use FP-POS=ALL, because that would generate four identical exposures; instead, we increment the FP-POS by hand.

Table 9.10: Overhead Values for FUV TIME-TAG with Modified BUFFER-TIME

Action	Phase I (s)	Chapter 9 (s)	APT Time (s)	Comment
Initial guide star acquisition	360	360	333	Required at start of a new visit
NUV ACQ/IMAGE with 10 s exposure	180	116 + 169 + 120 + 20 + 58 = 483	437 + 56	OSM1 starts at G130M, so move to NCM1 requires 116 s. OSM2 starts at G185M, so move to MIRRORA takes 169 s. Add 2 min ACQ/IMAGE setup, twice the exposure time, and memory readout.
First exposure overhead adjustment	N/A	–(116 + 169) = –285	–333	OSM1 and OSM2 movements may be hidden in guide star acquisition.
FUV G130M at 1327 Å, TIME-TAG, FP-POS=1, BUFFER-TIME=1210, 1310 s exposure	300 + 1310	109 + 71 + 1310 + 40 = 1530	197 + 1310 + 38	Move OSM1 from NCM1 to G130M (109 s); generic TIME-TAG set-up (71 s); exposure time; short TIME-TAG memory read-out (40 s)
TIME-TAG, FP-POS=2, BUFFER-TIME=1310, 1310 s exposure	120 + 1310	71 + 3 + 1310 + 116 = 1500	67 + 1310 + 114	Generic TIME-TAG set-up; move to FP-POS=2 (3 s); exp time; TIME-TAG memory readout
Total science time in orbit 1	2620	2620	2620	
Total time used in orbit 1	3580	3588	3529	
Guide star re-acquisition	240	240	222	Required at start of next orbit
TIME-TAG, FP-POS=3, BUFFER-TIME=1398, 1498 s exposure	120 + 1498	71 + 3 + 1498 + 40 = 1612	67 + 1498 + 38	As for FP-POS=2, but with short TIME-TAG memory read-out
TIME-TAG, FP-POS=4, BUFFER-TIME=1498, 1498 s exposure	120 + 1498	71 + 3 + 1498 + 116 = 1688	67 + 1498 + 114	As for FP-POS=2
Total science time in orbit 2	2996	2996	2996	
Total time used in orbit 2	3476	3540	3504	

9.7.6 Single CENWAVE Example for Non-CVZ Targets using 4 FP-POS in 1 Orbit

This example is a single orbit TIME-TAG observation using the G130M grating and the 1055 CENWAVE with FP-POS=ALL. It uses a 30 s ACQ/IMAGE target acquisition with MIRRORB and the BOA. The PSA is used for the science exposures.

Table 9.11: Overhead Values for FUV TIME–TAG with 4 FP–POS

Action	Phase I (s)	Chapter 9 (s)	APT Time (s)	Comment
Initial guide star acquisition	360	360	333	Required at start of a new visit
NUV ACQ/IMAGE with 30 s exposure	180	116 + 175 + 8 + 120 + 60+ 58 = 537	494 + 56 (dump)	COS starts at G130M on OSM1, so move to NCM1 requires 116 s. OSM2 home position is G185M, so move to MIRRORB takes 175 s. PSA to BOA change takes 8 s. Add 2 min ACQ/IMAGE setup, twice the exposure time, and memory readout.
First exposure overhead adjustment	N/A	–(116 + 175) = –291	–333	OSM1 and OSM2 movements may be hidden in guide-star acquisition.
FUV G130M at 1055 Å, TIME-TAG, FP-POS=ALL, BUFFER-TIME=500, 500 s exposure	500 + 300	71 + 109 + 8 + 500 + 116 = 804	188 + 500+ 114	Generic FUV TIME-TAG setup; change from MIRRORB to G130M (109 s); change from BOA to PSA (8 s); exp time; TIME-TAG memory readout
	500 + 120	71 + 3 + 500 + 116 = 690	67 + 500 + 114	Generic FUV TIME-TAG setup; change to FP-POS=2 (3 s); exp time; TIME-TAG memory readout
	500 + 120	71 + 3 + 500 + 116 = 690	67 + 500 + 114	Generic FUV TIME-TAG setup; change to FP-POS=3 (3 s); exp time; TIME-TAG memory readout
	500 + 120	71 + 3 + 500 + 116 = 690	67 + 500 + 114	Generic FUV TIME-TAG setup; change to FP-POS=4 (3 s); exp time; TIME-TAG memory readout
Total science time	2000	2000	2000	
Total time used in orbit	3200	3480	3395	

9.7.7 Single CENWAVE Example for Non-CVZ Targets with 4 FP-POS in 2 Orbits

This example is a TIME-TAG observation using the G130M grating and the 1055 CENWAVE with FP-POS=ALL spread over two orbits. It uses a 30 s ACQ/IMAGE target acquisition with MIRRORB and the BOA. The PSA is used for the science exposures.

Table 9.12: Overhead Values for FUV TIME-TAG with 4 FP-POS in 2 Orbits

Action	Phase I (s)	Chapter 9 (s)	APT Time (s)	Comment
Initial guide star acquisition	360	360	333	Required at start of a new visit
NUV ACQ/IMAGE with 30 s exposure	180	116 + 175 + 8 + 120 + 60+ 58 = 537	494 + 56 (dump)	COS starts at G130M on OSM1, so move to NCM1 requires 116 s. OSM2 home position is G185M, so move to MIRRORB takes 175 s. PSA to BOA change takes 8 s. Add 2 min ACQ/IMAGE setup, twice the exposure time, and memory readout.
First exposure overhead adjustment	N/A	–(116 + 175) = –291	–333	OSM1 and OSM2 movements may be hidden in guide-star acquisition.
FUV G130M at 1055 Å, TIME-TAG, FP-POS=1, BUFFER-TIME=1075, 1175 s exposure	1175 + 300	71 + 109 + 8 + 1175+ 40= 1443	188 + 1175 + 38	Generic FUV TIME-TAG setup; change from MIRRORB to G130M (109 s); change from BOA to PSA (8 s); exp time; short TIME-TAG memory readout (40s)
FUV G130M at 1055 Å, TIME-TAG, FP-POS=2, BUFFER-TIME=1075, 1175 s exposure	1175 + 120	71+ 3 + 1175 + 40= 1289	67 + 1175 + 38	Same as above but with FP-POS=2.
Total Science Time in Orbit 1	2350	2350	2350	
Total Time Used in Orbit 1	3310	3338	3307	
Guide star reacquisition	240	240	222	
FUV G130M at 1055 Å, TIME-TAG, FP-POS=3, BUFFER-TIME=1275, 1375 s exposure	1375 + 120	71 + 3 + 1375+ 40= 1489	67 + 1375 + 38	Generic FUV TIME-TAG setup; change to FP-POS=3 (3 s); exp time; short TIME-TAG memory readout (40s)
FUV G130M at 1055 Å, TIME-TAG, FP-POS=4, BUFFER-TIME=1275, 1375 s exposure	1375 + 120	71 + 3 + 1375+ 40= 1489	67 + 1375 + 38	Same as above but with FP-POS=4.
Total science time	2750	2750	2750	
Total time used in orbit	3230	3218	3258	

CHAPTER 10:

Bright-Object Protection

In this chapter…

10.1 Introduction

Both the FUV XDL and the NUV MAMA detectors are subject to damage or destruction by excessive illumination. An excessive local count rate can permanently reduce the sensitivity of the affected detector region. The most likely causes are a bright spectral emission line (XDL or MAMA) or a bright source observed in direct imaging (MAMA). A global over-illumination of the detector can result in its loss. To protect the detectors, onboard software monitors the local and global count rates. It shutters the instrument in case of a local violation and lowers the high voltage if a global count-rate violation is detected. The local rate is checked before an exposure is begun, while the global rate is monitored continuously during the exposure. Under certain circumstances damage can result despite the onboard safety measures, and in any event lowering the high voltage will disrupt the *HST* schedule and operations. Therefore, all proposed COS observations must meet count-rate screening limits with safety margins to allow for uncertainties. COS is currently the only *HST* instrument to use UV detectors for target acquisitions; such acquisitions must be screened, as well. It is the responsibility of the observer to screen all proposed targets and fields during Phase II preparation, and of STScI to check and enforce these limits. The COS Bright Object Protection (BOP) policies and procedures are described in this chapter.

Table 10.1: COS Count Rate Screening Limits

Detector	Source type	Type of limit	Limiting count rate (counts/s)
FUV	predictable	global	15,000 per segment [1]
		local	0.67 per pixel [2]
	irregular	global	6,000 per segment [1]
		local	0.67 per pixel[2]
NUV	predictable	global	170,000 (imaging) or 30,000 per stripe (spectroscopic)[1]
		local	50 per pixel[3] (imaging) or 70 per pixel (spectroscopic)
	irregular	global	68,000 (imaging) or 12,000 per stripe (spectroscopic)[1]
		local	50 per pixel (imaging) or 70 per pixel (spectroscopic)

1. The global count rate limit for observations using TIME-TAG mode is 30,000 counts/s
2. This local count rate screening limit is not applicable to the 1055 and 1096 cenwaves of the COS G130M grating. For these modes the limiting count rate is 0.2 count/s/pixel for both source types.
3. For imaging acquisitions, a count rate of 360 count/s in the 9×9-pixel box surrounding the target (as computed by the COS Imaging Acquisition ETC) represents an equivalent safe upper limit.

10.2 Screening Limits

The global and local count-rate screening limits for each COS configuration are given in Table 10.1. The limits are independent of observing mode (TIME-TAG or ACCUM). Compliance with these limits must be checked for all proposed COS targets by means of the Exposure Time Calculator (ETC), which issues warnings if they are exceeded. In Phase I, all proposed targets must be screened against these limits. In Phase II, the results of more detailed target and field checks must be submitted with the observing proposal; details are provided in Section 10.6. Note that the local count rate limits given in Table 1.2 and the local count rate screening limits given in Table 10.1 are not applicable to the 1055 and 1096 cenwaves of the COS G130M grating. For those modes the local limit is 0.2 count/s/pixel for both predictable and irregular sources.

10.3 Screening versus Data-Rate Limits

It is useful to compare the BOP limits with the 30,000 count/s limit on TIME-TAG exposures discussed in Section 5.2.1. In the FUV, a steep spectrum could exceed the BOP limit of 15,000 count/s per detector segment without exceeding the TIME-TAG limit. In the NUV, the BOP limit is considerably higher; a target that is perfectly safe could be far too bright to observe in TIME-TAG mode.

10.4 Source V Magnitude Limits

In the following tables, the screening limits in Table 10.1 are converted into *V* magnitude limits for a variety of sources. These values are not meant to be a substitute for the ETC, but rather an indication of whether a given object may be near the limit. The most sensitive spectroscopic setting and lowest rate limit (global or local) determine the listed values. Stellar spectra are assumed to be unreddened. Table 10.2 corresponds to spectroscopy through the PSA, Table 10.3 through the BOA, and Table 10.4 to NUV imaging for both apertures.

Table 10.2: V Magnitude Limits for PSA Spectroscopy

Spectral Class	FUV			NUV			
	G130M	G160M	G140L	G185M	G225M	G285M	G230L
O5 V	14.7	14.0	15.1	10.1	9.5	8.7	12.5
O7 V	14.5	13.8	14.9	10.0	9.5	8.6	12.4
O9 V	14.2	13.6	14.7	9.9	9.4	8.5	12.3
B0 V	14.2	13.5	14.6	9.8	9.3	8.4	12.2
B1 V	13.8	13.1	14.3	9.4	9.0	8.2	11.9
B3 V	12.8	12.5	13.4	8.8	8.4	7.7	11.3
B5 V	12.0	11.9	12.7	8.3	8.0	7.4	10.8
B8 V	10.9	11.0	11.5	7.5	7.2	6.7	10.0
A1 V	8.5	8.9	9.3	6.4	6.2	5.8	9.0
A3 V	6.4	7.8	8.3	6.1	6.0	5.6	8.7
A5 V	2.9	6.9	7.3	5.8	5.8	5.5	8.5
F0 V	–0.1	4.9	5.7	4.8	5.2	5.2	7.8
F2 V	–1.2	4.0	5.0	4.5	5.0	5.2	7.6
F5 V	–3.4	1.9	3.2	3.7	4.4	5.0	7.3
F8 V	–4.8	0.5	2.0	3.2	4.1	4.8	7.1
G2 V (Solar)	1.8	–0.5	3.4	1.4	2.7	4.4	6.8

Table 10.2: V Magnitude Limits for PSA Spectroscopy (Continued)

Spectral Class	FUV			NUV			
	G130M	G160M	G140L	G185M	G225M	G285M	G230L
G8 V (Tau Ceti)	3.0	–0.4	4.7	0.5	2.2	3.9	6.4
K2 V (Epsilon Eri)	4.0	–0.1	5.8	–0.8	1.1	3.2	6.1
KM III (Eta Ser)	–1.5	–1.4	0.2	–0.7	1.0	2.9	5.7
KM III (Alpha Boo)	–0.8	–2.3	0.9	–3.1	–1.1	0.9	4.7
KM III (Gamma Aql)	–2.3	–4.5	–0.5	–5.4	–3.9	–2.3	3.8
KM III (HD 146051)	–3.1	–5.0	–1.4	–7.0	–5.1	–3.1	3.3
KM III (Alpha Cet)	0.2	–1.5	1.9	–4.2	–1.9	–1.0	3.3
KM III (HD 123023)	0.0	–1.0	1.6	–3.2	–1.2	–0.3	3.7
KM III (Beta Gru)	–0.2	–0.6	1.5	–2.9	–1.0	0.7	3.4
T~50,000 K Blackbody	14.6	14.0	15.0	10.1	9.5	8.6	12.5
$F_\lambda \sim \lambda^{-1}$	11.0	10.6	11.5	7.2	7.2	6.7	9.9
F_λ = const surface brightness	11.1	10.9	11.8	7.7	8.0	7.6	10.7
F_λ = const point source	9.3	9.2	10.0	6.0	6.3	5.9	9.0

Table 10.3: V Magnitude Limits for BOA Spectroscopy

Spectral Class	FUV			NUV			
	G130M	G160M	G140L	G185M	G225M	G285M	G230L
O5 V	9.4	8.5	9.8	4.6	3.8	2.8	6.9
O7 V	9.2	8.4	9.6	4.4	3.7	2.7	6.8
O9 V	9.0	8.2	9.4	4.3	3.6	2.7	6.7
B0 V	8.9	8.0	9.3	4.2	3.5	2.6	6.6
B1 V	8.5	7.7	9.0	3.9	3.3	2.4	6.2
B3 V	7.5	7.0	8.1	3.2	2.7	1.9	5.6
B5 V	6.7	6.5	7.4	2.7	2.2	1.5	5.1
B8 V	5.5	5.5	6.2	1.9	1.5	0.8	4.3
A1 V	3.1	3.4	3.8	0.8	0.4	–0.1	3.3
A3 V	1.0	2.2	2.8	0.5	0.2	–0.3	3.0
A5 V	–2.5	1.4	1.8	0.2	0.0	–0.4	2.8

Table 10.3: V Magnitude Limits for BOA Spectroscopy (Continued)

Spectral Class	FUV			NUV			
	G130M	G160M	G140L	G185M	G225M	G285M	G230L
F0 V	–5.6	–0.7	0.1	-0.8	–0.6	–0.7	2.0
F2 V	–6.7	–1.6	–0.6	–1.2	–0.8	–0.8	1.7
F5 V	–8.8	–3.7	–2.4	–2.0	–1.4	–1.0	1.4
F8 V	–10.2	–5.0	–3.6	–2.5	–1.7	–1.1	1.2
G2 V (Solar)	–3.6	–6.1	–1.9	–4.3	–3.1	–1.5	0.8
G8 V (Tau Ceti)	–2.3	–5.9	–0.6	–5.2	–3.6	–2.0	0.3
K2 V (Epsilon Eri)	–1.2	–5.6	0.5	–6.4	–4.7	–2.7	0.1
KM III (Eta Ser)	–6.9	–6.9	–5.2	–6.3	–4.8	–3.1	-0.4
KM III (Alpha Boo)	–6.1	–7.8	–4.4	–8.7	–6.9	–5.1	–1.3
KM III (Gamma Aql)	–7.6	–10.0	–5.9	–11.1	–9.7	–8.2	–2.2
KM III (HD 146051)	–8.5	–10.5	–6.8	–12.6	–10.9	–9.0	–2.8
KM III (Alpha Cet)	–5.1	–7.0	–3.4	–9.7	–7.7	–7.0	–2.8
KM III (HD 123023)	–5.4	–6.5	–3.7	–8.8	–7.0	–6.4	–2.3
KM III (Beta Gru)	–5.6	–6.1	–3.8	–8.6	–6.8	–5.2	–2.6
T~50,000 K Blackbody	9.3	8.5	9.7	4.5	3.7	2.8	6.9
$F_\lambda \sim \lambda^{-1}$	5.7	5.1	6.2	1.6	1.4	0.8	4.2
F_λ = const surface brightness	5.8	5.4	6.4	2.2	2.2	1.7	5.0
F_λ = const point source	4.1	3.7	4.6	0.5	0.5	0.0	3.3

Table 10.4: V Magnitude Bright–Object Limits for Imaging

Spectral Class	PSA+MirrorA	PSA+MirrorB	BOA+MirrorA	BOA+MirrorB
O5 V	19.2	16.3	13.5	10.7
O7 V	19.1	16.1	13.4	10.5
O9 V	19.0	16.0	13.3	10.4
B0 V	18.9	15.9	13.2	10.3
B1 V	18.6	15.6	12.9	10.0
B3 V	18.1	15.0	12.4	9.3
B5 V	17.6	14.5	11.9	8.9
B8 V	16.9	13.7	11.1	8.0

Spectral Class	PSA+MirrorA	PSA+MirrorB	BOA+MirrorA	BOA+MirrorB
A1 V	15.8	12.6	10.1	6.9
A3 V	15.6	12.3	9.9	6.6
A5 V	15.3	12.0	9.6	6.2
F0 V	14.7	11.3	8.9	5.5
F2 V	14.4	11.0	8.6	5.2
F5 V	14.0	10.6	8.1	4.7
F8 V	13.7	10.3	7.8	4.4
G2 V (Solar)	13.0	9.6	7.1	3.7
G8 V (Tau Ceti)	12.6	9.1	6.6	3.2
K2 V (Epsilon Eri)	11.8	8.3	5.8	2.4
KM III (Eta Ser)	11.4	8.0	5.5	2.0
KM III (Alpha Boo)	9.6	6.1	3.6	0.2
KM III (Gamma Aql)	7.1	3.6	1.1	-2.3
KM III (HD 146051)	6.2	2.7	0.2	-3.3
KM III (Alpha Cet)	8.0	4.6	2.1	-1.3
KM III (HD 123023)	8.7	5.2	2.7	-0.7
KM III (Beta Gru)	8.9	5.5	3.0	-0.4
T~50,000 K Blackbody	19.2	16.2	13.5	10.6
$F_\lambda \sim \lambda^{-1}$	16.8	13.6	11.0	7.9
F_λ= const surface brightness	10.9	8.0	5.1	2.3
F_λ= const point source	15.8	12.6	10.1	6.9

10.5 Tools for Bright-Object Screening

10.5.1 The Bright Object Tool (BOT)

STScI has developed a Bright Object Tool (BOT) to facilitate field checking prior to COS program implementation. The BOT is implemented within APT (the Astronomer's Proposal Tool), using the Aladin interface, and reads target and exposure information from the Phase II proposal. Help files and training movies are available within APT. The BOT is based on displays of the Digital Sky Survey (DSS) and on automated analysis of the field using data from two catalogs: the second Guide Star Catalog (GSC2) and the *GALEX* catalog.

GSC2 provides two magnitudes (photographic *J* and *F*), hence one color, for most fields down to about magnitude 22, which, combined with conservative assumptions about spectral type vs. color, allow expeditious target and field checks. In some cases, the GSC2 is inadequate because of crowding or the absence of one filter. The APT/BOT automatically clears stars with only a single GSC2 magnitude if they are safe based on the assumption that the target is an unreddened O5V star. Any other unknown targets must be cleared by hand.

Automated *GALEX* screening is now available within the APT/BOT. The AIS (all-sky) sources are screened as unreddened O5V stars and reported as either safe, unsafe, or unknown. Because it is based directly on UV fluxes, *GALEX* screening can reveal, for example, previously unknown hot companions to late-type stars. If the field passes the BOT check, it is safe; unsafe and unknown objects require further investigation. ***Caveats:*** (1) The *GALEX* catalog does not cover the whole sky, so PIs must check that their COS field is fully covered by *GALEX*. (2) *GALEX* fluxes represent upper limits in crowded regions because of the instrument's relatively low spatial resolution. (3) The *GALEX* detectors suffer local non-linear effects at high count rates. The fluxes and magnitudes in the current version of the *GALEX* catalog are not corrected for these effects and may be underestimated for the brightest stars. A preliminary correction is presented in Morrissey et al. (2007, ApJS, 173, 682). The BOT now applies this correction to the *GALEX* catalog. As a result, it may report *GALEX* magnitudes that are brighter than those given in the *GALEX* catalog itself.

In general, a COS pointing with unconstrained telescope orientation requires the clearance of a field 43 arcsec in diameter. If any displacements from the default pointing (*e.g.,* acquisition scans, POS TARGs, patterns, or mosaics) are specified, then the field to be cleared increases commensurately. Because both the PSA and BOA are exposed to the sky at all times, no unsafe or unknown star may fall within 7 arcsec of either aperture at any allowed orientation. The BOT automatically accounts for the reduced throughput of the BOA and MIRRORB. The BOT automatically creates a macroaperture covering the expected field of view for an observation that accounts for a given combination of scans, POS-TARGs, patterns or mosaics. It also can account for the proper motion of the science target.

Note: Always check the science target with the ETC, rather than relying on the BOT field report. When constructing your Phase II proposal within APT, include the ETC exposure ID number to document your work and to facilitate the Phase II review.

10.5.2 The Exposure Time Calculator (ETC)

Should the tools available within the BOT be insufficient to clear a field object, its safety may be confirmed using the ETC.

An existing UV spectrogram of the target or class may be imported directly into the ETC. When using *IUE* data as input spectra in the ETC, consider only low-resolution spectra taken through the large aperture. Note that the ETC does not convolve imported spectra to the COS resolution. To be conservative, one must assume that the entire flux of an emission line falls within a single COS resolution element. The ETC can also have emission lines of a given intensity and width included in a calculation.

If model spectra are used in the ETC, the original Kurucz (not Castelli & Kurucz) models should be used for early-type stars. None of the provided models is adequate for late-type stars since the models lack chromospheric emission lines. Actual UV data must be used for late-type stars when possible. If a given star has only a *V* magnitude, it must be treated as an unreddened O5V star. If one color is available it may be processed as a reddened O5V star (which will always have a greater UV flux than an unreddened star of the same color).

If two colors are available, then the spectral type and reddening can be estimated separately. In some cases, the 2MASS *JHK* may be the only photometry available for an otherwise unknown star. The ETC supports direct entry of observed *J* and *H* magnitudes with E_{B-V}. It is also possible to estimate *V* and E_{B-V} from those data on the assumption of a reddened O5V star, and thus determine its count rates in the ETC. Martins & Plez (2006, A&A, 457, 637) derive $(J–H)_0 = –0.11$ for all O stars, and $(V–J)_0 = –0.67$ and $(V–H)_0 = –0.79$ for early O types. (The *K* band should be avoided for BOP purposes because of various instrumental and astrophysical complications.) Bessell & Brett (1988, PASP, 100, 1134), Appendix B, give relationships between the NIR reddenings and E_{B-V}.

10.6 Policies and Procedures

All COS exposures, whether target-acquisition, spectroscopic, or imaging, must be checked for bright objects. Any COS targets or fields that cannot be demonstrated to be safe to a reasonable level of certainty in the judgment of the Contact Scientist (CS) will not be observed. In that case, it is possible that equivalent alternative targets may be approved upon request. Any observations that trigger the onboard safety mechanisms will not be rescheduled.

COS GOs *must* enter the ETC calculation number for each discrete exposure into the appropriate field of the APT when preparing their Phase II material. A GO *must* also report any unsafe or unknown stars from APT/BOT for each field, and either show that the observations are safe or document any unresolved issues. (An exception is moving-target fields, which cannot be cleared until the scheduling windows have been established.) It is not expected that all such issues will be resolved by the Phase II deadline, but they should at least be identified and have planned resolutions by then.

Light from a bright nearby source could scatter into the PSA. For example, a target that is safe for the BOA may scatter enough light into the PSA to violate our screening limits. The region of concern is an annulus extending 5 to 15 arcsec from the center of the PSA. Any field object falling in this annulus may not produce a global count rate in excess of 1×10^5 count/s per segment for the FUV channel or 2×10^5 count/s for the NUV, or a local count rate over 3.3 count/s/pixel in the FUV or 250 count/s/pixel in the NUV. At present, the APT/BOT does not search for such objects, so they must be checked by hand. In such cases, count rates must be estimated using the ETC as though the source were at the center of the PSA.

In worst cases, new ground-based data or *HST* CCD UV exposures may be required to clear the fields for BOP; in general, the latter must be covered by the existing Phase I time allocation.

For unsafe targets, one solution is to change to a less sensitive instrument configuration: one could use the BOA, MIRRORB, or both (though the BOA is available-but-unsupported, see Section 2.4), a higher-resolution grating, or a less-sensitive wavelength setting. Note that the medium-resolution gratings actually have higher throughput than G140L when the data are rebinned, but are subject to brighter limits.

For unsafe field objects that threaten to fall into the non-target aperture, an orientation restriction (ORIENT) may be used to constrain the spacecraft roll angle and thus the position of the non-target aperture, but such constraints will limit the scheduling of the observation.

GOs planning COS observations of unpredictably variable targets, such as cataclysmic variables, should be aware of the special BOP procedures in effect for such cases. These include quiescence verification immediately preceding the COS observations, as detailed in ACS ISR 2006-04, which applies to all *HST* detectors subject to BOP. Observations of flare stars are allowed with COS (and STIS) only if the Contact Scientist is convinced that the target would not violate BOP limits even in its brightest state. STScI reserves the right to limit the number of visits requiring quiescence observations within 20 days or less of an *HST* observation to no more than 12 such visits per Cycle.

A pointing or configuration change after the targets and fields have been cleared by the STScI BOP review must be approved by the COS Team on the basis of a specific scientific justification and a new BOP review by the GO, which may be submitted via the CS.

10.7 On-Orbit Protection Procedures

Should an overly bright object be observed with COS, on-board software will typically act to protect the instrument from damage. The most serious response is to reduce the high voltage of the affected detector; subsequent observations will not take place until COS undergoes a safe-mode recovery procedure that is run from the ground. Activating any of the instrument protection levels listed below is regarded as a serious breach of our health and safety screening procedures and is cause for an investigation. Observers are responsible for ensuring that their observations do not endanger the instrument.

FUV Bright Object Protection

There are five levels of protection for the COS FUV detector:

1. At the lowest level are the screening limits imposed on observers in order to provide a margin of safety for the instrument. The screening limits (Table 10.1) are set a factor of two or more below actual risk levels, and we expect observers to work with us to ensure these limits are adhered to. They are determined by estimating the expected count rate from an object, both glob-

ally over the detector and locally in an emission line if appropriate. The COS ETC is the tool used for this check.

2. At the next level, within COS the "Take Data Flag" (TDF) is monitored during an exposure. If an event occurs that causes the TDF to drop (such as loss of lock on a guide star, which could lead to the telescope drifting), then the exposure will continue with the COS external shutter closed. Subsequent exposures in the visit may also be lost.
3. Next comes local rate monitoring. It is possible to permanently damage a localized region of the micro-channel plates without necessarily exceeding the global rate limits. This could occur if an object with bright emission lines were observed, for example. At the beginning of each exposure, the COS flight software bins the FUV spectrum by 4 pixels in x and 1024 in y; if the count rate in any bin exceeds 1000 counts per 15 s, the external shutter is closed and the calibration lamps turned off. All subsequent exposures until the next grating change or target acquisition are lost.
4. Global rate monitoring is next. The COS flight software continuously monitors the total event rate for both FUV detector segments. If the rate for either segment exceeds 600,000 counts in 10 s, the high voltage to both segments is turned off. Special commanding is required to turn on the FUV detector high voltage, so subsequent FUV observations will be lost, and the *HST* schedule will be disrupted.
5. At the highest level, the instrument is protected by software that senses an over-current condition in the high-voltage power supply; if triggered, the software shuts down the high voltage.

NUV Bright Object Protection

Similar protections also apply to the NUV detector:

1. At the lowest level are the screening limits imposed on observers to provide a margin of safety for the instrument. The screening limits (Table 10.1) are set a factor of two or more below actual risk levels, and we expect observers to work with us to ensure these limits are adhered to. They are determined by estimating the expected count rate from an object, both globally over the detector, and locally in an emission line if appropriate. The COS ETC is the tool used for this check.
2. At the next level, within COS the "Take Data Flag" (TDF) is monitored during an exposure. If an event occurs that causes the TDF to drop (such as loss of lock on a guide star, which could lead to the telescope's drifting), then the exposure will continue with the COS external shutter closed. Subsequent exposures in the visit may also be lost.
3. Next comes local rate monitoring. It is possible to permanently damage a small region of a micro-channel plate without exceeding the global rate limits. This could occur if an object were imaged or had a spectrum with bright emission lines, for example. Before each observation, the flight software takes a

0.3 s exposure, bins it in "superpixels" of 4 × 4 pixels each, and analyzes it in two passes. During the first pass, the flight software checks that each superpixel does not exceed the threshold values of 225 counts and 390 counts for imaging and spectroscopic observations, respectively. During the second pass, the software steps a box (of 1 × 2 superpixels for spectroscopic exposures and 2 × 2 pixels for imaging exposures) across the image, checking that the same limits are not exceeded in the larger area. The purpose of the second pass is to ensure that bright sources at the edge of the superpixels are not missed. This 0.3 s exposure is not recorded. If the local rate limit is exceeded, the COS flight software closes the external shutter and all subsequent exposures until the next grating change or target acquisition are lost.

4. Global rate monitoring is next. The COS flight software continuously monitors the total event rate for the NUV MAMA. If the total count rate exceeds 20,000 in 0.1 s the high voltage to the MAMA is turned off, the external shutter is closed, and the calibration lamps are turned off. The NUV detector can resume operations only after a safe-mode recovery procedure, so subsequent NUV exposures will be lost, and the *HST* schedule disrupted.

5. At the highest level, the NUV MAMA is protected by the detector electronics. The Bright-Scene Detector (BSD) monitors the output of every 2 anode wires across the detector, corresponding to every 32nd row of pixels. The wires are parallel to the dispersion axis. If the total count rate exceeds 17,000 in 138 ms, then the high voltage is turned off. COS can resume operations only after a safe-mode recovery procedure. BSD differs from global-rate monitoring in two ways: it is done in hardware, not software, and what is measured is not a digitized count rate, but current in the anode grid wires.

CHAPTER 11:

Data Products and Data Reduction

In this chapter…

11.1 Overview

Raw COS data are processed through the STScI Data Processing pipeline. Data first undergo Generic Conversion, by which bits from individual exposures are unpacked and combined into files containing raw, uncalibrated data. Next, the raw files are processed through the COS calibration pipeline, **calcos**, which performs image and spectroscopic reduction to produce output files useful for scientific analysis. Finally, the data are ingested into the Hubble Data Archive through the Data Archive and Distribution System (DADS). This system populates a database containing header keywords that is accessible to users via the Mikulski Archive for Space Telescopes (MAST). Both calibrated and uncalibrated data are then available for distribution by MAST to the user.

11.2 COS Data Files

When data are taken in TIME-TAG mode (the default), the raw data are in the form of a table of photon events containing the arrival time, *x* and *y* pixel coordinates, and pulse height (for FUV data) for each photon detected. Raw ACCUM data are in the form of a 2-D image. For FUV data, there will be two raw files for each exposure, one file for Segment A and one for Segment B. For NUV data, there will be one raw file for each exposure.

The calibrated data have the same general format for both FUV and NUV, although there are differences in detail. There is a "corrtag" file (the file name contains the string "corrtag") containing a corrected events table. The corrtag table includes all of the columns from the raw data file, plus these additional columns: a weight that accounts for the flat-field and dead-time corrections, a data-quality column, and a column that gives the pulse-height amplitude of each event. (Codes for the DQ flags are listed on the COS website.) The corrtag file provides several sets of corrected pixel coordinates for each event. These include X[Y]CORR, which are corrected for thermal drifts in the detector electronics, geometric distortions in the detector; and Y walk; XDOPP, which are the *x* coordinates corrected for orbital Doppler motions; X[Y]FULL, which are the XDOPP and YCORR coordinates corrected for OSM drift and recast into a coordinate system defined by the WAVECAL spectrum; and WAVELENGTH, which provides the wavelength corresponding to the XFULL coordinate. The corrtag file has a separate extension containing timeline information. It provides second-by-second values for the spacecraft position, solar and target altitude above the horizon, and count rates for the most prominent airglow lines and the background. The data in this extension can be useful when reprocessing TIME-TAG data, allowing the user to exclude, for example, data obtained during orbital day. For ACCUM data, the corrtag table has the same format, but all the values in the TIME column are a constant, half the exposure time. There is one row in this pseudo-TIME-TAG table for each count in the raw ACCUM image.

Additional calibrated files include the flt and counts images, which are created by binning the events in the corrtag table. Both images have units of counts/s, but the flt image is also corrected for flat-field and dead-time effects. For spectroscopic data, a 1-D extracted spectrum (or three spectra, for NUV exposures) will be written to an x1d file for each exposure. For data in an association (whereby multiple exposures are processed together—the usual case), the 1-D spectra for separate exposures will be averaged and written to an x1dsum table. If multiple FP-POS settings are used, there will be one x1dsum file for each FP-POS (x1dsum[1,2,3,4]), even if only one spectrum was obtained at each position. The distinction between the x1d and x1dsum files in such cases is that the data-quality weights, the DQ_WGT column of the x1d files, are used to eliminate bad or suspect data (such as detector dead spots). The x1dsum file without a number is the final sum of all of the exposures. It can be a weighted mean of all the x1dsum[n] files or, if a single exposure was obtained at a single FP-POS setting, a copy of the x1d file with the DQ_WGTs applied.

By default **calcos** will combine data taken at different `FP-POS` settings, but not at different central wavelengths. A new association is created when either the grating or central wavelength is changed, and **calcos** only combines data within an association. A tool for combining spectra is the "splice" task in the **ctools** package of **IRAF/PyRAF**. This program was written for STIS data, but it can be run on COS data, though not all of the input columns will be preserved.

Wavelength calibration can be performed in either of two ways. The default (specified as `FLASH=YES`) is to take line-lamp exposures ("wavecal" exposures) simultaneously with the science data. In this case, the wavecal spectra will be extracted and saved in lampflash tables. The alternative is to take separate wavecal exposures interspersed with the science exposures. These wavecals will be calibrated in the same way as science exposures, except that the calibrated wavecal data (`corrtag`, `flt`, `counts`, `x1d`) will not be corrected for the offset of the spectrum from the template, and no `x1dsum` file will be created for a wavecal.

11.3 Additional COS Files

Several additional files are used in the processing of COS data. These include association files (`asn`), which are used to control calibration processing; engineering support files (`spt`), which contain information used in the pipeline processing; and lampflash files (`lampflash`), which contain extracted wavelength calibration spectra used in the processing of `TIME-TAG` data with `FLASH=YES`. For a full description of these and other files, see the *COS Data Handbook*.

CHAPTER 12:

The COS Calibration Program

In this chapter...

12.1 Introduction

In this chapter, we provide a brief overview of the calibration observations obtained during ground testing and on-orbit through Cycle 23. Potential Cycle 24 observers should assume that all of these calibrations will be completed by the time that Cycle 24 begins.

Observers who wish to use instrument configurations that are not addressed by these calibration plans should assess their specific calibration needs and include time in their Phase I proposal for any additional calibrations that are required. Proposers who believe that more extensive calibration observations or analysis may be of general benefit to the COS user community should consider submitting a Cycle 24 Calibration Outsourcing Proposal (see the Cycle 24 Call for Proposals for details).

12.2 Ground Testing and Calibration

The COS Instrument Definition Team (Principal Investigator, James Green, University of Colorado) was responsible for the ground testing and ground calibration of COS. Most of the ground test data was obtained in 2003 and 2006 during thermal vacuum testing at Ball Aerospace and Goddard Space Flight Center, respectively. These tests characterized the basic properties of the optics, the detectors, and the mechanisms. While some measurements (e.g., FUV full-detector flat-field images) cannot be repeated in orbit, most of the ground-test data have been superseded by on-orbit measurements obtained during SMOV4.

12.3 SMOV4 Testing and Calibration

The primary goal of the Observatory Verification program for Servicing Mission 4 (SMOV4) was the timely commissioning of *HST* for normal science operations. For the newly-installed COS, this included testing the focus (internal and external), verifying the target-acquisition procedures, monitoring instrument stability (both in terms of image motions and sensitivity), and measuring plate scales, line-spread functions, and other instrument parameters. SMOV4 observations were completed in October 2009, and a series of Instrument Science Reports (ISRs) detailing the results of their analysis have been published. Those ISRs and the observing programs on which they are based are listed in Table 12.1.

Table 12.1: COS ISRs Resulting from SMOV4 Calibration Programs

Number	Title	Author	Associated SMOV Programs
2009-01	Preliminary Characterization of the Post-Launch Line-Spread Function of COS	Ghavamian et al.	11489, 11476
2010-01	SMOV Absolute Flux Calibration of the COS NUV Modes	Massa et al.	11479
2010-02	SMOV Absolute Flux Calibration of the COS FUV Modes	Massa et al.	11492
2010-03	COS Near-UV Flat Fields and High S/N Determination from SMOV Data	Ake et al.	11478, 11481
2010-04	SMOV: COS NUV On-Orbit Optical Alignment	Hartig et al.	11468, 11469
2010-05	SMOV: COS NUV Wavelength Calibration	Oliveira et al.	11470, 11474, 11475
2010-06	SMOV: COS FUV Wavelength Calibration	Oliveira et al.	11485, 11488, 11487
2010-07	SMOV: COS FUV Focus Determination	Lennon et al.	11484

Number	Title	Author	Associated SMOV Programs
2010-08	NUV Spectroscopic Performance	Beland & Ghavamian	11476, 11477
2010-09	FUV Spectroscopic Performance	Ghavamian et al.	11489, 11490
2010-10	SMOV: COS NUV Imaging Performance	Goudfrooij et al.	11473
2010-11	FUV Darks	Sahnow et al.	11356, 11482, 11484
2010-12	NUV Darks	Sahnow et al.	11355, 11466,
2010-13	NUV/FUV Structural and Thermal Stability	Smith & Keyes	11480, 11493
2010-14	COS Target Acquisition Guidelines, Recommendations, and Interpretation	Keyes & Penton	11471, 11472, 11486

12.4 COS Monitoring Programs

An overview of the COS monitoring programs is given in Table 12.2 along with the ID numbers of completed programs. Table 12.3 lists COS contingency programs. Details on special calibration programs that were undertaken in a particular Cycle are given the appropriate subsection below.

Table 12.2: COS Monitoring Calibration Program

Title	Accuracy Achieved	Program IDs	Products
NUV Monitors			
NUV MAMA Fold Distribution	<5% at the location of the peak of the fold distribution	11891 (Cycle 17) 12419 (Cycle 18) 12723 (Cycle 19) 13128 (Cycle 20) 13531 (Cycle 21) 13976 (Cycle 22) 14444 (Cycle 23)	ISR
NUV Dark Monitor	<0.2% in the global dark rate uncertainty	11894 (Cycle 17) 12420 (Cycle 18) 12720 (Cycle 19) 13126 (Cycle 20) 13528 (Cycle 21) 13974 (Cycle 22) 14442 (Cycle 23)	ISR

Table 12.2: COS Monitoring Calibration Program (Cont'd)

Title	Accuracy Achieved	Program IDs	Products
NUV Monitors			
NUV Spectroscopic Sensitivity Monitor	S/N ~ 30 at λ_{cen}	11896 (Cycle 17) 12421 (Cycle 18) 12719 (Cycle 19) 13125 (Cycle 20) 13527 (Cycle 21) 13973 (Cycle 22) 14441 (Cycle 23)	COS ISR 2010-15 Reference File
NUV Imaging Sensitivity	S/N ~ 60, observed to a predicted countrate accuracy of 0.1%	11899 (Cycle 17)	ISR Reference File
NUV Internal/External Wavelength Scale Monitor	1.7–3.7 pixels in wavelength scale accuracy	11900 (Ccyle17) 12422 (Ccyle18) 12722 (Ccyle19) 13127 (Cycle 20) 13529 (Cycle 21) 13975 (Cycle 22) 14443 (Cycle 23)	Reference File
NUV Flat Monitor	S/N = 20–25 per 3.3 pixel element	12721 (Cycle 19)	ISR
COS ACQ/IMAGE Performance Monitoring	WCA–PSA offsets to <0.5 pixels	13124 (Cycle 20) 13526 (Cycle 21) 13972 (Cycle 22) 14440 (Cycle 23)	
FUV Monitors			
FUV Dark Monitor	Rate < 10^{-6} count/pixel/s 0.1% in global dark rate uncertainty	11895 (Cycle 17) 12423 (Cycle 18) 12716 (Cycle 19) 13121 (Cycle 20) 13521 (cycle 21) 13968 (Cycle 22) 14436 (Cycle 23)	ISR
FUV Spectroscopic Sensitivity Monitor	S/N = 30 at λ_{cen}	11897 (Cycle 17) 12424 (Cycle 18) 12715 (Cycle 19) 13119 (Cycle 20) 13520 (Cycle 21) 13967 (Cycle 22) 14435 (Cycle 23)	COS ISR 2010-15 Reference File
FUV Internal/External Wavelength Monitor	Wavelength zeropoint accuracies: G130M: 5.7–7.5 pixels G160M: 5.8–7.2 pixels G140L: 7.5–12.5 pixels	11997 (Cycle 17) 12425 (Cycle 18) 12717 (Cycle 19) 13122 (Cycle 20) 13522 (Cycle 21) 13969 (Cycle 22) 14436 (Cycle 23)	Calibration Workshop Paper ISR Reference File

Table 12.3: COS Contingency Programs

Title	Program IDs
NUV Detector Recovery after Anomalous Shutdown	11892 (Cycle 17) 12430 (Cycle 18) 12724 (Cycle 19) 13129 (Cycle 20) 13533 (Cycle 21) 13978 (Cycle 22) 14446 (Cycle 23)
FUV Detector Recovery after Anomalous Shutdown	11893 (Cycle 17) 12431 (Cycle 18) 12718 (Cycle 19) 13123 (Cycle 20) 13532 (Cycle 21) 13977 (Cycle 22) 14445 (Cycle 23)

12.5 Cycle 17 Calibration Program

The Cycle 17 calibration program continued the testing begun during SMOV. It included long-term programs to monitor the sensitivity and wavelength scale of both the NUV and FUV detectors. Midway through Cycle 17, additional calibration programs were added. Brief descriptions of these monitoring programs are presented in Table 12.2. Table 12.4 lists additional special calibration programs that were undertaken in Cycle 17. A comprehensive review of the Cycle 17 calibration program was published in COS ISR 2012-02 (Osten et al. 2012).

Table 12.4: Cycle 17 Calibration Program

Program ID	Title	Accuracy Achieved	Products
12010	COS FUV Line Spread Function Characterization	Continuum S/N = 9.2 near 1530 Å	COS ISR 2009-01, Tables of LSF models
12052	COS NUV Grating Efficiency Test	Few percent uncertainty in count-rate ratios	Calibration Workshop paper, ISR
12080	G140L Focus Sweep	30% uncertainty in autocorrelation FWHM of spectra	ISR
12081	COS Flux Calibration Below 1150 Å with G140L/1280	3% for 900–1150 Å, 10% for 300–700 Å	ISR, Reference file
12082	Extending COS/ G130M Coverage Down to 905 Å with Two New Central Wavelengths	wavelength scale: ± 0.5 Å, sensitivity: ± 5–10%, resolution: 20–30%	ISR, Reference file
12083	G140L/1280 Wavecal Template	N/A	Reference file
12084	G140L/1280 Internal-to-External Wavelength Scales	7.5–12.5 pixel wavelength zero-point accuracy	Reference file
12085	STIS/E230M Data to Determine Internal-to-External Offsets in COS/G230L	Not evaluated yet.	Reference file
12086	Generation of 1-D Fixed-Pattern Templates	2%	Reference file, ISR
12096	COS FUV Detector Lifetime Position Test	min S/N per resel of 30 at λ_{cen}	ISR

12.6 Cycle 18 Calibration Program

The Cycle 18 calibration program continued the calibration and monitoring observations performed in Cycle 17, including long-term programs to monitor the sensitivity and wavelength scale of both the NUV and FUV detectors. Brief descriptions of these monitoring programs are presented in Table 12.2. Table lists additional special calibration programs that were undertaken in Cycle 18. A comprehensive review of the Cycle 18 calibration program was published in COS ISR 2013-04 (Kriss et al. 2012).

Table 12.5: Cycle 18 Calibration Program FUV Lifetime Position Calibration Program

Program ID	Title	Accuracy Achieved	Products
12414[1]	COS Observations of Geocoronal Lyman-α Emission	G140L: S/N = 2 per pixel at 1200 Å, G130M: S/N = 2 per pixel at 1213 Å	List of exposures on the COS website[2] that GOs may use to model and subtract Lyman-α
12426	FUV Sensitivity Characterization	S/N ~ 10/pixel	ISR, Reference file
12432	COS FUV Detector Gain Sag vs. High Voltage	1% over 2 Å bands	Decision on change of voltage or lifetime position

1. Coordinated parallel with STIS calibration program 12414.
2. http://www.stsci.edu/hst/cos/calibration/airglow.html.

As described in Section 4.1.7, gain sag affects spectra obtained with the FUV detector. To address this problem the COS team performed studies to move the Aperture Mechanism so that the FUV spectra fell on a different part of the detector, called a lifetime position. This work was divided into three phases. Table 12.6 lists the programs that were used to determine the location of the new lifetime position, enable science at that location, and finally calibrate observations obtained there. The additional lifetime calibration program "Second COS FUV Lifetime Position: Wavelength Scales (FCAL1)" uses observations from programs 12805, 12806, and 12796.

Table 12.6: Lifetime Position 2 Calibration Program

	I. Identify the New Lifetime Position
12676	COS/FUV Characterization of Detector Effects
12677	COS/FUV Mapping of the Stray PtNe Light through FCA
12678	COS/FUV Characterization of Optical Effects
	II. Enable Science at the New Lifetime Position
12793	Second COS FUV Lifetime Position: FUV Detector High Voltage Sweep (FENA1)
12795	Second COS FUV Lifetime Position: Verification of Aperture and FUV Spectrum Placement (FENA2)
12796	Second COS FUV Lifetime Position: Focus Sweep Enabling Program (FENA3)

12797	Second COS FUV Lifetime Position: FUV Target Acquisition Parameter Update (FENA4)
	III. Calibrate the New Lifetime Position
12805	Second COS FUV Lifetime Position: Wavelength and Resolution Calibration (FCAL2)
12806	Second COS FUV Lifetime Position: Flux and Flat-field Calibration and TDS Transfer (FCAL3)
12807	Second COS FUV Lifetime Position: Verification of FUV BOA Operations (FCAL4)

Phase I was part of Cycle 18. Phases II and III took place during Cycle 19.

12.7 Cycle 19 Calibration Program

The Cycle 19 calibration program continued the routine calibration and monitoring observations performed in Cycle 18, including long-term programs to monitor the sensitivity and wavelength scale of both the FUV and NUV detectors. Brief descriptions of these monitoring programs are presented in Table 12.7. Table 12.7 lists additional special calibration programs that were undertaken in Cycle 19. A comprehensive review of the Cycle 19 calibration programs is detailed in COS ISR 2014-01 (Duval et al., 2014).

Table 12.7: Cycle 19 Calibration Program

Program ID	Title	Accuracy Achieved	Products
12775[1]	COS Observations of Geocoronal Lyman-α Emission	G140L: S/N = 2 per pixel at 1200 Å, G130M: S/N = 2 per pixel at 1213 Å	List of exposures on the COS website[2] that GOs may use to model and subtract Lyman-α
13070	Characterization of the Spatial Resolution and Wavelength Solution of the New FUV Modes (C1055, C1096, C1222)	10% in residual difference between model and observations	ISR, LSFs for C1055, C1096, C1222

1. Coordinated parallel with STIS calibration program 12775.
2. http://www.stsci.edu/hst/cos/calibration/airglow.html.

12.8 Cycle 20 Calibration Program

The Cycle 20 calibration program continued the routine calibration and monitoring observations performed in Cycle 19, including long-term programs to monitor the sensitivity and wavelength scale of both the FUV and NUV detectors. Brief descriptions of these monitoring programs are presented in Table 12.2. Table 12.8. lists additional special calibration programs that were undertaken in Cycle 20.

Table 12.8: Cycle 20 Calibration Program

Program ID	Title	Accuracy Achieved	Products
13145[1]	COS Observations of Geocoronal Lyman-α Emission	G140L: S/N = 2 per pixel at 1200 Å, G130M: S/N = 2 per pixel at 1213 Å	List of exposures on the COS website[2] that GOs may use to model and subtract Lyman-α

1. Coordinated parallel with STIS calibration program 13145.
2. http://www.stsci.edu/hst/cos/calibration/airglow.html.

12.9 Cycle 21 Calibration Program

The Cycle 21 calibration program continued the routine calibration and monitoring observations performed in Cycle 20, including long-term programs to monitor the sensitivity and wavelength scale of both the FUV and NUV detectors. Brief descriptions of these monitoring programs are presented in Table 12.2. Table 12.9 lists additional special calibration programs that were undertaken in Cycle 21.

Table 12.9: Cycle 21 Calibration Program

Program ID	Title	Accuracy Achieved	Products
13523	PtNe Lamp Cross Calibration	lamp flash times to within 10%	ISR tables of lamp flash times for Lamp 2
13530	NUV Focus Sweep	Analysis in progress	ISR

12.10 Cycle 22 Calibration Program

The Cycle 22 calibration plans for COS (see Table 12.10) continued the routine calibration and monitoring observations performed in Cycles 17–21. Brief descriptions of these monitoring programs are presented in Table 12.2.

The program also included enabling and calibration programs designed to facilitate the move to Lifetime Position 3 (LP3).

Table 12.10: Cycle 22 Calibration Program

Program ID	Title	Accuracy Achieved	Products
13970	COS FUV Detector Gain Maps	NA	Gain maps of detector
13971	Characterization of HV change effect on sensitivity	NA	ISR

Table 12.11: Lifetime Position 3 Calibration Program

	I. Optimize New Lifetime Position
13617	Characterization of COS/FUV modal gain at lifetime position 3 {LOP1}
13618	Optimization of COS/FUV spectrum placement at lifetime position 3 {LOP2}

	II. Enable New Science at the New Lifetime Position
13634	Verification of Aperture and FUV Spectrum Placement for COS at LP3 {LENA1}
13635	FUV Focus Sweep Enabling Program for COS at LP3 (LENA2)
13636	Third COS FUV Lifetime Position: FUV Target Acquisition Parameter Update {LENA3}
13637	COS FUV Detector Response to New HV Management System at LP3 {LENA4}
	III. Calibrate the New Lifetime Position
13931	Third COS FUV Lifetime Position: Wavelength and Resolution Calibration (LCAL2)
13932	Third COS FUV Lifetime Position: Cross-Dispersion Profiles, Flux, and Flat-Field Calibration (LCAL3)
13933	Third COS FUV Lifetime Position: Verification of FUV BOA Operations (LCAL4)

12.11 Cycle 23 Calibration Program

The Cycle 23 calibration plans for COS continue the routine calibration and monitoring programs performed in previous Cycles. Brief descriptions of the programs are listed in Table 12.2. The full calibration plan for Cycle 23 is listed in Table 12.12.

Table 12.12: Cycle 23 Calibration Programs

Program Name	Program ID
NUV MAMA Fold Distribution	14444
NUV Detector Dark Monitor	14442
NUV Spectroscopic Sensitivity Monitor	14441
NUV Internal/External Wavelength Scale Monitor	14443
FUV Detector Dark Monitor	14436
FUV Spectroscopic Sensitivity Monitor	14435
FUV Internal/External Wavelength Scale Monitor	14437
COS FUV Detector Gain Maps	14439
COS Pure Parallel Observations of Geocoronal Ly alpha	14438
COS Target Acquisition Monitor	14440

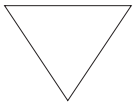

If your program requires calibrations beyond those described here, then you should explicitly include this calibration in your Phase I proposal.

CHAPTER 13:

Spectroscopic Reference Material

In this chapter...

13.1 Introduction

The information in this chapter will help you to select a detector, grating configuration, and observing aperture, and to develop your observing plan. For each grating, the following information is provided:

- A brief description of the grating, with special considerations for its use.
- Grating parameters, including the dispersion and plate scale.
- Plots showing the available central-wavelength settings and the range of wavelengths covered by each setting and (for the FUV gratings) `FP-POS` position.
- Plots and tables of sensitivities and effective areas as a function of wavelength.
- Plots of signal-to-noise ratio as a function of STMAG, F_λ, and exposure time.

Note that the quoted sensitivities are estimates for mid-Cycle 23 (April 2016). The COS Exposure Time Calculator (ETC) will be updated as the instrument's sensitivity continues to evolve. See the COS website for the latest information.

13.2 Using the Information in this Chapter

13.2.1 Grating Parameters

For each grating, the resolving power and dispersion are taken from Table 5.1. Plate scales are derived from data obtained during SMOV.

13.2.2 Wavelength Ranges

For each grating, we plot the wavelengths sampled by each central-wavelength setting. For the NUV gratings, the central wavelength is the approximate midpoint of stripe B. For the FUV gratings, the central wavelength is (approximately) the shortest wavelength recorded on Segment A. Wavelength ranges for each central wavelength at `FP-POS=3` are provided in tabular format in Table 5.3 and Table 5.4.

For the FUV gratings, the wavelength ranges sampled at each `FP-POS` position are plotted separately. For the NUV gratings, the total wavelength range sampled by all `FP-POS` positions is plotted for each central-wavelength setting.

Figure 13.1 shows how some wavelengths are covered by multiple modes, but on different parts of the FUV detectors.

Figure 13.1: Wavelength Coverage of the COS Gratings

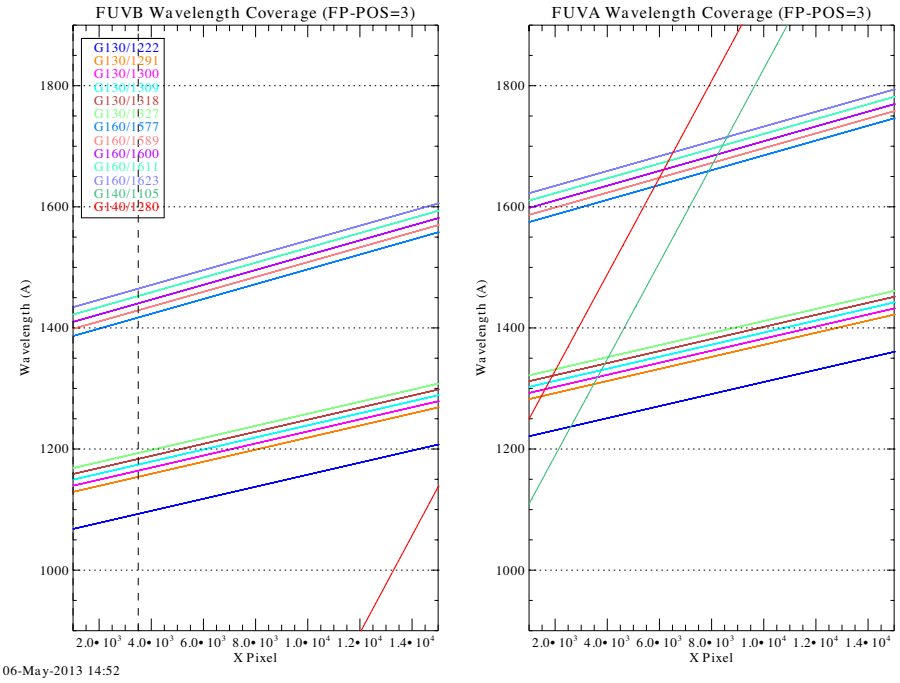

13.2.3 Grating Sensitivities and Effective Areas

This section presents sensitivities and effective areas as a function of wavelength for each grating. The target is assumed to be a point source centered in the PSA. For both the FUV and NUV detectors, the total systemic[1] *spectroscopic point-source sensitivity,* S_λ^p, has units of counts pix_λ^{-1} s^{-1} per incident erg cm^{-2} s^{-1} $Å^{-1}$, where

- pix_λ = a pixel in the dispersion direction, and
- counts refer to the total counts from a point source integrated over the PSF in the direction perpendicular to the dispersion.

The count rate per pixel is simply the product of the target flux and the point-source sensitivity at a given wavelength. To estimate the signal-to-noise ratio (S/N) achieved at a given count rate and exposure time, follow the directions in Section 7.3 or use the S/N plots in this chapter.

The effective area has units of cm^2.

13.2.4 Signal-to-Noise Plots

For each grating, a plot is provided to help you estimate the S/N that can be achieved from a point source observed at a fiducial wavelength near the peak of the effective-area curve. The fiducial wavelength is indicated in the ordinate label of each plot. To estimate the S/N at other wavelengths, scale your source flux or magnitude by the relative sensitivities at the wavelength of interest and at the fiducial. The plots show S/N as a function of F_λ and of STMAG for a range of exposure times. $STMAG_\lambda$ is the color-dependent correction from V magnitude to STMAG at wavelength λ. Values of $STMAG_\lambda$ for various stellar and extragalactic sources are presented in Table 13.1 and Table 13.2, respectively. In producing these plots, we assumed an average sky background (as described in Chapter 7) and the dark current appropriate for each detector. These plots should be used only for rough estimates of exposure times. When constructing your proposal, use the COS ETC to estimate S/N values.

Note the following.

- The point source S/N has been calculated per resolution element and has been integrated over the PSF to contain all of the flux in the cross-dispersion direction.
- The symbols in the S/N figures delineate regions of parameter space where the dark current contributes more than half the source counts.
- The vertical shaded area indicates the bright-object screening limit given in Table 10.1.

Follow these steps to use the S/N plots.

1. Look up, in Table 13.1, the effective temperature and wavelength region of interest (e.g., 5000 K at 2000 Å). Interpolate in the table to get $STMAG_\lambda$.

1. COS plus *HST* Optical Telescope Assembly (OTA).

2. Add the V magnitude of the target to get STMAG.
3. Find the appropriate plot for the desired grating and locate STMAG on the horizontal axis. Read off the S/N for the desired exposure time, or vice-versa. Alternatively, use F_λ directly on the horizontal axis.
4. To get accurate values for repeated, or `FP-POS`, exposures use the sub-exposure time when consulting the plot, and then multiply the resulting S/N by $\sqrt{N}$, where N is the number of sub-exposures to be averaged.

For example, consider a $V = 15$ mag star of spectral type B0V, for which we want to derive the S/N achieved in a 100 s exposure using the NUV grating G230L. The S/N calculations for G230L are presented in Figure 13.28, where we learn that the fiducial wavelength for this grating is 3001 Å. Assuming an effective temperature of 30,000 K, we obtain $\text{STMAG}_\lambda \sim -2.1$ at 3000 Å from Table 13.1, making STMAG = 12.9. Returning to Figure 13.28, we find this value on the horizontal axis. For an exposure time of 100 s, we find S/N ~ 9.5.

Table 13.1: STMAG_λ as a Function of Wavelength for Stellar Objects

Temp (K)	Wavelength (Å)									
	1000	1200	1500	2000	2500	3000	3500	4000	4500	5000
45000	–5.87	–5.46	–4.79	–3.87	–3.02	–2.36	–1.76	–1.27	–0.79	–0.37
30000	–5.38	–4.92	–4.37	–3.50	–2.70	–2.13	–1.56	–1.23	–0.76	–0.35
20000	–3.90	–3.38	–3.45	–2.73	–2.14	–1.66	–1.18	–1.13	–0.72	–0.33
15000	–1.68	–1.24	–2.68	–2.08	–1.53	–1.21	–0.83	–1.05	–0.68	–0.31
10000	9.18	6.27	–0.72	–0.68	–0.26	–0.21	–0.03	–0.88	–0.62	–0.29
9000	12.84	8.67	1.81	–0.19	0.15	0.05	0.16	–0.75	–0.58	–0.26
8000	17.10	11.79	6.33	0.51	0.58	0.21	0.24	–0.56	–0.46	–0.20
7000	20.97	15.07	9.29	1.86	1.26	0.36	0.24	–0.34	–0.32	–0.12
6000	N/A	19.44	14.17	5.50	2.92	0.94	0.47	0.02	–0.15	–0.04
5000	N/A	N/A	20.15	9.80	6.24	2.74	1.24	0.50	0.04	0.10
4000	N/A	N/A	N/A	14.74	9.70	5.53	2.37	0.97	0.24	0.58
3000	N/A	N/A	N/A	17.85	11.46	5.69	2.22	0.71	0.25	0.82

Table 13.2: $STMAG_\lambda$ as a Function of Wavelength for Non–Stellar Objects

Spectrum	Wavelength (Å)							
	1500	**2000**	**2500**	**3000**	**3500**	**4000**	**4500**	**5000**
Elliptical	3.35	3.19	4.17	2.92	1.60	0.70	0.17	0.15
S0	4.63	3.95	3.27	2.23	1.61	0.71	0.18	0.13
Sa	2.64	2.27	2.39	1.78	1.31	0.36	0.12	0.07
Sb	1.70	2.59	2.04	1.32	1.12	0.43	0.17	0.10
Sc	–0.18	0.44	–0.17	–0.68	–0.67	–0.51	–0.44	–1.25
Starburst, $E(B–V) < 0.1$	–1.71	–1.15	–0.68	–0.43	–0.13	–0.42	–0.23	–1.24
Starburst, $0.25 < E(B–V) < 0.35$	–0.95	–0.87	–0.33	–0.10	0.08	–0.19	–0.19	–0.28
Starburst, $0.51 < E(B–V) < 0.60$	–0.40	–0.18	0.01	0.23	0.03	–0.14	–0.12	–0.36
Starburst, $0.61 < E(–V) < 0.70$	0.05	0.31	0.31	0.15	0.27	–0.17	–0.13	–0.11

The $STMAG_\lambda$ values of Table 13.1 are derived from the stellar models of Castelli and Kurucz (2003, 2004), assuming solar metallicity ([Fe/H] = 0.0) and a surface gravity of $\log(g) = 4.5$. The $STMAG_\lambda$ values of Table 13.2 are based on observed spectra of each object type.

13.3 Gratings

For each COS grating, we present the resolving power, dispersion, plate scale, the wavelength range covered at each central wavelength setting and `FP-POS` position, sensitivities, effective areas, and a tool for estimating S/N. Advice on use is provided where appropriate.

Note that the quoted sensitivities are estimates for mid-Cycle 23 (April 2016). The COS ETC will be updated as the instrumental sensitivity evolves. Users should be aware that the BOA is not well calibrated below 1200 Å, and is an available-but-unsupported mode (See Section 2.4).

Wavelengths in this handbook, and in COS data products, are always measured in vacuum.

Gratings:

FUV Grating G130M

Description

The G130M grating samples wavelengths between about 900 and 1450 Å. (Its use at shorter wavelengths is discussed below.) It offers higher resolution and effective area than the G140L grating, but less spectral coverage.

Special Considerations

The gap between segments A and B spans 14.3 Å. To fill this gap requires exposures separated by two central-wavelength settings.

Grating	Resolving Power $R = \lambda/\Delta\lambda$	Dispersion (mÅ pixel^{-1})	Plate Scale (milliarcsec pixel^{-1})		FP-POS Step (Å step^{-1})
			Disp. Axis	Cross-Disp. Axis	
G130M	16,000 - 21,000[1]	9.97	22.9	100	2.5

1. See below for the 1055, 1096, and 1222 settings, which have $R < 13{,}000$.

Figure 13.2: Wavelength Ranges for the G130M Grating

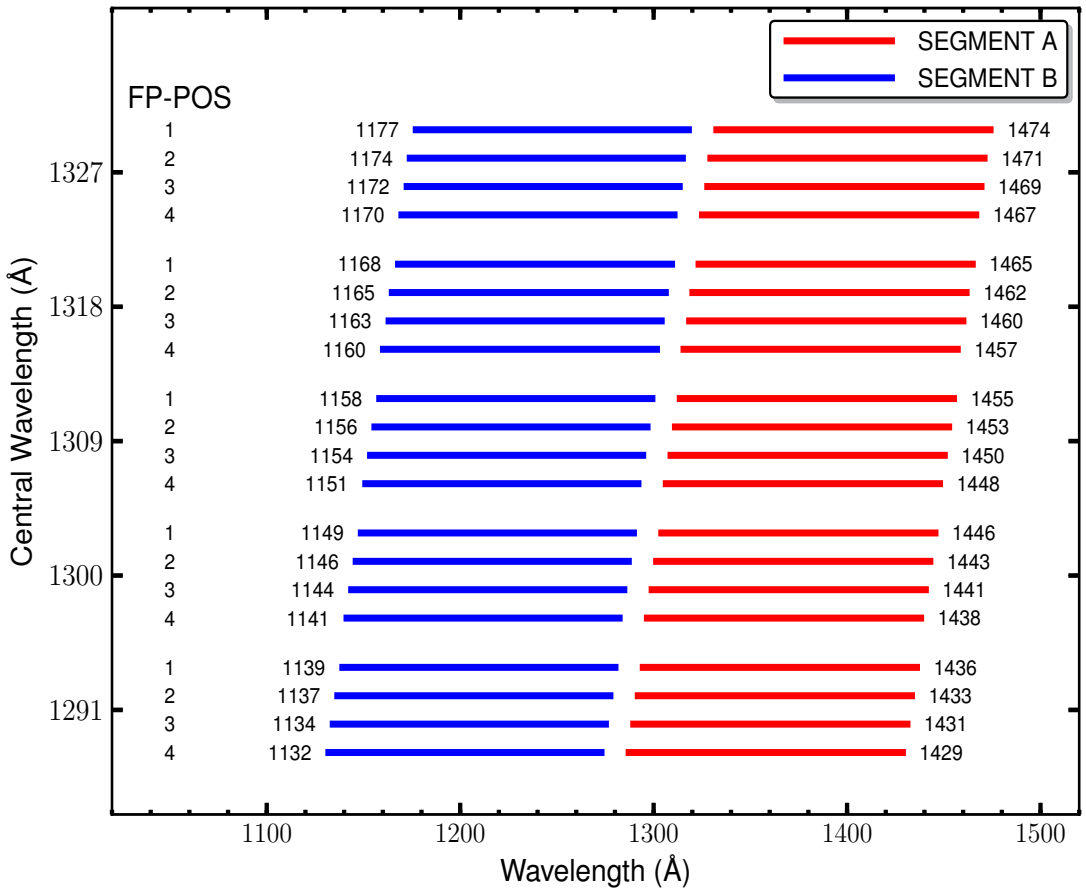

G130M Point-Source Sensitivity

Table 13.3: G130M Point–Source Sensitivity for PSA

Wavelength (Å)	Throughput	Sensitivity (counts pixel^{-1} sec^{-1} per erg cm^{-2} sec^{-1} Å^{-1})	Effective Area (cm^2)
1136	2.757e-02	7.1e+11	1.25e+03
1150	3.336e-02	8.7e+11	1.51e+03
1200	4.695e-02	1.3e+12	2.12e+03
1250	5.588e-02	1.6e+12	2.53e+03
1300	5.041e-02	1.5e+12	2.28e+03
1350	4.008e-02	1.2e+12	1.81e+03
1400	3.382e-02	1.1e+12	1.53e+03
1450	2.702e-02	8.9e+11	1.22e+03
1469	2.477e-02	8.3e+11	1.12e+03

Figure 13.3: G130M Point–Source Sensitivity for PSA and BOA

The throughput of the BOA is poorly characterized below 1200 Å and close to zero below 1150 Å.

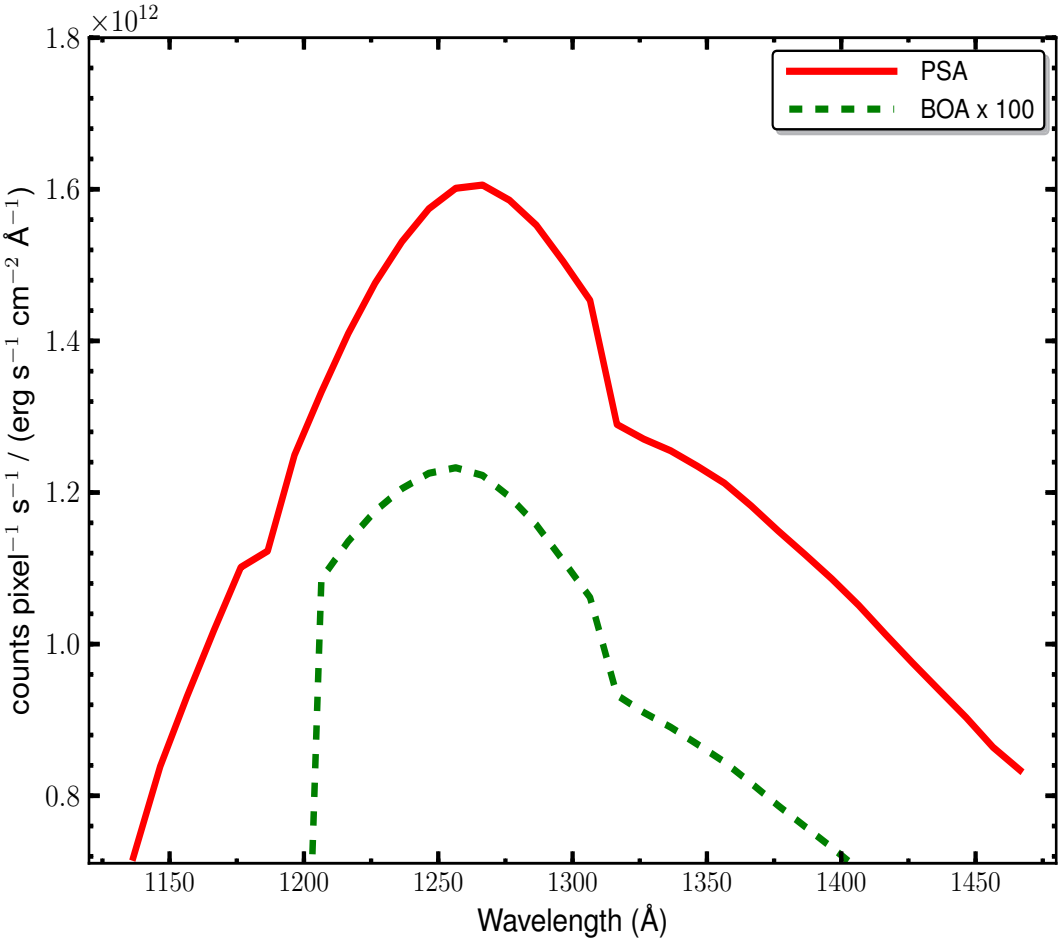

G130M Signal-to-Noise Ratio

Figure 13.4: Point–Source Signal–to–Noise as a Function of STMAG for G130M at 1310 Å

The top axis displays constant F_λ values corresponding to the STMAG units ($V+STMAG_\lambda$) on the bottom axis. Recall that STMAG = 0 is equivalent to F_λ = 3.63E-9 erg cm^{-2} s^{-1} Å^{-1}. Colors refer to exposure times in seconds. The edge of the shaded area corresponds to the bright-object screening limit. Use of the PSA is assumed.

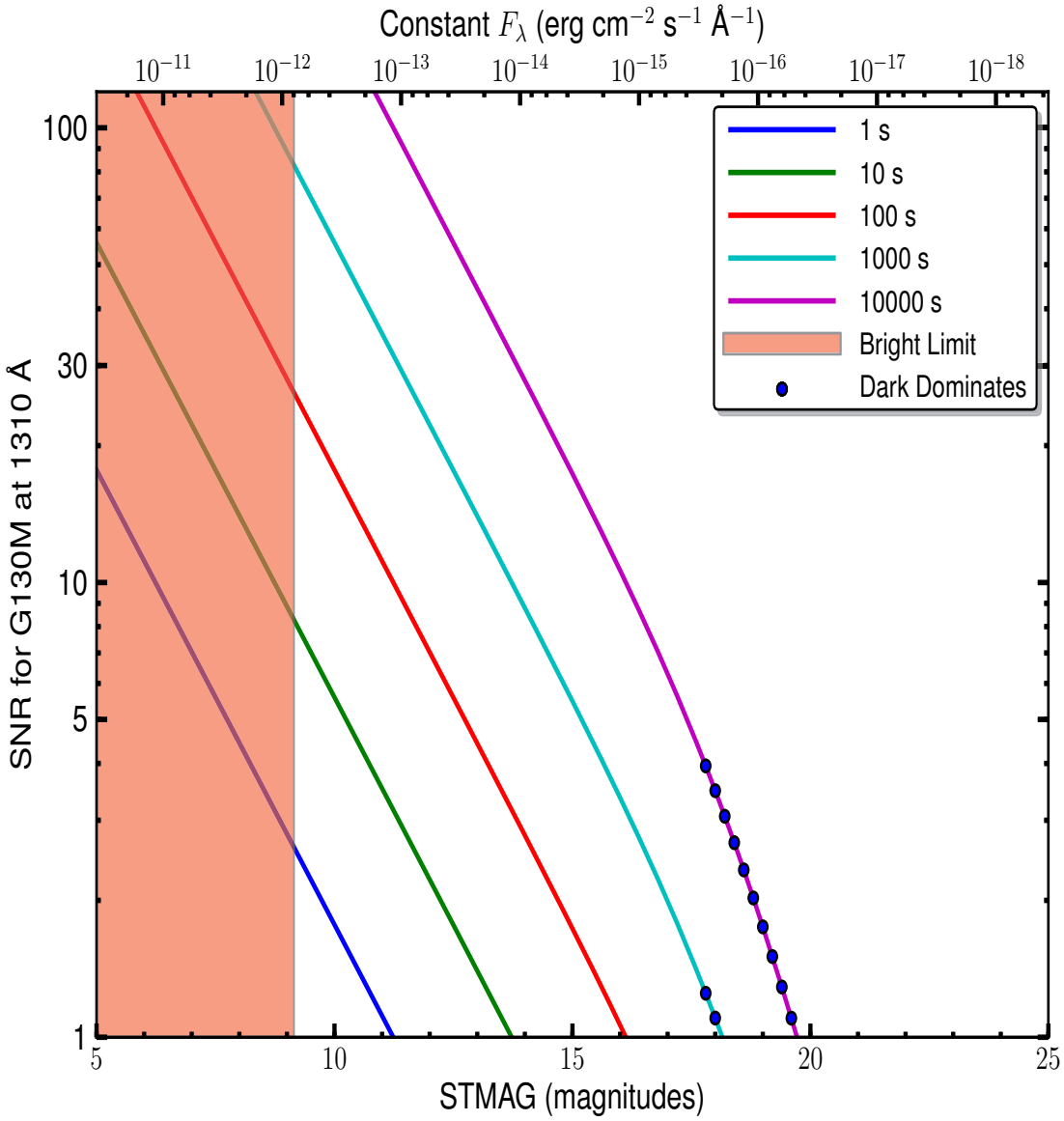

FUV Grating G130M with CENWAVE=1222

Description

When used with a central wavelength of 1222 Å, grating G130M samples wavelengths between about 1065 and 1365 Å with a resolving power $R > 10{,}000$. Its sensitivity is comparable to that of other G130M modes and considerably higher than G140L. Preliminary measurements indicate that the resolving power of this mode is $R > 13{,}000$ at 1135 Å and $R > 10{,}000$ at 1340 Å.

Special Considerations

A key advantage of this observing mode is that it places the Lyman-α airglow line in the gap between detector segments A and B, eliminating this source of damaging high-intensity flux.

Grating	Resolving Power $R = \lambda/\Delta\lambda$	Dispersion (mÅ pixel^{-1})	Plate Scale (milliarcsec pixel^{-1})		FP-POS Step (Å step^{-1})
			Disp. Axis	Cross-Disp. Axis	
G130M	13,000 - 10,000	9.97	22.9	100	2.5

Figure 13.5: Wavelength Ranges for the G130M/1222 Mode

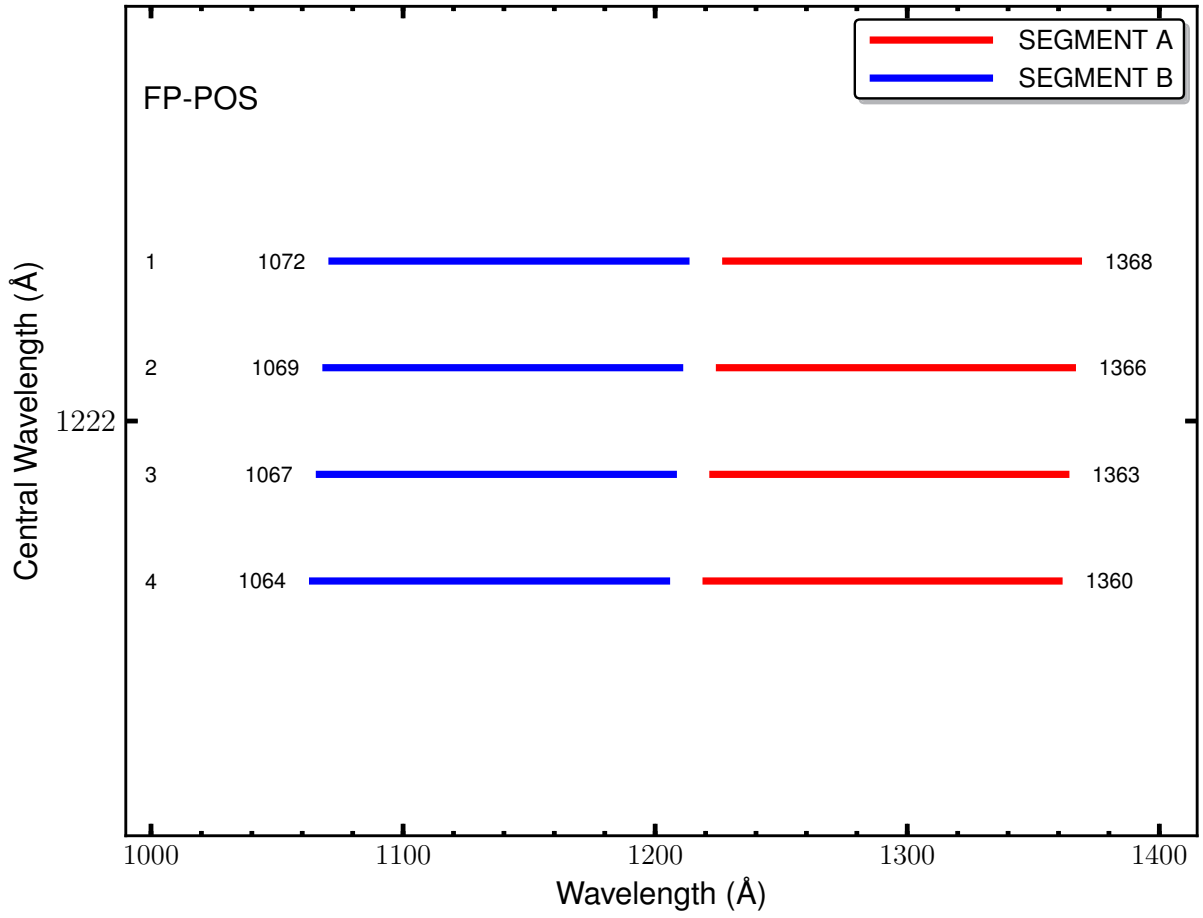

G130M/1222 Point-Source Sensitivity

Table 13.4: G130M/1222 Point–Source Sensitivity for PSA

Wavelength (Å)	Throughput	Sensitivity (counts pixel^{-1} sec^{-1} per erg cm^{-2} sec^{-1} Å^{-1})	Effective Area (cm^2)
1066	6.028e-04	1.5e+10	2.73e+01
1100	6.219e-03	1.6e+11	2.81e+02
1150	3.337e-02	8.7e+11	1.51e+03
1200	4.698e-02	1.3e+12	2.13e+03
1250	5.059e-02	1.4e+12	2.29e+03
1300	4.672e-02	1.4e+12	2.11e+03
1350	4.137e-02	1.3e+12	1.87e+03
1363	3.979e-02	1.2e+12	1.80e+03

Figure 13.6: G130M/1222 Point–Source Sensitivity for PSA

The sensitivity through the BOA is not shown, as its MgF_2 filter is opaque at wavelengths $\lambda <$ 1150 Å.

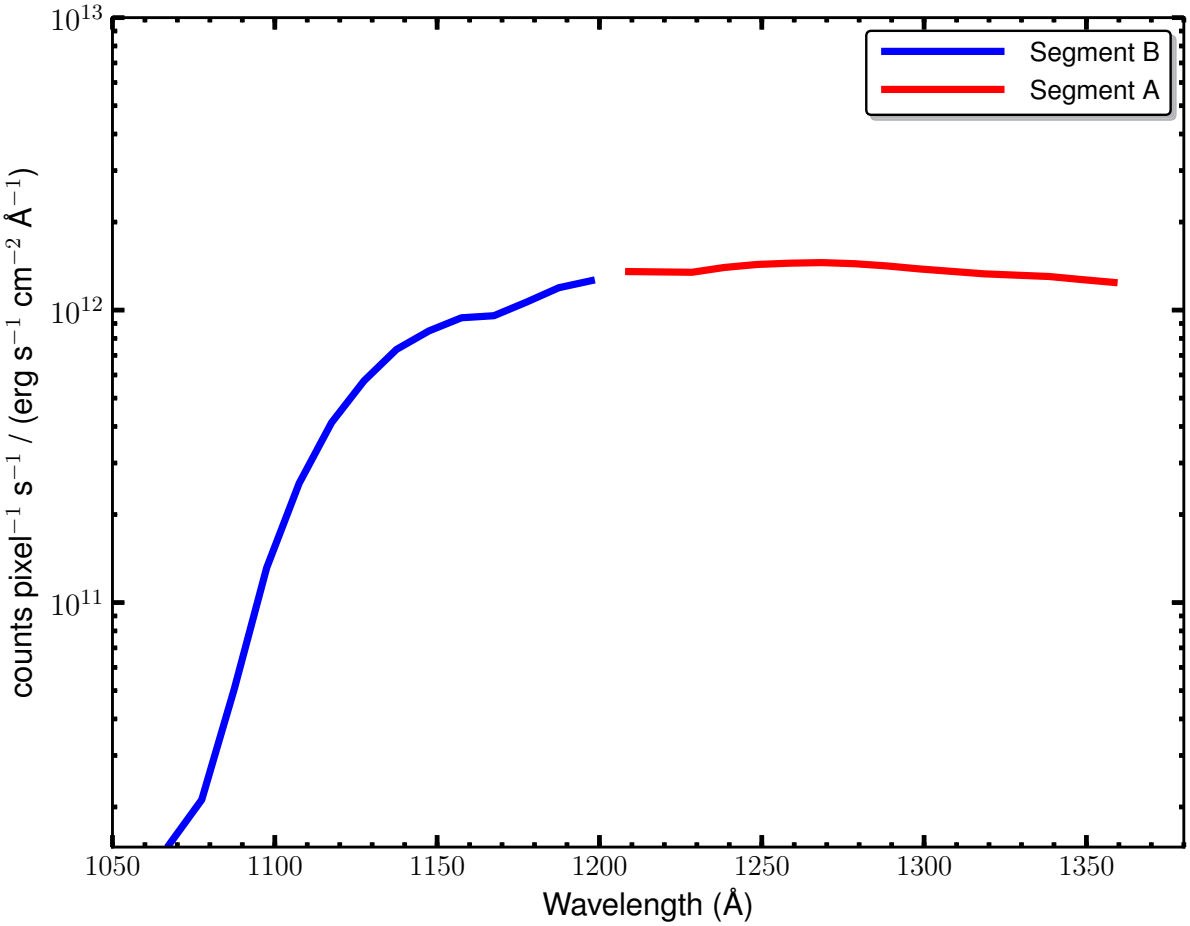

G130M/1222 Signal-to-Noise Ratio

Figure 13.7: Point–Source Signal–to–Noise as a Function of STMAG for G130M at 1135 Å

The top axis displays constant F_λ values corresponding to the STMAG units ($V+STMAG_\lambda$) on the bottom axis. Recall that STMAG = 0 is equivalent to F_λ = 3.63E-9 erg cm^{-2} s^{-1} Å^{-1}. Colors refer to exposure times in seconds. The edge of the shaded area corresponds to the bright-object screening limit. Use of the PSA is assumed.

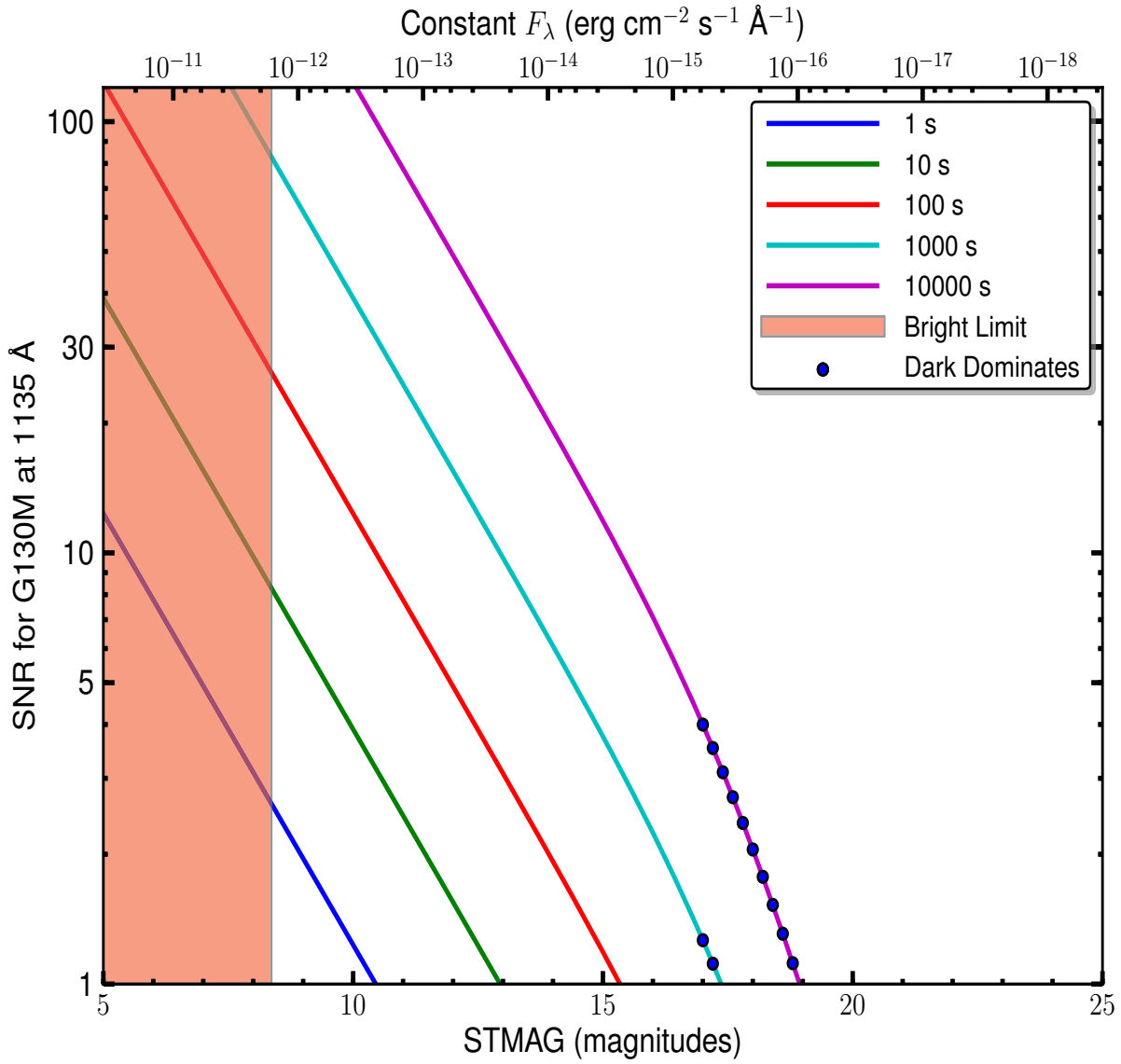

FUV Grating G130M with CENWAVE=1055 or 1096

Description

When used with a central wavelength of 1055 or 1096 Å, grating G130M samples wavelengths between about 900 and 1200 Å. Its resolution and effective area are higher than those of the G140L grating, but lower than those of G130M when used at longer central wavelengths.

Special Considerations

The COS sensitivity rises steeply between 1070 and 1150 Å. To observe bright targets near the Lyman limit, turn off detector segment A and use only segment B.

Grating	Resolving Power $R = \lambda/\Delta\lambda$	Dispersion (mÅ pixel^{-1})	Plate Scale (milliarcsec pixel^{-1})		FP-POS Step (Å step^{-1})
			Disp. Axis	Cross-Disp. Axis	
G130M Segment A	3000 - 8000	9.97	22.9	100	2.5
G130M Segment B	5000 - 12,000	9.97	22.9	100	2.5

Figure 13.8: Wavelength Ranges for the G130M/1055 and 1096 Modes

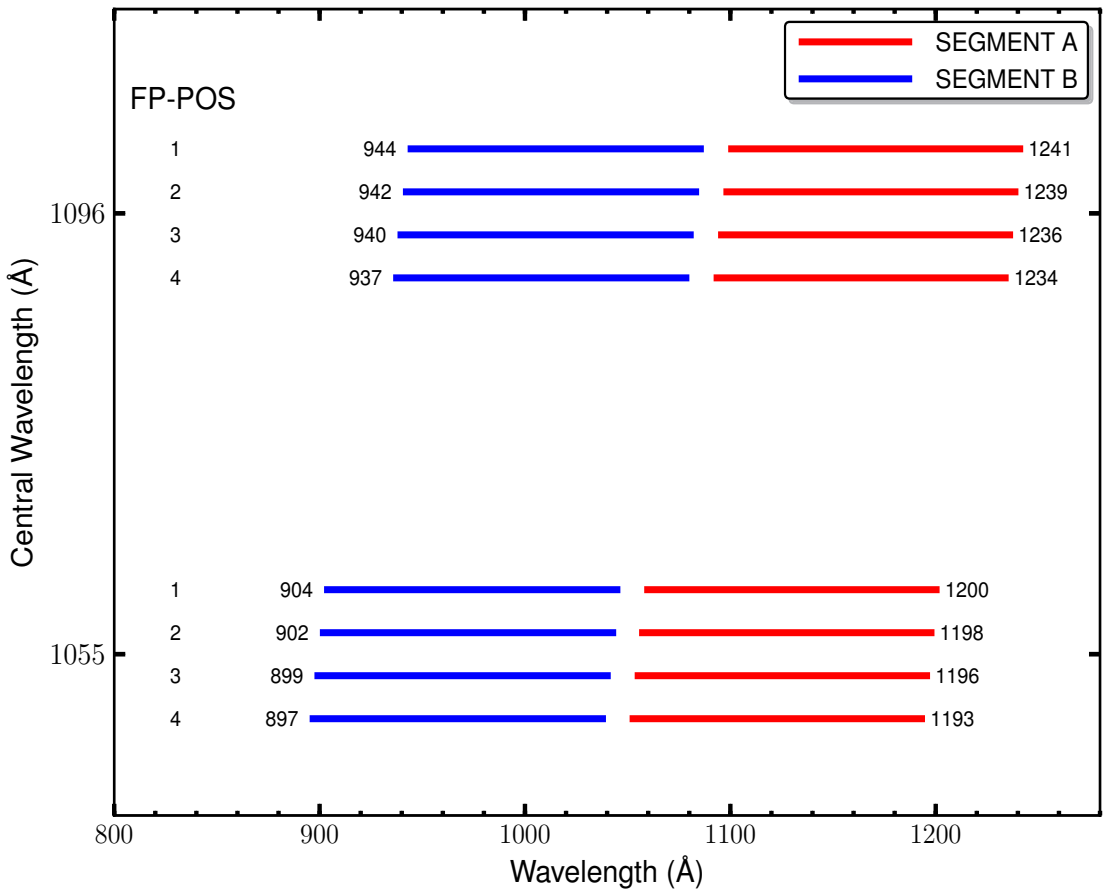

G130M/1055 and 1096 Point-Source Sensitivity

Table 13.5: G130M/1055 and 1096 Point–Source Sensitivity for PSA

Wavelength (Å)	Throughput	Sensitivity (counts pixel^{-1} sec^{-1} per erg cm^{-2} sec^{-1} Å^{-1})	Effective Area (cm^2)
901	1.611e-04	3.3e+09	7.29e+00
950	4.736e-04	1.0e+10	2.14e+01
1000	2.709e-04	6.1e+09	1.23e+01
1050	6.355e-04	1.5e+10	2.87e+01
1100	5.538e-03	1.4e+11	2.51e+02
1150	3.076e-02	8.0e+11	1.39e+03
1200	4.216e-02	1.1e+12	1.91e+03
1237	4.389e-02	1.2e+12	1.99e+03

Figure 13.9: G130M/1055 and 1096 Point–Source Sensitivity for PSA

The sensitivity through the BOA is not shown, as its MgF_2 filter is opaque at these wavelengths.

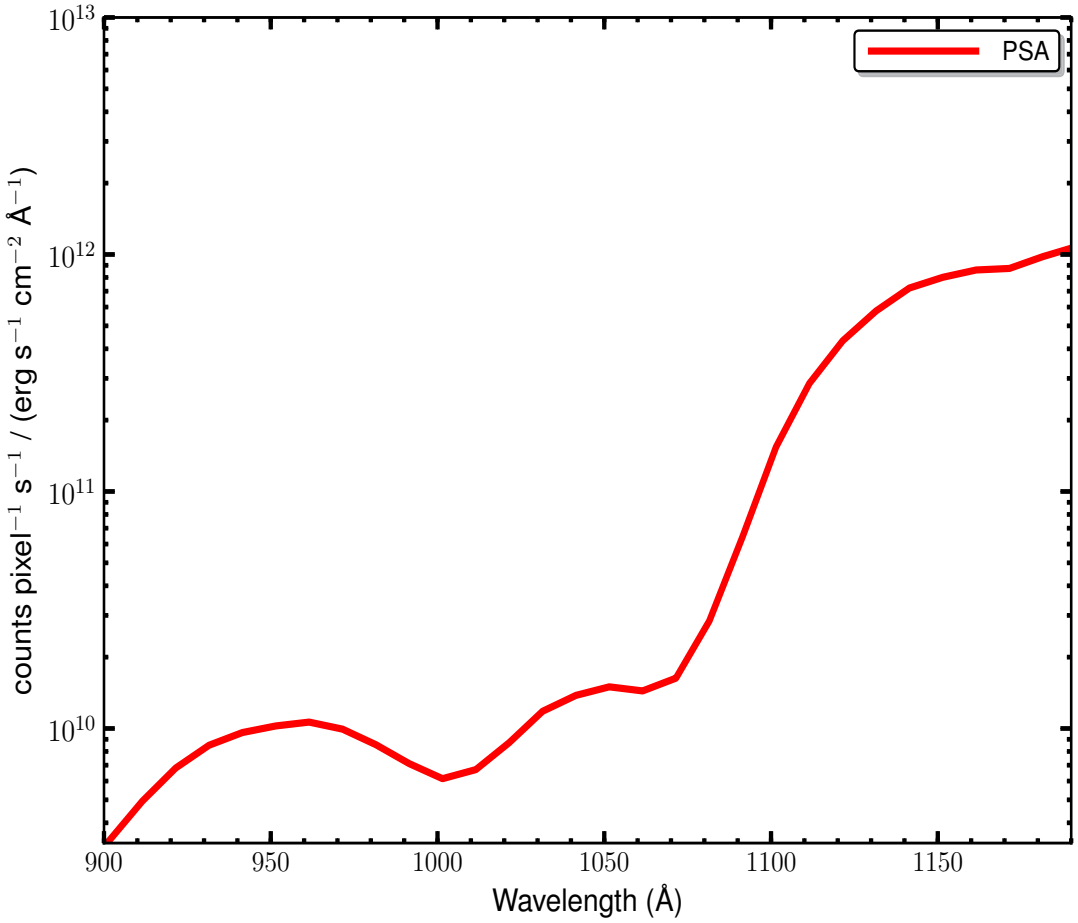

G130M/1055 and 1096 Signal-to-Noise Ratio

Figure 13.10: Point-Source Signal-to-Noise as a Function of STMAG for G130M at 1030 Å

The top axis displays constant F_λ values corresponding to the STMAG units ($V+STMAG_\lambda$) on the bottom axis. Recall that STMAG = 0 is equivalent to F_λ = 3.63E-9 erg cm^{-2} s^{-1} Å^{-1}. Colors refer to exposure times in seconds. The edge of the shaded area corresponds to the bright-object screening limit. Use of the PSA is assumed.

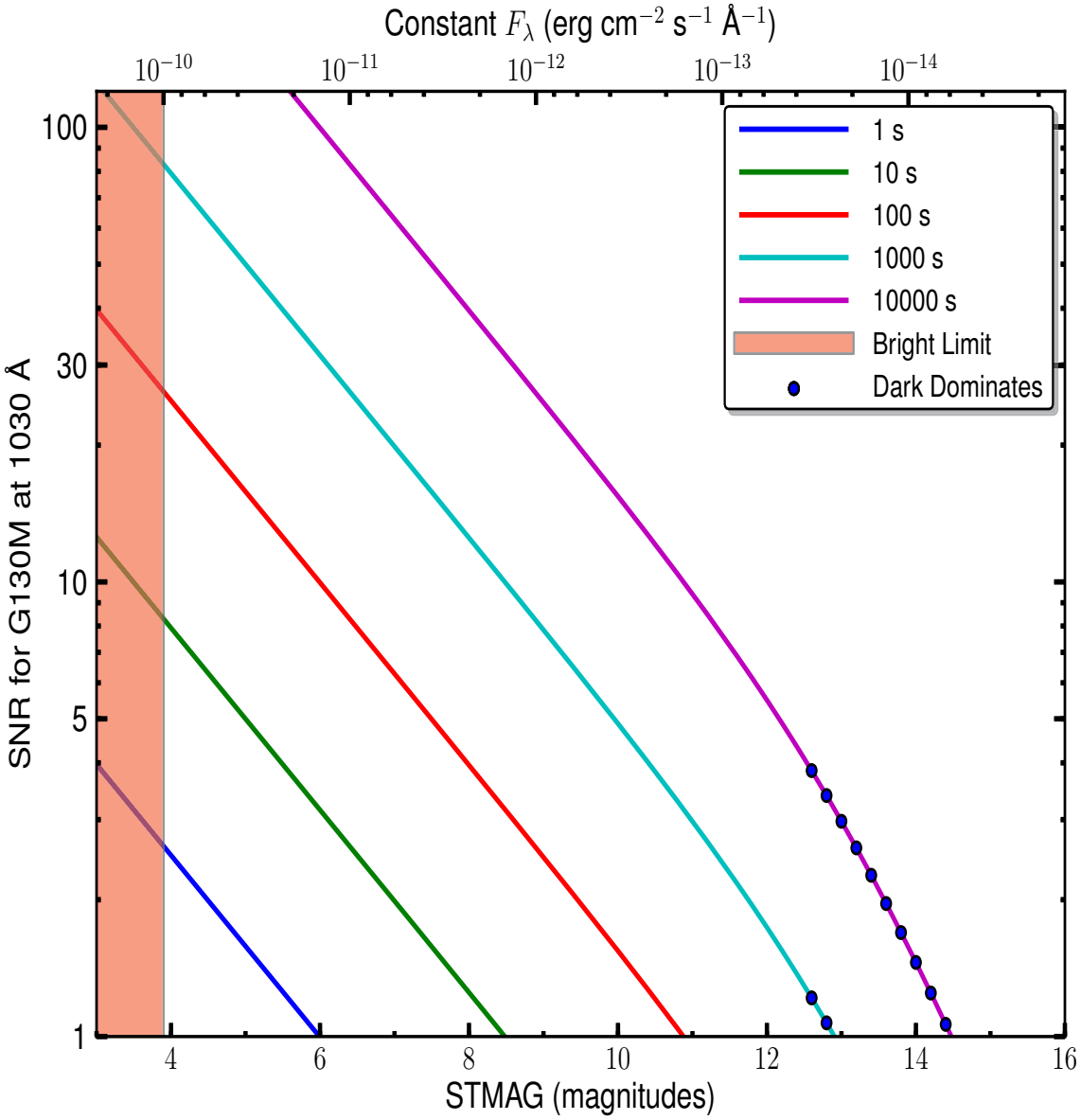

FUV Grating G160M

Description

The G160M grating samples wavelengths between about 1405 and 1775 Å. It offers higher resolution and effective area than the G140L grating, but less spectral coverage.

Special Considerations

The gap between segments A and B spans 18.1 Å. To fill this gap requires exposures separated by two central-wavelength settings.

Grating	Resolving Power $R = \lambda/\Delta\lambda$	Dispersion (mÅ pixel^{-1})	Plate Scale (milliarcsec pixel^{-1})		FP-POS Step (Å step^{-1})
			Disp. Axis	Cross-Disp. Axis	
G160M	16,000 - 21,000	12.23	24.3	90	3.1

Figure 13.11: Wavelength Ranges for the G160M Grating

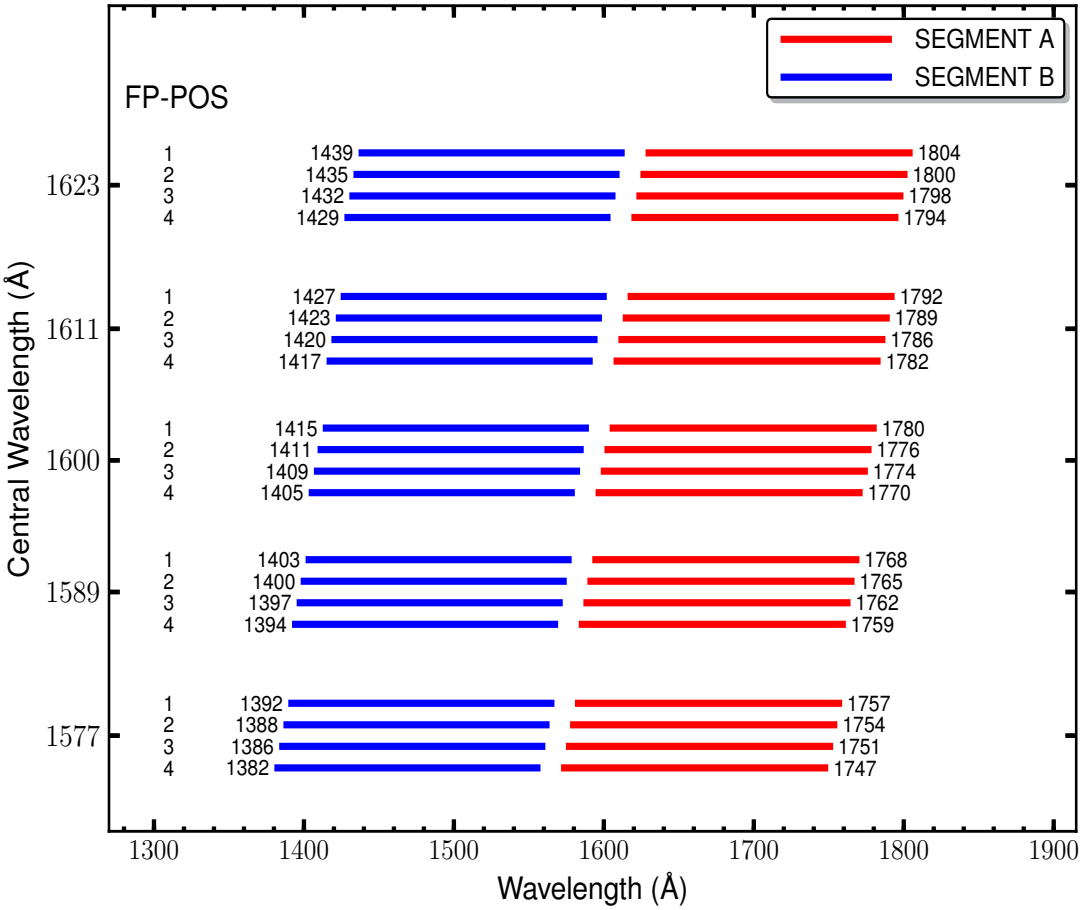

G160M Point-Source Sensitivity

Table 13.6: G160M Point–Source Sensitivity for PSA

Wavelength (Å)	Throughput	Sensitivity (counts pixel^{-1} sec^{-1} per erg cm^{-2} sec^{-1} Å^{-1})	Effective Area (cm^2)
1386	4.015e-02	1.6e+12	1.82e+03
1400	3.867e-02	1.5e+12	1.75e+03
1450	3.287e-02	1.3e+12	1.49e+03
1500	2.512e-02	1.1e+12	1.14e+03
1550	1.989e-02	8.6e+11	9.00e+02
1600	1.482e-02	6.6e+11	6.70e+02
1650	1.098e-02	5.0e+11	4.97e+02
1700	8.872e-03	4.2e+11	4.01e+02
1750	7.378e-03	3.6e+11	3.34e+02
1798	5.413e-03	2.7e+11	2.45e+02

Figure 13.12: G160M Point–Source Sensitivity for PSA and BOA

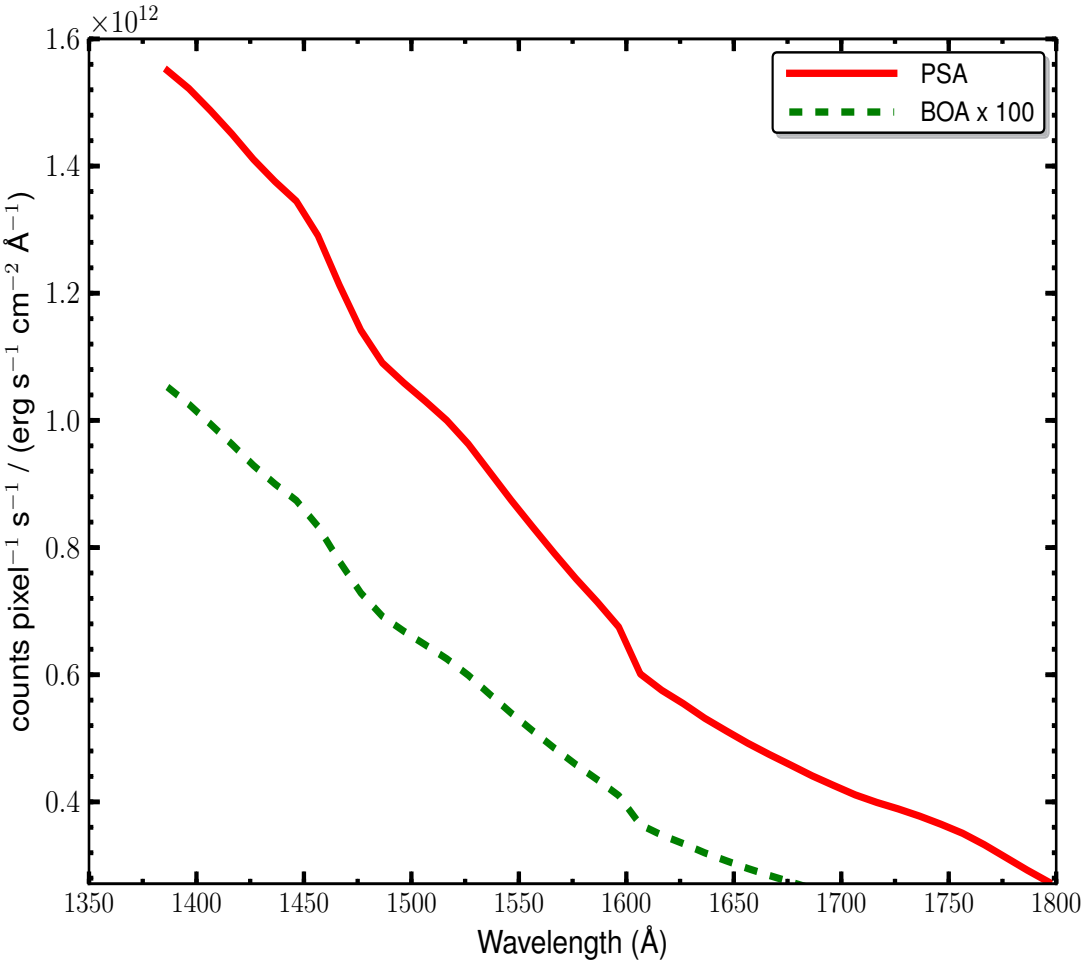

G160M Signal-to-Noise Ratio

Figure 13.13: Point-Source Signal-to-Noise as a Function of STMAG for G160M at 1610 Å

The top axis displays constant F_λ values corresponding to the STMAG units ($V+STMAG_\lambda$) on the bottom axis. Recall that STMAG = 0 is equivalent to F_λ = 3.63E-9 erg cm^{-2} s^{-1} Å^{-1}. Colors refer to exposure times in seconds. The edge of the shaded area corresponds to the bright-object screening limit. Use of the PSA is assumed.

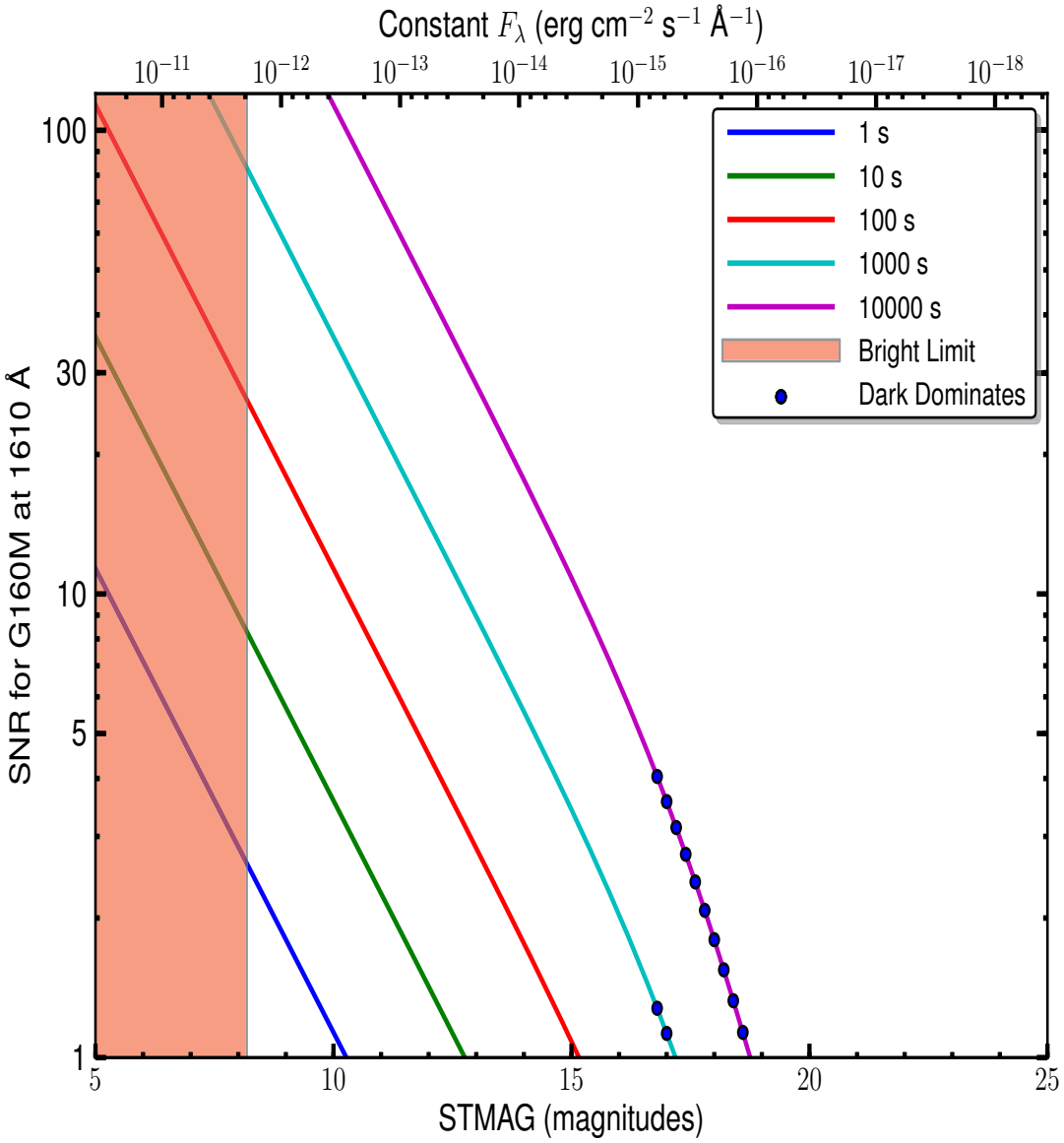

FUV Grating G140L

Description

G140L is a low-resolution grating (R ~ 2000) with wavelength coverage extending to 900 Å, and perhaps below. Its sensitivity at EUV wavelengths, marked in light blue in Figure 13.14, has not yet been calibrated. The grating has two central-wavelength settings, 1105 and 1280 Å.

Special Considerations

The gap between segments A and B spans 105 Å. To fill this gap requires exposures at both central-wavelength settings. When setting 1105 is used, the high voltage on Segment B must be lowered to avoid a dangerously high count rate from zero-order light. Wavelengths longer than 2150 Å may be contaminated by second-order light.

Grating	Resolving Power $R = \lambda/\Delta\lambda$	Dispersion (mÅ pixel^{-1})	Plate Scale (milliarcsec pixel^{-1})		FP-POS Step (Å step^{-1})
			Disp. Axis	Cross-Disp. Axis	
G140L	1,500 - 4,000	80.3	23.0	90	20.1

Figure 13.14: Wavelength Ranges for the G140L Grating

The COS sensitivity at EUV wavelengths (marked in light blue) is not yet known.

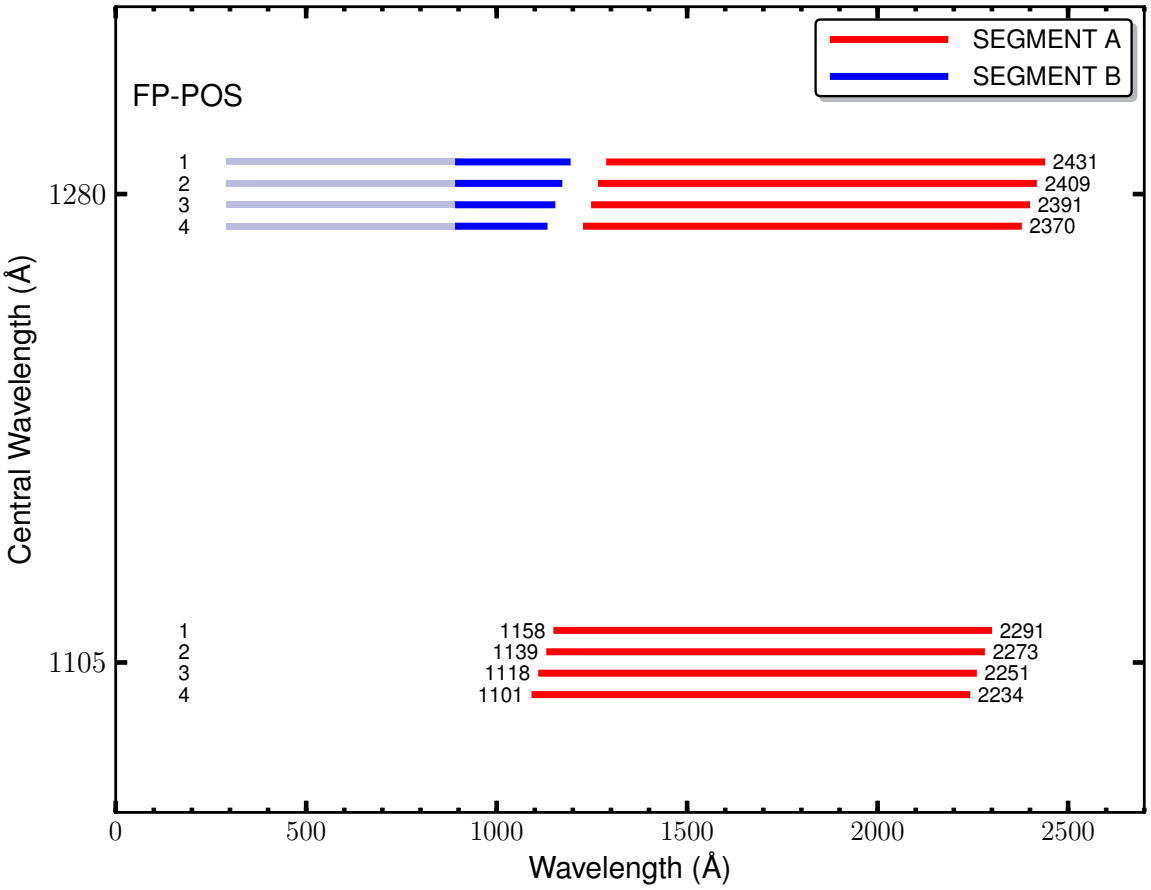

G140L Point-Source Sensitivity

Table 13.7: G140L Point–Source Sensitivity for PSA

Wavelength (Å)	Throughput	Sensitivity (counts pixel^{-1} sec^{-1} per erg cm^{-2} sec^{-1} Å^{-1})	Effective Area (cm^2)
914	1.907e-02	3.2e+12	8.63e+02
950	2.701e-04	4.6e+10	1.22e+01
1000	2.025e-04	3.7e+10	9.16e+00
1050	4.370e-04	8.3e+10	1.98e+01
1100	3.869e-03	7.7e+11	1.75e+02
1150	2.096e-02	4.4e+12	9.48e+02
1200	3.143e-02	6.8e+12	1.42e+03
1250	3.481e-02	7.9e+12	1.57e+03
1300	3.191e-02	7.5e+12	1.44e+03
1350	2.642e-02	6.5e+12	1.20e+03
1400	2.117e-02	5.4e+12	9.58e+02
1450	1.726e-02	4.5e+12	7.81e+02
1500	1.369e-02	3.7e+12	6.19e+02
1550	1.052e-02	2.9e+12	4.76e+02
1600	8.191e-03	2.4e+12	3.71e+02
1650	6.315e-03	1.9e+12	2.86e+02
1700	5.209e-03	1.6e+12	2.36e+02
1750	4.523e-03	1.4e+12	2.05e+02
1800	3.648e-03	1.2e+12	1.65e+02
1850	2.789e-03	9.3e+11	1.26e+02
1900	1.829e-03	6.3e+11	8.27e+01
1950	1.012e-03	3.6e+11	4.58e+01
2000	3.978e-04	1.4e+11	1.80e+01
2050	1.308e-04	4.9e+10	5.92e+00
2100	4.006e-05	1.5e+10	1.81e+00
2148	5.357e-06	2.1e+09	2.42e-01

Figure 13.15: G140L Point-Source Sensitivity for PSA and BOA

PSA × 10 is plotted to show sensitivity below 1100 Å.

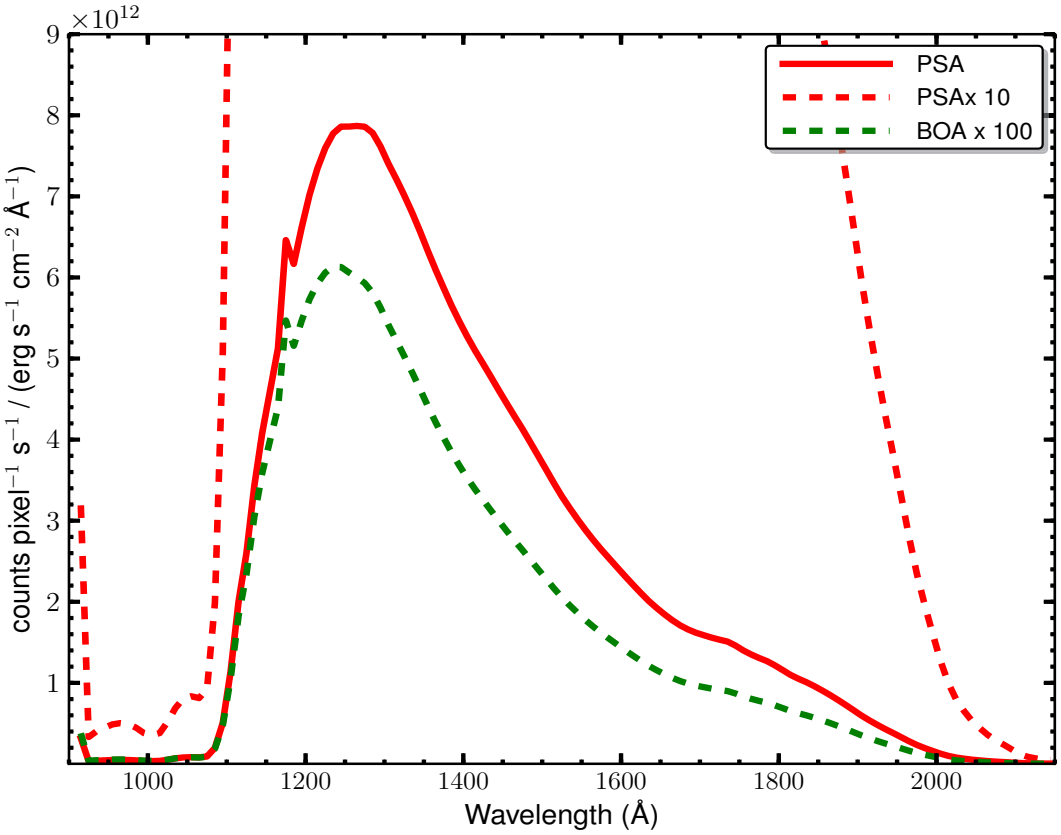

G140L Signal-to-Noise Ratio

Figure 13.16: Point–Source Signal–to–Noise as a Function of STMAG for G140L

The top axis displays constant F_λ values corresponding to the STMAG units ($V+STMAG_\lambda$) on the bottom axis. Recall that STMAG = 0 is equivalent to F_λ = 3.63E-9 erg cm^{-2} s^{-1} Å^{-1}. Colors refer to exposure times in seconds. The edge of the shaded area corresponds to the bright-object screening limit. Use of the PSA is assumed.

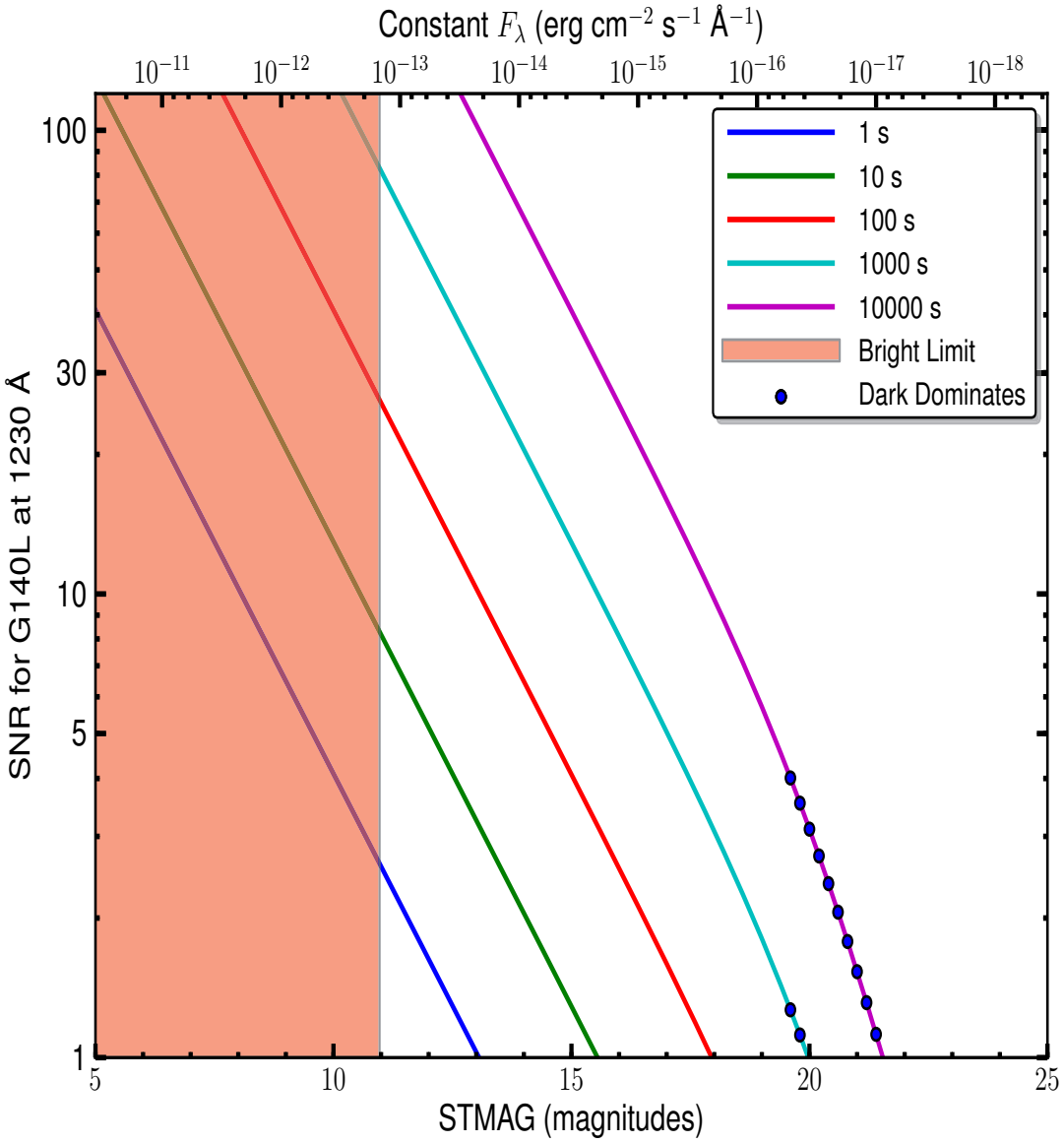

NUV Grating G185M

Description

The G185M grating samples wavelengths between about 1700 and 2100 Å. The grating has 15 central wavelength settings.

Special Considerations

G185M spectra consist of three 35 Å stripes separated by two 64 Å gaps. To acquire a complete spectrum requires the use of six central-wavelength settings.

Grating	Resolving Power $R = \lambda/\Delta\lambda$	Dispersion (mÅ pixel^{-1})	Spatial Resolution (milliarcsec pixel^{-1})	Plate Scale (milliarcsec pixel^{-1})		FP-POS Step (Å step^{-1})
				Disp. Axis	Cross-Disp. Axis	
G185M	16,000 - 20,000	37	75 ± 4	24.3	23.8	1.9

Figure 13.17: Wavelength Ranges for the G185M Grating

Dark lines represent wavelengths sampled by all four FP-POS positions.

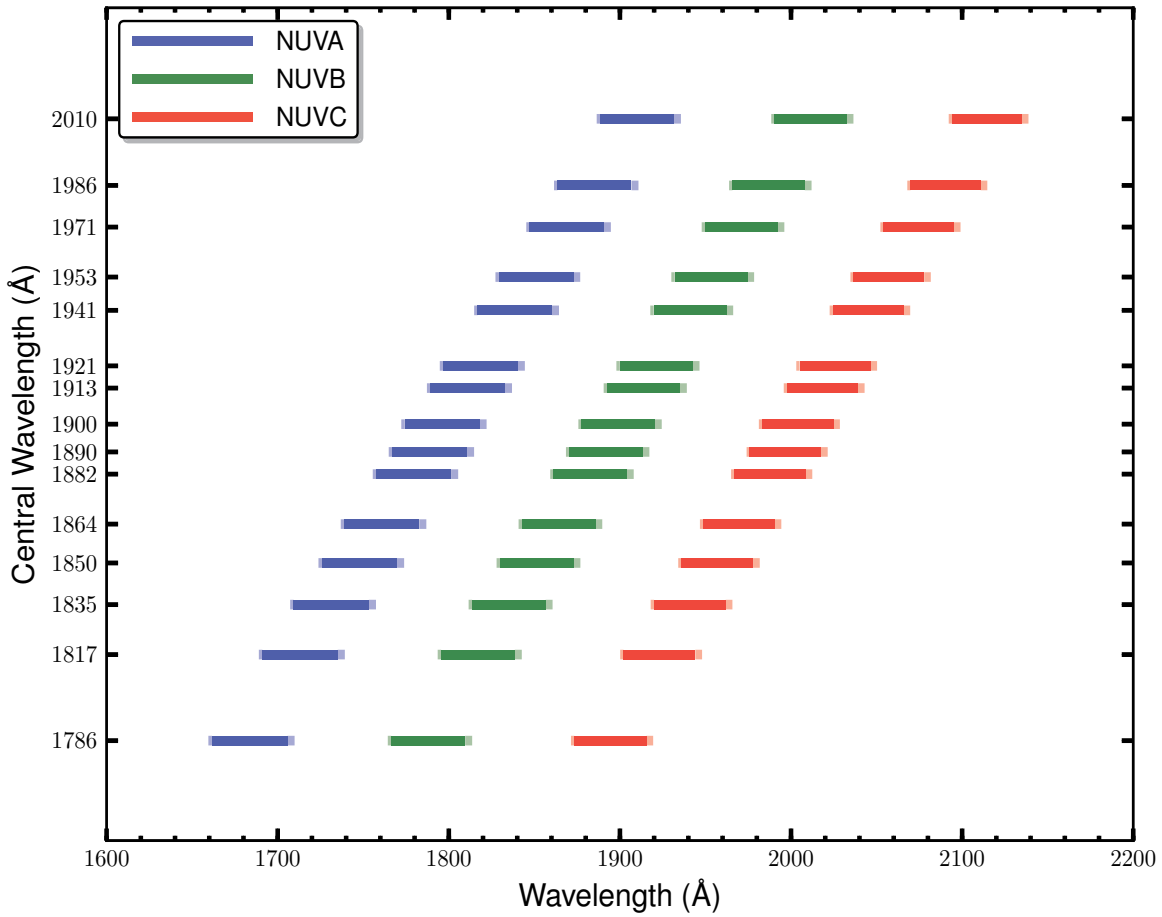

G165M Point-Source Sensitivity

Table 13.8: G185M Point–Source Sensitivity for PSA

Wavelength (Å)	Throughput	Sensitivity (counts pixel^{-1} sec^{-1} per erg cm^{-2} sec^{-1} Å^{-1})	Effective Area (cm^2)
1670	6.068e-03	8.4e+11	2.75e+02
1700	8.398e-03	1.2e+12	3.80e+02
1750	1.158e-02	1.7e+12	5.24e+02
1800	1.335e-02	2.0e+12	6.04e+02
1850	1.401e-02	2.2e+12	6.34e+02
1900	1.397e-02	2.2e+12	6.32e+02
1950	1.334e-02	2.2e+12	6.03e+02
2000	1.301e-02	2.2e+12	5.88e+02
2050	1.221e-02	2.1e+12	5.53e+02
2100	1.122e-02	2.0e+12	5.08e+02
2127	1.047e-02	1.9e+12	4.74e+02

Figure 13.18: G185M Point–Source Sensitivity for PSA and BOA

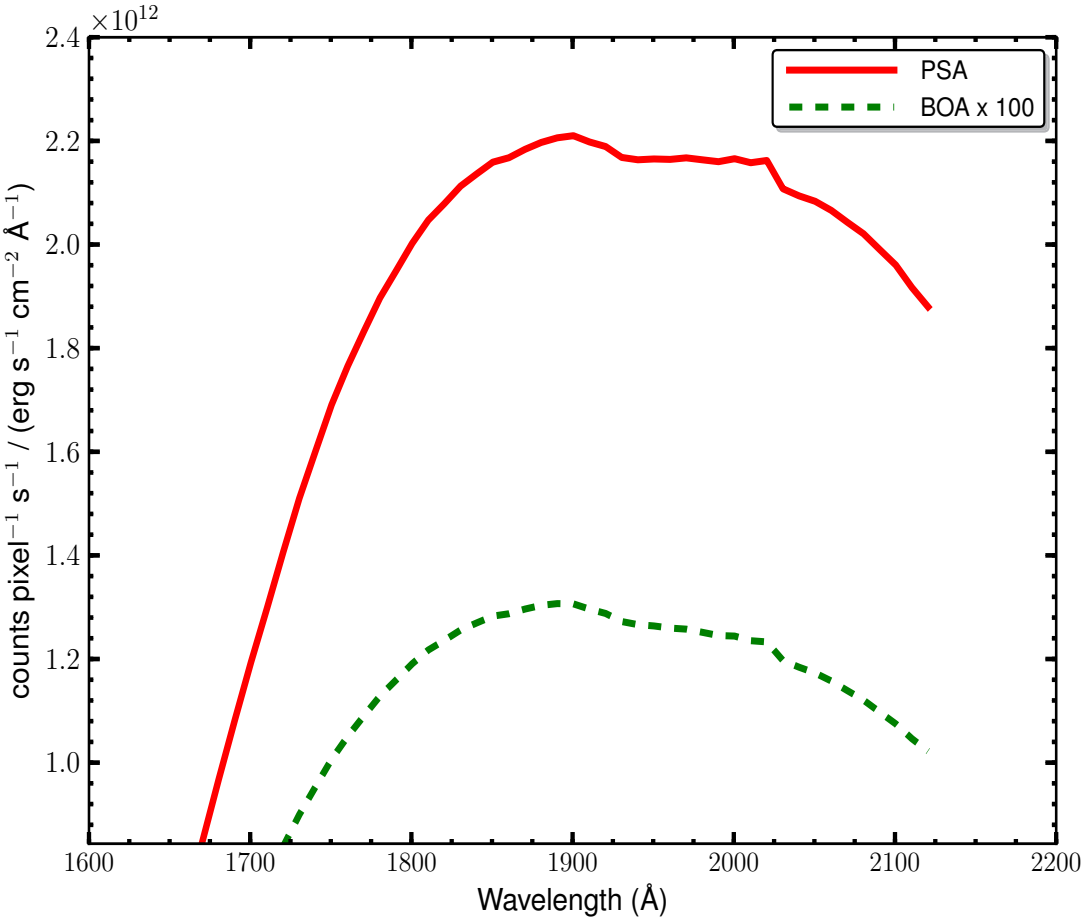

G185M Signal-to-Noise Ratio

Figure 13.19: Point-Source Signal-to-Noise as a Function of STMAG for G185M

The top axis displays constant F_λ values corresponding to the STMAG units ($V+STMAG_\lambda$) on the bottom axis. Recall that STMAG = 0 is equivalent to F_λ = 3.63E-9 erg cm^{-2} s^{-1} Å^{-1}. Colors refer to exposure times in seconds. The edge of the shaded area corresponds to the bright-object screening limit. Use of the PSA is assumed.

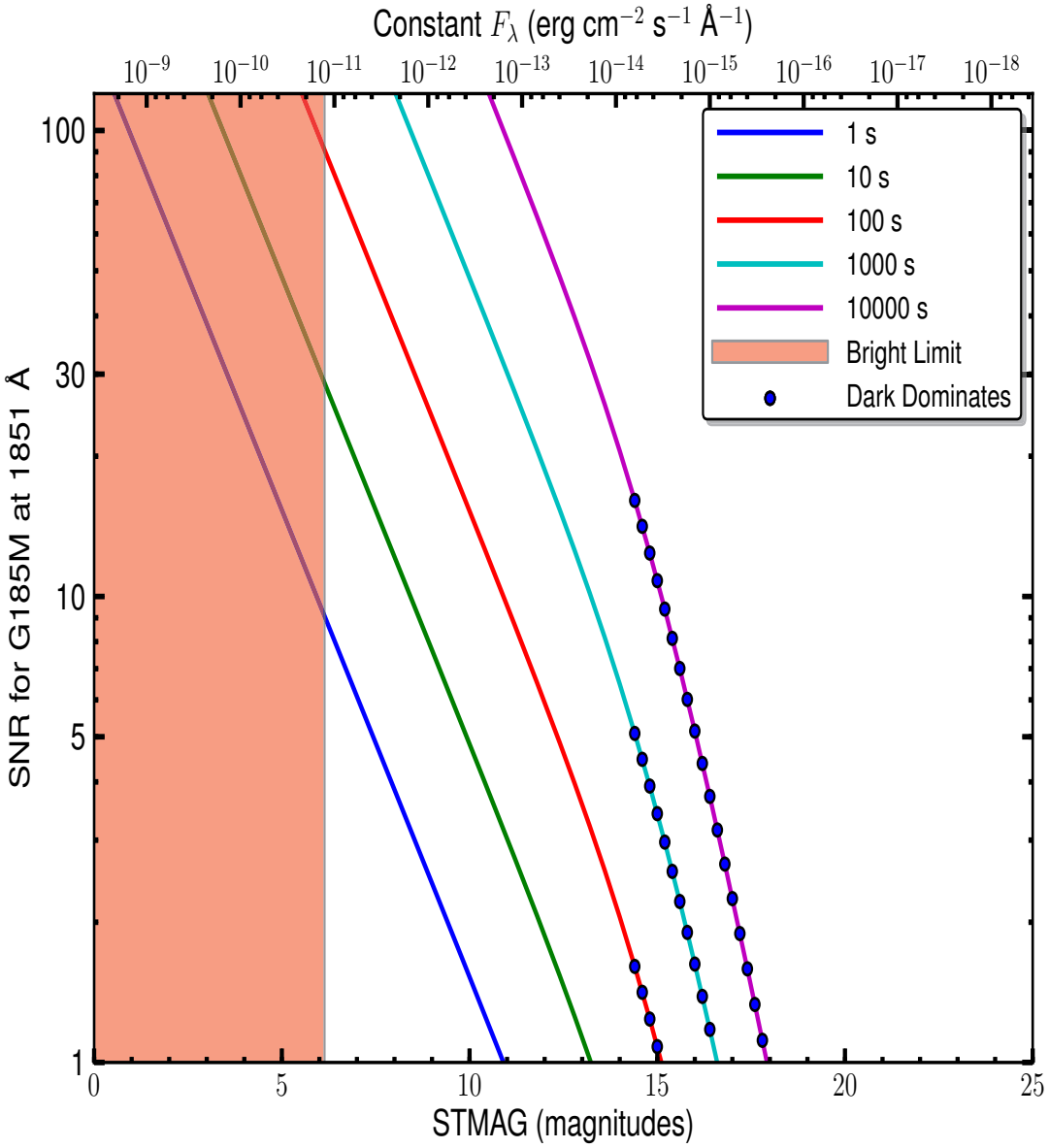

NUV Grating G225M

Description

The G225M grating samples wavelengths between about 2100 and 2500 Å. The grating has 13 central wavelength settings.

Special Considerations

G225M spectra consist of three 35 Å stripes separated by two 64 Å gaps. To acquire a complete spectrum requires the use of six central-wavelength settings.

Grating	Resolving Power $R = \lambda/\Delta\lambda$	Dispersion (mÅ pixel^{-1})	Spatial Resolution (milliarcsec pixel^{-1})	Plate Scale (milliarcsec pixel^{-1})		FP-POS Step (Å step^{-1})
				Disp. Axis	Cross-Disp. Axis	
G225M	20,000 - 24,000	33	58 ± 2	24.3	23.1	1.7

Figure 13.20: Wavelength Ranges for the G225M Grating

Dark lines represent wavelengths sampled by all four FP-POS positions.

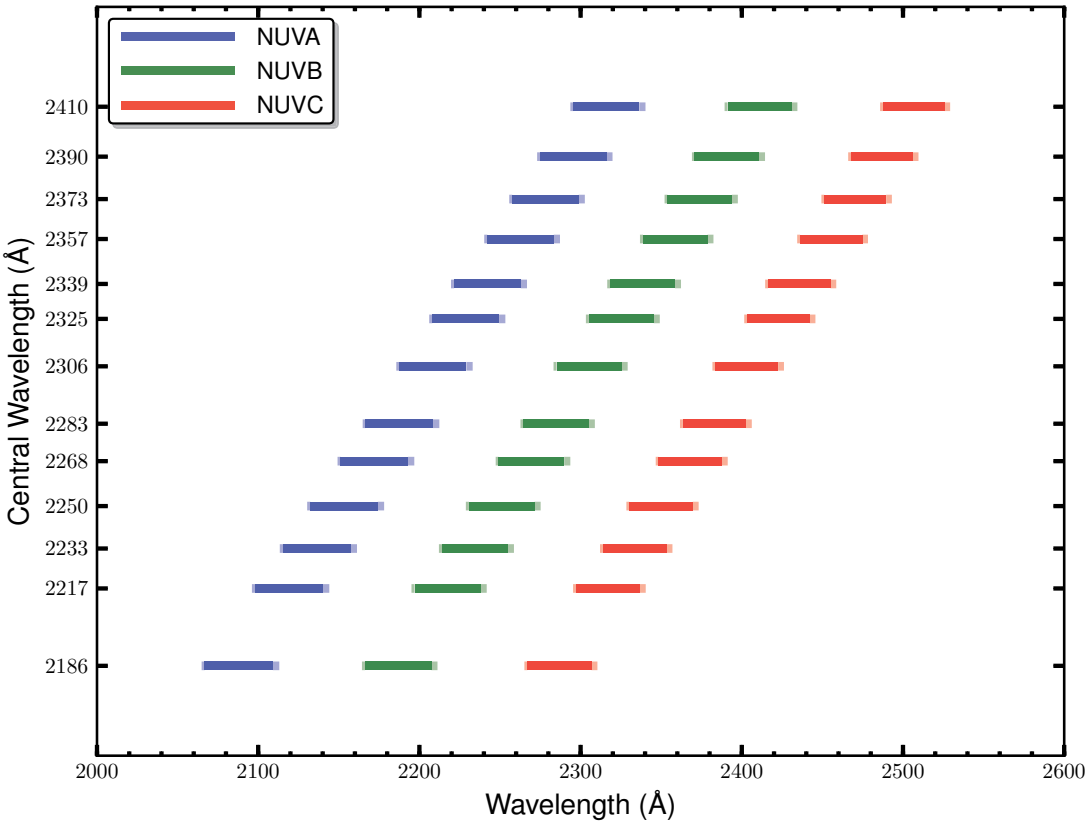

G225M Point-Source Sensitivity

Table 13.9: G225M Point–Source Sensitivity for PSA

Wavelength (Å)	Throughput	Sensitivity (counts pixel^{-1} sec^{-1} per erg cm^{-2} sec^{-1} Å^{-1})	Effective Area (cm^2)
2070	5.242e-03	8.5e+11	2.37e+02
2100	5.949e-03	9.8e+11	2.69e+02
2150	7.366e-03	1.2e+12	3.33e+02
2200	8.986e-03	1.5e+12	4.07e+02
2250	1.036e-02	1.8e+12	4.68e+02
2300	1.151e-02	2.1e+12	5.21e+02
2350	1.189e-02	2.2e+12	5.38e+02
2400	1.215e-02	2.3e+12	5.50e+02
2450	1.217e-02	2.3e+12	5.51e+02
2500	1.229e-02	2.4e+12	5.56e+02
2527	1.238e-02	2.4e+12	5.60e+02

Figure 13.21: G225M Point–Source Sensitivity for PSA and BOA

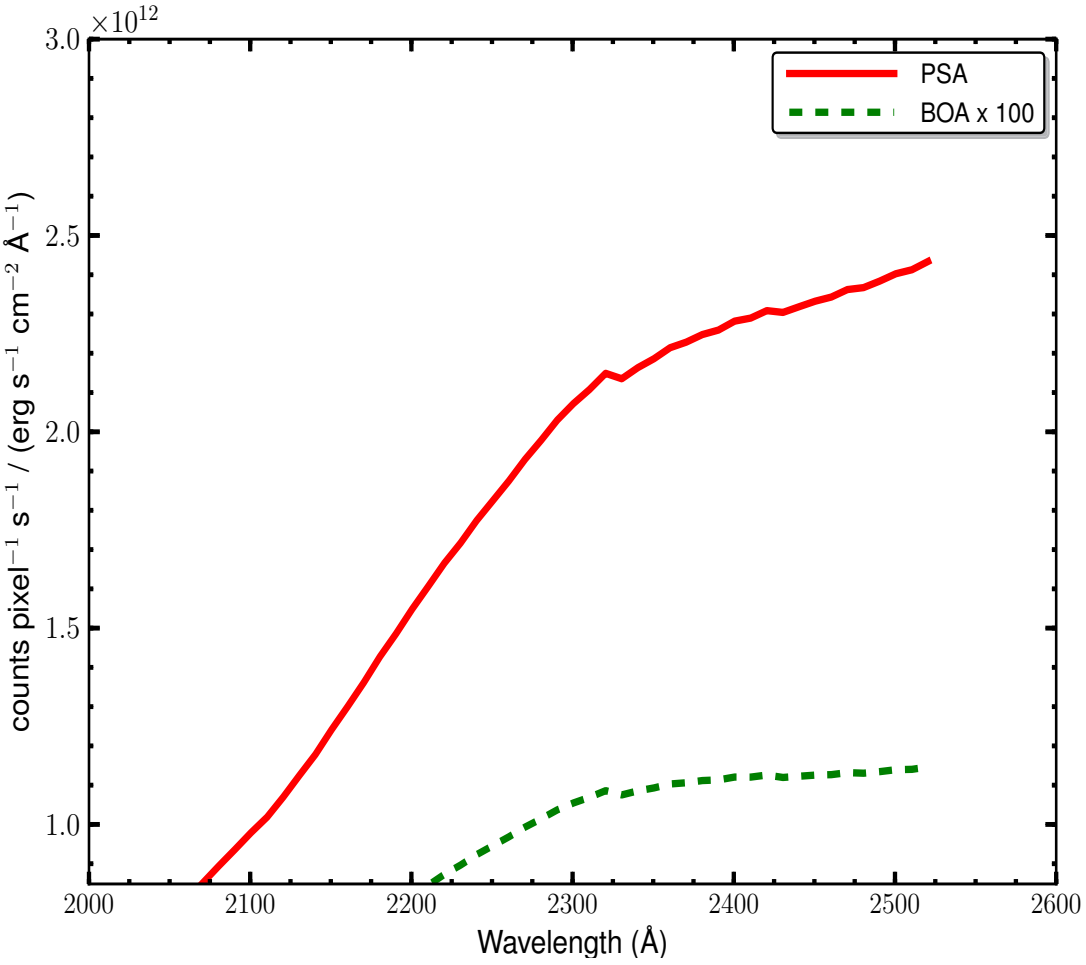

G225M Signal-to-Noise Ratio

Figure 13.22: Point–Source Signal–to–Noise as a Function of STMAG for G225M

The top axis displays constant F_λ values corresponding to the STMAG units ($V+STMAG_\lambda$) on the bottom axis. Recall that STMAG = 0 is equivalent to F_λ = 3.63E-9 erg cm^{-2} s^{-1} Å^{-1}. Colors refer to exposure times in seconds. The edge of the shaded area corresponds to the bright-object screening limit. Use of the PSA is assumed.

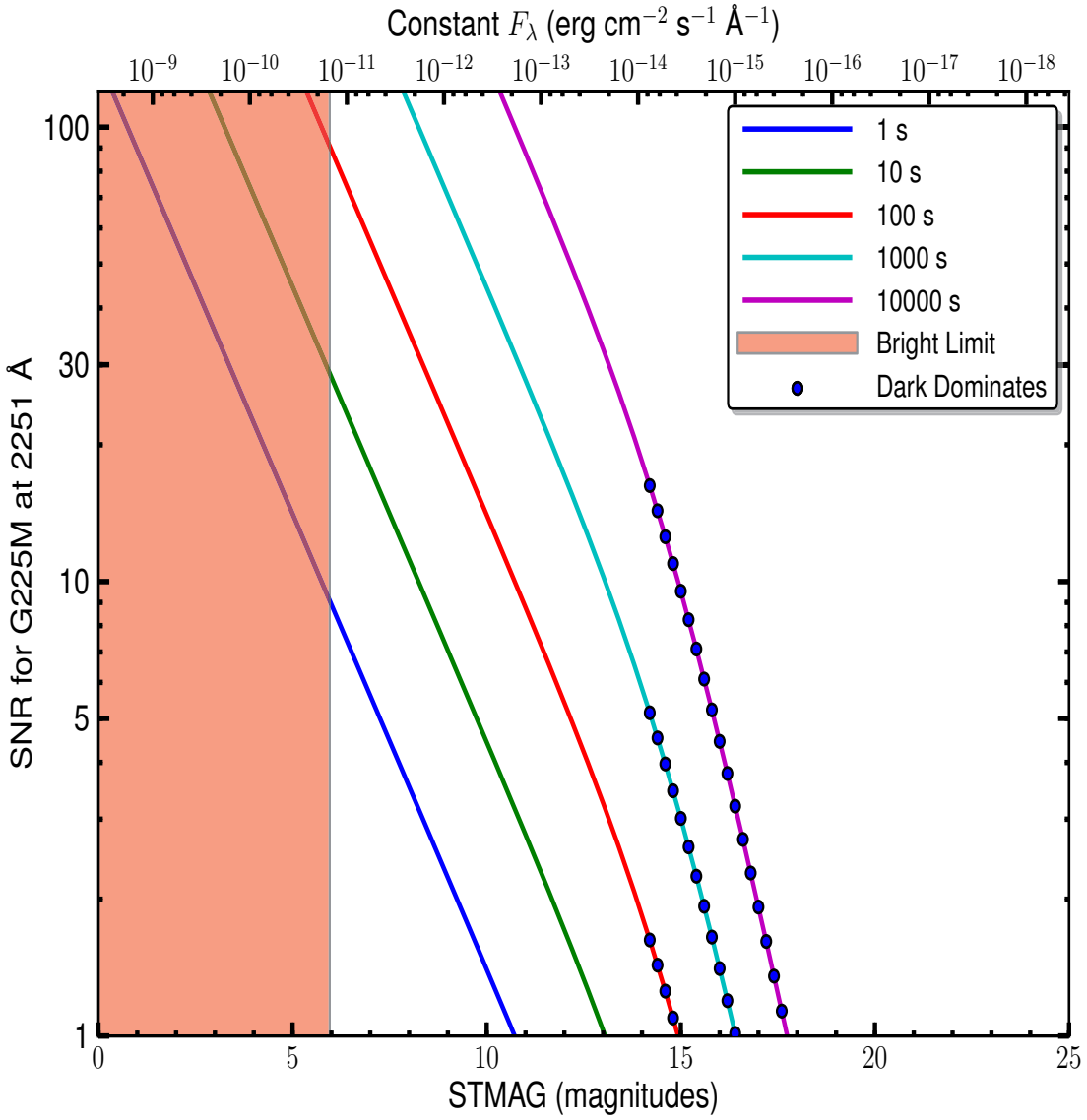

NUV Grating G285M

Description

The G285M grating samples wavelengths between about 2500 and 3200 Å. The grating has 17 central wavelength settings.

Special Considerations

G285M spectra consist of three 41 Å stripes separated by two 74 Å gaps. To acquire a complete spectrum requires the use of eight central-wavelength settings.

Grating	Resolving Power $R = \lambda/\Delta\lambda$	Dispersion (mÅ pixel^{-1})	Spatial Resolution (milliarcsec pixel^{-1})	Plate Scale (milliarcsec pixel^{-1})		FP-POS Step (Å step^{-1})
				Disp. Axis	Cross-Disp. Axis	
G285M	20,000 - 24,000	40	56 ± 1	24.3	24.4	2.1

Figure 13.23: Wavelength Ranges for the G285M Grating

Dark lines represent wavelengths sampled by all four FP-POS positions.

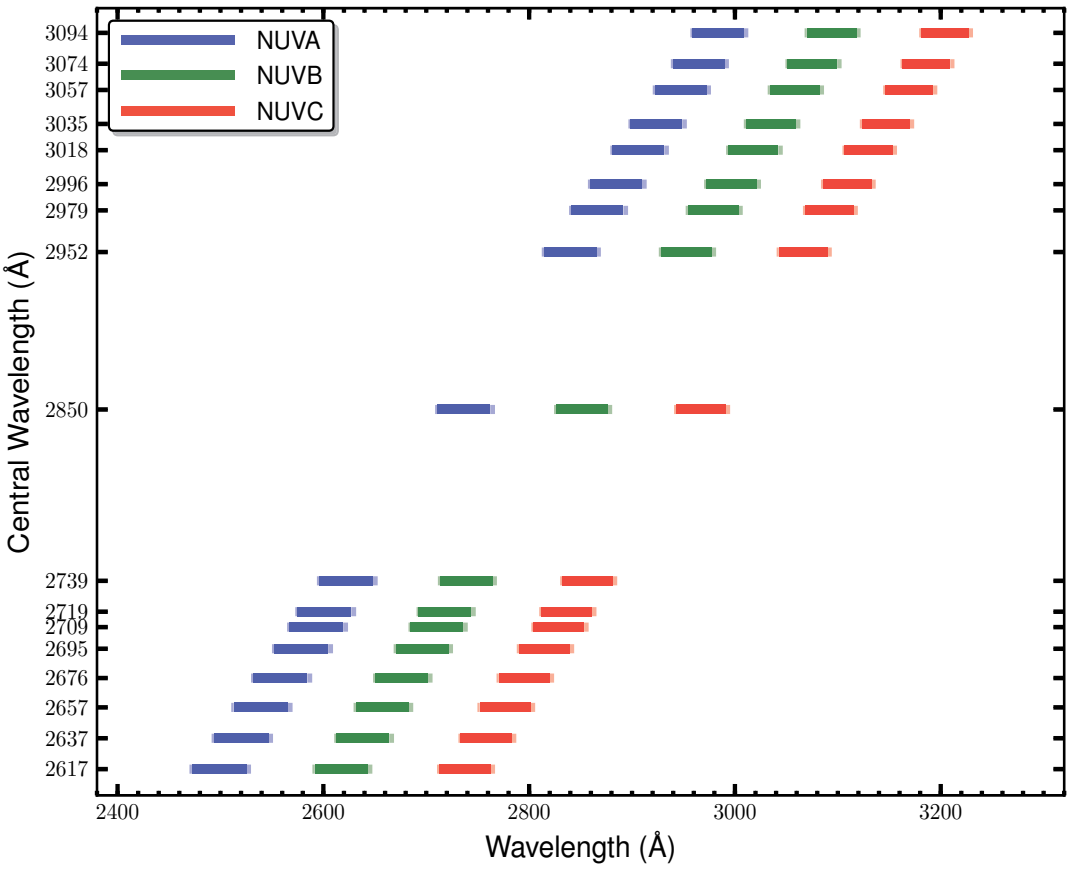

G285M Point-Source Sensitivity

Table 13.10: G285M Point–Source Sensitivity for PSA

Wavelength (Å)	Throughput	Sensitivity (counts pixel^{-1} sec^{-1} per erg cm^{-2} sec^{-1} Å^{-1})	Effective Area (cm^2)
2480	2.316e-03	5.3e+11	1.05e+02
2500	2.403e-03	5.6e+11	1.09e+02
2550	2.595e-03	6.1e+11	1.17e+02
2600	2.791e-03	6.7e+11	1.26e+02
2650	2.878e-03	7.0e+11	1.30e+02
2700	2.906e-03	7.2e+11	1.31e+02
2750	3.002e-03	7.6e+11	1.36e+02
2800	2.863e-03	7.4e+11	1.30e+02
2850	2.682e-03	7.1e+11	1.21e+02
2900	2.390e-03	6.4e+11	1.08e+02
2950	2.194e-03	6.0e+11	9.92e+01
3000	1.829e-03	5.1e+11	8.28e+01
3050	1.532e-03	4.3e+11	6.93e+01
3100	1.197e-03	3.4e+11	5.42e+01
3150	8.866e-04	2.6e+11	4.01e+01
3200	6.297e-04	1.9e+11	2.85e+01
3229	5.211e-04	1.6e+11	2.36e+01

Figure 13.24: G285M Point–Source Sensitivity for PSA and BOA

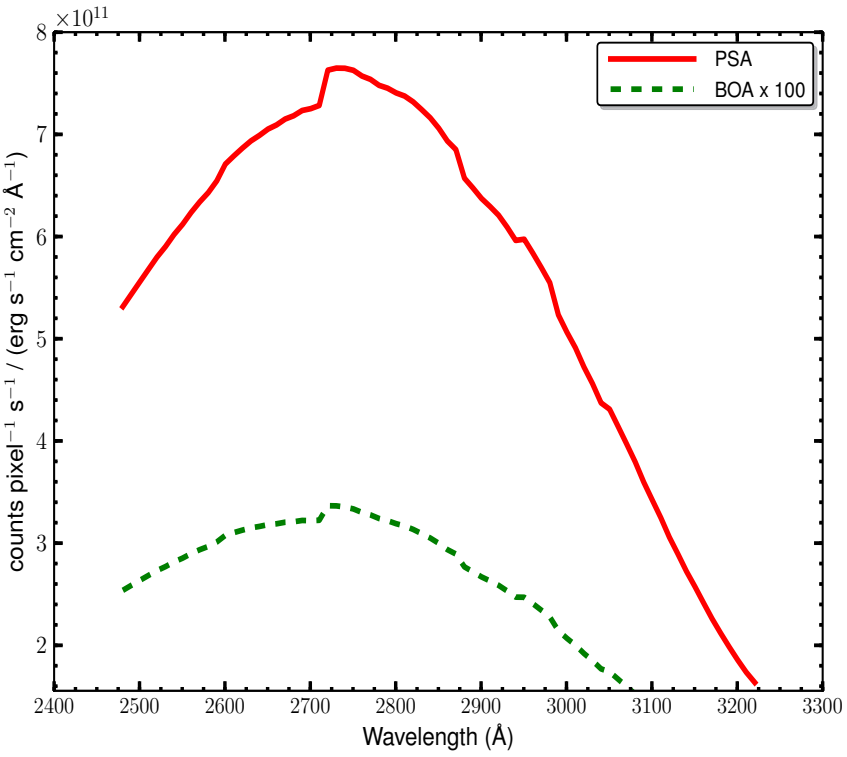

G285M Signal-to-Noise Ratio

Figure 13.25: Point–Source Signal–to–Noise as a Function of STMAG for G285M

The top axis displays constant F_λ values corresponding to the STMAG units ($V+STMAG_\lambda$) on the bottom axis. Recall that STMAG = 0 is equivalent to F_λ = 3.63E-9 erg cm^{-2} s^{-1} Å^{-1}. Colors refer to exposure times in seconds. The edge of the shaded area corresponds to the bright-object screening limit. Use of the PSA is assumed.

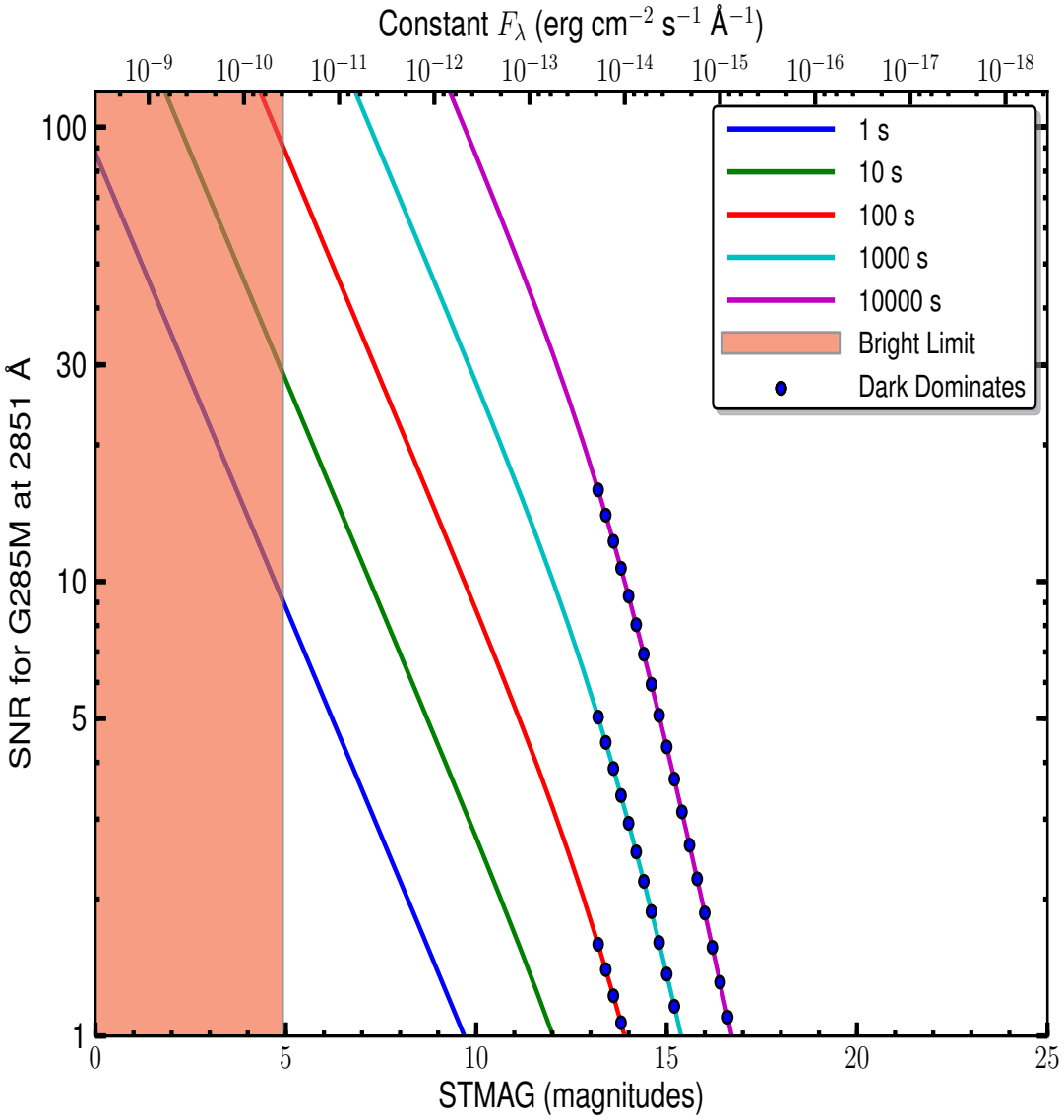

NUV Grating G230L

Description

G230L is a low-resolution grating (R~3000) with wavelength coverage extending from about 1650 to 3200 Å. The grating has four central-wavelength settings.

Special Considerations

G230L spectra consist of three 400-Å stripes separated by two 700-Å gaps. To acquire a complete spectrum requires the use of all four central-wavelength settings.

Only stripes A and B record first-order light, and even they may be contaminated by second-order light when central wavelength 3360 is used. See Table 5.4.

Grating	Resolving Power $R = \lambda/\Delta\lambda$	Dispersion (mÅ pixel^{-1})	Spatial Resolution (milliarcsec pixel^{-1})	Plate Scale (milliarcsec pixel^{-1})		FP-POS Step (Å step^{-1})
				Disp. Axis	Cross-Disp. Axis	
G230L	2,100 - 3,900	390	81 ± 1	24.3	24.0	20.3

Figure 13.26: Wavelength Ranges for the G230L Grating

Dark lines represent wavelengths sampled by all four FP-POS positions. Wavelengths above 3200 Å may be contaminated by second-order light.

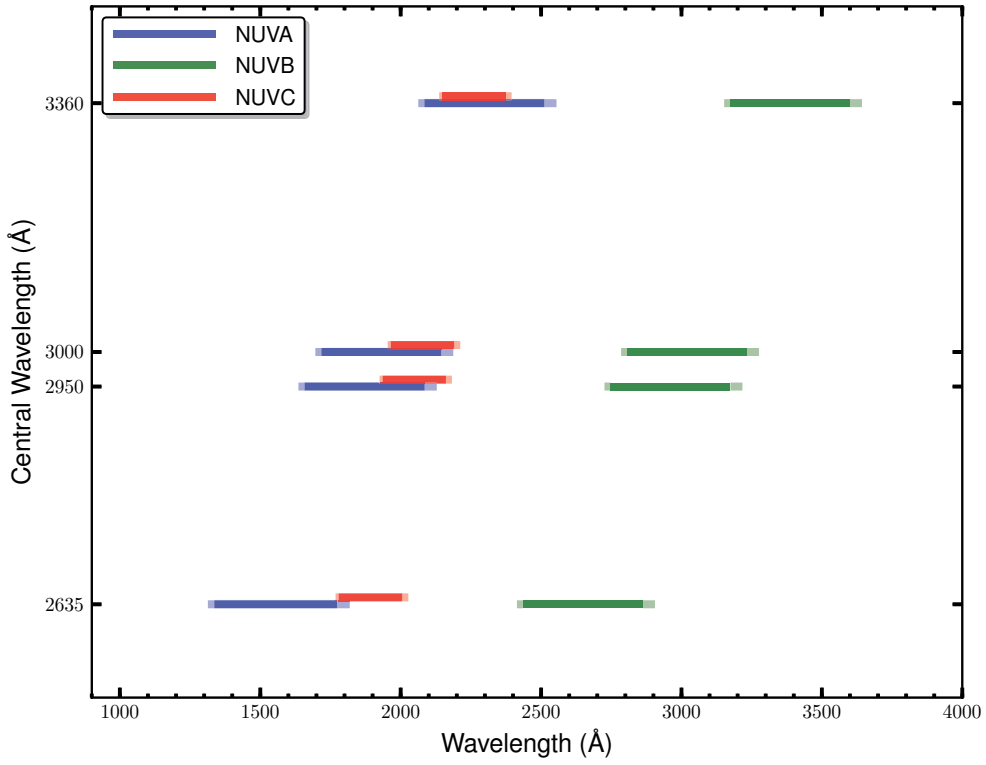

G230L Point-Source Sensitivity

Table 13.11: G230L Point–Source Sensitivity for PSA

Wavelength (Å)	Throughput	Sensitivity (counts pixel^{-1} sec^{-1} per erg cm^{-2} sec^{-1} Å^{-1})	Effective Area (cm^2)
1400	7.061e-09	7.4e+06	3.19e-04
1600	1.419e-04	1.7e+11	6.42e+00
1800	1.020e-02	1.4e+13	4.61e+02
2000	1.447e-02	2.2e+13	6.55e+02
2200	1.612e-02	2.6e+13	7.29e+02
2400	1.550e-02	2.8e+13	7.01e+02
2600	1.294e-02	2.5e+13	5.85e+02
2800	9.680e-03	2.0e+13	4.38e+02
3000	5.195e-03	1.2e+13	2.35e+02
3200	1.389e-03	3.3e+12	6.29e+01
3400	3.252e-03	8.2e+12	1.47e+02

Figure 13.27: G230L Point–Source Sensitivity for PSA and BOA

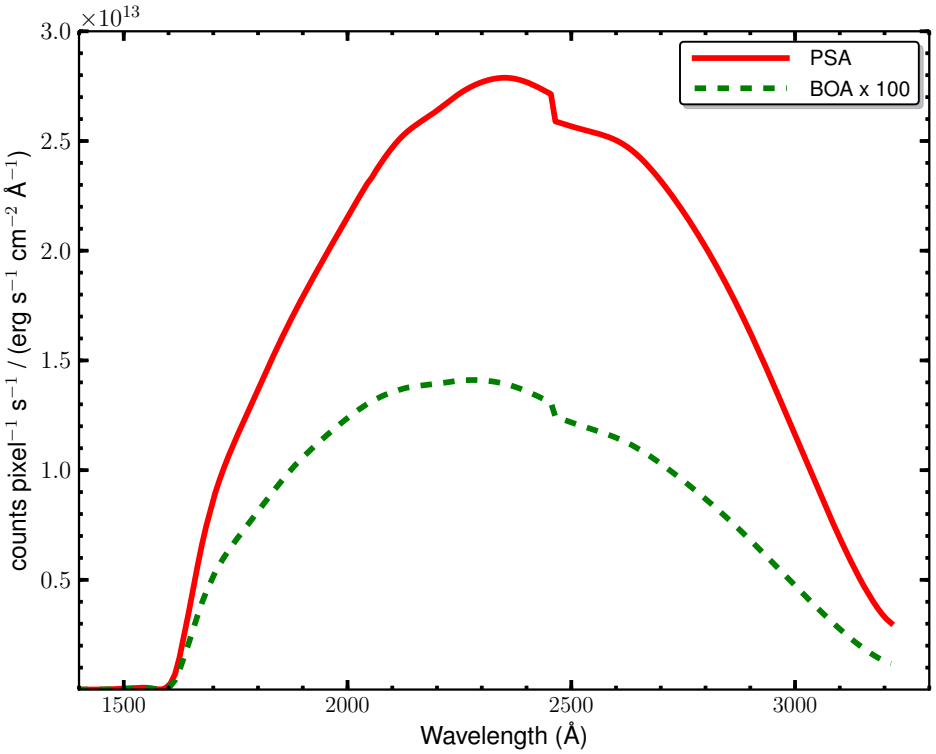

G230L Signal-to-Noise Ratio

Figure 13.28: Point–Source Signal–to–Noise as a Function of STMAG for G230L

The top axis displays constant F_λ values corresponding to the STMAG units ($V+STMAG_\lambda$) on the bottom axis. Recall that STMAG = 0 is equivalent to F_λ = 3.63E-9 erg cm^{-2} s^{-1} Å^{-1}. Colors refer to exposure times in seconds. The edge of the shaded area corresponds to the bright-object screening limit. Use of the PSA is assumed.

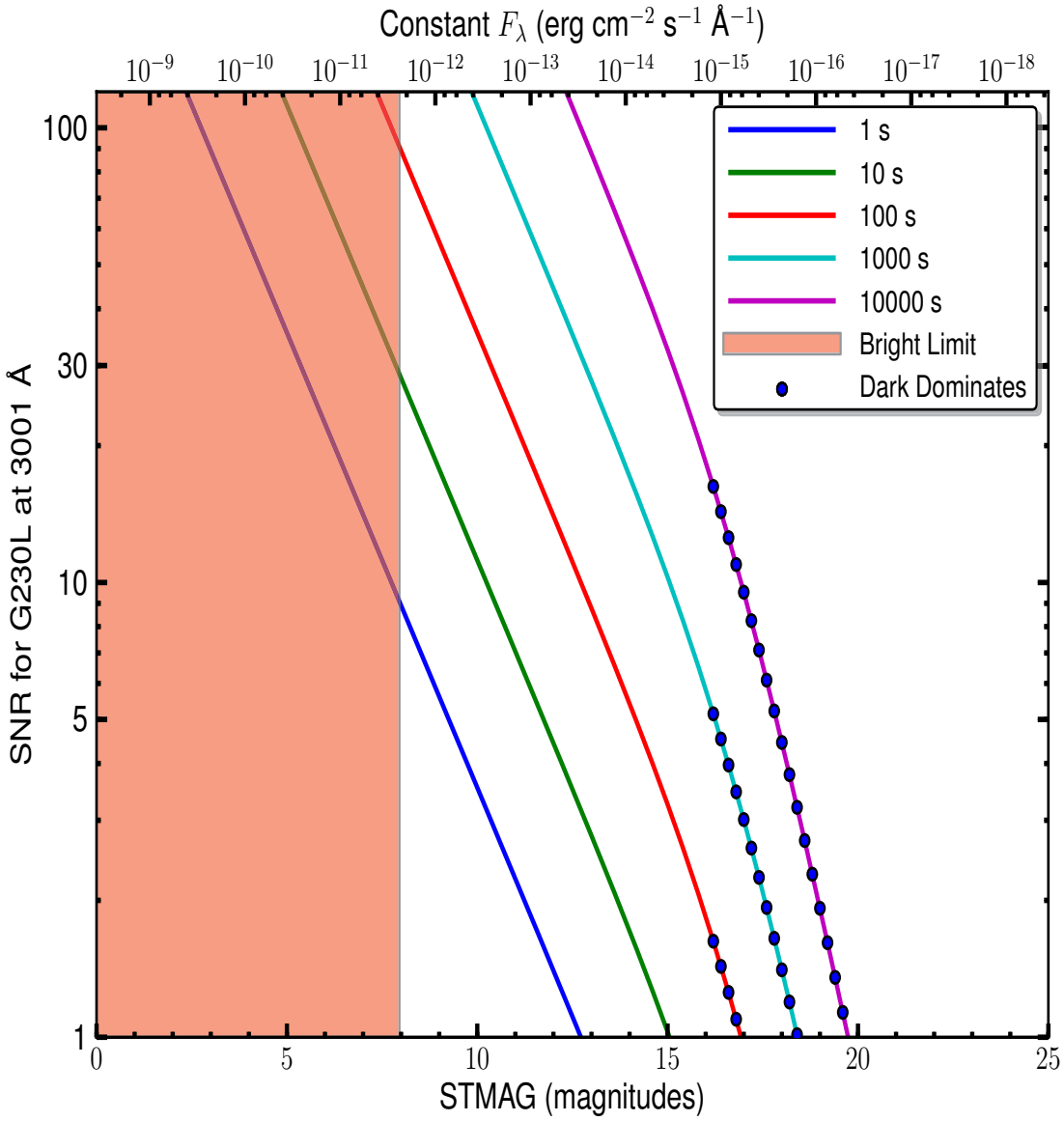

13.4 Spectrograph Design Parameters

13.4.1 FUV Channel

Table 13.12 presents design parameters of the FUV spectrograph and gratings. The FUV gratings are concave and have holographically-generated grooves to provide dispersion and correct for astigmatism. The gratings have aspherical surfaces to correct for *HST*'s spherical aberration. The FUV "M" gratings have been ion etched to produce triangular groove profiles for better efficiency. The G140L grating has grooves with a laminar profile. All FUV gratings are coated with MgF_2 over aluminum.

The surface of the optic is a sphere of the quoted radius, but with a deviation of $\Delta z = a_4 r^4 + a_6 r^6$, where z is measured along the vertex normal. The quantities γ, δ, r_c, and r_d are the standard positions of the recording sources as defined in Noda, Namioka, and Seya (1974, J. Opt. Soc. Amer., 64, 1031).

Table 13.12: Design Parameters for the FUV Spectrograph and Gratings

Dimension	G130M	G160M	G140L
secondary mirror vertex to aperture (z, mm)	6414.4		
V_1 axis to aperture (mm)	90.49		
aperture to grating (mm)	1626.57		
α (degrees)	20.1	20.1	7.40745
β (degrees)	8.6466	8.6466	–4.04595
$\alpha - \beta$ (degrees)	11.4534		
grating to detector (mm)	1541.25		
detector normal vs. central ray (degrees)	9.04664		
nominal groove density (lines mm $^{-1}$)	3800	3093.3	480
radius of curvature (mm)	1652	1652	1613.87
a_4	1.45789×10^{-9}	1.45789×10^{-9}	1.33939×10^{-9}
a_6	-4.85338×10^{-15}	-4.85338×10^{-15}	1.4885×10^{-13}
γ (degrees)	–71.0	–62.5	10.0
d (degrees)	65.3512	38.5004	24.0722
r_c (mm)	–4813.92	–4363.6	3674.09
r_d (mm)	5238.29	4180.27	3305.19
recording wavelength (Å)	4880		

13.4.2 NUV Gratings

Table 13.13 presents design parameters of the NUV gratings. The NUV gratings are flat and were not constructed holographically. The NUV MAMA has low but measurable sensitivity at FUV wavelengths, and with some gratings second-order light could contaminate the spectrum. To minimize this effect, the coated optics are optimized for wavelengths above 1600 Å. Given the four reflections used in the NUV channel, wavelengths below 1600 Å, including geocoronal Lyman-α, are effectively eliminated. In addition, gratings G230L and G285M have order-blocking filters mounted directly on them to block the second-order spectra below 1700 Å. Even with these filters, it is possible for second-order light to appear on the NUV MAMA when G230L is used, especially in the long-wavelength stripe.

Table 13.13: Design Parameters for the NUV Gratings

Dimension	G185M	G225M	G285M	G230L
groove density (mm^{-1})	4800	4800	4000	500
α (degrees)	27.24	33.621	35.707	5.565
β (degrees)	25.85	32.23	34.32	1.088
coating	Al + MgF_2	Al only	Al only	Al + MgF_2

13.5 The Location of COS in the *HST* Focal Plane

The location of the COS aperture in the *HST* focal plane is shown in Figure 13.29. Note the relative orientation of the *HST* V_2 and V_3 axes (the V_1 axis is along *HST*'s optical axis), as well as the relative locations and orientations of the other instruments. The COS aperture lies ~ 325 arcsec from the V_1 axis in the $+V_2, -V_3$ quadrant.

Figure 13.29: A Schematic View of the HST Focal Plane

This drawing shows the entire HST focal plane and the apertures of the scientific instruments. The view is from the rear of the telescope looking forward toward the sky, the opposite of the sense of Figure 13.30.

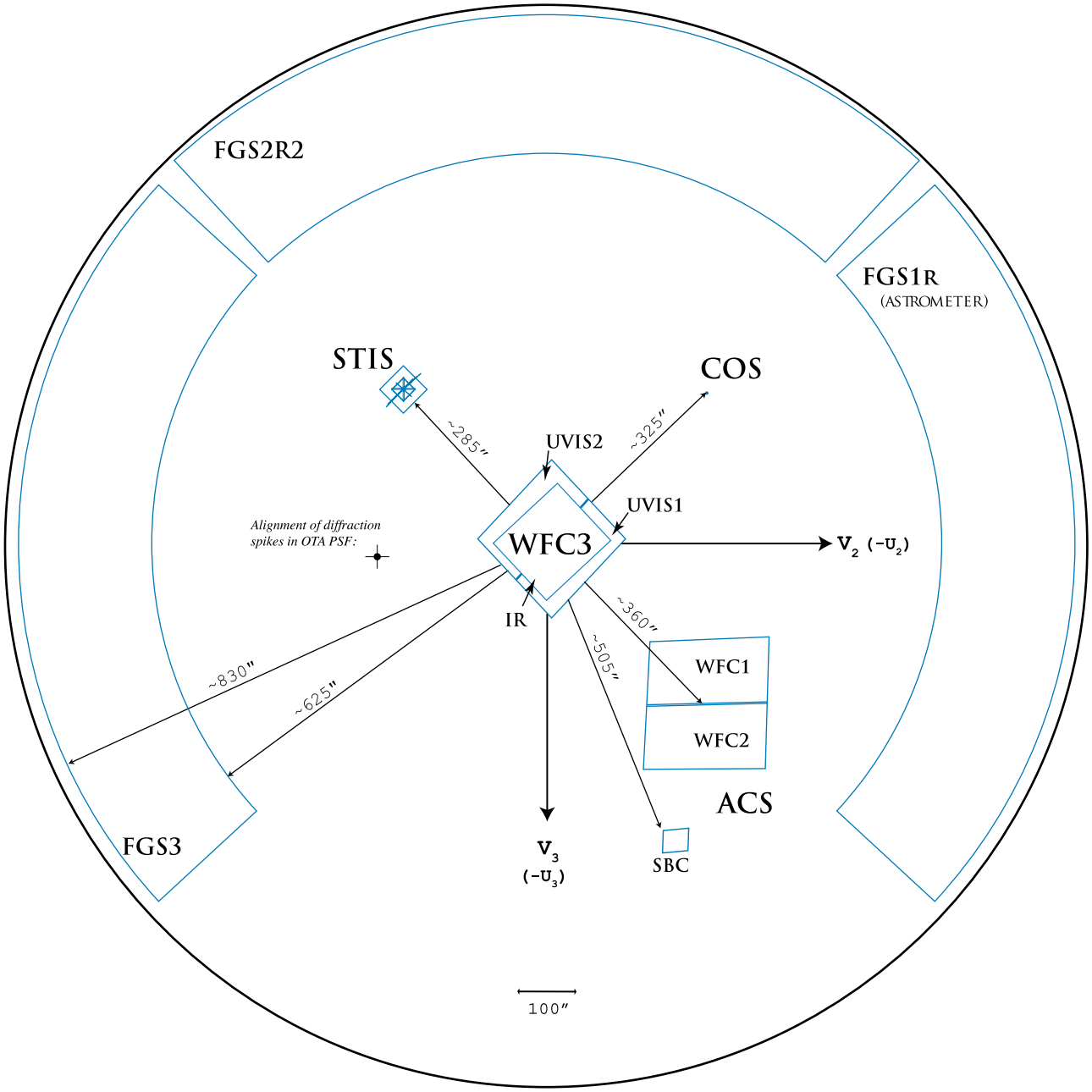

13.6 The COS User Coordinate System

Figure 13.30 presents a schematic layout of the COS focal plane. In this figure, the x and y axes denote the COS user coordinate system. In this system, x lies along the wavelength (dispersion) axis and increases with increasing wavelength for both the FUV and NUV channels. For the NUV channel, y increases with increasing wavelength in the cross-dispersion (XD) direction. All references to COS (including `POS TARG` specifications in APT, the Astronomer's Proposal Tool, detector pixel coordinates, and science header keywords) employ the user coordinate system.

Figure 13.30: Schematic Layout of the COS Detectors

This view is from the front of the telescope looking aft. The dashed arrows show the direction of increasing wavelength for the two detectors, and "XD" indicates the direction of increasing wavelength for the NUV cross-dispersion direction. The x and y axes denote the COS user coordinate system. For both the FUV and NUV channels, wavelength increases in the $+x$ or $(+V_2, -V_3)$ direction. Note that this diagram is purely schematic and it is intended to show only relative directions. This diagram does not show the locations of apertures. The bottom corner of this square (at V_1) corresponds to the center of the WF3 camera (see Figure 13.29).

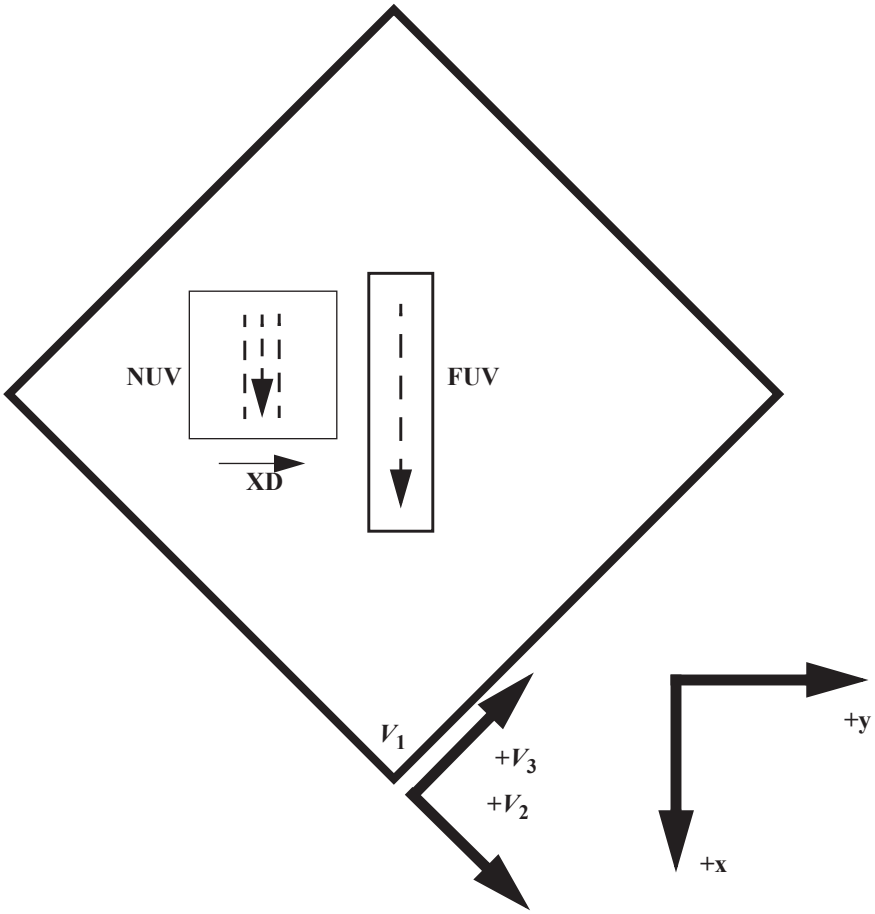

Glossary

A Glossary of Terms and Abbreviations

ACCUM

Operating mode for COS in which only the locations of detected photons are recorded; no time information is recorded. ACCUM mode is designed for bright objects with high count rates. See also TIME-TAG.

Along Dispersion (AD)

The dispersion direction, corresponding to the X axis on both the FUV and NUV detectors.

Aperture Mechanism (ApM)

The Aperture Mechanism is used to place either the BOA or PSA into position as the science aperture. The ApM is also moved to place the FCA into position if a flat-field exposure is to be taken.

APT

The Astronomer's Proposal Tool, software provided by STScI for writing Phase I proposals and Phase II programs. The use of APT is encouraged in all cases, even for Phase I proposals, because it provides an accurate estimate of the actual time needed to obtain an observation. For more information, go to

`http://apt.stsci.edu`

BOA

The Bright Object Aperture is 2.5 arcsec in diameter with a neutral-density filter that attenuates flux by a factor of about 200.

calcos

The COS calibration pipeline, a software package that performs image and spectroscopic data reduction to produce output files useful for scientific analysis.

central wavelength

For the NUV gratings, the central wavelength is the approximate midpoint of the stripe B spectrum. For the FUV gratings, the central wavelength refers approximately to the shortest wavelength recorded on Segment A.

channel (FUV or NUV)

One of the two COS optical systems, FUV and NUV, including mirrors, gratings, and detectors.

ETC

Exposure Time Calculator, software provided by STScI to estimate exposure times needed to achieve, say, a given signal-to-noise level on a source. Although information is provided in this handbook on exposure estimation, the ETC provides the most accurate way to determine the exposure times required to acquire or observe an object. The ETC is used together with the APT to plan *HST* observations. For more information, go to

http://www.stsci.edu/hst/cos/software/planning/etc

FCA

Flat-field Calibration Aperture, the aperture through which the on-board deuterium lamps illuminate the COS optical system.

FGS

Fine Guidance Sensor. By tracking guide stars, the three FGSs can maintain the pointing stability of *HST* with a precision of 2 mas or less.

FP-POS

A command used to move the spectrum on the detector (in the dispersion direction) to reduce the effects of fixed-pattern noise.

FUSE

Far Ultraviolet Spectroscopic Explorer, a moderate-resolution ($R \sim 15{,}000$), far-UV spectrograph that used micro-channel plate detectors similar to those employed by the FUV channel of COS.

FUV

The far-ultraviolet channel of COS can observe wavelengths from less than 900 to 1800 Å.

GALEX

Galaxy Evolution Explorer, a NASA mission observing the sky in two ultraviolet bandpasses. *GALEX* data are useful for determining the UV fluxes of COS targets. For more information, go to

http://www.galex.caltech.edu

GSC2/ICRS

Guide Star Catalog II / International Celestial Reference System. The GSC2 is an all-sky optical catalog based on 1" resolution scans of the photographic Sky Survey plates from the Polomar and UK Schmidt telescopes. The ICRS is the fundamental celestial reference system adopted by the International Astronomical Union for high-precision astrometry. Uncertainties in this system are dominated by the 0.3" uncertainty of the GSC2.

GTO

Guaranteed Time Observer, a member of the COS science team who has been granted a share of telescope time as part of their involvement in designing and building COS.

home position

The default position for a mechanism. COS is reconfigured at the start of each visit, and mechanisms are returned to their home positions. For the ApM, the home is the PSA; for OSM1, home is G130M, `CENWAVE=1309`; and for OSM2, home is G185M, `CENWAVE=1850`.

IDT

Instrument Development Team, NASA's term for the group that proposed and built COS.

LSF

Line Spread Function, the shape of a spectral feature emitted by a monochromatic point source.

MAMA

Multi-Anode Micro-channel Array, a photon-counting UV detector, used in the NUV channel.

MAST

The Mikulski Archive for Space Telescopes, which makes available data from a number of NASA missions, including *HST*. Go to

`http://archive.stsci.edu`

MCP

Micro-Channel Plate, a resistive glass plate with 10–15 micron-sized holes used within both the XDL and MAMA detectors to amplify photo-electrons into charge pulses large enough for electronic processing.

MIRRORA, MIRRORB

MIRRORA and MIRRORB are used for NUV imaging in COS. MIRRORA provides the highest throughput. MIRRORB uses a reflection off of the order-sorting filter of MIRRORA to get lower throughput, which can be helpful when observing bright targets.

NUV

The near-ultraviolet channel of COS can observe wavelengths from ~ 1650 to 3200 Å.

OSM1, OSM2

The Optics Select Mechanisms place gratings or mirrors in the optical path.

OTA

Optical Telescope Assembly, *HST*'s optical system of primary and secondary mirrors, plus the structure that holds them and maintains alignment.

pixel

The basic stored unit of data. In the NUV channel, MAMA pixels correspond to physical portions of the detector. In the FUV channel, the position of a detected event is assigned to a pixel based on calculations, but there are no physical pixels as such.

PHD

Pulse-Height Distribution, a histogram of the charge cloud sizes collected in a particular exposure or portion thereof. The PHD is a useful measure of data quality and is recorded as a data product for FUV exposures. PHD data are not available for NUV exposures.

POS TARG

The "`POS TARG X, Y`," special requirement is used to request a target offset in APT. POS TARG offsets are specified in the COS user coordinate system, which is used in all COS data products (section 13.6). Note that the POS TARG coordinates represent motion of the target in the aperture; the telescope moves in the opposite direction.

PSA

Primary Science Aperture, a circular aperture 2.5 arcsec in diameter and completely open.

PSF

Point Spread Function, the two-dimensional distribution of light produced by the *HST*+COS optics.

resel

Resolution element of a spectrum or image. For spectra, a resel corresponds to the FWHM of a narrow emission line. Using pre-flight data, resels were determined to be roughly 6 pixels wide (dispersion direction) by 10 tall for the FUV channel and 3 × 3 pixels for the NUV. On-orbit data suggests that the FUV resel is somewhat larger than this, while the NUV resel is somewhat smaller. Note that spectra are recorded in pixel units and that any rebinning into resels is performed on the ground during data reduction.

segment

The COS FUV detector consists of two independent segments. In all spectroscopic modes, the long-wavelength end of the spectrum falls on Segment A, and the short-wavelength end on Segment B.

SMOV

Servicing Mission Observatory Verification, the period immediately following a servicing mission in which *HST*'s instruments are activated, tested, and made ready for science observing. Only a minimal set of calibrations are done in SMOV to confirm instrument performance; more detailed calibrations are performed in the ensuing cycle.

stim pulse

Artificially-induced events on each segment of the FUV detector. The stim pulses allow for the correction of thermal distortion and aid in determining the dead-time correction.

STMAG

In this system, the flux density is expressed per unit wavelength, and the reference spectrum is flat in F_λ. $STMAG = -2.5 \log F_\lambda - 21.10$.

stripe

To accommodate the NUV detector format, COS NUV spectra are split into three non-contiguous stripes, each of which covers a relatively small range in wavelength.

TAGFLASH

Use of TIME-TAG mode with FLASH=YES selected. In this mode, wavelength-calibration spectra are obtained at periodic intervals during a PSA TIME-TAG observation so that any drifts of the spectrum due to residual motion of the optics can be removed.

TIME-TAG

A COS observing mode in which the locations (pixels) and times (to the nearest 32 msec) are recorded for each detected photon. Doing this consumes memory but allows great flexibility in reducing and analyzing the data.

wavecal

A wavelength calibration exposure; i.e., an exposure of the Pt-Ne wavelength calibration lamp through the WCA.

WCA

Wavelength Calibration Aperture, which is illuminated by a Pt-Ne wavelength calibration lamp.

XD

Cross-dispersion direction, corresponding to the Y axis on both the FUV and NUV detectors.

XDL

Cross Delay Line, the type of detector used in the FUV channel of COS.